From Inhibition to Benefit: Exploring the Relationship Between Zika Virus NS4A and ANKLE2

By

ADAM FISHBURN
DISSERTATION

Submitted in partial satisfaction of the requirements for the degree of

DOCTOR OF PHILOSOPHY

in

Microbiology

in the

OFFICE OF GRADUATE STUDIES

of the

UNIVERSITY OF CALIFORNIA

DAVIS

Approved:

_____

Priya Shah, Chair

_____

Lark Coffey

_____

Bennett Penn

Committee in Charge

2024

Acknowledgments

My Ph.D. and this thesis would not be possible without the enduring support of those around me. First, I would like to extend my most sincere appreciation for my advisor Dr. Priya Shah. Her enthusiasm and demeanor are what originally got me interested in these topics. She provided me with comfort when things did not go as I wished and tempered my often over-ambitious nature to do everything all at once. Her candidness as a scientist, professor, and mentor has taught me so much about what it means to be in her position and inspires me to follow a similar path. I cannot recall a single moment when I felt uncomfortable, unsupported, or unwanted. I thank her for allowing me the opportunity to continue that which she started and for allowing me to influence the project in my own ways. I would not be where I am, or be who I am, without her guidance and mentorship.

I would like to thank the members of my Dissertation Committee Dr. Lark Coffey and Dr. Bennett Penn. They have both supported me through my Qualifying Exam and the years of research that followed. Their encouragement and supply of new ideas has been instrumental in the development of my projects. I would also like to extend thanks to Dr. Bruce Draper who served as a mentor and member of this committee in the early stages of my Ph.D.

Next, I would like to acknowledge and thank those who have contributed to my research projects presented here. I would like to thank the members of the Shah Lab that have helped me weather the hardships and grow over the last 5 ½ years. The science we do is undoubtedly difficult, and they have all made it bearable. I would like to thank Dr. Nitin Beesabathuni, Dr. Shiaki Minami, and Matthew Kenaston for standing by me all the times I came to complain when things failed and shared my joy when things worked. Each of them has contributed so much to the scientific progress of my projects and I consider them all to be close friends. I would like to thank Nicholas Lopez, Thomas Klaessens, and Cole Florio who worked tirelessly alongside me and helped execute my vision. Each of them has contributed so much to this work and I could not have done

this all without them. I would like to thank the current and former post-doctoral researchers in the lab Dr. Marine Petit, Dr. Robert Stott, Dr. Efra Rivera-Serrano, Dr. Oanh Pham, and Dr. Liuba Cherkashchenko who have all taught me so much. I would like to thank other present and past members of the lab Shruthi Garimella, Neil Adia, Chase Skawinski, Ritika Gangarju, and Ariana Nagainis who have each contributed to my journey in their own ways. I would like to thank all the undergraduate students that have worked with me and assisted with projects: Traci Shiu, Tulika Singhal, Shahabal Khan, Sophia Haggard, Danny Kuei, Michelle Ramos, and Sydney Becker. Finally, I would like to thank all the trainees and rotations students that have joined me over the years: Natalie Sahabandu, Inglis Tucker, Zoila Estrada-Tobar, Jeannine Stroup, Vivian Hoang, Julia Godinez, Lucy Moore, and Marcella Mirabelli. I would also like to extend my appreciation to all the collaborators who have shared their time, resources, and advice to help progress our goals.

I would like to thank those closest to me for always encouraging me. Thank you to my close friends Derek Hamilton, Nawraz Bashir, and Marshall Everett for always being there when I needed a break from my studies. Thank you to thank my parents, Debbie and Scott, and my brother Jordan for their unwavering love and support. Thank you to my dog Stormy for being there every step of the way with me. Finally, I would like to thank my wife, partner, and best friend Judith. I know for certain that I would not have done this and could not have finished this without your encouragement and unending devotion. You inspire me every day to be the best version of myself that I can be. I hope that I have made you all proud.

Abstract

Flaviviruses are arthropod-transmitted positive-sense single stranded RNA viruses, capable of causing significant human disease. Their RNA genomes are translated by host machinery and produce a viral polypeptide of ten viral proteins, three structural and seven non-structural. The non-structural proteins are essential for mediating virus genome replication, host defense silencing, and cell remodeling. Much of this is accomplished through physical interactions between viral protein and host proteins, which interrupts or otherwise impacts their cellular function for virus benefit. Inhibition of host protein function during these interactions can be connected to viral pathogenesis and disease. In the case of Zika virus (ZIKV) the primary disease outcome of concern is birth defects or fetal demise that occur in fetuses that are infected *in utero* via vertical transmission from the infected mother. Birth defects arising from ZIKV infection are broad and collectively termed congenital Zika syndrome (CZS). Most infamous of these is microcephaly, a condition where brain and head are not fully grown at birth. Microcephaly is associated with a wide range of debilitating development problems that last throughout life. The molecular mechanisms that contribute to microcephaly observed in CZS cases are not fully understood and likely multifactorial.

To understand if ZIKV-host protein-protein interactions are contributing to neurodevelopmental defect, global proteomics was previously performed on ZIKV proteins to identify host interactors. This revealed the interaction between ZIKV non-structural 4A (NS4A) and the host protein ankyrin repeat and LEM domain containing 2 (ANKLE2). ANKLE2 is involved in nuclear envelope dynamics during mitosis and asymmetric cell division during neurogenesis, a key step in brain development. Mutations in ANKLE2 are associated with primary congenital microcephaly in humans. Expression of ZIKV NS4A *in vivo* results in abnormal brain development in fruit flies. This phenotype is rescued by overexpression of human ANKLE2. Together this data supports the hypothesis that NS4A physically interacts with ANKLE2, inhibiting its function during

neurodevelopment to cause microcephaly. However, the basis for the physical interaction and the specific ways NS4A inhibits ANKLE2 function through it are still mysterious. Beyond this is the question of why NS4A interacts with ANKLE2 to begin with? Is the interaction, and the pathogenesis that follows, purely coincidental, or does NS4A interact with ANKLE2 to serve in some aspect of ZIKV replication?

This work serves to explore the questions revolving the NS4A-ANKLE2 interaction. First, we establish that ANKLE2 has the opportunity to impact ZIKV replication by showing colocalization of ANKLE2 with ZIKV factors during virus replication. To explore if ANKLE2 is actively participating in some aspect of virus replication we then genetically deplete ANKLE2 using CRISPRi knockdown or CRISPR mutagenesis. Cells with diminished or depleted ANKLE2 were infected with ZIKV and had reduced replication across multiple conditions and cell lines. This work provides substantial evidence that ANKLE2 supports ZIKV replication in human cells. During a flavivirus transmission cycle the virus must efficiently replicate in both human and mosquito cells. In collaboration with another group, we show that depletion of the Ankle2 ortholog in mosquito Aag2 cells also leads to reduced ZIKV replication, supporting that Ankle2 is beneficial to virus replication across hosts. Further, we show that physical interaction between ANKLE2 and NS4A is conserved across four other mosquito-borne flaviviruses and that ANKLE2 plays a role in the replication of some of these viruses.

In order to investigate the physical determinants of the ANKLE2-NS4A interaction we developed a series of truncation mutants that serially express fewer domains of each protein. To test physical interaction between the proteins, we performed co-transfection and co-immunoprecipitation experiments. This revealed the N-terminal region of ANKLE2 interacts with the C-terminal region of NS4A. Further, we show that this non-interacting ANKLE2 mutant does not colocalize with ZIKV NS4A during infection. However, the data suggest that there are multiple contact sites between ANKLE2 and NS4A, across separate domains.

ANKLE2 is a scaffolding protein that modulates the cell cycle through physical protein interactions. To explore how these interactions may be perturbed during infection and how new interactions may be driven to benefit virus replication, we performed affinity-purification and mass spectrometry on ANKLE2 with and without ZIKV infection. These revealed hundreds of candidate protein interactions which enlighten both how ZIKV inhibits normal ANKLE2 function and also potential pathways through which ANKLE2 promotes virus replication. Altogether, this work vastly expands on our understanding of the ZIKV NS4A-ANKLE2 interaction and supplies avenues for future exploration.

Table of Contents

List of Figures and Tables

Copyright Acknowledgements

- Chapter 2 contains material originally published in Frontiers in Microbiology:

  Fishburn A.T., Pham O.H., Kenaston M.W., Beesabathuni N.S., Shah P.S. (2022) “Let’s get physical: Flavivirus-host protein-protein interactions in replication and pathogenesis” *Frontiers in Microbiology.* DOI: 10.3389/fmicb.2022.847588

- Chapter 3 contains material accepted to *Disease Models and Mechanisms*:

  Fishburn A.T., Florio C.J., Lopez N.J., Link N.L., and Shah P.S. (2024) “Molecular functions of ANKLE2 and implications in human disease” Accepted to *Disease Models and Mechanisms*.

- Chapter 4 and 5 contains material pre-printed on BioRxiv:

  Fishburn A.T., Kenaston M.W., Lopez N.J., Hoang V., Shiu T.N., Haggard Arcé S.T., Khan S.S., and Shah P.S (2022) “Zika virus NS4A hijacks host ANKLE2 to promote viral replication” DOI: 10.1101/2022.03.15.484510

These articles have been modified to comply with the formatting requirement of this thesis.

Chapter 1: Introduction

The molecular nature of viruses is contradictory to their biological size. Compared to multicellular eukaryotic organisms and even unicellular prokaryotes, most viruses have a minuscule genome and proteome (1). Despite this, viruses infiltrate organisms in every branch of the tree of life without fail. In many cases, their existence within their host is that of a shadow, endlessly present and shifting, but overall harmless. After all, killing your host means not being able to replicate in it. However, not all viruses follow this trend. Certain viruses must destroy their host cell to continue forward (2). The recent COVID-19 pandemic stands as the extreme example of the devastation viruses can unleash on humankind. Thus, it goes without saying that the study of viruses is essential for our collective ability to counter their advances, combat them within our bodies, and treat the diseases they cause. These three components: transmission, replication, and pathogenesis are at the forefront of virus research worldwide. And so, we return to the contradiction underlying viruses, the complexity concealed within the simplicity. How do they accomplish transmission between different cells, tissues, and hosts? How do they enter their host's cells, replicate their genomes, produce more viruses, all while silencing and counteracting the host's inherent defenses? How does their replication cause intentional or accidental detriment to the host? Finally, how do these seemingly simple entities, which are not even qualified as being alive by traditional metrics, accomplish all these complicated molecular feats with relatively few genes and proteins? This question serves as the bedrock for all the following work. At the base of all my study is the search for how viruses can circumvent their genetic size and perform things we would consider biologically miraculous. At the most basic level, viruses use their limited toolbox of proteins to hijack their host's much larger set to remodel, silence, rewire, create, or destroy whatever they need to replicate. This is often accomplished through physical protein-protein interactions (PPIs) between viruses and their target host proteins. These interactions can have many consequences on the target host protein including the alteration of subcellular

localization, functional changes through post-translational modification leading to inhibition or enhancement of enzymatic activity, or destruction through proteolytic cleavage or targeting to cellular degradation pathways, as will be discussed in Chapter 2. The underlying goal of this work is to explore how flaviviruses mediate their replication and cause disease through specific virus-host PPIs. In the rest of this Chapter, we will introduce and review the history of Zika virus, and the findings that serve as the foundation for this work. In Chapter 2 we will review PPIs between orthoflaviviruses and their hosts, and how these mediate virus replication and pathogenesis. In Chapter 3 we will review the cellular biology of the host protein ANKLE2. In Chapter 4 we present original work on the role of ANKLE2 in promoting orthoflavivirus replication. In Chapter 5 we present experiments that serve to understand the biochemical nature of the PPI. In Chapter 6 we present an initial proteomic study of ANKLE2 interactions and how these change during virus infection. Finally, in Chapter 7 we will present preliminary work and propose unanswered questions that will serve as the basis for future work.

The origin of Zika virus and ties to congenital birth defects

The virus family *Flaviviridae* consists of four genera of positive-sense single-stranded RNA viruses, including Pestivirus, Pegivirus, Hepacivirus, and Orthoflavivirus. The name *Flaviviridae* originates from the latin “flavi” for yellow, arising from individuals with jaundice, a signature symptom of yellow fever disease. In the late 1800’s to early 1900’s it was discovered that this disease was transmitted by mosquitoes and that the causative agent was a virus, appropriately named yellow fever virus (YFV) (3). YFV was one of the earliest known viruses and the first to be discovered in humans. Recently, to differentiate from the family name *Flaviviridae,* the genera orthoflavivirus was renamed from its original flavivirus. This name roughly translates from latin to mean “true flavivirus” or “proper flavivirus”, since this genus includes the original YFV and related viruses (4). Orthoflaviviruses are enveloped, arthropod-transmitted viruses with RNA genomes of

approximately 11 kb. The molecular virology of flaviviruses and the interactions with their hosts are extensively reviewed in Chapter 2.

The following work will primarily focus on Zika virus (ZIKV). ZIKV is an orthoflavivirus accidently discovered in 1947 in Uganda on an expedition to isolate YFV from monkeys in the Ziika forest (5). The virus they isolated from one monkey was similar to other endemic orthoflaviviruses like dengue virus (DENV) and YFV but did not cross-react with antibodies against these viruses. This suggested to the researchers that their isolated virus was a novel orthoflavivirus member, and so it was named Zika virus after the place it was discovered. In the decades following its discovery, human cases of ZIKV infection and detection of the virus in local monkey populations were rare (6). ZIKV has a similar transmission cycle to that of other orthoflaviviruses. In dense tropical forests it is transmitted by forest-dwelling mosquitoes between non-human primates (7). This is referred to as the sylvatic cycle. The concern with all viruses such as these is when human habitation closely borders these forests, and the risk arises of virus spillover from sylvatic cycle into humans.

The first notable outbreak of ZIKV occurred in 2007 on the small Pacific Island of Yap. In this outbreak, 185 cases of suspected ZIKV infection occurred, with 49 later being confirmed by PCR. No cases were severe enough to cause death or even warrant hospitalization (8,9). Prior to this, only 16 cases of ZIKV disease in humans had been documented (6). Between 2010 and 2015, there were sporadic cases of ZIKV infection throughout Asia, including a Canadian traveler who was infected in Thailand (10). This clinical isolate, termed PLCal, will serve as the model for many experiments in the following work. Also in 2013, a larger outbreak of ZIKV occurred in French Polynesia, another island in the Pacific Ocean. Over 8,500 cases were suspected with 396 being diagnostically confirmed by PCR or ELISA, although many more cases were estimated and likely unreported. Alarmingly, of these 396, 40 individuals were diagnosed with Guillain-Barré syndrome (GBS) within three months (11–13). GBS is a form of autoimmune disease that damages

peripheral nerves and causes tingling in the extremities, muscle weakness, and paralysis. Further, two mothers gave birth during this epidemic and their newborns tested positive for ZIKV in their serum, suggesting for the first time that ZIKV could be transmitted transplacentally to the developing fetus (14). Thankfully in these two cases, both mothers and newborns were clinically unharmed by the infection. The French Polynesia outbreak served as the first significant alarm to the global health community that ZIKV may emerge as a significant public health threat.

In early 2015, Brazilian health officials noticed an unusually high number of cases of patients presenting with neurological syndromes (15,16). In May 2015, the Pan American Health Organization (PAHO) issued their first epidemiological alert regarding ZIKV. A second alert in November updated the public to the association of ZIKV with neurological syndromes and congenital birth defects (6,17). In January 2016, the US CDC issued a formal travel advisory to warn pregnant women against traveling to affected areas due to the suspected risk (18). By the middle of 2016, the causality between *in utero* ZIKV infection with adverse birth defects was clear to most of the scientific community, based on a number of published single case descriptions, as well as several larger studies (19–24). A retrospective review of the 2013 French Polynesia outbreak also revealed 8 cases of ZIKV-associated neurodevelopmental birth defects (25).

The observed disease consists of a broad set of birth defects and was collectively termed congenital Zika syndrome (CZS). The most severe and notable symptom of CZS is microcephaly, which is clinically characterized as head and brain size smaller than two standard deviations (SD) from mean for a given sex and age. Severe microcephaly is characterized as smaller than 3 SD from the mean. ZIKV is not the only pathogen known to cause congenital birth defects or microcephaly. An established group called the TORCH pathogens (which stands for Toxoplasmosis, other, Rubella, Cytomegalovirus [CMV], and Herpes) all cause severe disease in the fetus or newly born offspring (26). ZIKV now soundly resides in the “other” group along with HIV, Syphilis, Chickenpox, and Parvovirus. Microcephaly in CZS is often accompanied by fetal

brain disruption sequence (FBDS), in which the morphology and development of the cranium itself is severely abnormal (27). While FBDS is not unique to CZS, it is rarely reported otherwise, and much more common in CZS associated cases. CZS also often leads to intracranial subcortical calcifications. This is divergent from the pathology of CMV, which also causes similar congenital microcephaly, but results in periventricular calcifications, suggesting the molecular etiology of disease is not entirely shared. In addition to calcifications, many neurological abnormalities have been described in CZS brains, including hypoplasia of the corpus collosum or cerebellum, abnormal gyral patterns, increased fluid spaces, and cortical thinning. Additionally, an array of ocular abnormalities, congenital contractures, and hip displacement are common manifestations of CZS (28–30). CZS-associated microcephaly has a mortality rate of approximately 10% (31,32), and in non-lethal cases, CZS is highly detrimental to the health and wellbeing of affected individuals. Severe CZS is often associated with dramatic neurological deficits and developmental delays including cognitive, speech, and motor ability. More rarely, defects in hearing or vision development, irritability, or predisposition to seizures have been observed (29). Follow-up studies of infants affected by CZS are limited, however studies suggest that neurological, ocular, and motor impairments are maintained over the first several years of life (33,34). Interestingly, physical therapy regiments have been shown to marginally improve motor function of CZS infants (35,36). To date, no other treatments, therapeutics, or preventatives have been fully developed to aid in battling ZIKV or CZS in humans, although vaccines are in development (37). The burden of ZIKV has waned significantly since the 2015-2016 epidemic, although it still resides primarily within Brazil, with several thousand confirmed cases every year since the epidemic (38). This persistence is likely contributed to by the establishment of a sylvatic cycle in the tropical forests of the region (39).

Current molecular models for ZIKV pathogenesis.

In the years following the ZIKV epidemic, the molecular mechanisms by which ZIKV causes CZS remained mysterious. It is clear that ZIKV can be transmitted vertically from a person infected in pregnancy to their fetus and can infect neurons in the fetal brain. However, the molecular, cellular, and organismal events that ultimately lead to birth defects and microcephaly remained nebulous and unclear. It is important to preface that the causes of CZS are likely multifactorial, likely arising from any number of genetic, environmental, viral, or cellular contributors. In the seven years since the ZIKV epidemic, several groups have developed potential models to explain how ZIKV induces CZS and microcephaly.

Temporally and spatially, the first step in CZS-associated pathogenesis is overcoming the placental barrier, which serves to protect the developing fetus. Several hypotheses have been generated for how ZIKV is able to subvert this barrier and access the fetal compartment. One of the main routes proposed is via transplacental infection, in which ZIKV infects placental cells, damaging the barrier integrity and increasing permeability (40). It is possible this is mediated by secreted non-structural protein 1 (NS1), which has been shown to induce vascular leakage and permeability (41,42). ZIKV has also been shown to induce apoptosis in placental cells, which could compromise barrier function (43,44). Infection of placental cells is also associated with dramatic shifts in proteomic profile (45,46). Alternatively, mechanisms involving paracellular movement of virions between cells by disrupting tight junctions or transcytosis through infected barrier cells have been proposed (47,48).

Once past the placental barrier, the blood-brain barrier must be overcome to infect the fetal brain and cause disease. Whether the blood brain barrier integrity is compromised to allow for virus passage is contested in the field, with some studies supporting barrier disruption (49–51), and other suggesting that barrier integrity is maintained (52,53). Similar mechanisms of paracellular migration and transcytosis have been proposed to circumvent this barrier as well (47).

Transmigration into the brain through infection of monocytes has also been proposed *in vitro* (54). Transmigration into the fetal brain has also been supported *in vivo* via yolk sac derived microglia, although depletion of these cells did not completely eliminate fetal infection (55). Altogether, these studies provide plenty of potential routes for fetal nervous system infection. It is entirely possible that ZIKV is not limited to only one pathway, instead using a combination of these mechanisms to circumvent the blood-brain barrier.

Considering that neurodevelopmental defects are the major disease outcome of concern, many groups have explored how ZIKV infects, alters, and damages neurons. ZIKV readily infects human neural progenitor cells (hNPCs) and alters their cell division (56,57). ZIKV infection in these cells is associated with DNA damage which leads to S-phase mitotic arrest, nuclear morphology defects, and increases in virus replication (58,59).

The developmental process of neurogenesis involves generation of neurons in the brain, and defective or inhibited neurogenesis is considered one of the primary routes to microcephaly. Thus, the effects of ZIKV on neurogenesis were rapidly explored after the epidemic. Intracranial ZIKV infection of immunocompetent embryonic mice leads to mild microcephaly and defects in NPC division and cell survival (60). Expression of ZIKV proteins NS4A and impairs neurogenesis using human neurospheres (61). In another study, ZIKV infection in human neurospheres reduced growth by depleting the pool of hNPCs (62). ZIKV infection or expression of NS2A alone was able to dysregulate neurogenesis by disrupting the adherens junctions between cortical neurons (63). Additionally, several other studies have shown dysregulation of developmental pathways and proteins involved in neurogenesis (64–66).

Neurons are not the only cells in the brain susceptible to or negatively affected by ZIKV infection. Neurons in the central nervous system (CNS) are supported by a cast of cells collectively called glial cells, which include astrocytes, oligodendrocytes, and microglia. Astrocytes provide metabolic and structural support to neurons and vastly outnumber neurons in the brain. ZIKV

readily infects astrocytes and data suggests that infection impairs aspects of synapse control, axon guidance, and neurodevelopment (67–69). Many other studies have explored alternative routes of ZIKV pathogenesis. The rates of naturally occurring genetic variants in key host genes has been explored in cohorts of microcephalic newborns and their mothers, although molecular follow-up on the role of these genes is still required (70–72). Multi-omics approaches on infected fetal mouse brains identified dysregulation of NAD+ metabolism as an underlying factor in ZIKV-induced cell death and microcephaly (73). ZIKV-induced degeneration of retinal neurons through induction of inflammatory and ER stress genes has been shown in developing mice (74). ZIKV Capsid has been shown to cause neurodevelopmental defects by interacting with and inhibiting the key antiviral protein Dicer in developing neural stem cells (75). These studies collectively suggest multiple avenues for ZIKV-associated disruption of CNS development and function. It is clear that CZS severity and the likelihood of microcephaly is increased the earlier in gestation the infection occurs (76), although it is unclear if this is due to increased susceptibility related to incomplete barrier formation (either placental or blood-brain) or because simply dysregulating brain development earlier results in more damage.

Uncovering the connection between Zika virus NS4A, ANKLE2, and microcephaly

At the onset of the ZIKV epidemic the labs of Raul Andino and Nevan Krogan at UCSF aimed to identify ZIKV-host PPIs that may contribute to CZS. At the time, they had been working to map DENV interactions and were poised to easily adapt their studies to include ZIKV, since the polypeptide organization is very similar. To accomplish this the Krogan lab used global proteomics to systematically express each viral protein (prey) in cells and co-purify interacting proteins (bait). These bait proteins were then identified using affinity-purification coupled to tandem mass spectrometry (AP-MS). Using control prey proteins to account for non-specific identifications and

unbiased scoring algorithms, an interaction network can be generated for each viral protein (77). This approach had been used to map the global interaction networks of viruses at the time and several more since (78–81).

For ZIKV, interaction networks with human proteins from HEK293T cells were successfully generated for five viral proteins: capsid, NS2B3, NS3, NS4A, and NS5. Hundreds of specific interactions were identified along with enrichment for specific pathways and complexes (82). Review of human proteins revealed seven involved in neurodevelopment, including the host protein ANKLE2, which interacted with NS4A. ANKLE2 is a scaffolding protein that mediates nuclear envelope dynamics during cell division (83) and is extensively reviewed in Chapter 3. Full-length ANKLE2 is 938 amino acids in length, with a mass of approximately 104 kDa. It is composed of thirteen protein-coding exons, and six protein isoforms have been identified (Appendix A-1), however the function of these isoforms has not been studied. At the time the NS4A-ANKLE2 interaction was identified, relatively little was known about ANKLE2 beyond its function in cell division and one study that identified its role in brain development and microcephaly (84). In this study by Hugo Bellen at Baylor College of Medicine, fruit flies (*Drosophila melanogaster*) were used to identify novel genes involved in nervous system function and development by way of a forward genetic screen. In this experiment, male flies were randomly mutagenized using ethyl methane-sulfonate (EMS). Flies were screened for multiple phenotypes or defects including in the bristles or eyes, which would indicate abnormal neurodevelopment. Ultimately, mutations from the screen were mapped to gene loci, some of which had human homologs previously identified to have roles in human disease. To identify new human disease genes, the homologs of 237 fly genes identified in the screens were searched for any genetic variants within whole-exome sequencing data from undiagnosed cases of Mendelian disease. A L326H missense mutation in the *Drosophila* gene *l(1)G0222* (renamed to *dAnkle2*), the homolog to human *ANKLE2*, caused developmental defects in thoracic bristles and sensory organs.

Whole-exome sequencing data identified variants in *ANKLE2* that appeared to be responsible for recessive microcephaly. The proband, with compound heterozygous mutations in *ANKLE2* (Q782X/L573V), was born with significant developmental defects and microcephaly. The parents of the proband had another child, who was also born with the same mutations in *ANKLE2* and severe congenital microcephaly, and unfortunately only survived ~24 hours due to congenital cardiac complications. To connect the apparent association of *ANKLE2* mutations with congenital microcephaly, larval brains of *dAnkle2* mutagenized flies were observed. In these experiments the Bellen lab measured significant brain volume reduction in third instar larval brains, as well as reduction in the number of neuroblasts and an increase in apoptosis using a TUNEL assay. Remarkably, these phenotypes were completely rescued when human *ANKLE2* cDNA was ubiquitously expressed in these mutants, suggesting that human ANKLE2 and *Drosophila dAnkle2* have a conserved function in brain development (Figure 1-1A) (84). This work established ANKLE2 has a novel primary microcephaly (MCPH) gene (Appendix A-2).

Given the physical interaction between NS4A and ANKLE2, and the strong association between ANKLE2 and MCPH, the team hypothesized that NS4A induces microcephaly during CZS by perturbing ANKLE2 function. To explore this a collaboration was formed between the labs at UCSF and Hugo Bellen's group at Baylor College of Medicine that had previously explored *dAnkle2*. NS4A was transgenically expressed in fruit flies and brain size of third instar larvae was measured as was done previously for *dAnkle2* mutants. In this experiment, NS4A expression led to a decrease in brain size that was similar to the reduction observed when *dAnkle2* was mutated. Importantly, the NS4A phenotype could be rescued by the simultaneous expression of wild-type human ANKLE2, but not the loss-of-function mutant Q782X (Figure 1-1B) (82). *Drosophila* Ankle2 was also able to rescue the phenotype, and DENV NS4A also partially reduced brain volume. Cell death in larval brains was also increased in NS4A expressing animals, as measured by TUNEL assay. Interestingly, *dAnkle2* heterozygous flies had normal brain development, but when NS4A

was expressed in these heterozygotes, brain development phenotypes were much more severe. This, combined with the observation that overexpression of human ANKLE2 could rescue the NS4A phenotype, led to the hypothesis that the stoichiometry between NS4A and functional ANKLE2 was a critical component of this phenomenon (82).

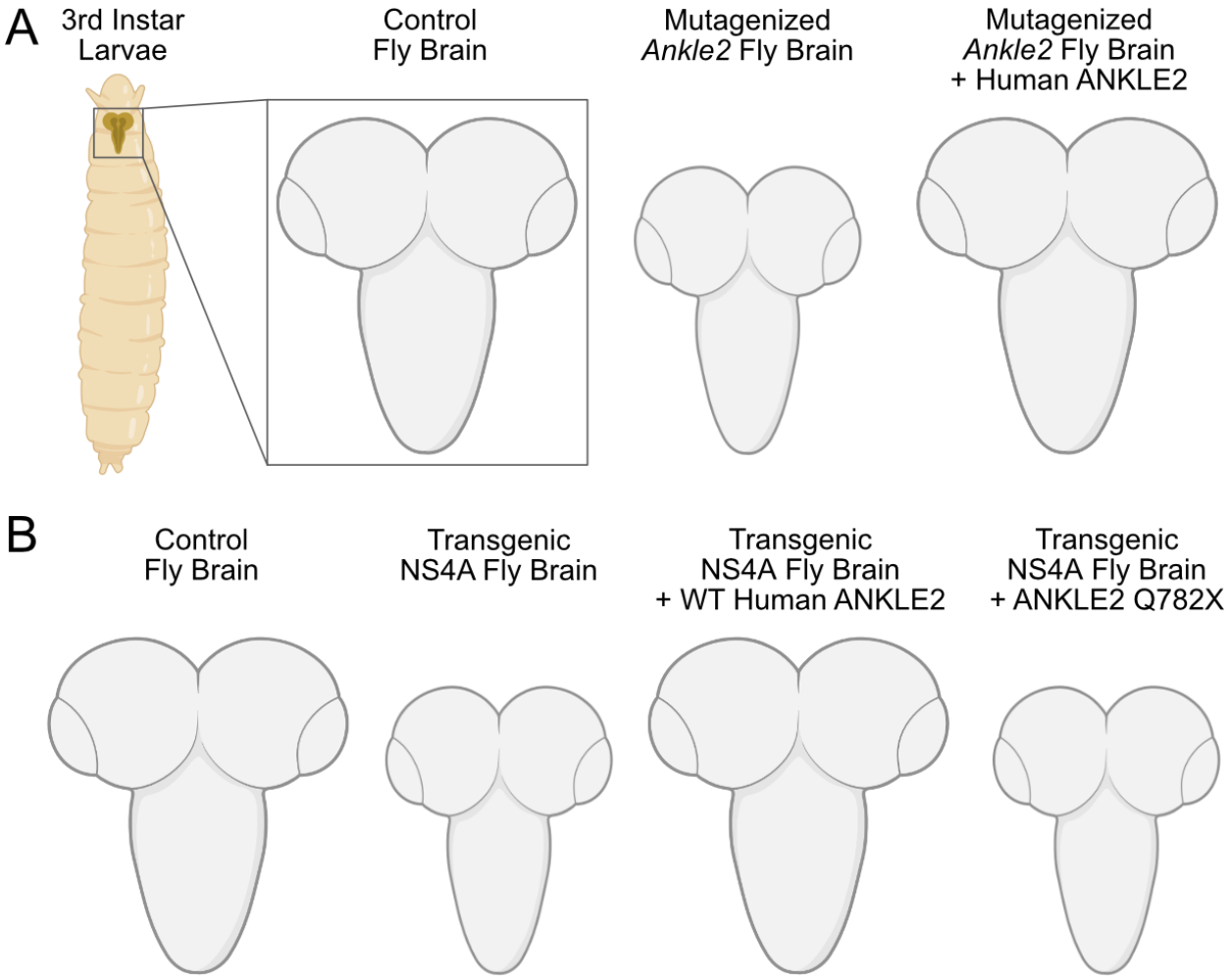

Figure 1-1: Cartoon summarization of fruit fly models of Ankle2- and NS4A-induced microcephaly. (A) The developing brain of third instar *Drosophila* larvae are dissected and evaluated to assess neurodevelopment. In mutagenized *Ankle2* larvae, brain volume is dramatically reduced. This phenotype is rescued upon expression of human ANKLE2 cDNA, suggesting that *Drosophila* and human ANKLE2 have a conserved role in brain development (84). (B) Similar reductions in larval brain size were observed when ZIKV NS4A was transgenically

expressed. This phenotype could also be rescued by the expression of wild-type human ANKLE2, but not the loss-of-function variant Q782X. This suggests that NS4A induces microcephaly in an ANKLE2-dependent manner (82).

Following this study, questions remained regarding the mechanism by which disruption of Ankle2 function leads to microcephaly. Given that the previous *Drosophila Ankle2* mutants contained only a single missense mutation (L326H) (referred to as $Ankle2^{A}$ in this study), the impact of complete disruption of Ankle2 on brain development was explored. Null mutants were generated by integrating a CRISPR-Cas9-mediated MIMiC-like (CRIMIC) into the 5th intron of *Ankle2,* (referred to as $Ankle2^{CRIMIC}$) (85). This resulted in truncated Ankle2 and animals that died as third instar larvae. The brain size of $Ankle2^{CRIMIC}$ animals was significantly reduced compared to controls, and dramatically smaller than $Ankle2^{A}$ animals. Expression of C-terminally tagged Ankle2-GFP fusion could rescue both brain development and survival phenotypes in $Ankle2^{A}$ and $Ankle2^{CRIMIC}$ animals. As seen previously, expression of wild-type human ANKLE2 could rescue brain size phenotypes in $Ankle2^{A}$ animals. However, expression of the human pathogenic variants Q782X, A109P, or G201W, could not rescue these phenotypes. These experiments solidified the role of Ankle2 in brain development and that human ANKLE2 has a conserved role in this process. Immunofluorescence revealed that $Ankle2^{A}$ neuroblasts had irregular Sec61β and Calnexin 99a localization, suggesting the ER and nuclear envelope may be disrupted. Further observation revealed that these neuroblasts had severely defective localization of partitioning proteins, vital for the asymmetric division which ultimately produces neurons. Specifically, this phenotype consists of misalignment of the mitotic spindle with the polarity of fate-inducing factors (explained further in Chapter 3). Expression of ZIKV NS4A also resulted in defective asymmetric division, suggesting that NS4A may inhibit Ankle2's role in this process to cause microcephaly (85).

Altogether, these studies support a model in which ZIKV NS4A inhibits the function of ANKLE2 in brain development contributing to the development of microcephaly. Yet several unresolved questions remain. Is the physical interaction between NS4A and ANKLE2 necessary for inhibition of its function in brain development? Does ZIKV benefit from the interaction with ANKLE2? How do NS4A and ANKLE2 physically interact? In what ways does ZIKV impact ANKLE2-host interactions, and what can this tell us about mechanisms of disease? Thus, the goal of the work presented here is to further explore this model and answer these unresolved questions.

References

1. Fenner F, Bachmann PeterA, Gibbs EPJ, Murphy FA, Studdert MJ, White DO. Structure and Composition of Viruses. Veterinary Virology. 1987;3–19.
2. Snyder JC, Young MJ. Lytic viruses infecting organisms from the three domains of life. Biochemical Society Transactions. 2013 Jan 29;41(1):309–13.
3. Staples JE, Monath TP. Yellow Fever: 100 Years of Discovery. JAMA. 2008 Aug 27;300(8):960–2.
4. Postler TS, Beer M, Blitvich BJ, Bukh J, de Lamballerie X, Drexler JF, et al. Renaming of the genus Flavivirus to Orthoflavivirus and extension of binomial species names within the family Flaviviridae. Arch Virol. 2023 Aug 10;168(9):224.
5. Dick GWA, Kitchen SF, Haddow AJ. Zika Virus (I). Isolations and serological specificity. Transactions of The Royal Society of Tropical Medicine and Hygiene. 1952 Sep 1;46(5):509–20.
6. Kindhauser MK, Allen T, Frank V, Santhana RS, Dye C. Zika: the origin and spread of a mosquito-borne virus. Bull World Health Organ. 2016 Sep 1;94(9):675-686C.
7. Valentine MJ, Murdock CC, Kelly PJ. Sylvatic cycles of arboviruses in non-human primates. Parasit Vectors. 2019 Oct 2;12:463.

8. Duffy MR, Chen TH, Hancock WT, Powers AM, Kool JL, Lanciotti RS, et al. Zika Virus Outbreak on Yap Island, Federated States of Micronesia. New England Journal of Medicine. 2009 Jun 11;360(24):2536–43.

9. Lanciotti RS, Kosoy OL, Laven JJ, Velez JO, Lambert AJ, Johnson AJ, et al. Genetic and Serologic Properties of Zika Virus Associated with an Epidemic, Yap State, Micronesia, 2007. Emerg Infect Dis. 2008 Aug;14(8):1232–9.

10. Fonseca K, Meatherall B, Zarra D, Drebot M, MacDonald J, Pabbaraju K, et al. First case of Zika virus infection in a returning Canadian traveler. Am J Trop Med Hyg. 2014 Nov;91(5):1035–8.

11. Ioos S, Mallet HP, Leparc Goffart I, Gauthier V, Cardoso T, Herida M. Current Zika virus epidemiology and recent epidemics. Médecine et Maladies Infectieuses. 2014 Jul 1;44(7):302–7.

12. Oehler E, Watrin L, Larre P, Leparc-Goffart I, Lastère S, Valour F, et al. Zika virus infection complicated by Guillain-Barré syndrome – case report, French Polynesia, December 2013. Eurosurveillance. 2014 Mar 6;19(9):20720.

13. Cao-Lormeau VM, Blake A, Mons S, Lastère S, Roche C, Vanhomwegen J, et al. Guillain-Barré Syndrome outbreak associated with Zika virus infection in French Polynesia: a case-control study. Lancet. 2016 Apr 9;387(10027):1531–9.

14. Besnard M, Lastère S, Teissier A, Cao-Lormeau VM, Musso D. Evidence of perinatal transmission of Zika virus, French Polynesia, December 2013 and February 2014. Eurosurveillance. 2014 Apr 3;19(13):20751.

15. Campos GS, Bandeira AC, Sardi SI. Zika Virus Outbreak, Bahia, Brazil. Emerg Infect Dis. 2015 Oct;21(10):1885–6.

16. Kleber de Oliveira W, Cortez-Escalante J, De Oliveira WTGH, do Carmo GMI, Henriques CMP, Coelho GE, et al. Increase in Reported Prevalence of Microcephaly in Infants Born to Women Living in Areas with Confirmed Zika Virus Transmission During the First

Trimester of Pregnancy - Brazil, 2015. MMWR Morb Mortal Wkly Rep. 2016 Mar 11;65(9):242–7.

17. Mitchell C. Pan American Health Organization / World Health Organization. 2016 [cited 2022 Feb 22]. PAHO/WHO | Zika Cumulative Cases. Available from: https://www3.paho.org/hq/index.php?option=com_content&view=article&id=12390:zika-cumulative-cases&Itemid=42090&lang=en

18. HAN Archive - 00385|Health Alert Network (HAN) [Internet]. 2018 [cited 2023 Nov 7]. Available from: https://emergency.cdc.gov/han/han00385.asp

19. Dain Gandelman Horovitz D, da Silva Pone MV, Moura Pone S, Dias Saad Salles TR, Bastos Boechat MC. Cranial bone collapse in microcephalic infants prenatally exposed to Zika virus infection. Neurology. 2016 Jul 5;87(1):118–9.

20. Driggers RW, Ho CY, Korhonen EM, Kuivanen S, Jääskeläinen AJ, Smura T, et al. Zika Virus Infection with Prolonged Maternal Viremia and Fetal Brain Abnormalities. N Engl J Med. 2016 Jun 2;374(22):2142–51.

21. Mlakar J, Korva M, Tul N, Popović M, Poljšak-Prijatelj M, Mraz J, et al. Zika Virus Associated with Microcephaly. N Engl J Med. 2016 Mar 10;374(10):951–8.

22. Brasil P, Pereira JP, Moreira ME, Ribeiro Nogueira RM, Damasceno L, Wakimoto M, et al. Zika Virus Infection in Pregnant Women in Rio de Janeiro. N Engl J Med. 2016 Dec 15;375(24):2321–34.

23. de Araújo TVB, Rodrigues LC, de Alencar Ximenes RA, de Barros Miranda-Filho D, Montarroyos UR, de Melo APL, et al. Association between Zika virus infection and microcephaly in Brazil, January to May, 2016: preliminary report of a case-control study. Lancet Infect Dis. 2016 Dec;16(12):1356–63.

24. Rasmussen SA, Jamieson DJ, Honein MA, Petersen LR. Zika Virus and Birth Defects--Reviewing the Evidence for Causality. N Engl J Med. 2016 May 19;374(20):1981–7.

25. Besnard M, Eyrolle-Guignot D, Guillemette-Artur P, Lastère S, Bost-Bezeaud F, Marcelis L, et al. Congenital cerebral malformations and dysfunction in fetuses and newborns following the 2013 to 2014 Zika virus epidemic in French Polynesia. Euro Surveill. 2016;21(13).

26. Stegmann BJ, Carey JC. TORCH Infections. Toxoplasmosis, Other (syphilis, varicella-zoster, parvovirus B19), Rubella, Cytomegalovirus (CMV), and Herpes infections. Curr Womens Health Rep. 2002 Aug;2(4):253–8.

27. Russell LJ, Weaver DD, Bull MJ, Weinbaum M. In utero brain destruction resulting in collapse of the fetal skull, microcephaly, scalp rugae, and neurologic impairment: the fetal brain disruption sequence. Am J Med Genet. 1984 Feb;17(2):509–21.

28. Campo M del, Feitosa IML, Ribeiro EM, Horovitz DDG, Pessoa ALS, França GVA, et al. The phenotypic spectrum of congenital Zika syndrome. American Journal of Medical Genetics Part A. 2017;173(4):841–57.

29. Moore CA, Staples JE, Dobyns WB, Pessoa A, Ventura CV, Fonseca EB da, et al. Characterizing the Pattern of Anomalies in Congenital Zika Syndrome for Pediatric Clinicians. JAMA Pediatr. 2017 01;171(3):288–95.

30. Fonseca JO da, Vianna RA de O, Carvalho FR, Velarde LGC, Oliveira SA de, Cardoso CAA, et al. The Hip of Children with Congenital Zika Syndrome: A Prospective Observational Study. The Journal of Pediatrics. 2023 May 1;256:27–32.

31. N. Costa MC, Cardim LL, Teixeira MG, Barreto ML, de Carvalho-Sauer R de CO, R. Barreto F, et al. Case Fatality Rate Related to Microcephaly Congenital Zika Syndrome and Associated Factors: A Nationwide Retrospective Study in Brazil. Viruses. 2020 Oct 29;12(11):1228.

32. Paixao ES, Rodrigues LC, Costa M da CN, de Carvalho-Sauer R de CO, Oliveira WK, Cardim LL, et al. Population-based surveillance for congenital zika virus syndrome: a latent

class analysis of recorded cases from 2015–2018. BMC Pregnancy and Childbirth. 2022 Jun 29;22(1):530.

33. Rua EC, de Oliveira SA, de Oliveira Vianna RA, Dalcastel LAB, de Castro Sarmet Dos Santos TC, Cardoso CAA, et al. Two-year follow-up of children with congenital Zika syndrome: the evolution of clinical patterns. Eur J Pediatr. 2022 Mar;181(3):991–9.

34. Dos Santos MLB, Lima LCSDS, Zin AA, Moreira MEL, De Vasconcelos ZFM, Neves LMDA, et al. Evaluation and monitoring of eye findings in children exposed to Zika virus during gestation: 3 years of follow-up. J Trop Pediatr. 2023 Sep 7;69(5):fmad030.

35. Gama GL, Ramos de Amorim MM, Alves da Silva Júnior R, Cristina de Sousa Santos A, Assunção PL, de Sales Tavares J, et al. Effect of Intensive Physiotherapy Training for Children With Congenital Zika Syndrome: A Retrospective Cohort Study. Arch Phys Med Rehabil. 2021 Mar;102(3):413–22.

36. Müller WIM, Gama GL, Borges MCD, Bastos BMAM, Tavares JS, Barros ES, et al. Effect of neurodevelopmental treatment in children with congenital Zika syndrome: A pilot study. J Paediatr Child Health. 2022 Nov;58(11):2008–15.

37. Dutta SK, Langenburg T. A Perspective on Current Flavivirus Vaccine Development: A Brief Review. Viruses. 2023 Mar 28;15(4):860.

38. PAHO/WHO Data - ZIKA [Internet]. [cited 2024 Feb 28]. Available from: https://www3.paho.org/data/index.php/en/mnu-topics/zika-weekly-en/

39. Terzian ACB, Zini N, Sacchetto L, Rocha RF, Parra MCP, Del Sarto JL, et al. Evidence of natural Zika virus infection in neotropical non-human primates in Brazil. Sci Rep. 2018 Oct 30;8:16034.

40. Noronha L de, Zanluca C, Azevedo MLV, Luz KG, Santos CNDD. Zika virus damages the human placental barrier and presents marked fetal neurotropism. Mem Inst Oswaldo Cruz. 2016 May;111(5):287–93.

41. Puerta-Guardo H, Glasner DR, Espinosa DA, Biering SB, Patana M, Ratnasiri K, et al. Flavivirus NS1 Triggers Tissue-Specific Vascular Endothelial Dysfunction Reflecting Disease Tropism. Cell Rep. 2019 Feb 5;26(6):1598-1613.e8.

42. Puerta-Guardo H, Tabata T, Petitt M, Dimitrova M, Glasner DR, Pereira L, et al. Zika Virus Nonstructural Protein 1 Disrupts Glycosaminoglycans and Causes Permeability in Developing Human Placentas. J Infect Dis. 2020 Jan 2;221(2):313–24.

43. Muthuraj PG, Sahoo PK, Kraus M, Bruett T, Annamalai AS, Pattnaik A, et al. Zika virus infection induces endoplasmic reticulum stress and apoptosis in placental trophoblasts. Cell Death Discov. 2021 Jan 26;7(1):24.

44. Zhao Z, Li Q, Ashraf U, Yang M, Zhu W, Gu J, et al. Zika virus causes placental pyroptosis and associated adverse fetal outcomes by activating GSDME. Elife. 2022 Aug 16;11:e73792.

45. Borges-Vélez G, Rosado-Philippi J, Cantres-Rosario YM, Carrasquillo-Carrion K, Roche-Lima A, Pérez-Vargas J, et al. Zika virus infection of the placenta alters extracellular matrix proteome. J Mol Histol. 2022 Apr;53(2):199–214.

46. Rosa-Fernandes L, Bandeira C, Pour SZ, Benedetti V de F, Ferreira D, Lorenzon AR, et al. The impact of Zika virus exposure on the placental proteomic profile. Biochim Biophys Acta Mol Basis Dis. 2022 Jan 1;1868(1):166270.

47. Chiu CF, Chu LW, Liao IC, Simanjuntak Y, Lin YL, Juan CC, et al. The Mechanism of the Zika Virus Crossing the Placental Barrier and the Blood-Brain Barrier. Front Microbiol. 2020;11:214.

48. Villalobos-Sánchez E, Burciaga-Flores M, Zapata-Cuellar L, Camacho-Villegas TA, Elizondo-Quiroga DE. Possible Routes for Zika Virus Vertical Transmission in Human Placenta: A Comprehensive Review. Viral Immunology. 2022 Jul;35(6):392–403.

49. Leda AR, Bertrand L, Andras IE, El-Hage N, Nair M, Toborek M. Selective Disruption of the Blood-Brain Barrier by Zika Virus. Front Microbiol. 2019;10:2158.

50. Panganiban AT, Blair RV, Hattler JB, Bohannon DG, Bonaldo MC, Schouest B, et al. A Zika virus primary isolate induces neuroinflammation, compromises the blood-brain barrier and upregulates CXCL12 in adult macaques. Brain Pathol. 2020 Nov;30(6):1017–27.

51. Kim J, Alejandro B, Hetman M, Hattab EM, Joiner J, Schroten H, et al. Zika virus infects pericytes in the choroid plexus and enters the central nervous system through the blood-cerebrospinal fluid barrier. PLoS Pathog. 2020 May;16(5):e1008204.

52. Mladinich MC, Schwedes J, Mackow ER. Zika Virus Persistently Infects and Is Basolaterally Released from Primary Human Brain Microvascular Endothelial Cells. mBio. 2017 Jul 11;8(4):e00952-17.

53. Papa MP, Meuren LM, Coelho SVA, Lucas CG de O, Mustafá YM, Lemos Matassoli F, et al. Zika Virus Infects, Activates, and Crosses Brain Microvascular Endothelial Cells, without Barrier Disruption. Front Microbiol. 2017;8:2557.

54. de Carvalho GC, Borget MY, Bernier S, Garneau D, da Silva Duarte AJ, Dumais N. RAGE and CCR7 mediate the transmigration of Zika-infected monocytes through the blood-brain barrier. Immunobiology. 2019 Nov 1;224(6):792–803.

55. Xu P, Shan C, Dunn TJ, Xie X, Xia H, Gao J, et al. Role of microglia in the dissemination of Zika virus from mother to fetal brain. PLOS Neglected Tropical Diseases. 2020 Jul 6;14(7):e0008413.

56. Tang H, Hammack C, Ogden SC, Wen Z, Qian X, Li Y, et al. Zika Virus Infects Human Cortical Neural Precursors and Attenuates Their Growth. Cell Stem Cell. 2016 May 5;18(5):587–90.

57. Onorati M, Li Z, Liu F, Sousa AMM, Nakagawa N, Li M, et al. Zika Virus Disrupts Phospho-TBK1 Localization and Mitosis in Human Neuroepithelial Stem Cells and Radial Glia. Cell Rep. 2016 Sep 6;16(10):2576–92.

58. Hammack C, Ogden SC, Madden JC, Medina A, Xu C, Phillips E, et al. Zika Virus Infection Induces DNA Damage Response in Human Neural Progenitors That Enhances Viral Replication. J Virol. 2019 Oct 15;93(20):e00638-19.

59. Rychlowska M, Agyapong A, Weinfeld M, Schang LM. Zika Virus Induces Mitotic Catastrophe in Human Neural Progenitors by Triggering Unscheduled Mitotic Entry in the Presence of DNA Damage While Functionally Depleting Nuclear PNKP. J Virol. 2022 May 11;96(9):e0033322.

60. Li C, Xu D, Ye Q, Hong S, Jiang Y, Liu X, et al. Zika Virus Disrupts Neural Progenitor Development and Leads to Microcephaly in Mice. Cell Stem Cell. 2016 Nov 3;19(5):672.

61. Liang Q, Luo Z, Zeng J, Chen W, Foo SS, Lee SA, et al. Zika Virus NS4A and NS4B Proteins Deregulate Akt-mTOR Signaling in Human Fetal Neural Stem Cells to Inhibit Neurogenesis and Induce Autophagy. Cell Stem Cell. 2016 Nov 3;19(5):663–71.

62. Garcez PP, Nascimento JM, de Vasconcelos JM, Madeiro da Costa R, Delvecchio R, Trindade P, et al. Zika virus disrupts molecular fingerprinting of human neurospheres. Sci Rep. 2017 Jan 23;7:40780.

63. Yoon KJ, Song G, Qian X, Pan J, Xu D, Rho HS, et al. Zika-Virus-Encoded NS2A Disrupts Mammalian Cortical Neurogenesis by Degrading Adherens Junction Proteins. Cell Stem Cell. 2017 Sep 7;21(3):349-358.e6.

64. Thulasi Raman SN, Latreille E, Gao J, Zhang W, Wu J, Russell MS, et al. Dysregulation of Ephrin receptor and PPAR signaling pathways in neural progenitor cells infected by Zika virus. Emerg Microbes Infect. 2020 Dec;9(1):2046–60.

65. Rosa-Fernandes L, Cugola FR, Russo FB, Kawahara R, de Melo Freire CC, Leite PEC, et al. Zika Virus Impairs Neurogenesis and Synaptogenesis Pathways in Human Neural Stem Cells and Neurons. Front Cell Neurosci. 2019 Mar 15;13:64.

66. He J, Yang L, Chang P, Yang S, Wang Y, Lin S, et al. Zika Virus Induces Degradation of the Numb Protein Required through Embryonic Neurogenesis. Viruses. 2023 May 27;15(6):1258.

67. Huang Y, Li Y, Zhang H, Zhao R, Jing R, Xu Y, et al. Zika virus propagation and release in human fetal astrocytes can be suppressed by neutral sphingomyelinase-2 inhibitor GW4869. Cell Discov. 2018;4:19.

68. Sher AA, Glover KKM, Coombs KM. Zika Virus Infection Disrupts Astrocytic Proteins Involved in Synapse Control and Axon Guidance. Front Microbiol. 2019;10:596.

69. Shereen MA, Bashir N, Su R, Liu F, Wu K, Luo Z, et al. Zika virus dysregulates the expression of astrocytic genes involved in neurodevelopment. PLoS Negl Trop Dis. 2021 Apr;15(4):e0009362.

70. Rossi ÁD, Faucz FR, Melo A, Pezzuto P, de Azevedo GS, Schamber-Reis BLF, et al. Variations in maternal adenylate cyclase genes are associated with congenital Zika syndrome in a cohort from Northeast, Brazil. J Intern Med. 2019 Feb;285(2):215–22.

71. Santos CNO, Ribeiro DR, Cardoso Alves J, Cazzaniga RA, Magalhães LS, de Souza MSF, et al. Association Between Zika Virus Microcephaly in Newborns With the rs3775291 Variant in Toll-Like Receptor 3 and rs1799964 Variant at Tumor Necrosis Factor-α Gene. J Infect Dis. 2019 Oct 22;220(11):1797–801.

72. Santos CNO, Magalhães LS, Fonseca AB de L, Bispo AJB, Porto RLS, Alves JC, et al. Association between genetic variants in TREM1, CXCL10, IL4, CXCL8 and TLR7 genes with the occurrence of congenital Zika syndrome and severe microcephaly. Sci Rep. 2023 Mar 1;13(1):3466.

73. Pang H, Jiang Y, Li J, Wang Y, Nie M, Xiao N, et al. Aberrant NAD+ metabolism underlies Zika virus–induced microcephaly. Nat Metab. 2021 Aug;3(8):1109–24.

74. Li Y, Shi S, Xia F, Shan C, Ha Y, Zou J, et al. Zika virus induces neuronal and vascular degeneration in developing mouse retina. Acta Neuropathol Commun. 2021 May 25;9(1):97.

75. Zeng J, Dong S, Luo Z, Xie X, Fu B, Li P, et al. The Zika Virus Capsid Disrupts Corticogenesis by Suppressing Dicer Activity and miRNA Biogenesis. Cell Stem Cell. 2020 Oct 1;27(4):618-632.e9.

76. Rasmussen SA, Jamieson DJ. Teratogen update: Zika virus and pregnancy. Birth Defects Research. 2020;112(15):1139–49.

77. Shah PS, Beesabathuni NS, Fishburn AT, Kenaston MW, Minami SA, Pham OH, et al. Systems Biology of Virus-Host Protein Interactions: From Hypothesis Generation to Mechanisms of Replication and Pathogenesis. Annu Rev Virol. 2022 Sep 29;9(1):397–415.

78. Ramage HR, Kumar GR, Verschueren E, Johnson JR, Von Dollen J, Johnson T, et al. A combined proteomics/genomics approach links hepatitis C virus infection with nonsense-mediated mRNA decay. Mol Cell. 2015 Jan 22;57(2):329–40.

79. Li M, Johnson JR, Truong B, Kim G, Weinbren N, Dittmar M, et al. Identification of antiviral roles for the exon-junction complex and nonsense-mediated decay in flaviviral infection. Nat Microbiol. 2019;4(6):985–95.

80. Gordon DE, Hiatt J, Bouhaddou M, Rezelj VV, Ulferts S, Braberg H, et al. Comparative host-coronavirus protein interaction networks reveal pan-viral disease mechanisms. Science. 2020 Dec 4;370(6521):eabe9403.

81. Haas KM, McGregor MJ, Bouhaddou M, Polacco BJ, Kim EY, Nguyen TT, et al. Proteomic and genetic analyses of influenza A viruses identify pan-viral host targets. Nat Commun. 2023 Sep 27;14(1):6030.

82. Shah PS, Link N, Jang GM, Sharp PP, Zhu T, Swaney DL, et al. Comparative Flavivirus-Host Protein Interaction Mapping Reveals Mechanisms of Dengue and Zika Virus Pathogenesis. Cell. 2018 13;175(7):1931-1945.e18.

83. Asencio C, Davidson IF, Santarella-Mellwig R, Ly-Hartig TBN, Mall M, Wallenfang MR, et al. Coordination of Kinase and Phosphatase Activities by Lem4 Enables Nuclear Envelope Reassembly during Mitosis. Cell. 2012 Jul 6;150(1):122–35.

84. Yamamoto S, Jaiswal M, Charng WL, Gambin T, Karaca E, Mirzaa G, et al. A *Drosophila* genetic resource of mutants to study mechanisms underlying human genetic diseases. Cell. 2014 Sep 25;159(1):200–14.

85. Link N, Chung H, Jolly A, Withers M, Tepe B, Arenkiel BR, et al. Mutations in ANKLE2, a ZIKA Virus Target, Disrupt an Asymmetric Cell Division Pathway in *Drosophila* Neuroblasts to Cause Microcephaly. Dev Cell. 2019 Dec 16;51(6):713-729.e6.

Chapter 2: Flavivirus-Host Protein–Protein Interactions in Replication and Pathogenesis

Flaviviruses comprise a genus of viruses that pose a significant burden on human health worldwide. Transmission by both mosquito and tick vectors, and broad host tropism contribute to the presence of flaviviruses globally. Like all viruses, they require utilization of host molecular machinery to facilitate their replication through physical interactions. Their RNA genomes are translated using host ribosomes, synthesizing viral proteins that cooperate with each other and host proteins to reshape the host cell into a factory for virus replication. Thus, dissecting the physical interactions between viral proteins and their host protein targets is essential in our comprehension of how flaviviruses replicate and how they alter host cell behavior. Beyond replication, even single interactions can contribute to immune evasion and pathogenesis, providing potential avenues for therapeutic intervention. In this Chapter, we review protein interactions between flavivirus and host proteins that contribute to virus replication, immune evasion, and disease.

Introduction

Flavivirus is a genus of positive-sense, single-stranded RNA (ssRNA+), arthropod-transmitted viruses within the family *Flaviviridae*. The ssRNA genome contains a single open-reading frame which is translated by host ribosomes into a large viral polyprotein. This polyprotein is co-translationally processed by viral and host proteases into ten individual viral proteins. Three of these proteins are referred to as structural proteins which include Capsid (C), pre-Membrane (prM), and Envelope (Env) proteins, which form the physical virion. The remaining seven proteins are referred to as non-structural (NS) proteins which include NS1, NS2A, NS2B, NS3, NS4A, NS4B, and NS5. These proteins are not components of infectious virions but rather play broad

roles within infected cells in generating virus progeny. Four distinct enzymatic activities are encoded within two NS proteins. NS3 serves as the helicase. It also interacts with NS2B as a cofactor (NS2B3) to form the viral protease (1). NS5 is both the RNA-dependent RNA-polymerase and methyltransferase, which synthesizes and caps new RNA genomes (2–4). The RNA genome also contains 3' and 5' untranslated regions (UTRs) with loop-like structures that play roles in genome stability and translation (5, 6). Genome replication occurs within the remodeled ER in involuted structures referred to as virus replication organelles or replication compartments (7). These substructures serve to concentrate replication substrates and hide viral nucleic acids from detection by the host immune response. Here, the viral NS proteins assemble into the replication complex, which performs the enzymatic steps of RNA synthesis (8, 9). Viral ssRNA+ is initially used as a template for the synthesis of negative-sense ssRNA, which in turn is used as a template to synthesize more ssRNA+. As replication progresses these genomes are either further amplified or packaged into progeny virions. In addition to genome replication by the replication complex, viral NS proteins mediate different aspects of virus replication, such as ER remodeling and modulating the host immune response.

The most well studied flaviviruses are those that cause significant disease in humans. For mosquito-transmitted viruses this includes dengue virus (DENV), Zika virus (ZIKV), West Nile virus (WNV), yellow fever virus (YFV), and Japanese encephalitis virus (JEV). These flaviviruses are all transmitted by mosquitoes of either *Aedes* or *Culex* spp. (10). DENV is the most widespread and threatening flavivirus. Currently, there are four well- described serotypes of DENV, referred to as DENV1-DENV4, that each have distinct molecular and physiological characteristics (11, 12). World-wide there are an estimated 390 million cases of DENV infection per year, occurring across 128 countries, although most infections occur in Asia (13, 14). Recently, the emergence of a 5th DENV serotype (DENV5) with a sylvatic replication cycle has been reported (15, 16). However, DENV5 remains a controversial topic, as the evidence to support the

existence of this serotype is limited and mathematical modeling suggests a low probability for the emergence of new DENV serotypes (17). ZIKV recently received major research attention due to the 2015-16 epidemic and the revelation that congenital ZIKV infection causes birth defects, collectively referred to as congenital Zika syndrome (CZS) (18, 19). ZIKV infection in adults is usually limited to mild flu-like illness but can be rarely associated with Guillain-Barré Syndrome, a condition where nerves are damaged, usually in the extremities (20). While less common, WNV and JEV can also cause encephalitis (21, 22). Tick-borne flaviviruses are transmitted by many different ticks, including *Haemaphysalis, Ixodes, Dermacentor,* and *Ornithidoros* spp. (23). These account for much fewer total human infections compared to the mosquito-borne flaviviruses, many of which are in vastly different geographical settings compared to the tropical climates which more prevalently host mosquitoes. The most studied of these are tick-borne encephalitis virus (TBEV) and Powassan virus (POWV). While the number of human infections arising from tick-borne viruses is relatively limited the resulting disease can be very severe. Encephalitis resulting from TBEV infection can appear in several forms, with an overall mortality rate of around 2% (24). Given the severity of disease caused by flaviviruses, it is critical to understand mechanisms of replication and pathogenesis.

In general, flaviviruses have a conserved replication cycle, which includes viral entry, virion fusion with the endosome and release of viral RNA, genome replication and protein production in the ER, virion packaging and processing through the secretory pathway, and viral release via exocytosis (Figure 1). At each of these stages, flaviviruses are dependent on host machinery to perform necessary functions. The limited flavivirus genome size requires them to maximize the functions of each protein they encode. Flavivirus replication is therefore largely dependent on the interactions between viral proteins and host proteins to manipulate their biology through direct and indirect mechanisms. These protein interactions can be identified using targeted and comprehensive screening approaches (25–34). This Chapter will focus on virus-host protein-

protein interactions (PPIs) emerging from both targeted and comprehensive studies that directly facilitate flavivirus replication, dampen host immune response, or disrupt cellular processes to cause disease. While not covered here, it is worth noting that additional virus-host interactions, such as RNA-protein, and RNA-RNA interactions also play important roles in flavivirus replication and disease (35–38).

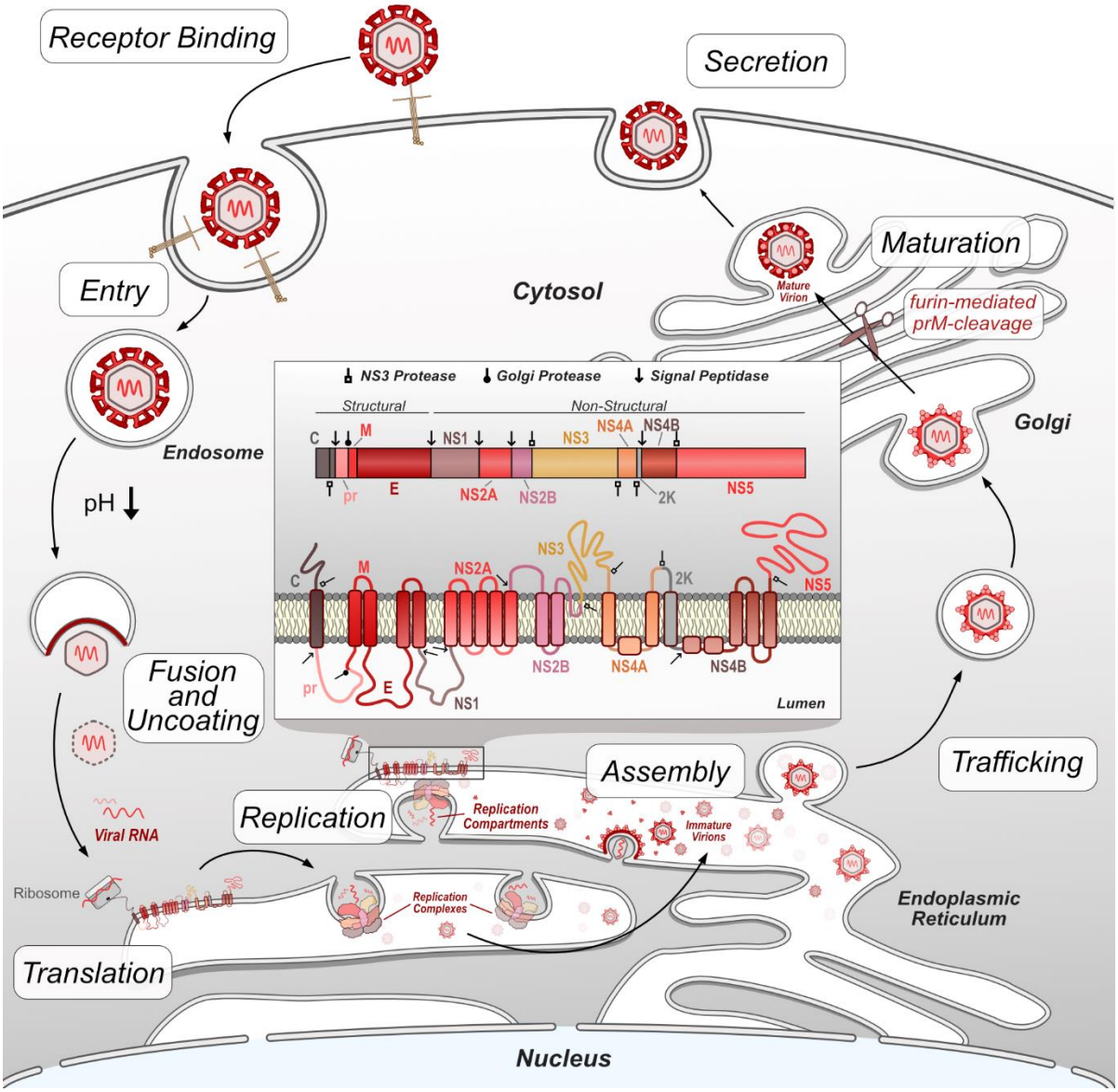

Figure 2-1: Flavivirus replication cycle. Flavivirus infection begins by receptor-mediated binding to the host cell and entry via clathrin-mediated endocytosis. Decreases in endosome pH trigger virion envelope fusion with the endosome membrane, releasing the genome into the host cytosol. After uncoating, the viral RNA genome is translated by host ribosomes into the viral polypeptide, which is co-translationally processed, including insertion of transmembrane proteins into the ER and cleavage of the polypeptide by host and viral proteases into individual proteins. Non-structural viral proteins form replication complexes which replicate viral RNA genomes within invaginated ER compartments. Structural viral proteins are assembled and loaded with viral genetic material in the ER prior to entering the trans-Golgi network. In the Golgi, immature virions are processed by furin protease cleavage of prM, resulting in mature, infectious virions. These virions exit the cell by exocytosis and continue the replication cycle by initiating infection of other host cells.

Flavivirus-host PPIs facilitate fundamental aspects of flavivirus replication

In this section we review the data emerging from both comprehensive and targeted studies of flavivirus-host PPIs as they relate to various stages of flavivirus replication.

Virus attachment factors

The first step in any virus replication cycle is entry into the host cell and involves the classic virus-host protein interaction between a virion structural protein and a host attachment factor. In the case of flaviviruses, Env proteins on the virion exterior interact and attach to host factors on the plasma membrane surface. Flavivirus Env proteins are quite promiscuous and can bind many different host factors. While each flavivirus appears to bind multiple host factors, not all flaviviruses use the same set of host factors for entry. Generally, flaviviruses use TAM (*e.g.* Tyro3, Axl, Mer)

family receptor tyrosine kinases (39, 40), phosphatidyl serine receptor T-cell immunoglobulin (TIM) (41–43), C-type lectin receptors (*e.g*. DC-SIGN) (44–46), integrins (47, 48), heat-shock proteins 70/90 (49–51), laminin receptor (LAMR1) (52, 53), and heparan sulfate (54, 55) as means of attachment. Subtle differences in Env protein sequence likely contribute to differences in host factor usage, and distinct tissue tropisms between flaviviruses. The well-established flavivirus-host attachment factors are described in Figure 2; however, it is essential to note that there are likely others that each virus uses that have not been identified.

Interestingly, some entry determinants are dependent on specific intracellular virus-host interactions that provide newly generated progeny virions with additional receptor targets. A recent study elegantly showed how the interaction between TRIM7, an E3-ubiquitin ligase, and Env resulted in specific polyubiquitination in the infected cell that allowed progeny virion binding toTim-1 of the new target cell (56). Here, ZIKV Env was ubiquitinated on three lysine residues: K38, K63, and K281. A recombinant virus in which one of these lysines was swapped with arginine (E-K38R) was significantly attenuated in JEG-3 placental trophoblast cells and *in vivo* in mice, but not in mosquitoes. Intriguingly, the ZIKV E-K38R titers *in vivo* varied significantly by tissue, suggesting that Env ubiquitination may drive tissue specific tropism. To further explore this, they generated TRIM7 knockout cells which attenuated ZIKV replication in JEG-3 cells but did not affect DENV replication in A549 lung epithelial cells. Similar results were observed in *Trim7*$^{-/-}$ knockout mice. In this model ZIKV replicated similarly to WT in the heart, liver, lung, and muscle, whereas ZIKV replication in the brain, eyes, and reproductive tissues was significantly reduced. Finally, they identified that Tim-1 interacted with wild-type ZIKV but very minimally with K38R viral particles, suggesting that ubiquitination at this site is critical for the interaction and virus entry through Tim-1. This was supported both by reduced attachment of ZIKV to Tim-1 knockout JEG-3 cells and reduced replication of ZIKV in the brains of *Tim1*$^{-/-}$ knockout mice (56). All together, these results indicate an important interaction between ZIKV Env and TRIM7, providing

ubiquitination that mediates entry into the brain and other tissues that are major contributors to ZIKV pathogenesis. Currently, it is unknown if other flaviviruses use TRIM7 ubiquitination of Env to mediate entry via TIM-1, as many other flaviviruses use TIM-1 as a host receptor (39, 41–43).

Intriguingly, a recent study identified this same ZIKV Env ubiquitination is also targeted by host factors and restricts virus infection (57). The laminin receptor LAMR1 consists of an intracellular domain, a transmembrane domain, and a larger extracellular domain which is known to be utilized as an attachment factor by several flaviviruses that are not ZIKV (52, 53, 58, 59). Unsurprisingly, ZIKV Env was also found to interact with LAMR1. However, it only interacts with the intracellular region, not the extracellular region that would mediate extracellular virion attachment. Overexpression of LAMR1 reduced virus replication and repression of LAMR1 by shRNA resulted in significant increases in viral titer. The interaction between ZIKV Env and LAMR1 is mediated by a single amino acid in Env, G282. Interestingly, G282 is very highly conserved among ZIKV strains, but is not conserved at all with other flaviviruses. Further, the authors found that LAMR1 recruits eukaryotic translation initiation factor 3 subunit 5 (EIF3S5), a member of the ubiquitin proteasome system (UPS). Knockdown of EIF3S5 reduced Env deubiquitination and increased the levels of NS5, Env, and viral RNA in infected HeLa cells (57). Thus, Env ubiquitination can have opposing effects mediated by different Env-host protein interactions.

It is worth noting that there is plentiful information on the host entry factors of mosquito-borne flaviviruses. However, knowledge on the attachment factors utilized by tick-borne flaviviruses is extremely limited. One recent study attempted to identify attachment factors for Langat virus (LGTV). They found that LGTV did not utilize heparin sulfate, *O*- or *N*-linked glycans, or glycolipids for entry, suggesting that the host receptor is protein in nature. However, they were unable to definitively identify such a protein (60). A pair of studies suggests one such attachment factor might be LAMR1, although additional studies are required (61, 62). Another recently published study used multiple methods to identify TIM-1 as an entry factor for TBEV (43).

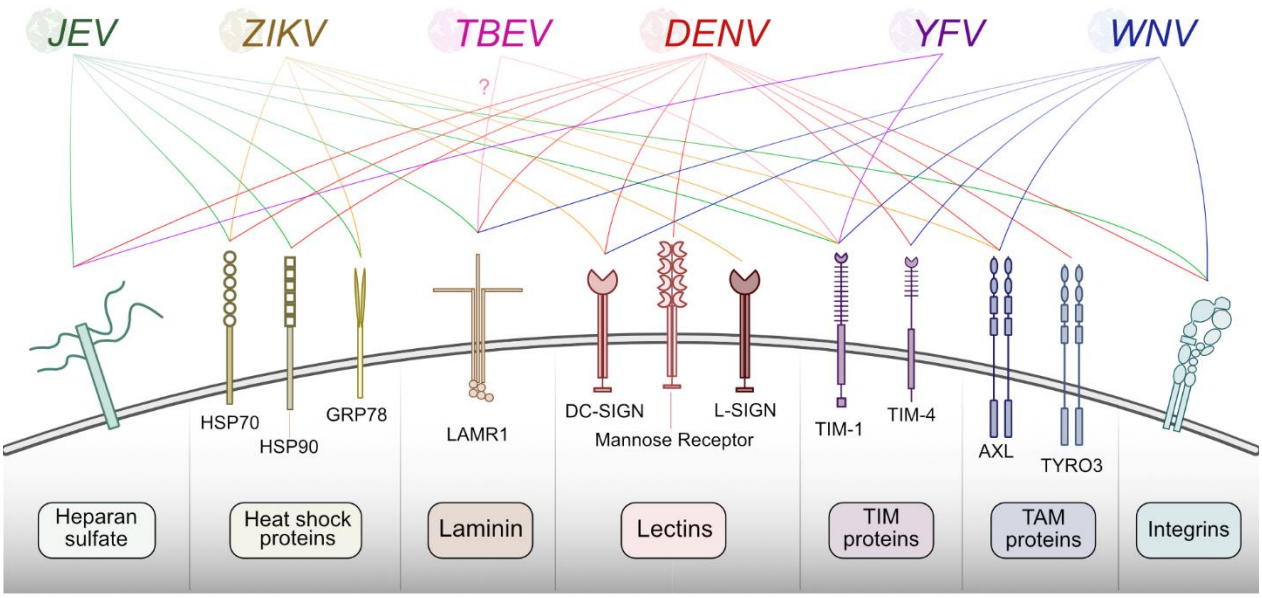

Figure 2-1: Summary of host proteins used by flaviviruses for entry. Flaviviruses recognize and bind plasma membrane host factors to initiate entry into the host cell. Different flaviviruses utilize a similar pool of host proteins for entry.

Fusion and uncoating

After a flavivirus binds to an extracellular host entry factor, it enters the intracellular space by clathrin-mediated endocytosis (63, 64). There are several cargo internalization factors involved in this process that are necessary for flavivirus infection. Specifically, LY6E has been shown to reorganize itself into tubule-like structures to support entry of WNV, ZIKV, and DENV (65), though direct virus-host interactions have yet to be identified in this case. Following endocytosis, the membrane of the virus envelope must fuse with the endosome membrane. This process happens through an indirect mechanism, not requiring any physical virus-host protein interactions. V-ATPase pumps protons from the cytoplasm into the lumen of various organelles, including endosomes, decreasing the intra-endosomal pH (66, 67). This triggers conformational changes in viral Env proteins that ultimately lead to their insertion into the endosome membrane and

formation of the fusion pore, releasing the nucleocapsid to the cytosol (68, 69). Once released the viral genome is not immediately capable of being translated. It first must be stripped of the capsid proteins that otherwise stabilize and protect viral RNA. This occurs through the ubiquitination of Capsid proteins by host UBA1 (70), with subsequent nucleocapsid disassembly shown to be mediated by VCP (71). Once uncoated, the flavivirus RNA genome may be translated into the viral polyprotein.

Interactions Involved in Viral Protein Translation and Stability

Translation of flavivirus genomes into functional viral proteins is dependent on the activity of several host pathways. As is true of all viruses, host ribosomes are required to initially translate the genome into the viral polyprotein. Several host proteases are necessary for polyprotein cleavage into singular proteins. However, many of these NS proteins contain multiple transmembrane domains, specifically NS2A, NS2B, NS4A, and NS4B, which all must be correctly inserted into the ER membrane in the correct orientation in order to be functional (72–75). The stability and insertion of these proteins is performed by the signal-recognition particle (SRP), host SEC61 translocon, and ER membrane complex (EMC). These complexes have been shown to be critical host factors for many viruses, including flaviviruses (76–79). In this section, we will review recent work that has advanced our understanding of how flaviviruses co-opt these complexes during infection (Figure 3).

SRP-Translocon Pathway

Flaviviruses replicate within the ER and utilize ER-associated ribosomes for translation. The translated polyprotein contains many transmembrane domains that must be properly integrated into the ER membrane. This function is performed by the SRP-translocon pathway, in which the

SRP ribonucleotide complex binds and identifies a hydrophobic transmembrane region of the nascent polypeptide, arrests translation, and brings the ribosome to a translocon where translation continues (80). In eukaryotes, the Sec translocon is made up of the SEC61 complex (SEC61α/β/γ), SEC62/63, and a number of other proteins that can vary depending on substrate (81). Flavivirus polypeptide insertion into the ER membrane is thus at least partially reliant on the interaction with SRP and SEC proteins. Unsurprisingly, these proteins have been found in several flavivirus-host protein interaction studies, including interactions between ZIKV/DENV NS4A with SEC62, SEC61γ, and SRPR, NS4A/2B with SEC61β, and NS4B with SEC61α (26, 27). Along with these interaction-based screens, these proteins have been identified in genetic screens as host factors supporting flavivirus replication (76, 78, 79, 82, 83). Interestingly, while the SEC61 translocon is essential for protein biogenesis, pharmacological modulation of this complex inhibits DENV and ZIKV replication (27, 77, 84). Together these results highlight the importance of the SRP/SEC61 translocon on flavivirus replication and the potential for a pan-flaviviral drug target.

ER Membrane Complex

The ER membrane complex (EMC) co-translationally interacts with nascent proteins and prevents their degradation by associating with chaperones. The EMC preferentially stabilizes multipass membrane proteins that may otherwise have difficulty being inserted into the ER membrane, thereby avoiding misfolding and degradation (85, 86). Similar to the SEC61 complex, EMC proteins have been identified in a number of flavivirus protein interactions (25, 27) and genetic screens (78, 83, 87, 88), underlining their importance. Three recent papers dissect their role in flavivirus replication. Through a combination of biochemical assays and pulse-chase experiments with gene knockdown, Lin and colleagues demonstrated that EMC1 promoted NS4B biogenesis, but not its post-translational stability. Interestingly, NS4B's dependence on the EMC arises from its two N-terminal transmembrane regions, which are marginally hydrophobic, as altering the

nature of these regions in either direction, more or less hydrophobic, rescued expression in EMC knockout cells. Together, this suggests that the generation and co-translational stability of flavivirus multi-pass proteins, including NS4B, depends on the interaction with EMC for protection from degradation and integration into the membrane. (89). Similar inhibition of virus replication and decreases in viral protein production were also shown by Ngo et al., 2019, using a similar CRISPR knockout setup. Using a dual-fluorescence reporter system they were able to identify that NS4B's underlying reliance on the EMC stems from its link to NS4A through the 2K peptide, a transmembrane region which serves as a signal sequence for the translocation of NS4B (90). Barrows et al., 2019 additionally found that knockout of EMC4 led to near complete loss in replication of DENV, ZIKV, and YFV, but did not affect WNV replication at all. They speculated this difference may arise from the WNV being transmitted by *Culex* mosquitoes, rather than *Aedes*. This vector specific hypothesis was supported by their finding that DENV titer in *Aedes* mosquito midguts was reduced after siRNA targeting of EMC2/3/4, although the decreases in replication were not nearly as severe as what was observed in human cells (91). Altogether, the EMC is a vital host factor utilized by *Aedes*-transmitted flaviviruses for correct viral protein insertion into the ER membrane.

Signal Peptidase and Oligosaccharyltransferase Complexes

Gene perturbation screens have long been used to identify essential flavivirus host factors. With the advances of CRISPR, these screens have become even more powerful. A pair of such screens published together in 2016 mapped host factors of multiple flaviviruses (78, 79). Unsurprisingly, proteins involved in ER translocation of and polypeptide stability, including SEC61B and EMC proteins, were among the hits in these screens. Additionally, signal peptidase complex (SPCS) and oligosaccharyltransferase (OST) complex were found to be essential for replication of many flaviviruses. Knockout of SPCS1, a major component of the SPCS, in

HEK293T embryonic kidney cells completely ablated replication of all tested flaviviruses, but had little effect on other unrelated RNA viruses, suggesting its role in virus replication was specific to *Flaviviridae.* Further experiments revealed that the SPCS1 is responsible for several polyprotein cleavage events, specifically C-prM, prM-E, E-NS1, and 2K-NS4B (79). The cleavage between NS1 and NS2A occurs through an unknown signal peptidase pathway mechanism. Interestingly, the OST complex plays a role in replication separate from its enzymatic activity. Normally the OST complex is responsible for the *N*-linked glycosylation of host proteins. Knockout of major OST complex component STT3A had major effects on the replication of DENV, YFV, WNV, JEV, and ZIKV (78, 79). However, these replication defects could be rescued by the expression of catalytically dead STT3A mutants, suggesting that the OST complex serves virus replication through function outside its ability to glycosylate proteins (78). Physical interactions with flavivirus replication complex members NS1, NS2B, NS3, and NS4B along with its close association with sites of virus replication in the ER suggest that the OST complex may serve a structural role in genome replication (78, 92).

ER remodeling and virus replication compartment formation

The majority of flavivirus replication occurs within the ER membrane. Flaviviruses employ a variety of mechanisms to remodel the host ER into a niche which maximizes the efficiency of genome replication and viral packaging. The task of remodeling the ER is primarily performed by the viral NS proteins through a combination of direct remodeling and specific virus-host interactions. NS4A and NS4B contain transmembrane domains which pass through the ER and helices that lie in the plane of the ER lumen to induce positive curvature of the membrane (72, 93, 94). Membrane alteration is further driven by the oligomerization of NS4A (95). In addition to the action of these viral proteins on their own, they recruit and hijack the function of a number of other host proteins involved in ER morphology. The highly curved and tubular host ER membrane

system is stabilized and maintained by several protein families including the reticulon (RTN) family, the atlastin (ATL) family, and the Lunapark (LNP) protein (96, 97). Even beyond these canonically ER proteins, other host factors have been shown to be involved in flavivirus-mediated ER modifications. Recently several groups have evaluated the roles of these protein families in flavivirus replication and ER remodeling during infection.

Reticulon

Proteins in the RTN family all have a domain including two transmembrane regions separated by a single hydrophilic loop which, similarly to NS4A, induces membrane curvature (98). Reticulon 3A (RTN3A) is known to be involved in the replication of other viruses, including the *Flaviviridae* family member Hepatitis C virus (HCV) (99–101). Aktepe et al., 2017 found that the broadly expressed RTN3.1A plays a role in the replication of several flaviviruses, including WNV, DENV, and ZIKV. RTN3.1A colocalized with sites of virus replication and siRNA silencing resulted in significant decreases in viral titer after infection. ZIKV infection in RTN3.1A-silenced cells displayed dramatically less membrane curvature with fewer replication complexes. Using a combination of immunofluorescence microscopy and fluorescence resonance energy transfer (FRET) the authors determined that RTN3.1A specifically interacted with WNV NS4A, whereas ZIKV and DENV NS4A did not (102). However, later proteomics studies did identify an interaction between ZIKV NS4A and RTN3 (27). A yeast-two hybrid screen also showed that ZIKV NS4A and NS2B interact with RTN1, suggesting that flaviviruses may utilize RTN family members differentially for roles in ER remodeling (31).

Atlastins

The ATL family of proteins is composed of three (ATL1/2/3) membrane-bound, dynamin-related GTPases that function in maintaining Golgi (ATL1) and ER (ATL2/3) morphogenesis through the formation of three-way junctions (103, 104). ZIKV is known to actively remodel the ER and induce the formation of large ER-derived cytoplasmic vacuoles. Ultimately this results in cell death through paraptosis, a caspase-independent, non-apoptotic form of cell death (84). The formation of these vacuoles in HeLa cells is dependent on the activity of ATLs. Knockout of ATL2 and ATL3 led to nearly a complete loss in the formation of these vacuoles during ZIKV infection and significant reduction in ZIKV replication. These phenotypes could be rescued by expression of wild-type ATL3, but not a GTPase-deficient mutant (105). Another group similarly found that knockdown of ATL2/3 reduced the replication of both ZIKV and DENV and that ATL3 played an important role in DENV maturation (106). There appears to be multiple methods by which flaviviruses physically interact with ATL proteins. Using co-immunoprecipitation (Co-IP) and immunofluorescence analysis, one group determined that ATL3 strongly interacted with both ZIKV NS2A and NS2B3, although they did identify partial interaction with both NS4A and NS4B as well (105). ATL2/3 were found to interact with DENV NS2B, NS3, and NS5. Interestingly, ATL3 was also found to further interact with DENV NS1, envelope, and capsid proteins (106). Flavivirus-ATL interactions have also been identified in a number of proteomic screens including WNV NS4B with ATL2 (29) and ZIKV NS4A and NS2A with both ATL1 and ATL2 (25). Thus, while multiple flaviviruses hijack atlastin proteins, the molecular mechanisms appear to be unique.

Lunapark

While RTN family proteins induce curvature within the ER membrane and ATL form three-way tubular junction, the LNP protein stabilizes these junctions and is required for their mobility, a necessary feature of the dynamic ER (107). Similar to RTN and ATL, siRNA silencing of LNP

results in significant reduction in flavivirus induced replication compartments and corresponding decreases in genome replication. Using Co-IP, Tran et al, 2021 identified that TBEV NS4B interacted with LNP through its C-terminal region (108). Additionally, ZIKV NS4A has been identified to interact with LNP, and may constitute virus-specific mechanisms of ER-remodeling (27). All together these findings show that flaviviruses physically hijack a number of host pathways to remodel the ER membrane system to create a space conducive to virus replication.

TMEM41B and VMP1

A recent CRISPR genetic screen assessed host factors involved in flavivirus infection (83). In addition to identifying many ER proteins discussed previously, the authors also identified two transmembrane ER proteins, TMEM41B and VMP1. These proteins function as phospholipid scramblases and have similar roles in lipid mobilization, lipoprotein biogenesis, autophagy, and the induction of membrane curvature (109–112). Knockout of either gene dramatically inhibited the replication of a wide range of mosquito- and tick-borne flaviviruses. TMEM41B was also shown to be critical for infection across multiple cell types, including mosquito C6/36 cells. The authors found TMEM41B interacts and colocalizes with ZIKV NS4A and YFV NS4B during infection, which is supported by the previous identification of ZIKV NS4B's interaction with TMEM41B (26). Given its role in inducing membrane curvature, this suggested that TMEM41B may be involved in the formation of viral replication compartments in the ER. Intriguingly, TMEM41B-deficient cells were observed to have heightened innate immune responses after infection. Using YFV replicons this was elegantly shown to be due to increased sensing of viral dsRNA in TMEM41B knockout cells (83). Together, these results show that TMEM41B is a pan-flavivirus host factor that is likely involved in the formation of replication compartments in the ER, and loss of this protein results in the inability to retain viral dsRNA in the ER, leading to detection by host immune response sensors.

Vimentin

The RTN, ATL, and LNP family proteins are logical targets for virus-mediated ER remodeling based on their canonical roles in regulating ER morphology. However, flaviviruses are also capable of hijacking host proteins with more divergent functions to establish replication compartments within the ER. A 2014 study by Teo and Chu established that DENV NS4A interacted with host vimentin, a major component of cytoskeletal intermediate filaments, to anchor replication compartments in the ER. They found that the N-terminal cytoplasmic region of NS4A mediated this interaction and that DENV infection increasing the phosphorylation of vimentin, promoting depolymerization and reassembly to the perinuclear region where it was utilized for virus replication. Phosphorylation of vimentin was shown to be crucial for replication as siRNA silencing of the vimentin-targeting kinase CaMKIIγ led to significant decreases in DENV replication (113).

RACK1

The Receptor for Activated C Kinase 1 (RACK1) protein is a known scaffolding protein with roles in protein shuttling, anchoring, and stabilization, as well as mediating cellular pathways through protein interactions (114). The interaction between DENV NS1 and host RACK1 was first identified in a DENV NS1 specific proteomics screen (92) but the role of this interaction was not fully explored until recently by Shue et al 2021. They performed a genome-wide CRISPR knockout screen in Huh7 cells to identify host genes involved in ZIKV replication. This identified several potential host genes including members of the ER membrane complex (EMC) (discussed earlier in this Chapter), as well as RACK1. Additionally, they found that silencing of RACK1 impacted the replication of several flaviviruses including ZIKV, DENV, WNV, POWV, and LGTV, and even SARS-CoV-2. However, they found that YFV, herpes simplex virus (a DNA virus), and vesicular stomatitis virus (negative-strand ssRNA virus) were not affected by RACK1 silencing. Using a

Renilla luciferase DENV replicon they determined that RACK1 specifically played a role in viral genome replication, rather than viral entry or translation. Using replication-independent expression system that induces the formation of replication compartments in the ER without virus infection they found that RACK1 silencing led to reduced formation of these compartments in the ER (115). These studies are a great example of the power of integrating proteomic and genetic screens to identify mechanisms of virus replication. In the future utilization of existing screens will advance our understanding of these mechanisms and identify new interactions that are necessary for flavivirus replication.

One interesting feature of flavivirus infection worth noting is the induction of convoluted membranes (Figure 3). These peculiar membranous structures contain vast arrangements of smooth ER, however they appear to form only under certain conditions, as their presence can vary with virus or cell type (116–119). Convoluted membranes contain viral proteins but lack viral RNA, suggesting these are not sites of genome replication (8). The virus-host PPIs that contribute to the formation of these membrane structures are still under investigation. It has been shown that NS4B associated with mitochondria physically contact these structures, potentially to tether them near sites of virus replication or assembly or to dampen innate immune response signaling (120).

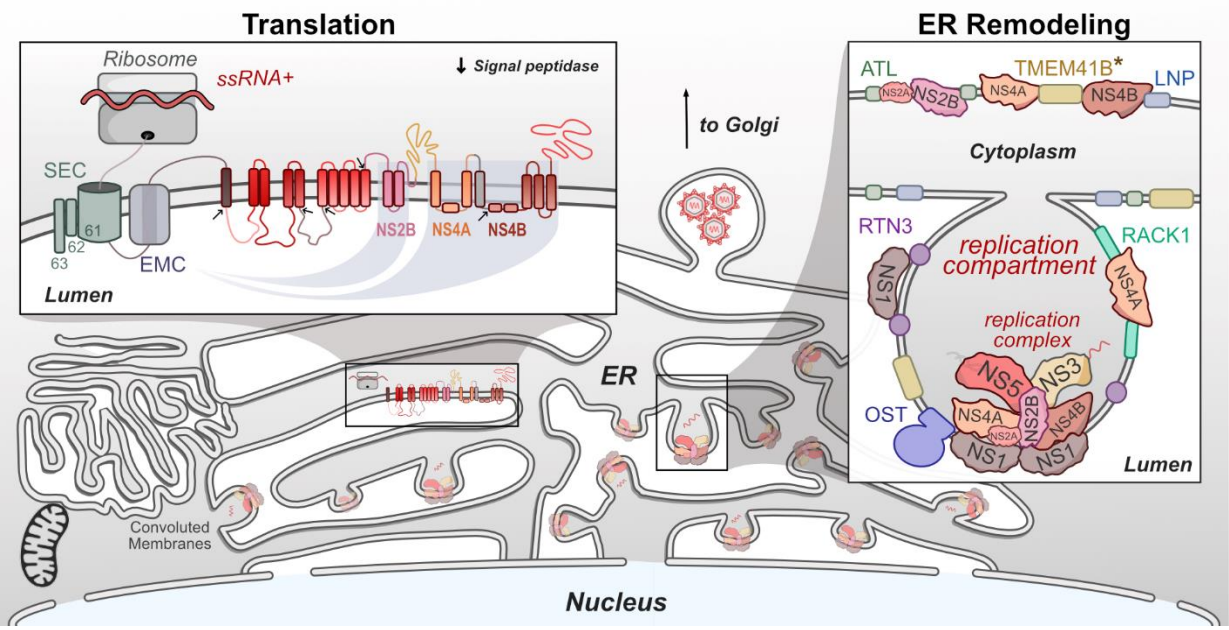

Figure 2-3: Flaviviruses co-opt host proteins to remodel the ER. Flaviviruses dramatically alter the morphology of the host ER to create a niche that maximizes the efficiency of genome replication and virion packaging. Replication compartments are formed by the involution of the ER membrane by both viral and host proteins. Viral replication complexes reside within these compartments and carry out RNA replication. These complexes also physically associate with host proteins. Viral ssRNA+ genomes are translated on the ER by host ribosomes. The resulting viral polyprotein is co-translationally processed to ensure its stability, insertion into the ER membrane, and proper cleavage into individual viral proteins. *TMEM41B is known to interact with either ZIKV NS4A or YFV NS4B and may facilitate ER remodeling.

Flavivirus interactions for host processes outside the ER

While the ER is a major site of flavivirus replication, virus-host protein interactions in other organelles are critical for replication. Soluble viral proteins such as NS3 and NS5 are known to have dispersed localizations during infection, thus it is unsurprising that identified interacting host

proteins also have a wide range of localizations. Here, we will review important and recently identified virus-host PPIs outside context of ER replication that promote virus replication.

Trafficking

After virions are packaged and assembled in the ER lumen they must be processed prior to release. Specifically, the prM protein on the outermost part of the virion must be cleaved by furin, a host protease within the Golgi apparatus. Cleavage sites on prM are only made accessible by the relatively acidic environment of the Golgi and secretory vesicles (121–123). This prM maturation is required to allow future viral entry into host cells after release. Vesicles containing immature virions reach the Golgi through the host's secretory pathway or trans-Golgi network (TGbN). Golgi proteins and others involved in TGN trafficking have been identified in proteomic screens (124), but in-depth studies on the role of these interactions in flavivirus replication are very limited. Recently several specific virus-host PPIs have been identified here with roles in virus maturation and replication.

As trafficking through the TGN is essential for flaviviruses, one anti-viral host mechanism is to limit this processing by halting virion progression at the Golgi, preventing release. One well-studied protein with this function is bone marrow stromal cell antigen 2 (BST2), also known as tetherin. BST2 is known to restrict the replication of many viruses, including filoviruses, retroviruses, and alphaviruses, by tethering virions to the cell surface or by interrupting virion release from the TGN prior to exit from the cell (125–128). Accordingly, several viruses have evolved measures to counteract this inhibition. For example, the Vpu protein of HIV-1 inhibits the anti-viral tethering effects of BST2, allowing release of infectious virions from the cell (129). However, there are some conflicting reports about the effects of BST2 on flaviviruses. A 2012 study described significant BST2-mediated inhibition of DENV release from Huh7 cells (130). Conversely, another study found only modest effects on non-infectious, "virus-like particle"

release from TRex HEK293 cells expressing BST2 and transfected to express DENV Env (128). Whether these discrepancies are methodological or cell-type derived is unclear. More recently, Li et al. investigated the potential mechanisms by which JEV escapes BST2 restriction. Endogenous BST2 proteins levels were actively decreased during JEV infection and expression of JEV Env alone was sufficient to reduce BST2 expression. JEV Env physically interacted with BST2 at its transmembrane and cytoplasmic loop domains, and targeted it for lysosomal degradation (131). Thus, the interaction between Env and BST2 promotes virus replication by eliminating the anti-viral activity of BST2. Whether other flaviviruses interact with and inhibit BST2 using similar mechanisms requires further study. Previously we also discussed the interaction between ATL3 and multiple viral proteins, and the role of this interaction in ER remodeling. Interestingly, this study also identified a role of ATL3 in flavivirus maturation and furin recycling. Knockdown of ATL3 increased levels of extracellular un-cleaved prM and altered furin localization away from the Golgi. The relocalization of furin was specifically observed after knockdown of ATL2 and ATL3, whereas knockdown of other ER remodeling proteins RTN3 and LNP had no effect (106).

Autophagy

Autophagy is an essential intracellular degradative process that recycles cytoplasmic components (132). Autophagy involves three major steps, the formation of autophagosomes and simultaneous capture of cytoplasmic material, the fusion of autophagosomes with lysosomes to form autolysosomes, and the turnover of autolysosomes. The cytoplasmic components, often referred to as cargo, can either be selectively or non-selectively degraded (133). For selective autophagy, cargo such as mitochondria is tagged by cargo receptors which are then encapsulated and degraded by autophagy. Autophagy is involved in the replication of various flaviviruses. The overall role of autophagy as proviral or antiviral in flavivirus replication is complex and has no

clear consensus (134–136). Here, we discuss the studies that have implicated the role of autophagy-related proteins in virus replication through physical interactions with viral proteins.

DENV and ZIKV hijack various aspects of selective autophagy for efficient virus replication. Regulation of lipid metabolism during DENV infection has been reported by multiple groups (137–141). DENV NS4A physically interacts with unubiquitinated AUP1 to translocate lipid droplets to autophagosomes to induce lipophagy (142). Interestingly, DENV NS4B or DENV infection is essential for this interaction. Ubiquitination of AUP1 impeded its interaction with NS4A, which led to defective lipophagy and reduced viral titers. This study highlights the importance of lipophagy during virus infection that is regulated by virus-host protein interactions. Regulation of apoptosis through autophagy is another strategy utilized by DENV for prolonged virus replication (143), and DENV NS1 interacts with Beclin-1 to activate autophagy and prevent apoptosis at early stages of infection (144). FAM134B, an ER phagy (reticulophagy) selective cargo receptor was identified to interact with DENV and ZIKV NS2B3 (145). The researchers demonstrated that DENV and ZIKV NS2B3 cleave FAM134B to inhibit the degradation of viral proteins through reticulophagy. Additionally, overexpression of FAM134B leads to decreased virus replication. These results indicate selective degradation of ER is subverted by viruses even though overall autophagy could be upregulated during infection. In a recent study, Ponia and colleagues observed inhibition of mitophagy through the interaction of ZIKV NS5 with the host protein Ajuba (146). Ajuba is a key regulator of mitophagy and is translocated to depolarized mitochondria to initiate PINK1-Parkin mediated mitophagy. NS5 interaction with Ajuba impeded its translocation to depolarize mitochondria, thus inhibiting mitophagy. The authors further use *in vivo* ZIKV infection studies in mice to demonstrate increased early pro-inflammatory chemokines and viral load in tissue due to inhibition of mitophagy, further underlining the importance of the NS5-Ajuba interaction. These studies point towards the regulation of selective autophagy by DENV and ZIKV. Systematic measurements of degraded cargo during virus infection can provide key insights. In the future, it

will also be valuable to explore if modulation of selective autophagy is a common theme for other flaviviruses and other types of selective autophagy (*e.g.,* pexophagy, and xenophagy).

Interactions of general autophagy-related proteins with WNV and JEV proteins have also been identified. WNV Capsid protein interacts with AMPK, an autophagy inducer (147). This interaction mediated the degradation of AMPK through the proteasome pathway and led to the accumulation of ubiquitinated protein aggregates. A mutant Capsid protein reduced the interaction with AMPK and its degradation. Even though disrupting this interaction did not affect virus replication, it led to lower protein aggregates in mouse brain and reduced neurological symptoms. For JEV, Sharma et al have shown that autophagy acts as an antiviral response during JEV infection in neuronal cells (148). They also observed NS1 colocalization with LC3-I, an important autophagy protein whose depletion caused decreased viral titers. In a more recent study, the same group also demonstrated Capsid protein interaction with LC3-I, using immunoprecipitation (149). The functional role of these interactions in virus replication and autophagy is uncharacterized and could be a potential study.

Future efforts can be focused on investigating known uncharacterized physical interactions. The mTOR pathway is an important autophagy pathway that is differentially regulated during flavivirus infection (139, 150–153). Moreover, viral protein interactions with mTOR were also found using proteomic approaches (27). However, characterizing the role of virus-mTOR PPIs in the context of virus infection is largely unexplored and could be a potential future direction. Selective autophagy during virus infection is another interesting attribute for potential study. Viruses appear to exploit the selective nature of autophagy by variably regulating specific cargo degradation. For example, DENV upregulates lipophagy while downregulating reticulophagy for effective replication (142, 145). Thus, further investigating the interactions found between the viral proteins and cargo receptors could be a promising direction. We explored the literature to generate a list of virus-autophagy PPIs that have been identified in various proteomic screens which could

further explain the role of autophagy during virus infection (Table 1). Interestingly, while many autophagy proteins were identified in these screens, none were pursued mechanistically in those published studies, leaving the door open to many systematic studies of these PPIs. Finally, capturing the temporal change in cargo degraded during virus infection may also provide novel insights into the dynamic replication cycle.

Autophagy protein	Autophagy related role	Viral proteins
ACBD5	Pexophagy receptor	NS4A[1]
AMBRA1	Key regulator of autophagy by modulating the BECN1-PIK3C3 complex	NS1[7], NS2B[7]
ATG9A	Supplies membrane for the growing autophagosome	Env[7]
BNIP3 (NIP3)	Mitophagy receptor	NS5[1,2]
EI24 (EPG4)	Regulates formation of degradative autolysosomes	NS1[2], NS4B[3]
LGALS8	Restricts infection by initiating autophagy via interaction with CALCOCO2/NDP52	NS3[6]
MTOR	Key regulator of autophagy through phosphorylation of ULK1, DAP, AMBRA1, and RUBCNL	NS4A[1,2]
PHB2	Mitophagy receptor	NS2B3[3], NS4B[3]
SQSTM1 (p62)	Multiple cargo receptor	NS4B[2]
STX17	Regulates autophagosome fusion with lysosomes	NS2A[7]
VCP	Essential for the maturation of ubiquitin-containing autophagosomes and the clearance of ubiquitinated protein by autophagy	NS2B3[5]
WAC	Regulator of autophagy	NS2B[6]
AUP1	Lipophagy regulator	NS2A[4], NS4B[3,4]
FAM134C	Reticulophagy receptor	NS4A[1], NS4B[3]
RTN3	Reticulophagy receptor	NS4A[1]
SEC62	Reticulophagy receptor	NS4A[2]
CALCOCO1	Reticulophagy receptor	NS5[5]
NBR1	Aggrephagy, pexophagy and xenophagy receptor	NS2A[4]
VMP1	Required for autophagosome biogenesis	NS4A[4]
TMEM41B	Required for autophagosome biogenesis	NS4B[3]

Table 2-1: Protein-protein interactions between flavivirus proteins and host autophagy factors. PPI found between autophagy proteins and viral proteins from 7 data sets (25–27, 29, 31, 33). PPI that were found significant by the authors were considered for the search. Approximately 100 autophagy proteins were probed for interactions based on a list of proteins mentioned in these studies (133, 154, 155). [1]Shah 2018 (ZIKV), [2]Shah 2018 (DENV), [3]Scaturro 2018 (ZIKV), [4]Coyaud 2018 (ZIKV), [5]Li 2019 (WNV), [6]Golubeva 2020 (ZIKV), and [7]Zeng 2020 (ZIKV)

Mitochondrial Dynamics and Morphology

Mitochondria are dynamic organelles with widespread functions in cellular homeostasis including ATP production, immune response signaling, and apoptosis activation. Unsurprisingly, many viruses interact with and perturb these functions to benefit their own replication (156). Recently the mechanisms and protein interactions that flaviviruses use to modulate these mitochondrial functions have revealed dynamic alterations in mitochondrial morphology that impact virus replication.

The morphology of host mitochondria are constantly changing. The constant fusion and fission of mitochondria is critical for cellular homeostasis. The fusion of mitochondria together is mediated by mitofusin 1 (MFN1) and MFN2 in the outer mitochondrial membrane and optic atrophy protein 1 (OPA1) in the inner membrane. Fission is mediated by dynamin-related protein 1 (DRP1) which is soluble and recruited to mitochondria by mitochondrial fission protein 1 (FIS1) (157). ZIKV and DENV both impact mitochondrial morphology, albeit in cell-type and virus specific manners (120, 158–160). DENV and ZIKV infection in Huh7 hepatocytes induces dramatic mitochondrial elongation. This is associated with significant decreases in DRP1 fission activity, specifically through decreased phosphorylation at S616, a site which induces fission by DRP1. NS4B interacts with many mitochondrial proteins (26, 27) and its expression alone is sufficient to alter

mitochondrial morphology (120). NS4B expression is linked with decreased expression of CDK1, the kinase which phosphorylates DRP1 at S616. Knockdown of DRP1 further increases DENV and ZIKV replication, while increasing fusion through knockdown of MFN2 decreases replication (120, 158). Interestingly, knockdown of DRP1 did not impact the replication of fellow flavivirus WNV or the closely related HCV (120). Together, this suggests that DENV and ZIKV specifically induce the elongation of mitochondria in these cells. It appears this elongation may serve two functions for virus replication. Firstly, elongated mitochondria have increased respiratory function, resulting in greater energy production which may be utilized directly for virus replication or promote host cell survival (158). Secondly, this elongation impedes mitochondrial innate immune response signaling by preventing the translocation of RIG-I to mitochondrial-associated membranes, decreasing MAVS-associated IFN production (120, 161). The interplay between flaviviruses and innate immune signaling, including through MAVS and RIG-I, will be discussed in more detail later in this Chapter.

Intriguingly, mechanisms that promote mitochondrial fission, rather than fusion, have been observed during DENV and ZIKV infection in other cell types (160, 161). In A549 cells, DENV infection also leads to abnormal mitochondrial dynamics, however independent of DRP1. Rather, MFN1 and MFN2 are cleaved by the DENV NS2B3 protease, resulting in decreased fusion and more mitochondrial fragmentation. Specifically, cleavage of MFN1 results in decreased MAVS-mediated IFN production, while cleavage of MFN2 decreased the activation of cell-death associated caspases. Again, this activity does not appear to be conserved across all flaviviruses, as NS2B3 from JEV was unable to perform the same cleavage events (161). This specificity may contribute to the unique pathogenesis of some flaviviruses. Congenital ZIKV is associated with the development of neurological and ocular abnormalities which are not observed with other flaviviruses (162, 163). It is possible that perturbation of mitochondrial processes by viruses are especially potent in these tissues, as metabolic demands are high and these tissues are very

sensitive to mitochondrial dysfunction (164, 165) In ZIKV-infected neural stem cells (NSCs) mitochondria numbers and size are significantly decreased, associated with concomitant decreases in MFN2 protein expression, whereas the other fusion/fission proteins (MFN1, OPA1, DRP1, and FIS1) were unchanged (160). ZIKV had similar effects on the mitochondria of retinal pigment epithelial (RPE) cells, with mitochondria appearing more fragmented and punctate in nature (159). In both cases, ZIKV-associated morphology changes involved the loss of mitochondrial membrane potential, resulting in diminished ATP production and mitochondrial function. Whether ZIKV NS2B3 performs similar cleavage of MFN2 as the DENV protease or if ZIKV relies on other unique interactions requires further experimentation.

Antagonism of host immunity by flavivirus-host PPIs

While some interactions between viral proteins and host proteins associated with the immune system restrict flavivirus replication and pathogenesis (166–168), flaviviruses have evolved numerous mechanisms to sabotage the host innate immune response via interactions with host proteins. Here, we review the major mechanisms of antagonism associated with IFN production, IFN signaling, and the complement system (Figure 4).

IFN production

Pattern-recognition receptors (PRRs) sense flaviviruses upon entry. The major PRRs relevant for flaviviruses are TLR3 and TLR7/8, which are located primarily in endosomal vesicles and recognize viral RNA of incoming virions (169, 170); retinoic-acid inducible gene-I (RIG-I) and myeloma differentiation factor 5 (MDA5), which recognize cytosolic RNA (171); and cyclic GMP-AMP synthase (cGAS) which recognize cytosolic DNA (172). Mechanistically, activated TLR3 and TLR7 recruited adaptor protein MyD88 and TRIF to initiate further changes regulating the

expression of cytokines, chemokines, and type I IFNs (173). After sensing viral RNA, RIG-I and MDA5 move from the cytosol to mitochondria and interact with their adaptor, mitochondrial antiviral signaling protein (MAVS), to continue further downstream signaling that activates IRF3 and NF-kβ (174). cGAS activation after recognizing cytosolic DNA catalyzes the synthesis of cyclic GAMP (cGAMP) which activates STING, which subsequently activates IFN expression (175). The signaling induced by these sensors converges on a common cascade that induces the production of interferon (IFN) and downstream genes stimulated by IFN called interferon-stimulated genes (ISGs) (176).

Flaviviruses have evolved different strategies to interfere with the host production of IFNs. A major mechanism for flaviviruses is to disrupt double-stranded RNA-sensing pathway. NS3 from DENV and ZIKV binds 14-3-3ε, an important protein in antiviral immunity (177), via a conserved phosphomimetic motif on NS3 and prevent the translocation of RIG-I to mitochondria, and consequently IFN production (178, 179). During DENV infection, DENV NS4A also physically interacts with MAVS to prevent RIG-I from forming complexes with MAVS in mitochondria-associated endoplasmic reticulum membranes (MAMs), leading to the disruption of RIG-I-induced IRF3 activation and subsequently suppression of IFN production (180).

Further down in the RIG-I-induced type I IFN pathway, DENV serotypes 1, 2, 4 (DENV1, DENV2, DENV4) NS2A and NS4B proteins inhibit RIG-I/MDA5-regulated interferon beta (IFN-β) induction by blocking TBK1/IRF3 (181). DENV NS2B3 interacts with IKKε to prevent IRF3 phosphorylation (182) potentially changing the activation of multiple antiviral genes including type I IFN. JEV inhibits IFN-β production by suppressing IFR3 and NF-kβ (183). Mechanistically, JEV NS5 interacts with nuclear transport proteins KPN2, KPN3, KPN4 and block their interaction with IRF3 and P65, therefore preventing nuclear translocation of IRF3 and NF-kβ and reducing type I IFN production.

Even as RNA viruses, flaviviruses also antagonize IFN production by interfering with cytosolic DNA-sensing pathway by cGAS and its adaptor STING. Specifically, as DENV infection triggers innate immune response through mtDNA sensing by cGAS (184), DENV NS2B protease targets the DNA sensor cGAS and degrades it to prevent the detection of mitochondrial DNA released during DENV infection, blocking the activation of cGAS/STING pathway and the induction of type I IFN (185). DENV NS2B3 also physically interacts with and cleaves STING to inhibit type I IFN production in species-specific manner (186, 187). During ZIKV infection, cGAS is targeted and cleaved by NS1-stablized caspase-1, leading to enhanced NLRP3 inflammation activation and reduced type I induction to benefit the infection (188). The multiple mechanisms by which flaviviruses antagonize DNA sensing suggest that this is an important mechanism of immune evasion for RNA viruses and represents a new frontier of investigation for virus-host interactions.

Flavivirus NS5 proteins also antagonize innate immunity upstream of IFN production and signaling, primarily through interactions with host gene expression machinery in the nucleus. The extent of NS5 localization to the nucleus varies depending on flavivirus species, yet some nuclear localization and nuclear/cytoplasmic shuttling appears to occur for nearly all NS5s, with the exception of duck Tembusu virus (189–196). NS5 protein interactions with host gene expression machinery have been noted through several unbiased screens, including mass spectrometry and yeast-two-hybrid screens (25–27, 29, 197–199). Several of these protein interactions have been linked back to NS5 perturbation of host gene expression. For example, a proteomic study of DENV NS5 during infection revealed interactions with CD2BP2 and DDX23, core components of U5 small nuclear ribonucleoprotein particles (U5 snRNPs) that ultimately interfere splicing efficiency (199). DENV NS5 also dysregulates host splicing by physically interacting with RBM10, a splicing factor that regulates spermidine/spermine-N1-acetyltransferase (SAT1) splicing and promoting RBM10 proteasomal degradation. The interaction potentially restricts RBM10 from its proinflammatory function and benefits DENV replication (200). In our recent studies on DENV-

human protein interactions, we identified an interaction with PAF1C (27), which regulates the transcription elongation of many immune response genes (201, 202). Our recent work dissecting the NS5-PAF1C interaction demonstrated that PAF1C regulates immune response genes upstream of type I IFN production, including the RIG-I/DDX58 signaling axis. Breaking the NS5-PAF1C interaction through mutagenesis of NS5 rescued PAF1-dependent gene expression, underlining the importance of this protein interaction (196).

The recurring theme of NS5 nuclear localization and interactions with nuclear proteins has led to much speculation in the field regarding why the polymerase and methyltransferase of a cytoplasmic RNA virus would have such behavior. There is mounting evidence that flavivirus NS5 protein can perturb host gene expression, both through dissection of virus-host protein interactions, and through more generalized gene expression studies. For example, independent studies of ZIKV, WNV, and DENV NS5 all point to overall inhibition of immune gene expression (196, 203, 204). On the other hand, studies involving infection have not revealed *in vitro* or *in vivo* phenotypes for DENV mutants that reduce NS5 nuclear localization (192, 193, 195), resulting in skepticism regarding the biological significance of NS5 nuclear localization. However, for studies involving DENV serotype 2, it should be noted that there are two distinct nuclear localization signals (NLSs) that contribute to nuclear localization. In fact, mutation of a single NLS still results in substantial NS5 nuclear localization (~1:1 nuclear:cytoplasmic ratio). In our own studies, we show that only mutation of both NLSs truly excludes NS5 from the nucleus and disrupts the NS5-PAF1C interaction (196). Thus, a modest amount of NS5 nuclear localization may be sufficient for its role in perturbing host gene expression. Using a double NLS mutant to study protein interactions and virus replication phenotypes will be essential to understanding the true function of nuclear NS5. Creating similar NLS mutants for other flavivirus NS5 will also strengthen the evidence supporting a role for nuclear NS5 in general.

IFN signaling

Although flaviviruses actively exploit various strategies to suppress the production of IFN by infected cells, secreted IFN can still bind to the heterodimeric IFN receptor, IFNR1 and IFNR2, that are present on most cells. Binding of IFN to the receptors triggers the activation of JAK1 and Tyk2 to phosphorylate cytoplasmic STAT1 and STAT2 (205). The phosphorylated STAT1 and STAT2 form a heterotrimeric complex with interferon regulatory factor 9 (IFR9) known as IFN-stimulated gene factor 3 (ISGF3) which translocate to the nucleus and binds to interferon-stimulated response element (ISRE) to regulate the transcription of IFN-stimulated genes (ISGs), many of which are antiviral (206).

Multiple studies have shown that flaviviruses use different ways to manipulate IFN signaling. DENV NS2A, NS4A, and NS4B block the IFN-induced transduction cascade in human A549 cells by interfering STAT1 phosphorylation, resulting in decreased IFN-induced ISRE-promoter activation and enhanced DENV2 virus replication (207, 208). NS5 also inhibits IFN signaling via multiple mechanisms that appear to be virus-specific (191, 209–213), and we will highlight mechanisms for which the role of NS5-host protein interactions has been dissected. NS5 of Langat virus (LGTV), a member of tick-borne encephalitis complex of viruses, also interacts with IFN-a/b receptor subunit (IFNAR2) and IFN-g receptor subunit (IFNGR1) to block Jak1 and Tyk2 phosphorylation (209, 212). TBEV NS5 protein also interacts with hScrib, a protein expressed at the membrane of mammalian cells and controls cell-to-cell contact, resulting in impaired pSTAT1 formation in response to IFN-a/b and IFN-g (214). TBEV and WNV NS5 can also inhibit IFNAR1 mutation and accumulation at the cell surface through an interaction with PEPD (215). DENV and ZIKV NS5 interact with and target STAT2 for proteasome-mediated degradation to inhibit IFN-induced signaling (191, 216–218). Interestingly, DENV and ZIKV NS5 can target and degrade human STAT2 (hSTAT2) but not mouse STAT2 (191, 219). Thus, STAT2 is a species-specific target of a flaviviral nonstructural protein, similar to STING. Given the many emerging flaviviruses

that circulate in non-human reservoirs, exploring the biophysical and biochemical differences underlying species-specific virus restriction could help predict the constraints to emergence.

Complement system

The complement system is an important part of innate immunity to control early infection. It contains more than 50 plasma proteins and membrane proteins expressed on cell surface (220). Complement activities occur in plasma, in tissues, or within cells (221). The activation of complement happens through three distinct target-dependent pathways: classical, lectin, and alternative pathways. The classical pathway is initiated by the direct binding of C1q to the pathogen surface or antigen-antibody complexes; the lectin pathway is activated when mannose binding lectin (MBL), a serum protein, binds to mannose-containing carbohydrates on pathogens; and the alternative pathway is active when a spontaneously activated complement component binds to the pathogen surface (220). Each pathway has its own protease to target and process different antigens, but they all generate a protease called C3 convertase and share common terminal outcomes after C3 cleavage: pathogen opsonization, regulation of inflammation, clearance of immune complexes and cell debris. Complement activation is a bridge linking innate immune response and adaptive response by B cells and T cells in viral infection (222, 223).

Flaviviruses have evolved mechanisms to antagonize this part of the innate immune system. Among NS proteins from flavivirus, NS1 has been recognized as an immune invasion protein that interferes with the complement system. A study by Avirutnan showed that NS1 from DENV, WNV, and YFV reduced complement activation pathways by interacting and forming a complex with C4 and C1s, leading to reduced classical pathway C4b deposition and C3 convertase (C4b2a) activity and consequent protection of DENV from complement-regulated neutralization (224). In another study, NS1 from these flaviviruses directly binds to C4b binding protein (C4BP), a regulatory plasma protein of the classical and lectin pathway, to inactivate C4b in both cell surface and fluid;

thereby protecting the viruses from complement attack (225). WNV NS1 also binds to factor H (fH), a key regulator of the alternative pathway, and facilitates factor I-mediated cleavage of C3b. Additionally, cell surface-associated NS1 recruits fH and reduces C3b deposition and C5b–9 membrane attack complexes on cell surfaces, reducing the recognition of infected cells by complement system (226). For the lectin pathway, insect-derived DENV NS1 not only bind to human C1s, C4, and C4b-binding protein to suppress classical pathway of complement activation but also bind to mannose binding lection (MBL) to disrupt neutralization by the lectin pathway (227). DENV NS1 was also reported to interact with other proteins and interfere with the terminal pathway of complement activation. Specifically, NS1 interacts with complement regulator vitronectin (VN) and inhibits membrane attack complex (MAC) formation, suggesting a role of NS1 in antagonizing complement activation (228).

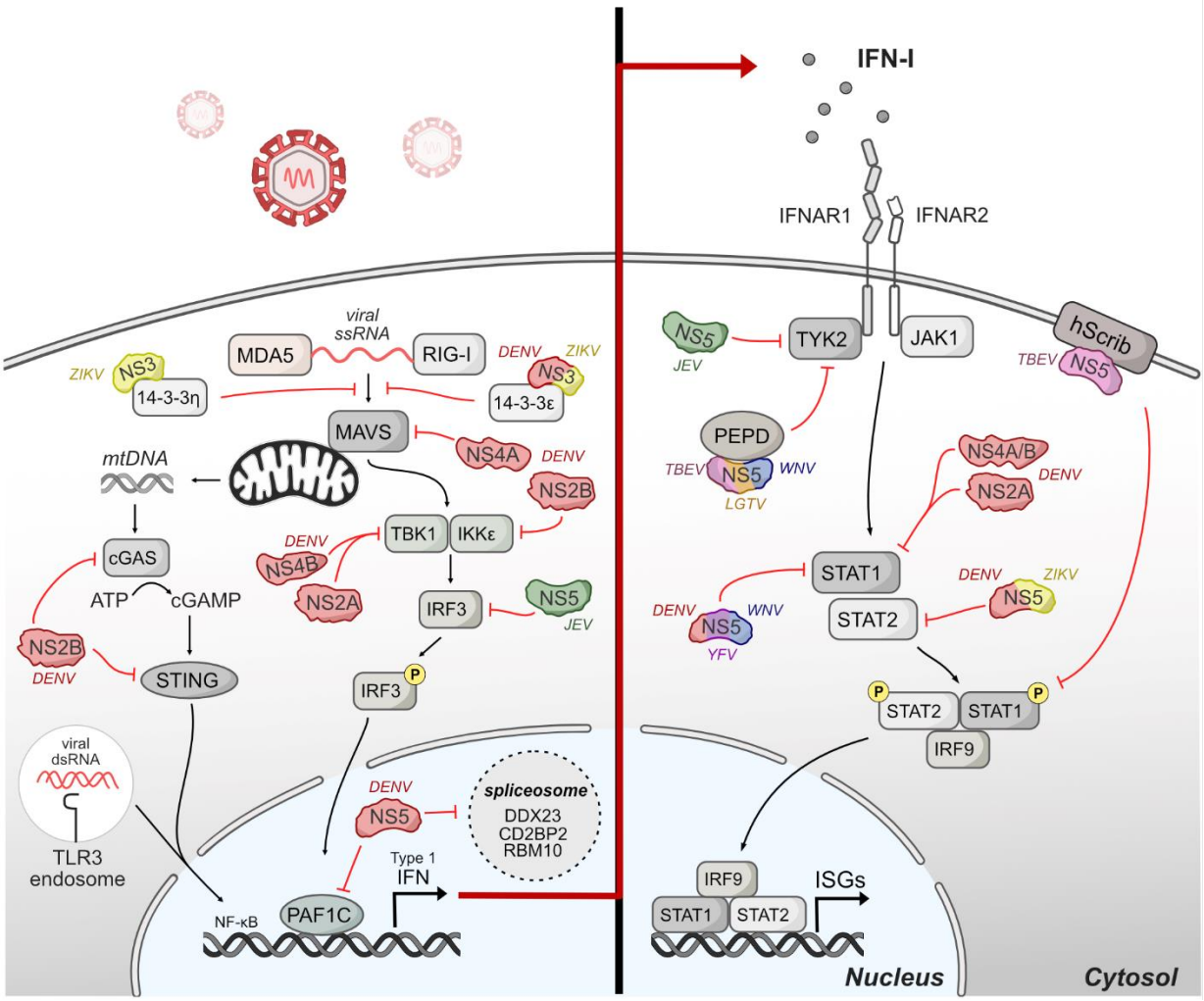

Figure 2-4: Host innate immune response is antagonized by flavivirus protein interactions. Upon entry, flaviviruses are sensed by different pattern-recognition receptors (PRRs) such as TLR-3 and RIG-I. The signaling induced by these sensors converges on a common cascade that induces the production of interferon (IFN) and downstream genes stimulated by IFN called interferon-stimulated genes (ISGs). Flaviviruses have evolved invasive strategies to interfere with host immune response by antagonizing different protein components of innate immune signaling pathways associated with IFN production and IFN signaling.

Flavivirus-host PPIs involved in disease

While identifying virus-host PPIs is important to inform on the fundamental mechanisms driving their replication, they can also be critical to understanding pathogenesis. Indeed, in recent years several individual interactions have sparked interest in how flaviviruses alter host cellular behavior to cause disease. ZIKV has deservedly received significant research attention due to its unique association CZS. The most notable presentation of CZS is microcephaly, a condition in which head and brain size are dramatically reduced at birth (19). Many studies have provided insight into the mechanisms by which ZIKV causes CZS. Notably, however, is that many of these studies focus on virus strain/variants, placental damage, the innate immune response *in utero* (229–234). Here, we review how flavivirus-host PPIs directly dysregulate important developmental pathways to cause CZS.

In our own global proteomics screen, we identified an interaction between ZIKV NS4A and host ANKLE2 (27), mutations in which are known to be associated with hereditary microcephaly in humans and small-brain phenotypes in *Drosophila melanogaster* (flies) (235). NS4A expression alone in flies is sufficient to induce similar brain size defects in an ANKLE2-dependent manner. Further investigation revealed ANKLE2 is critical for spindle pole alignment during asymmetric division of fly neuroblasts, akin to mammalian neuroprogenitor cells that are targeted by ZIKV, and expression of NS4A results in similar division defects. Elegant fly genetics were used to demonstrate that NS4A inhibits the ANKLE2 pathway specifically (236). Together, this demonstrates NS4A interacts with and disrupts ANKLE2 function, which in susceptible neuroblasts can disturb brain development. The extent to which this specific interaction impacts vertebrate brain development requires further investigation. Additionally, these studies bring to light the interplay between host genetics and viral pathogenesis. In flies Ankle2 mutation heterozygosity results in normal brain development. However, NS4A expression in these flies is dramatically more severe than in wild-type flies (27, 236), suggesting that host genetics can pre-

dispose an organism to disease that may be associated with virus-host PPIs. Another example of this phenomenon involves the previously discussed host-factor TMEM41B. Naturally occurring single nucleotide polymorphisms that lead to Ile266Val/Leu substitutions are prevalent in certain human populations but fail to rescue flavivirus replication in TMEM41B KO cells. This suggests these variants cannot be utilized by flaviviruses for the function they require to effectively replicate (83).

One of the most common clinical findings associated with CZS is intracranial calcifications (237). A recent study explored how ZIKV induces these calcifications through the specific interaction between the viral protease NS3 and host bone morphogenic protein 2 (BMP2). BMP2 is an essential signaling protein in the process of osteogenesis, inducing the expression of downstream genes that ultimately facilitate bone growth. BMP2 normally must be cleaved by furin-type proteases prior to secretion, where it then induces these signaling cascades. Infection with ZIKV leads to increased expression of BMP2 and downstream genes, and subsequent calcification *in vitro* and *in vivo*. In fact, the expression of NS3 alone is sufficient to induce these phenotypes in U2OS osteosarcoma epithelial cells, but not a protease-defective mutant, suggesting that ZIKV NS3 cleavage of BMP2 initiates osteogenesis in the brain, leading to intracranial calcifications (238).

Beyond these examples, several other ZIKV-host interactions have been found to impact brain development and may ultimately play a role in human pathogenesis. Even while the ZIKV epidemic was ongoing it was shown that expression of ZIKV NS4A and NS4B specifically impaired the growth of neural stem cells by perturbing autophagy, while corresponding DENV proteins did not (151). This is not the only example of ZIKV-specific effects. Expression of ZIKV NS2A *in vivo* disrupts neurogenesis through physical interactions with adherens junctions in radial glial cells (239). In another recent study, systematic proteomics in neural stem cells (NSCs) revealed the interaction between ZIKV Capsid and Dicer, a pivotal protein in the host RNAi pathway with

implications in neurodevelopment (33). Amongst flaviviruses this interaction is also unique to ZIKV. Mechanistically, Dicer is a host restriction factor and ZIKV Capsid interaction inhibits this antiviral function, as infection with a H41R mutation which ablates this interaction leads to less viral burden *in vivo*. Indeed, even ZIKV Capsid expression alone, dependent on its interaction with Dicer, is sufficient to induce severe defects in brain development.

Together, these studies highlight how certain aspects of pathogenesis may be uniquely derived from single virus-host PPIs. However, given the incredible complexity of human development, it is not likely that any single interaction during infection is solely responsible for disease outcome. More realistically in the case of ZIKV, it is the culmination of these perturbations and dysregulation of brain development by multiple mechanisms that results in CZS. Intriguingly, the intersection of flavivirus-host PPIs and disease, including host factors implicated in hereditary disease, opens the door to the possibility of host genetics being a major and overlooked contributing factor to susceptibility to CZS. For example, loss-of-function variants for host factors like ANKLE2, which are haplo-sufficient for their role in development in the absence of a virus-host PPI, but haplo-insufficient in the context of a virus-host PPI, could tip the balance in the favor of disease in an otherwise healthy individual. Future studies exploring this concept are warranted.

Concluding Remarks

Flaviviruses are arthropod-borne viruses that cause significant human disease worldwide. Their limited genome requires them to co-opt host proteins through physical interactions during infection to properly replicate. Some of these interactions appear to be broadly conserved amongst flaviviruses, while other unique interactions contribute to observed differences in host tropism and pathogenesis. Flaviviruses employ a wide range of host receptors utilized for entry into host cells. Replication within the ER involves vast remodeling into a microenvironment well-suited to the

generation of viral progeny. Even outside the ER viral proteins orchestrate modulation of host cell systems. This includes physical interaction with other cellular pathways and organelles critical to virus replication and with different protein components of the host innate immune system. These virus-host PPIs can be influential in the development of pathogenesis. Thus, understanding these mechanisms is essential for creating new therapeutics to alleviate human disease caused by flaviviruses.

References

1. Falgout B, Pethel M, Zhang YM, Lai CJ. Both nonstructural proteins NS2B and NS3 are required for the proteolytic processing of dengue virus nonstructural proteins. J Virol. 1991 May;65(5):2467–75.
2. Tan BH, Fu J, Sugrue RJ, Yap EH, Chan YC, Tan YH. Recombinant dengue type 1 virus NS5 protein expressed in Escherichia coli exhibits RNA-dependent RNA polymerase activity. Virology. 1996 Feb 15;216(2):317–25.
3. Egloff MP, Benarroch D, Selisko B, Romette JL, Canard B. An RNA cap (nucleoside-2'-O-)-methyltransferase in the flavivirus RNA polymerase NS5: crystal structure and functional characterization. EMBO J. 2002 Jun 3;21(11):2757–68.
4. Ray D, Shah A, Tilgner M, Guo Y, Zhao Y, Dong H, et al. West Nile virus 5'-cap structure is formed by sequential guanine N-7 and ribose 2'-O methylations by nonstructural protein 5. J Virol. 2006 Sep;80(17):8362–70.
5. Alvarez DE, De Lella Ezcurra AL, Fucito S, Gamarnik AV. Role of RNA structures present at the 3'UTR of dengue virus on translation, RNA synthesis, and viral replication. Virology. 2005 Sep 1;339(2):200–12.
6. Lodeiro MF, Filomatori CV, Gamarnik AV. Structural and functional studies of the promoter element for dengue virus RNA replication. J Virol. 2009 Jan;83(2):993–1008.

7. Gillespie LK, Hoenen A, Morgan G, Mackenzie JM. The endoplasmic reticulum provides the membrane platform for biogenesis of the flavivirus replication complex. J Virol. 2010 Oct;84(20):10438–47.

8. Welsch S, Miller S, Romero-Brey I, Merz A, Bleck CKE, Walther P, et al. Composition and three-dimensional architecture of the dengue virus replication and assembly sites. Cell Host Microbe. 2009 Apr 23;5(4):365–75.

9. Yi Z, Yuan Z, Rice CM, MacDonald MR. Flavivirus replication complex assembly revealed by DNAJC14 functional mapping. J Virol. 2012 Nov;86(21):11815–32.

10. Huang YJS, Higgs S, Horne KM, Vanlandingham DL. Flavivirus-Mosquito Interactions. Viruses. 2014 Nov 24;6(11):4703–30.

11. Chandramouli S, Joseph JS, Daudenarde S, Gatchalian J, Cornillez-Ty C, Kuhn P. Serotype-Specific Structural Differences in the Protease-Cofactor Complexes of the Dengue Virus Family. J Virol. 2010 Mar;84(6):3059–67.

12. Yung CF, Lee KS, Thein TL, Tan LK, Gan VC, Wong JGX, et al. Dengue Serotype-Specific Differences in Clinical Manifestation, Laboratory Parameters and Risk of Severe Disease in Adults, Singapore. Am J Trop Med Hyg. 2015 May 6;92(5):999–1005.

13. Brady OJ, Gething PW, Bhatt S, Messina JP, Brownstein JS, Hoen AG, et al. Refining the Global Spatial Limits of Dengue Virus Transmission by Evidence-Based Consensus. PLOS Neglected Tropical Diseases. 2012 Aug 7;6(8):e1760.

14. Bhatt S, Gething PW, Brady OJ, Messina JP, Farlow AW, Moyes CL, et al. The global distribution and burden of dengue. Nature. 2013 Apr 25;496(7446):504–7.

15. da Silva Voorham JM. [A possible fifth dengue virus serotype]. Ned Tijdschr Geneeskd. 2014;158:A7946.

16. Mustafa MS, Rasotgi V, Jain S, Gupta V. Discovery of fifth serotype of dengue virus (DENV-5): A new public health dilemma in dengue control. Med J Armed Forces India. 2015 Jan;71(1):67–70.

17. Sánchez-González G, Belak ZR, Lozano L, Condé R. Probability of consolidation constrains novel serotype emergence in dengue fever virus. PLOS ONE. 2021 Apr 5;16(4):e0248765.

18. de Araújo TVB, Rodrigues LC, de Alencar Ximenes RA, de Barros Miranda-Filho D, Montarroyos UR, de Melo APL, et al. Association between Zika virus infection and microcephaly in Brazil, January to May, 2016: preliminary report of a case-control study. Lancet Infect Dis. 2016 Dec;16(12):1356–63.

19. Moore CA, Staples JE, Dobyns WB, Pessoa A, Ventura CV, Fonseca EB da, et al. Characterizing the Pattern of Anomalies in Congenital Zika Syndrome for Pediatric Clinicians. JAMA Pediatr. 2017 01;171(3):288–95.

20. Cao-Lormeau VM, Blake A, Mons S, Lastère S, Roche C, Vanhomwegen J, et al. Guillain-Barré Syndrome outbreak associated with Zika virus infection in French Polynesia: a case-control study. Lancet. 2016 Apr 9;387(10027):1531–9.

21. Solomon T, Dung NM, Kneen R, Gainsborough M, Vaughn DW, Khanh VT. Japanese encephalitis. Journal of Neurology, Neurosurgery & Psychiatry. 2000 Apr 1;68(4):405–15.

22. DeBiasi RL, Tyler KL. West Nile virus meningoencephalitis. Nat Clin Pract Neurol. 2006 May;2(5):264–75.

23. de la Fuente J, Antunes S, Bonnet S, Cabezas-Cruz A, Domingos AG, Estrada-Peña A, et al. Tick-Pathogen Interactions and Vector Competence: Identification of Molecular Drivers for Tick-Borne Diseases. Front Cell Infect Microbiol. 2017 Apr 7;7:114.

24. Ruzek D, Avšič Županc T, Borde J, Chrdle A, Eyer L, Karganova G, et al. Tick-borne encephalitis in Europe and Russia: Review of pathogenesis, clinical features, therapy, and vaccines. Antiviral Res. 2019 Apr;164:23–51.

25. Coyaud E, Ranadheera C, Cheng D, Gonçalves J, Dyakov BJA, Laurent EMN, et al. Global Interactomics Uncovers Extensive Organellar Targeting by Zika Virus. Mol Cell Proteomics. 2018;17(11):2242–55.

26. Scaturro P, Stukalov A, Haas DA, Cortese M, Draganova K, Płaszczyca A, et al. An orthogonal proteomic survey uncovers novel Zika virus host factors. Nature. 2018 Sep;561(7722):253–7.

27. Shah PS, Link N, Jang GM, Sharp PP, Zhu T, Swaney DL, et al. Comparative Flavivirus-Host Protein Interaction Mapping Reveals Mechanisms of Dengue and Zika Virus Pathogenesis. Cell. 2018 13;175(7):1931-1945.e18.

28. Cao YQ, Yuan L, Zhao Q, Yuan JL, Miao C, Chang YF, et al. Hsp40 Protein DNAJB6 Interacts with Viral NS3 and Inhibits the Replication of the Japanese Encephalitis Virus. Int J Mol Sci. 2019 Nov 14;20(22):E5719.

29. Li M, Johnson JR, Truong B, Kim G, Weinbren N, Dittmar M, et al. Identification of antiviral roles for the exon-junction complex and nonsense-mediated decay in flaviviral infection. Nat Microbiol. 2019;4(6):985–95.

30. Wang Y, Zhang S, Tang Y, Diao Y. Screening of Duck Tembusu Virus NS3 Interacting Host Proteins and Identification of Its Specific Interplay Domains. Viruses. 2019 Aug 12;11(8):E740.

31. Golubeva VA, Nepomuceno TC, Gregoriis G de, Mesquita RD, Li X, Dash S, et al. Network of Interactions between ZIKA Virus Non-Structural Proteins and Human Host Proteins. Cells. 2020 Jan 8;9(1):E153.

32. Tan MJA, Brown NG, Chan KWK, Jin JY, Zu Kong SY, Vasudevan SG. Mutations in the cytoplasmic domain of dengue virus NS4A affect virus fitness and interactions with other non-structural proteins. J Gen Virol. 2020 Sep;101(9):941–53.

33. Zeng J, Dong S, Luo Z, Xie X, Fu B, Li P, et al. The Zika Virus Capsid Disrupts Corticogenesis by Suppressing Dicer Activity and miRNA Biogenesis. Cell Stem Cell. 2020 Oct 1;27(4):618-632.e9.

34. Lemasson M, Caignard G, Unterfinger Y, Attoui H, Bell-Sakyi L, Hirchaud E, et al. Exploration of binary protein-protein interactions between tick-borne flaviviruses and Ixodes ricinus. Parasit Vectors. 2021 Mar 6;14(1):144.

35. Funk A, Truong K, Nagasaki T, Torres S, Floden N, Balmori Melian E, et al. RNA structures required for production of subgenomic flavivirus RNA. J Virol. 2010 Nov;84(21):11407–17.

36. Chavali PL, Stojic L, Meredith LW, Joseph N, Nahorski MS, Sanford TJ, et al. Neurodevelopmental protein Musashi-1 interacts with the Zika genome and promotes viral replication. Science. 2017 Jul 7;357(6346):83–8.

37. Damas ND, Fossat N, Scheel TKH. Functional Interplay between RNA Viruses and Non-Coding RNA in Mammals. Noncoding RNA. 2019 Jan 14;5(1):7.

38. Ooi YS, Majzoub K, Flynn RA, Mata MA, Diep J, Li JK, et al. An RNA-centric dissection of host complexes controlling flavivirus infection. Nat Microbiol. 2019 Dec;4(12):2369–82.

39. Meertens L, Carnec X, Lecoin MP, Ramdasi R, Guivel-Benhassine F, Lew E, et al. The TIM and TAM Families of Phosphatidylserine Receptors Mediate Dengue Virus Entry. Cell Host Microbe. 2012 Oct 18;12(4):544–57.

40. Richard AS, Shim BS, Kwon YC, Zhang R, Otsuka Y, Schmitt K, et al. AXL-dependent infection of human fetal endothelial cells distinguishes Zika virus from other pathogenic flaviviruses. Proc Natl Acad Sci U S A. 2017 Feb 21;114(8):2024–9.

41. Dejarnac O, Hafirassou ML, Chazal M, Versapuech M, Gaillard J, Perera-Lecoin M, et al. TIM-1 Ubiquitination Mediates Dengue Virus Entry. Cell Rep. 2018 May 8;23(6):1779–93.

42. Niu J, Jiang Y, Xu H, Zhao C, Zhou G, Chen P, et al. TIM-1 Promotes Japanese Encephalitis Virus Entry and Infection. Viruses. 2018 Nov 14;10(11):630.

43. Zhang X, Liang C, Wang H, Guo Z, Rong H, Pan J, et al. T-Cell Immunoglobulin and Mucin Domain 1 (TIM-1) Is a Functional Entry Factor for Tick-Borne Encephalitis Virus. mBio. 2022 Jan 25;e0286021.

44. Miller JL, de Wet BJM, deWet BJM, Martinez-Pomares L, Radcliffe CM, Dwek RA, et al. The mannose receptor mediates dengue virus infection of macrophages. PLoS Pathog. 2008 Feb 8;4(2):e17.

45. Pereira LHS, de Souza TPP, Camargos VN, de Oliveira Barbosa LA, Taranto AG, Junior MC, et al. Assays with recombinant soluble isoforms of DC-SIGN, a dengue virus ligand, show variation in their ability to bind to mannose residues. Arch Virol. 2019 Nov 1;164(11):2793–7.

46. Routhu NK, Lehoux SD, Rouse EA, Bidokhti MRM, Giron LB, Anzurez A, et al. Glycosylation of Zika Virus is Important in Host-Virus Interaction and Pathogenic Potential. Int J Mol Sci. 2019 Oct 21;20(20):E5206.

47. Chu JJ hann, Ng ML. Interaction of West Nile Virus with αvβ3 Integrin Mediates Virus Entry into Cells *. Journal of Biological Chemistry. 2004 Dec 24;279(52):54533–41.

48. Schmidt K, Keller M, Bader BL, Korytář T, Finke S, Ziegler U, et al. Integrins modulate the infection efficiency of West Nile virus into cells. J Gen Virol. 2013 Aug;94(Pt 8):1723–33.

49. Reyes-Del Valle J, Chávez-Salinas S, Medina F, Del Angel RM. Heat shock protein 90 and heat shock protein 70 are components of dengue virus receptor complex in human cells. J Virol. 2005 Apr;79(8):4557–67.

50. Das S, Laxminarayana SV, Chandra N, Ravi V, Desai A. Heat shock protein 70 on Neuro2a cells is a putative receptor for Japanese encephalitis virus. Virology. 2009 Mar 1;385(1):47–57.

51. Pujhari S, Brustolin M, Macias VM, Nissly RH, Nomura M, Kuchipudi SV, et al. Heat shock protein 70 (Hsp70) mediates Zika virus entry, replication, and egress from host cells. Emerg Microbes Infect. 2019;8(1):8–16.

52. Tio PH, Jong WW, Cardosa MJ. Two dimensional VOPBA reveals laminin receptor (LAMR1) interaction with dengue virus serotypes 1, 2 and 3. Virol J. 2005 Mar 25;2:25.

53. Thongtan T, Wikan N, Wintachai P, Rattanarungsan C, Srisomsap C, Cheepsunthorn P, et al. Characterization of putative Japanese encephalitis virus receptor molecules on microglial cells. J Med Virol. 2012 Apr;84(4):615–23.

54. Chen Y, Maguire T, Hileman RE, Fromm JR, Esko JD, Linhardt RJ, et al. Dengue virus infectivity depends on envelope protein binding to target cell heparan sulfate. Nat Med. 1997 Aug;3(8):866–71.

55. Germi R, Crance JM, Garin D, Guimet J, Lortat-Jacob H, Ruigrok RWH, et al. Heparan Sulfate-Mediated Binding of Infectious Dengue Virus Type 2 and Yellow Fever Virus. Virology. 2002 Jan 5;292(1):162–8.

56. Giraldo MI, Xia H, Aguilera-Aguirre L, Hage A, van Tol S, Shan C, et al. Envelope protein ubiquitination drives entry and pathogenesis of Zika virus. Nature. 2020 Sep;585(7825):414–9.

57. Hu D, Wang Y, Li A, Li Q, Wu C, Shereen MA, et al. LAMR1 restricts Zika virus infection by attenuating the envelope protein ubiquitination. Virulence. 2021 Dec;12(1):1795–807.

58. Sakoonwatanyoo P, Boonsanay V, Smith DR. Growth and production of the dengue virus in C6/36 cells and identification of a laminin-binding protein as a candidate serotype 3 and 4 receptor protein. Intervirology. 2006;49(3):161–72.

59. Bogachek MV, Protopopova EV, Loktev VB, Zaitsev BN, Favre M, Sekatskii SK, et al. Immunochemical and single molecule force spectroscopy studies of specific interaction between the laminin binding protein and the West Nile virus surface glycoprotein E domain II. J Mol Recognit. 2008 Feb;21(1):55–62.

60. Rodrigues R, Danskog K, Överby AK, Arnberg N. Characterizing the cellular attachment receptor for Langat virus. PLoS One. 2019;14(6):e0217359.

61. Protopopova EV, Konavalova SN, Loktev VB. [Isolation of a cellular receptor for tick-borne encephalitis virus using anti-idiotypic antibodies]. Vopr Virusol. 1997 Dec;42(6):264–8.

62. Malygin AA, Bondarenko EI, Ivanisenko VA, Protopopova EV, Karpova GG, Loktev VB. C-terminal fragment of human laminin-binding protein contains a receptor domain for venezuelan equine encephalitis and tick-borne encephalitis viruses. Biochemistry (Mosc). 2009 Dec;74(12):1328–36.

63. Acosta EG, Castilla V, Damonte EB. Functional entry of dengue virus into *Aedes albopictus* mosquito cells is dependent on clathrin-mediated endocytosis. J Gen Virol. 2008 Feb;89(Pt 2):474–84.

64. van der Schaar HM, Rust MJ, Chen C, van der Ende-Metselaar H, Wilschut J, Zhuang X, et al. Dissecting the cell entry pathway of dengue virus by single-particle tracking in living cells. PLoS Pathog. 2008 Dec;4(12):e1000244.

65. Hackett BA, Cherry S. Flavivirus internalization is regulated by a size-dependent endocytic pathway. Proc Natl Acad Sci U S A. 2018 Apr 17;115(16):4246–51.

66. Lafourcade C, Sobo K, Kieffer-Jaquinod S, Garin J, Goot FG van der. Regulation of the V-ATPase along the Endocytic Pathway Occurs through Reversible Subunit Association and Membrane Localization. PLOS ONE. 2008 Jul 23;3(7):e2758.

67. Kozik P, Hodson NA, Sahlender DA, Simecek N, Soromani C, Wu J, et al. A Human Genome-wide Screen for Regulators of Clathrin-coated Vesicle Formation Reveals an Unexpected Role for the V-ATPase. Nat Cell Biol. 2013 Jan;15(1):50–60.

68. Allison SL, Schalich J, Stiasny K, Mandl CW, Kunz C, Heinz FX. Oligomeric rearrangement of tick-borne encephalitis virus envelope proteins induced by an acidic pH. J Virol. 1995 Feb;69(2):695–700.

69. Chao LH, Klein DE, Schmidt AG, Peña JM, Harrison SC. Sequential conformational rearrangements in flavivirus membrane fusion. Jahn R, editor. eLife. 2014 Dec 5;3:e04389.

70. Byk LA, Iglesias NG, De Maio FA, Gebhard LG, Rossi M, Gamarnik AV. Dengue Virus Genome Uncoating Requires Ubiquitination. mBio. 2016 Jun 28;7(3):e00804-16.

71. Ramanathan HN, Zhang S, Douam F, Mar KB, Chang J, Yang PL, et al. A Sensitive Yellow Fever Virus Entry Reporter Identifies Valosin-Containing Protein (VCP/p97) as an Essential Host Factor for Flavivirus Uncoating. mBio. 2020 Apr 14;11(2):e00467-20.

72. Miller S, Kastner S, Krijnse-Locker J, Bühler S, Bartenschlager R. The non-structural protein 4A of dengue virus is an integral membrane protein inducing membrane alterations in a 2K-regulated manner. J Biol Chem. 2007 Mar 23;282(12):8873–82.

73. Xie X, Gayen S, Kang C, Yuan Z, Shi PY. Membrane Topology and Function of Dengue Virus NS2A Protein. J Virol. 2013 Apr;87(8):4609–22.

74. Li Y, Li Q, Wong YL, Liew LSY, Kang C. Membrane topology of NS2B of dengue virus revealed by NMR spectroscopy. Biochim Biophys Acta. 2015 Oct;1848(10 Pt A):2244–52.

75. Li Y, Wong YL, Lee MY, Li Q, Wang QY, Lescar J, et al. Secondary Structure and Membrane Topology of the Full-Length Dengue Virus NS4B in Micelles. Angew Chem Int Ed Engl. 2016 Sep 19;55(39):12068–72.

76. Sessions OM, Barrows NJ, Souza-Neto JA, Robinson TJ, Hershey CL, Rodgers MA, et al. Discovery of insect and human dengue virus host factors. Nature. 2009 Apr 23;458(7241):1047–50.

77. Heaton NS, Moshkina N, Fenouil R, Gardner TJ, Aguirre S, Shah PS, et al. Targeting Viral Proteostasis Limits Influenza Virus, HIV, and Dengue Virus Infection. Immunity. 2016 Jan 19;44(1):46–58.

78. Marceau CD, Puschnik AS, Majzoub K, Ooi YS, Brewer SM, Fuchs G, et al. Genetic dissection of Flaviviridae host factors through genome-scale CRISPR screens. Nature. 2016 Jul 7;535(7610):159–63.

79. Zhang R, Miner JJ, Gorman MJ, Rausch K, Ramage H, White JP, et al. A CRISPR screen defines a signal peptide processing pathway required by flaviviruses. Nature. 2016 Jul 7;535(7610):164–8.

80. Keenan RJ, Freymann DM, Stroud RM, Walter P. The signal recognition particle. Annu Rev Biochem. 2001;70:755–75.

81. Denks K, Vogt A, Sachelaru I, Petriman NA, Kudva R, Koch HG. The Sec translocon mediated protein transport in prokaryotes and eukaryotes. Mol Membr Biol. 2014 May;31(2–3):58–84.

82. Krishnan MN, Ng A, Sukumaran B, Gilfoy FD, Uchil PD, Sultana H, et al. RNA interference screen for human genes associated with West Nile virus infection. Nature. 2008 Sep 11;455(7210):242–5.

83. Hoffmann HH, Schneider WM, Rozen-Gagnon K, Miles LA, Schuster F, Razooky B, et al. TMEM41B Is a Pan-flavivirus Host Factor. Cell. 2021 Jan 7;184(1):133-148.e20.

84. Monel B, Compton AA, Bruel T, Amraoui S, Burlaud-Gaillard J, Roy N, et al. Zika virus induces massive cytoplasmic vacuolization and paraptosis-like death in infected cells. EMBO J. 2017 Jun 14;36(12):1653–68.

85. Jonikas MC, Collins SR, Denic V, Oh E, Quan EM, Schmid V, et al. Comprehensive characterization of genes required for protein folding in the endoplasmic reticulum. Science. 2009 Mar 27;323(5922):1693–7.

86. Shurtleff MJ, Itzhak DN, Hussmann JA, Schirle Oakdale NT, Costa EA, Jonikas M, et al. The ER membrane protein complex interacts cotranslationally to enable biogenesis of multipass membrane proteins. Ron D, editor. eLife. 2018 May 29;7:e37018.

87. Ma H, Dang Y, Wu Y, Jia G, Anaya E, Zhang J, et al. A CRISPR-Based Screen Identifies Genes Essential for West-Nile-Virus-Induced Cell Death. Cell Reports. 2015 Jul 28;12(4):673–83.

88. Savidis G, McDougall WM, Meraner P, Perreira JM, Portmann JM, Trincucci G, et al. Identification of Zika Virus and Dengue Virus Dependency Factors using Functional Genomics. Cell Reports. 2016 Jun 28;16(1):232–46.

89. Lin DL, Inoue T, Chen YJ, Chang A, Tsai B, Tai AW. The ER Membrane Protein Complex Promotes Biogenesis of Dengue and Zika Virus Non-structural Multi-pass Transmembrane Proteins to Support Infection. Cell Rep. 2019 May 7;27(6):1666-1674.e4.

90. Ngo AM, Shurtleff MJ, Popova KD, Kulsuptrakul J, Weissman JS, Puschnik AS. The ER membrane protein complex is required to ensure correct topology and stable expression of flavivirus polyproteins. Gao G, Kirkegaard K, Sanyal S, editors. eLife. 2019 Sep 13;8:e48469.

91. Barrows NJ, Anglero-Rodriguez Y, Kim B, Jamison SF, Le Sommer C, McGee CE, et al. Dual roles for the ER membrane protein complex in flavivirus infection: viral entry and protein biogenesis. Sci Rep. 2019 Jul 4;9(1):9711.

92. Hafirassou ML, Meertens L, Umaña-Diaz C, Labeau A, Dejarnac O, Bonnet-Madin L, et al. A Global Interactome Map of the Dengue Virus NS1 Identifies Virus Restriction and Dependency Host Factors. Cell Rep. 2017 Dec 26;21(13):3900–13.

93. Roosendaal J, Westaway EG, Khromykh A, Mackenzie JM. Regulated cleavages at the West Nile virus NS4A-2K-NS4B junctions play a major role in rearranging cytoplasmic membranes and Golgi trafficking of the NS4A protein. J Virol. 2006 May;80(9):4623–32.

94. Kaufusi PH, Kelley JF, Yanagihara R, Nerurkar VR. Induction of endoplasmic reticulum-derived replication-competent membrane structures by West Nile virus non-structural protein 4B. PLoS One. 2014;9(1):e84040.

95. Lee CM, Xie X, Zou J, Li SH, Lee MYQ, Dong H, et al. Determinants of Dengue Virus NS4A Protein Oligomerization. J Virol. 2015 Jun;89(12):6171–83.

96. Goyal U, Blackstone C. Untangling the web: mechanisms underlying ER network formation. Biochim Biophys Acta. 2013 Nov;1833(11):2492–8.

97. Wang S, Tukachinsky H, Romano FB, Rapoport TA. Cooperation of the ER-shaping proteins atlastin, lunapark, and reticulons to generate a tubular membrane network. Kozlov M, editor. eLife. 2016 Sep 13;5:e18605.

98. Zurek N, Sparks L, Voeltz G. Reticulon short hairpin transmembrane domains are used to shape ER tubules. Traffic. 2011 Jan;12(1):28–41.

99. Tang WF, Yang SY, Wu BW, Jheng JR, Chen YL, Shih CH, et al. Reticulon 3 binds the 2C protein of enterovirus 71 and is required for viral replication. J Biol Chem. 2007 Feb 23;282(8):5888–98.

100. Diaz A, Wang X, Ahlquist P. Membrane-shaping host reticulon proteins play crucial roles in viral RNA replication compartment formation and function. Proc Natl Acad Sci U S A. 2010 Sep 14;107(37):16291–6.

101. Barajas D, Xu K, Sharma M, Wu CY, Nagy PD. Tombusviruses upregulate phospholipid biosynthesis via interaction between p33 replication protein and yeast lipid sensor proteins during virus replication in yeast. Virology. 2014 Dec;471–473:72–80.

102. Aktepe TE, Liebscher S, Prier JE, Simmons CP, Mackenzie JM. The Host Protein Reticulon 3.1A Is Utilized by Flaviviruses to Facilitate Membrane Remodelling. Cell Rep. 2017 Nov 7;21(6):1639–54.

103. Rismanchi N, Soderblom C, Stadler J, Zhu PP, Blackstone C. Atlastin GTPases are required for Golgi apparatus and ER morphogenesis. Hum Mol Genet. 2008 Jun 1;17(11):1591–604.

104. Hu J, Shibata Y, Zhu PP, Voss C, Rismanchi N, Prinz WA, et al. A class of dynamin-like GTPases involved in the generation of the tubular ER network. Cell. 2009 Aug 7;138(3):549–61.

105. Monel B, Rajah MM, Hafirassou ML, Sid Ahmed S, Burlaud-Gaillard J, Zhu PP, et al. Atlastin Endoplasmic Reticulum-Shaping Proteins Facilitate Zika Virus Replication. J Virol. 2019 Dec 1;93(23):e01047-19.

106. Neufeldt CJ, Cortese M, Scaturro P, Cerikan B, Wideman JG, Tabata K, et al. ER-shaping atlastin proteins act as central hubs to promote flavivirus replication and virion assembly. Nat Microbiol. 2019 Dec;4(12):2416–29.

107. Chen S, Desai T, McNew JA, Gerard P, Novick PJ, Ferro-Novick S. Lunapark stabilizes nascent three-way junctions in the endoplasmic reticulum. Proc Natl Acad Sci U S A. 2015 Jan 13;112(2):418–23.

108. Tran PTH, Asghar N, Johansson M, Melik W. Roles of the Endogenous Lunapark Protein during Flavivirus Replication. Viruses. 2021 Jul;13(7):1198.

109. Zhao YG, Chen Y, Miao G, Zhao H, Qu W, Li D, et al. The ER-Localized Transmembrane Protein EPG-3/VMP1 Regulates SERCA Activity to Control ER-Isolation Membrane Contacts for Autophagosome Formation. Mol Cell. 2017 Sep 21;67(6):974-989.e6.

110. Moretti F, Bergman P, Dodgson S, Marcellin D, Claerr I, Goodwin JM, et al. TMEM41B is a novel regulator of autophagy and lipid mobilization. EMBO Rep. 2018 Sep;19(9):e45889.

111. Morita K, Hama Y, Mizushima N. TMEM41B functions with VMP1 in autophagosome formation. Autophagy. 2019 May;15(5):922–3.

112. Huang D, Xu B, Liu L, Wu L, Zhu Y, Ghanbarpour A, et al. TMEM41B acts as an ER scramblase required for lipoprotein biogenesis and lipid homeostasis. Cell Metab. 2021 Aug 3;33(8):1655-1670.e8.

113. Teo CSH, Chu JJH. Cellular vimentin regulates construction of dengue virus replication complexes through interaction with NS4A protein. J Virol. 2014 Feb;88(4):1897–913.

114. Adams DR, Ron D, Kiely PA. RACK1, A multifaceted scaffolding protein: Structure and function. Cell Commun Signal. 2011 Oct 6;9:22.

115. Shue B, Chiramel AI, Cerikan B, To TH, Frölich S, Pederson SM, et al. Genome-Wide CRISPR Screen Identifies RACK1 as a Critical Host Factor for Flavivirus Replication. J Virol. 2021 Nov 23;95(24):e0059621.

116. Junjhon J, Pennington JG, Edwards TJ, Perera R, Lanman J, Kuhn RJ. Ultrastructural characterization and three-dimensional architecture of replication sites in dengue virus-infected mosquito cells. J Virol. 2014 May;88(9):4687–97.

117. Hanners NW, Eitson JL, Usui N, Richardson RB, Wexler EM, Konopka G, et al. Western Zika Virus in Human Fetal Neural Progenitors Persists Long Term with Partial Cytopathic and Limited Immunogenic Effects. Cell Rep. 2016 Jun 14;15(11):2315–22.

118. Cortese M, Goellner S, Acosta EG, Neufeldt CJ, Oleksiuk O, Lampe M, et al. Ultrastructural Characterization of Zika Virus Replication Factories. Cell Rep. 2017 Feb 28;18(9):2113–23.

119. Offerdahl DK, Dorward DW, Hansen BT, Bloom ME. Cytoarchitecture of Zika virus infection in human neuroblastoma and *Aedes albopictus* cell lines. Virology. 2017 Jan 15;501:54–62.

120. Chatel-Chaix L, Cortese M, Romero-Brey I, Bender S, Neufeldt CJ, Fischl W, et al. Dengue Virus Perturbs Mitochondrial Morphodynamics to Dampen Innate Immune Responses. Cell Host Microbe. 2016 Sep 14;20(3):342–56.

121. Stadler K, Allison SL, Schalich J, Heinz FX. Proteolytic activation of tick-borne encephalitis virus by furin. J Virol. 1997 Nov;71(11):8475–81.

122. Yu IM, Zhang W, Holdaway HA, Li L, Kostyuchenko VA, Chipman PR, et al. Structure of the immature dengue virus at low pH primes proteolytic maturation. Science. 2008 Mar 28;319(5871):1834–7.

123. Zheng A, Yuan F, Kleinfelter LM, Kielian M. A toggle switch controls the low pH-triggered rearrangement and maturation of the dengue virus envelope proteins. Nat Commun. 2014 May 20;5(1):3877.

124. Carpp LN, Rogers RS, Moritz RL, Aitchison JD. Quantitative proteomic analysis of host-virus interactions reveals a role for Golgi brefeldin A resistance factor 1 (GBF1) in dengue infection. Mol Cell Proteomics. 2014 Nov;13(11):2836–54.

125. Jouvenet N, Neil SJD, Zhadina M, Zang T, Kratovac Z, Lee Y, et al. Broad-spectrum inhibition of retroviral and filoviral particle release by tetherin. J Virol. 2009 Feb;83(4):1837–44.

126. Sakuma T, Noda T, Urata S, Kawaoka Y, Yasuda J. Inhibition of Lassa and Marburg virus production by tetherin. J Virol. 2009 Mar;83(5):2382–5.

127. Liu Y, Luo S, He S, Zhang M, Wang P, Li C, et al. Tetherin restricts HSV-2 release and is counteracted by multiple viral glycoproteins. Virology. 2015 Jan 15;475:96–109.

128. Ooi YS, Dubé M, Kielian M. BST2/Tetherin Inhibition of Alphavirus Exit. Viruses. 2015 Apr;7(4):2147–67.

129. Neil SJD, Zang T, Bieniasz PD. Tetherin inhibits retrovirus release and is antagonized by HIV-1 Vpu. Nature. 2008 Jan 24;451(7177):425–30.

130. Pan XB, Han JC, Cong X, Wei L. BST2/Tetherin Inhibits Dengue Virus Release from Human Hepatoma Cells. PLOS ONE. 2012 Dec 7;7(12):e51033.

131. Li M, Wang P, Zheng Z, Hu K, Zhang M, Guan X, et al. Japanese encephalitis virus counteracts BST2 restriction via its envelope protein E. Virology. 2017 Oct 1;510:67–75.

132. Bento CF, Renna M, Ghislat G, Puri C, Ashkenazi A, Vicinanza M, et al. Mammalian Autophagy: How Does It Work? Annu Rev Biochem. 2016 Jun 2;85:685–713.

133. Gatica D, Lahiri V, Klionsky DJ. Cargo recognition and degradation by selective autophagy. Nat Cell Biol. 2018 Mar;20(3):233–42.

134. Choi Y, Bowman JW, Jung JU. Autophagy during viral infection — a double-edged sword. Nat Rev Microbiol. 2018 Jun;16(6):341–54.

135. Ke PY. The Multifaceted Roles of Autophagy in Flavivirus-Host Interactions. Int J Mol Sci. 2018 Dec 7;19(12):3940.

136. Echavarria-Consuegra L, Smit JM, Reggiori F. Role of autophagy during the replication and pathogenesis of common mosquito-borne flavi- and alphaviruses. Open Biol. 2019 Mar 29;9(3):190009.

137. Heaton NS, Randall G. Dengue virus-induced autophagy regulates lipid metabolism. Cell Host Microbe. 2010 Nov 18;8(5):422–32.

138. Perera R, Riley C, Isaac G, Hopf-Jannasch AS, Moore RJ, Weitz KW, et al. Dengue Virus Infection Perturbs Lipid Homeostasis in Infected Mosquito Cells. PLOS Pathogens. 2012 Mar 22;8(3):e1002584.

139. Jordan TX, Randall G. Dengue Virus Activates the AMP Kinase-mTOR Axis To Stimulate a Proviral Lipophagy. J Virol. 2017 Jun 1;91(11):e02020-16.

140. Chotiwan N, Andre BG, Sanchez-Vargas I, Islam MN, Grabowski JM, Hopf-Jannasch A, et al. Dynamic remodeling of lipids coincides with dengue virus replication in the midgut of *Aedes aegypti* mosquitoes. PLOS Pathogens. 2018 Feb 15;14(2):e1006853.

141. Koh C, Islam MN, Ye YH, Chotiwan N, Graham B, Belisle JT, et al. Dengue virus dominates lipid metabolism modulations in Wolbachia-coinfected *Aedes aegypti*. Commun Biol. 2020 Sep 18;3(1):1–14.

142. Zhang J, Lan Y, Li MY, Lamers MM, Fusade-Boyer M, Klemm E, et al. Flaviviruses Exploit the Lipid Droplet Protein AUP1 to Trigger Lipophagy and Drive Virus Production. Cell Host Microbe. 2018 Jun 13;23(6):819-831.e5.

143. McLean JE, Wudzinska A, Datan E, Quaglino D, Zakeri Z. Flavivirus NS4A-induced Autophagy Protects Cells against Death and Enhances Virus Replication. J Biol Chem. 2011 Jun 24;286(25):22147–59.

144. Lu ZY, Cheng MH, Yu CY, Lin YS, Yeh TM, Chen CL, et al. Dengue Nonstructural Protein 1 Maintains Autophagy through Retarding Caspase-Mediated Cleavage of Beclin-1. Int J Mol Sci. 2020 Dec 19;21(24):E9702.

145. Lennemann NJ, Coyne CB. Dengue and Zika viruses subvert reticulophagy by NS2B3-mediated cleavage of FAM134B. Autophagy. 2017 Feb;13(2):322–32.

146. Ponia SS, Robertson SJ, McNally KL, Subramanian G, Sturdevant GL, Lewis M, et al. Mitophagy antagonism by ZIKV reveals Ajuba as a regulator of PINK1 signaling, PKR-dependent inflammation, and viral invasion of tissues. Cell Reports. 2021 Oct 26;37(4):109888.

147. Kobayashi S, Yoshii K, Phongphaew W, Muto M, Hirano M, Orba Y, et al. West Nile virus capsid protein inhibits autophagy by AMP-activated protein kinase degradation in neurological disease development. PLoS Pathog. 2020 Jan 23;16(1):e1008238.

148. Sharma KB, Chhabra S, Aggarwal S, Tripathi A, Banerjee A, Yadav AK, et al. Proteomic landscape of Japanese encephalitis virus-infected fibroblasts. J Gen Virol. 2021 Sep;102(9).

149. Sarkar R, Sharma KB, Kumari A, Asthana S, Kalia M. Japanese encephalitis virus capsid protein interacts with non-lipidated MAP1LC3 on replication membranes and lipid droplets. J Gen Virol. 2021 Jan;102(1).

150. Shives KD, Beatman EL, Chamanian M, O'Brien C, Hobson-Peters J, Beckham JD. West Nile Virus-Induced Activation of Mammalian Target of Rapamycin Complex 1 Supports Viral Growth and Viral Protein Expression. Journal of Virology. 2014 Aug;88(16):9458.

151. Liang Q, Luo Z, Zeng J, Chen W, Foo SS, Lee SA, et al. Zika Virus NS4A and NS4B Proteins Deregulate Akt-mTOR Signaling in Human Fetal Neural Stem Cells to Inhibit Neurogenesis and Induce Autophagy. Cell Stem Cell. 2016 Nov 3;19(5):663–71.

152. Sahoo BR, Pattnaik A, Annamalai AS, Franco R, Pattnaik AK. Mechanistic Target of Rapamycin Signaling Activation Antagonizes Autophagy To Facilitate Zika Virus Replication. J Virol. 2020 Oct 27;94(22):e01575-20.

153. Lahon A, Arya RP, Banerjea AC. Dengue Virus Dysregulates Master Transcription Factors and PI3K/AKT/mTOR Signaling Pathway in Megakaryocytes. Front Cell Infect Microbiol. 2021;11:715208.

154. Galluzzi L, Baehrecke EH, Ballabio A, Boya P, Bravo-San Pedro JM, Cecconi F, et al. Molecular definitions of autophagy and related processes. EMBO J. 2017 Jul 3;36(13):1811–36.

155. Gubas A, Dikic I. A guide to the regulation of selective autophagy receptors. FEBS J. 2022 Jan;289(1):75–89.

156. Anand SK, Tikoo SK. Viruses as modulators of mitochondrial functions. Adv Virol. 2013;2013:738794.

157. Westermann B. Mitochondrial fusion and fission in cell life and death. Nat Rev Mol Cell Biol. 2010 Dec;11(12):872–84.

158. Barbier V, Lang D, Valois S, Rothman AL, Medin CL. Dengue virus induces mitochondrial elongation through impairment of Drp1-triggered mitochondrial fission. Virology. 2017 Jan;500:149–60.

159. García CC, Vázquez CA, Giovannoni F, Russo CA, Cordo SM, Alaimo A, et al. Cellular Organelles Reorganization During Zika Virus Infection of Human Cells. Frontiers in Microbiology. 2020;11:1558.

160. Yang S, Gorshkov K, Lee EM, Xu M, Cheng YS, Sun N, et al. Zika Virus-Induced Neuronal Apoptosis via Increased Mitochondrial Fragmentation. Front Microbiol. 2020 Dec 23;11:598203.

161. Yu CY, Liang JJ, Li JK, Lee YL, Chang BL, Su CI, et al. Dengue Virus Impairs Mitochondrial Fusion by Cleaving Mitofusins. PLOS Pathogens. 2015 Dec 30;11(12):e1005350.

162. Roach T, Alcendor DJ. Zika virus infection of cellular components of the blood-retinal barriers: implications for viral associated congenital ocular disease. J Neuroinflammation. 2017 Mar 3;14(1):43.

163. Carod-Artal FJ. Neurological complications of Zika virus infection. Expert Review of Anti-infective Therapy. 2018 May 4;16(5):399–410.

164. Norat P, Soldozy S, Sokolowski JD, Gorick CM, Kumar JS, Chae Y, et al. Mitochondrial dysfunction in neurological disorders: Exploring mitochondrial transplantation. npj Regen Med. 2020 Nov 23;5(1):1–9.

165. Pacheu-Grau D, Rucktäschel R, Deckers M. Mitochondrial dysfunction and its role in tissue-specific cellular stress. Cell Stress. 2(8):184–99.

166. Sun E, Zhao J, TaoYang, Xu Q, Qin Y, Wang W, et al. Antibodies generated by immunization with the NS1 protein of West Nile virus confer partial protection against lethal Japanese encephalitis virus challenge. Vet Microbiol. 2013 Sep 27;166(1–2):145–53.

167. Douradinha B, McBurney SP, Soares de Melo KM, Smith AP, Krishna NK, Barratt-Boyes SM, et al. C1q binding to dengue virus decreases levels of infection and inflammatory molecules transcription in THP-1 cells. Virus Research. 2014 Jan 22;179:231–4.

168. Wessel AW, Doyle MP, Engdahl TB, Rodriguez J, Crowe JE, Diamond MS. Human Monoclonal Antibodies against NS1 Protein Protect against Lethal West Nile Virus Infection. mBio. 2021 Oct 26;12(5):e0244021.

169. Heil F, Hemmi H, Hochrein H, Ampenberger F, Kirschning C, Akira S, et al. Species-Specific Recognition of Single-Stranded RNA via Toll-like Receptor 7 and 8. Science. 2004 Mar 5;303(5663):1526–9.

170. Tsai YT, Chang SY, Lee CN, Kao CL. Human TLR3 recognizes dengue virus and modulates viral replication in vitro. Cellular Microbiology. 2009;11(4):604–15.

171. Yoneyama M, Kikuchi M, Matsumoto K, Imaizumi T, Miyagishi M, Taira K, et al. Shared and Unique Functions of the DExD/H-Box Helicases RIG-I, MDA5, and LGP2 in Antiviral Innate Immunity. The Journal of Immunology. 2005 Sep 1;175(5):2851–8.

172. Sun L, Wu J, Du F, Chen X, Chen ZJ. Cyclic GMP-AMP synthase is a cytosolic DNA sensor that activates the type I interferon pathway. Science. 2013 Feb 15;339(6121):786–91.

173. Kawasaki T, Kawai T. Toll-Like Receptor Signaling Pathways. Frontiers in Immunology. 2014;5:461.

174. Chiang JJ, Davis ME, Gack MU. Regulation of RIG-I-like receptor signaling by host and viral proteins. Cytokine Growth Factor Rev. 2014 Oct;25(5):491–505.

175. Cai X, Chiu YH, Chen ZJ. The cGAS-cGAMP-STING pathway of cytosolic DNA sensing and signaling. Mol Cell. 2014 Apr 24;54(2):289–96.

176. Nasirudeen AMA, Wong HH, Thien P, Xu S, Lam KP, Liu DX. RIG-I, MDA5 and TLR3 Synergistically Play an Important Role in Restriction of Dengue Virus Infection. PLOS Neglected Tropical Diseases. 2011 thg 1;5(1):e926.

177. Liu HM, Loo YM, Horner SM, Zornetzer GA, Katze MG, Gale M. The mitochondrial targeting chaperone 14-3-3ε regulates a RIG-I translocon that mediates membrane association and innate antiviral immunity. Cell Host Microbe. 2012 May 17;11(5):528–37.

178. Chan YK, Gack MU. A phosphomimetic-based mechanism of dengue virus to antagonize innate immunity. Nat Immunol. 2016 May;17(5):523–30.

179. Riedl W, Acharya D, Lee JH, Liu G, Serman T, Chiang C, et al. Zika Virus NS3 Mimics a Cellular 14-3-3-Binding Motif to Antagonize RIG-I- and MDA5-Mediated Innate Immunity. Cell Host & Microbe. 2019 Oct 9;26(4):493-503.e6.

180. He Z, Zhu X, Wen W, Yuan J, Hu Y, Chen J, et al. Dengue Virus Subverts Host Innate Immunity by Targeting Adaptor Protein MAVS. J Virol. 2016 Jul 27;90(16):7219–30.

181. Dalrymple NA, Cimica V, Mackow ER. Dengue Virus NS Proteins Inhibit RIG-I/MAVS Signaling by Blocking TBK1/IRF3 Phosphorylation: Dengue Virus Serotype 1 NS4A Is a Unique Interferon-Regulating Virulence Determinant. mBio. 2015 May 12;6(3):e00553-00515.

182. Angleró-Rodríguez YI, Pantoja P, Sariol CA. Dengue Virus Subverts the Interferon Induction Pathway via NS2B/3 Protease-IκB Kinase ε Interaction. Clinical and Vaccine Immunology. 2014 Jan 1;21(1):29–38.

183. Ye J, Chen Z, Li Y, Zhao Z, He W, Zohaib A, et al. Japanese Encephalitis Virus NS5 Inhibits Type I Interferon (IFN) Production by Blocking the Nuclear Translocation of IFN Regulatory Factor 3 and NF-κB. J Virol. 2017 Apr 15;91(8):e00039-17.

184. Sun B, Sundström KB, Chew JJ, Bist P, Gan ES, Tan HC, et al. Dengue virus activates cGAS through the release of mitochondrial DNA. Sci Rep. 2017 Jun 15;7(1):3594.

185. Aguirre S, Luthra P, Sanchez-Aparicio MT, Maestre AM, Patel J, Lamothe F, et al. Dengue virus NS2B protein targets cGAS for degradation and prevents mitochondrial DNA sensing during infection. Nat Microbiol. 2017 Mar 27;2:17037.

186. Aguirre S, Maestre AM, Pagni S, Patel JR, Savage T, Gutman D, et al. DENV inhibits type I IFN production in infected cells by cleaving human STING. PLoS Pathog. 2012;8(10):e1002934.

187. Yu CY, Chang TH, Liang JJ, Chiang RL, Lee YL, Liao CL, et al. Dengue Virus Targets the Adaptor Protein MITA to Subvert Host Innate Immunity. PLOS Pathogens. 2012 Jun 28;8(6):e1002780.

188. Zheng Y, Liu Q, Wu Y, Ma L, Zhang Z, Liu T, et al. Zika virus elicits inflammation to evade antiviral response by cleaving cGAS via NS1-caspase-1 axis. EMBO J. 2018 Sep 14;37(18):e99347.

189. Hannemann H, Sung PY, Chiu HC, Yousuf A, Bird J, Lim SP, et al. Serotype-specific differences in dengue virus non-structural protein 5 nuclear localization. J Biol Chem. 2013 Aug 2;288(31):22621–35.

190. Zhao Y, Soh TS, Zheng J, Chan KWK, Phoo WW, Lee CC, et al. A Crystal Structure of the Dengue Virus NS5 Protein Reveals a Novel Inter-domain Interface Essential for Protein Flexibility and Virus Replication. PLoS Pathog. 2015 Mar 16;11(3):e1004682.

191. Grant A, Ponia SS, Tripathi S, Balasubramaniam V, Miorin L, Sourisseau M, et al. Zika Virus Targets Human STAT2 to Inhibit Type I Interferon Signaling. Cell Host Microbe. 2016 Jun 8;19(6):882–90.

192. Kumar A, Hou S, Airo AM, Limonta D, Mancinelli V, Branton W, et al. Zika virus inhibits type-I interferon production and downstream signaling. EMBO Rep. 2016 Dec;17(12):1766–75.

193. Tay MYF, Smith K, Ng IHW, Chan KWK, Zhao Y, Ooi EE, et al. The C-terminal 18 Amino Acid Region of Dengue Virus NS5 Regulates its Subcellular Localization and Contains a

Conserved Arginine Residue Essential for Infectious Virus Production. PLOS Pathogens. 2016 thg 9;12(9):e1005886.

194. Duan Y, Zeng M, Zhang W, Liu P, Yang C, Wang M, et al. Expression and purification of the truncated duck DTMUV NS5 protein and the subcellular localization of NS5 in vitro. Poultry Science. 2019 Jul 1;98(7):2989–96.

195. Cheng CX, Alvin Tan MJ, Chan KWK, Watanabe S, Wang S, Choy MM, et al. In Vitro and In Vivo Stability of P884T, a Mutation that Relocalizes Dengue Virus 2 Non-structural Protein 5. ACS Infect Dis. 2021 Dec 10;7(12):3277–91.

196. Petit MJ, Kenaston MW, Pham OH, Nagainis AA, Fishburn AT, Shah PS. Nuclear dengue virus NS5 antagonizes expression of PAF1-dependent immune response genes. PLoS Pathog. 2021 Nov 19;17(11):e1010100.

197. Khadka S, Vangeloff AD, Zhang C, Siddavatam P, Heaton NS, Wang L, et al. A physical interaction network of dengue virus and human proteins. Mol Cell Proteomics. 2011 Dec;10(12):M111.012187.

198. Le Breton M, Meyniel-Schicklin L, Deloire A, Coutard B, Canard B, de Lamballerie X, et al. Flavivirus NS3 and NS5 proteins interaction network: a high-throughput yeast two-hybrid screen. BMC Microbiol. 2011 Oct 20;11:234.

199. De Maio FA, Risso G, Iglesias NG, Shah P, Pozzi B, Gebhard LG, et al. The Dengue Virus NS5 Protein Intrudes in the Cellular Spliceosome and Modulates Splicing. PLoS Pathog. 2016 Aug;12(8):e1005841.

200. Pozzi B, Bragado L, Mammi P, Torti MF, Gaioli N, Gebhard LG, et al. Dengue virus targets RBM10 deregulating host cell splicing and innate immune response. Nucleic Acids Res. 2020 Jul 9;48(12):6824–38.

201. Marazzi I, Ho JSY, Kim J, Manicassamy B, Dewell S, Albrecht RA, et al. Suppression of the antiviral response by an influenza histone mimic. Nature. 2012 Mar;483(7390):428–33.

202. Parnas O, Jovanovic M, Eisenhaure TM, Herbst RH, Dixit A, Ye CJ, et al. A Genome-wide CRISPR Screen in Primary Immune Cells to Dissect Regulatory Networks. Cell. 2015 Jul 30;162(3):675–86.

203. López-Denman AJ, Tuipulotu DE, Ross JB, Trenerry AM, White PA, Mackenzie JM. Nuclear localisation of West Nile virus NS5 protein modulates host gene expression. Virology. 2021 Jul;559:131–44.

204. Zhao Z, Tao M, Han W, Fan Z, Imran M, Cao S, et al. Nuclear localization of Zika virus NS5 contributes to suppression of type I interferon production and response. J Gen Virol. 2021 Mar;102(3).

205. Darnell JE, Kerr IM, Stark GR. Jak-STAT pathways and transcriptional activation in response to IFNs and other extracellular signaling proteins. Science. 1994 Jun 3;264(5164):1415–21.

206. Haller O, Kochs G, Weber F. The interferon response circuit: Induction and suppression by pathogenic viruses. Virology. 2006 Jan 5;344(1):119–30.

207. Muñoz-Jordán JL, Sánchez-Burgos GG, Laurent-Rolle M, García-Sastre A. Inhibition of interferon signaling by dengue virus. PNAS. 2003 Nov 25;100(24):14333–8.

208. Muñoz-Jordán JL, Laurent-Rolle M, Ashour J, Martínez-Sobrido L, Ashok M, Lipkin WI, et al. Inhibition of Alpha/Beta Interferon Signaling by the NS4B Protein of Flaviviruses. Journal of Virology. 2005 Jul 1;79(13):8004–13.

209. Best SM, Morris KL, Shannon JG, Robertson SJ, Mitzel DN, Park GS, et al. Inhibition of Interferon-Stimulated JAK-STAT Signaling by a Tick-Borne Flavivirus and Identification of NS5 as an Interferon Antagonist. Journal of Virology. 2005 Oct 15;79(20):12828–39.

210. Guo JT, Hayashi J, Seeger C. West Nile Virus Inhibits the Signal Transduction Pathway of Alpha Interferon. Journal of Virology. 2005 Feb 1;79(3):1343–50.

211. Lin RJ, Chang BL, Yu HP, Liao CL, Lin YL. Blocking of interferon-induced Jak-Stat signaling by Japanese encephalitis virus NS5 through a protein tyrosine phosphatase-mediated mechanism. J Virol. 2006 Jun;80(12):5908–18.

212. Park GS, Morris KL, Hallett RG, Bloom ME, Best SM. Identification of Residues Critical for the Interferon Antagonist Function of Langat Virus NS5 Reveals a Role for the RNA-Dependent RNA Polymerase Domain. Journal of Virology. 2007 Jul 1;81(13):6936–46.

213. Laurent-Rolle M, Boer EF, Lubick KJ, Wolfinbarger JB, Carmody AB, Rockx B, et al. The NS5 Protein of the Virulent West Nile Virus NY99 Strain Is a Potent Antagonist of Type I Interferon-Mediated JAK-STAT Signaling. Journal of Virology. 2010 Apr 1;84(7):3503–15.

214. Werme K, Wigerius M, Johansson M. Tick-borne encephalitis virus NS5 associates with membrane protein scribble and impairs interferon-stimulated JAK-STAT signalling. Cellular Microbiology. 2008;10(3):696–712.

215. Lubick KJ, Robertson SJ, McNally KL, Freedman BA, Rasmussen AL, Taylor RT, et al. Flavivirus Antagonism of Type I Interferon Signaling Reveals Prolidase as a Regulator of IFNAR1 Surface Expression. Cell Host Microbe. 2015 Jul 8;18(1):61–74.

216. Ashour J, Laurent-Rolle M, Shi PY, García-Sastre A. NS5 of Dengue Virus Mediates STAT2 Binding and Degradation. Journal of Virology. 2009 Jun 1;83(11):5408–18.

217. Mazzon M, Jones M, Davidson A, Chain B, Jacobs M. Dengue Virus NS5 Inhibits Interferon-α Signaling by Blocking Signal Transducer and Activator of Transcription 2 Phosphorylation. The Journal of Infectious Diseases. 2009 Oct 1;200(8):1261–70.

218. Morrison J, Laurent-Rolle M, Maestre AM, Rajsbaum R, Pisanelli G, Simon V, et al. Dengue Virus Co-opts UBR4 to Degrade STAT2 and Antagonize Type I Interferon Signaling. PLOS Pathogens. 2013 thg 3;9(3):e1003265.

219. Ashour J, Morrison J, Laurent-Rolle M, Belicha-Villanueva A, Plumlee CR, Bernal-Rubio D, et al. Mouse STAT2 Restricts Early Dengue Virus Replication. Cell Host Microbe. 2010 Nov 18;8(5):410–21.

220. Merle NS, Church SE, Fremeaux-Bacchi V, Roumenina LT. Complement System Part I – Molecular Mechanisms of Activation and Regulation. Frontiers in Immunology. 2015;6:262.

221. Kolev M, Friec GL, Kemper C. Complement — tapping into new sites and effector systems. Nat Rev Immunol. 2014 Dec;14(12):811–20.

222. Mehlhop E, Diamond MS. Protective immune responses against West Nile virus are primed by distinct complement activation pathways. Journal of Experimental Medicine. 2006 May 1;203(5):1371–81.

223. Merle NS, Noe R, Halbwachs-Mecarelli L, Fremeaux-Bacchi V, Roumenina LT. Complement System Part II: Role in Immunity. Frontiers in Immunology. 2015;6:257.

224. Avirutnan P, Fuchs A, Hauhart RE, Somnuke P, Youn S, Diamond MS, et al. Antagonism of the complement component C4 by flavivirus nonstructural protein NS1. J Exp Med. 2010 Apr 12;207(4):793–806.

225. Avirutnan P, Hauhart RE, Somnuke P, Blom AM, Diamond MS, Atkinson JP. Binding of Flavivirus Nonstructural Protein NS1 to C4b Binding Protein Modulates Complement Activation. The Journal of Immunology. 2011 Jul 1;187(1):424–33.

226. Chung KM, Liszewski MK, Nybakken G, Davis AE, Townsend RR, Fremont DH, et al. West Nile virus nonstructural protein NS1 inhibits complement activation by binding the regulatory protein factor H. PNAS. 2006 Dec 12;103(50):19111–6.

227. Thiemmeca S, Tamdet C, Punyadee N, Prommool T, Songjaeng A, Noisakran S, et al. Secreted NS1 Protects Dengue Virus from Mannose-Binding Lectin–Mediated Neutralization. The Journal of Immunology. 2016 Nov 15;197(10):4053–65.

228. Conde JN, da Silva EM, Allonso D, Coelho DR, Andrade I da S, de Medeiros LN, et al. Inhibition of the Membrane Attack Complex by Dengue Virus NS1 through Interaction with Vitronectin and Terminal Complement Proteins. J Virol. 2016 Nov 1;90(21):9570–81.

229. Miner JJ, Cao B, Govero J, Smith AM, Fernandez E, Cabrera OH, et al. Zika virus infection during pregnancy in mice causes placental damage and fetal demise. Cell. 2016 May 19;165(5):1081–91.

230. Jagger BW, Miner JJ, Cao B, Arora N, Smith AM, Kovacs A, et al. Gestational stage and IFN-λ signaling regulate ZIKV infection in utero. Cell Host Microbe. 2017 Sep 13;22(3):366-376.e3.

231. Rosenfeld AB, Doobin DJ, Warren AL, Racaniello VR, Vallee RB. Replication of early and recent Zika virus isolates throughout mouse brain development. Proc Natl Acad Sci U S A. 2017 Nov 14;114(46):12273–8.

232. Yuan L, Huang XY, Liu ZY, Zhang F, Zhu XL, Yu JY, et al. A single mutation in the prM protein of Zika virus contributes to fetal microcephaly. Science. 2017 Nov 17;358(6365):933–6.

233. Platt DJ, Smith AM, Arora N, Diamond MS, Coyne CB, Miner JJ. Zika virus-related neurotropic flaviviruses infect human placental explants and cause fetal demise in mice. Sci Transl Med. 2018 Jan 31;10(426):eaao7090.

234. Yockey LJ, Jurado KA, Arora N, Millet A, Rakib T, Milano KM, et al. Type I interferons instigate fetal demise after Zika virus infection. Sci Immunol. 2018 Jan 5;3(19):eaao1680.

235. Yamamoto S, Jaiswal M, Charng WL, Gambin T, Karaca E, Mirzaa G, et al. A *Drosophila* genetic resource of mutants to study mechanisms underlying human genetic diseases. Cell. 2014 Sep 25;159(1):200–14.

236. Link N, Chung H, Jolly A, Withers M, Tepe B, Arenkiel BR, et al. Mutations in ANKLE2, a ZIKA Virus Target, Disrupt an Asymmetric Cell Division Pathway in *Drosophila* Neuroblasts to Cause Microcephaly. Dev Cell. 2019 Dec 16;51(6):713-729.e6.

237. Pool KL, Adachi K, Karnezis S, Salamon N, Romero T, Nielsen-Saines K, et al. Association Between Neonatal Neuroimaging and Clinical Outcomes in Zika-Exposed Infants From Rio de Janeiro, Brazil. JAMA Network Open. 2019 Jul 31;2(7):e198124.

238. Chen W, Foo SS, Hong E, Wu C, Lee WS, Lee SA, et al. Zika virus NS3 protease induces bone morphogenetic protein-dependent brain calcification in human fetuses. Nat Microbiol. 2021 Apr;6(4):455–66.

239. Yoon KJ, Song G, Qian X, Pan J, Xu D, Rho HS, et al. Zika-Virus-Encoded NS2A Disrupts Mammalian Cortical Neurogenesis by Degrading Adherens Junction Proteins. Cell Stem Cell. 2017 Sep 7;21(3):349-358.e6.

Chapter 3: Molecular functions of ANKLE2 and its implications in human disease.

Ankyrin repeat and LEM domain containing 2 (ANKLE2) is a scaffolding protein with established roles in cell division and development, the dysfunction of which is increasingly implicated in human disease. ANKLE2 regulates nuclear envelope disassembly at the onset of mitosis and its reassembly after chromosome segregation. Its dysfunction is associated with abnormal nuclear morphology and cell division. ANKLE2 regulates the nuclear envelope by mediating protein-protein interactions with barrier to autointegration factor (BAF/BANF1) and with the kinase and phosphatase that modulate BAF's phosphorylation state. In brain development, ANKLE2 is crucial for proper asymmetric division of neural progenitor cells. In humans, pathogenic loss-of-function mutations in *ANKLE2* are associated with primary congenital microcephaly, a condition in which the brain is not properly developed at birth. ANKLE2 is also linked to other disease pathologies, including congenital Zika syndrome, cancer, and tauopathy. Here, we review the molecular roles of ANKLE2 and the recent literature on human diseases caused by its dysfunction.

Introduction

ANKLE2, also known as LEM4, KIAA0692, or MCPH16, is named after its LEM and ankyrin repeat domains (1). LEM domains form globular motifs composed of two parallel α-helices of ~40 amino acids and are mostly found in inner nuclear membrane (INM) proteins (2) (Appendix A-3). Named after the proteins in which they were first discovered: LAP2, emerin, and MAN1 (3,4), LEM domains mediate protein-protein interactions with barrier-to-autointegration factor (BAF, also known as BANF1) (5–7). BAF has distinct functions in the nucleus during different phases of the cell cycle. During interphase BAF has high mobility within the nucleoplasm where it binds chromatin and many nuclear proteins (8). During nuclear envelope reassembly BAF binds to

chromatin and membrane-bound LEM domain proteins, including ANKLE2, tethering DNA to the reforming nuclear envelope (9–11). This creates a meshwork with the nuclear lamina to provide stability to the nuclear envelope (Appendix A-3).

The second functional domain of ANKLE2 is its ankyrin repeat domain. Ankyrin repeat domains are widely found in proteins across the tree of life. Composed of 33 residues with a clear consensus sequence (12,13), these domains confer protein stability and scaffolding function for protein-protein interactions (14). They often occur in 2-7 tandem repeats, but can repeat up to 33 times (13). Given the high prevalence of ankyrin repeats in many proteins, their function is linked to many cellular processes, including molecule transport, adhesion, signaling, cytoskeletal stability, and cell division. Unsurprisingly, mutations in the ankyrin repeats of these proteins contribute to a wide array of human diseases (15).

The combination of both a LEM domain and ankyrin repeat domain in a single protein is rare, shared only by ANKLE2 and ANKLE1 (also known as LEM3). Like ANKLE2, ANKLE1 interacts with chromatin via a physical interaction with BAF (16). However, the functional similarities between these two proteins appear to end here, as ANKLE1 then acts as an endonuclease to cleave genomic or mitochondrial DNA (16–18). By contrast, ANKLE2 lacks any known enzymatic domains or activity, instead functioning as a scaffold for other protein-protein interactions. Several canonical ANKLE2-protein interactions mediate the stability of the nuclear envelope, assisting in cell division. However, proteomic studies suggest ANKLE2 likely has many other interacting partners (19–22), and is speculated to have diverse roles in cell biology and human disease as we will discuss later.

This review aims to provide background on the molecular structure and function of ANKLE2 and relate this to human disease. We review reported insights into the molecular and cellular functions of ANKLE2. Finally, we explore recent findings that suggest novel roles for ANKLE2 in neurodevelopment, cancer, neurodegenerative diseases, immune system development, and virus pathogenesis.

Conservation of ANKLE2 Molecular Architecture

ANKLE2 is conserved throughout metazoans. LEM proteins and the LEM domain are proposed to have coevolved with BAF to act as INM tethers (23). ANKLE2 contains both characterized and uncharacterized structural domains predicted by AlphaFold, and the organization of these motifs within ANKLE2 is consistent across orthologs (Figure 3-1). In humans and many other vertebrates ANKLE2 begins with an N-terminal transmembrane (TM) domain, which acts as an anchor to the INM and endoplasmic reticulum (ER) membrane. In human cells loss of this TM domain causes ANKLE2 to mislocalize to the cytoplasm (24,25). Interestingly, invertebrates do not have this TM domain (Figure 3-1B), although *Drosophila melanogaster* Ankle2 maintains INM and ER localization through an unknown mechanism (26). The LEM domain follows the TM domain, and its standard helix-linker-helix structure is maintained throughout vertebrates (Figure 3-1). Invertebrates have no recognizable LEM domain, although a LEM domain-equivalent might have a different organization or structure. Given the absence of a conserved LEM domain in invertebrates, it is especially interesting that the uncharacterized structure that follows the LEM domain (amino acids 197-252 in human ANKLE2) is present in all species examined (Figure 3-1B). This structure consists of 50-60 amino acids and is predicted to form a β sheet-α helix-β sheet-α helix (Figure 3-1A). In certain databases this region is annotated as a Caulimovirus viroplasmin VI domain, which in *Caulimoviruses* mediates the formation of viral inclusion bodies and acts as a site of virus assembly (27). For the sake of this review, we refer to this structured region as the Caulimovirus domain. It is worth noting that no study has determined if this region arose via horizontal gene transfer from these viruses or through convergent evolution. The potential function of the Caulimovirus domain in mediating specific ANKLE2 interactions will be discussed in more detail later.

Following the Caulimovirus domain is the ankyrin repeat domain, which acts as the scaffolding domain for protein-protein interactions (Figure 3-1A). The amino acids of the LEM and ankyrin

repeat domains are more highly conserved across orthologs compared to the rest of the protein (Figure 3-1C-E). Immediately following the ankyrin repeat domain is a large, structured region (amino acids 472-620 in human ANKLE2) of unknown significance or function. This region's presence and its overall organization is broadly conserved (Figure 3-1B). Given its proximity to the ankyrin repeat domain, this structured region might stabilize or expand its function. In vertebrates, the remainder of ANKLE2 appears to be disordered except for a small, structured region that coils back to interact with the previously mentioned uncharacterized structure. The space between each of these structured regions seemingly consists of intrinsically disordered protein (Appendix A-3). Intrinsically disordered regions are known to regulate protein-protein interactions and serve as sites for protein regulation and signaling (28,29). The molecular functions of these uncharacterized structured regions are largely unknown. However, they likely play key roles in ANKLE2 function as mutations that disrupt these regions are linked to human disease, as we discuss later in this review.

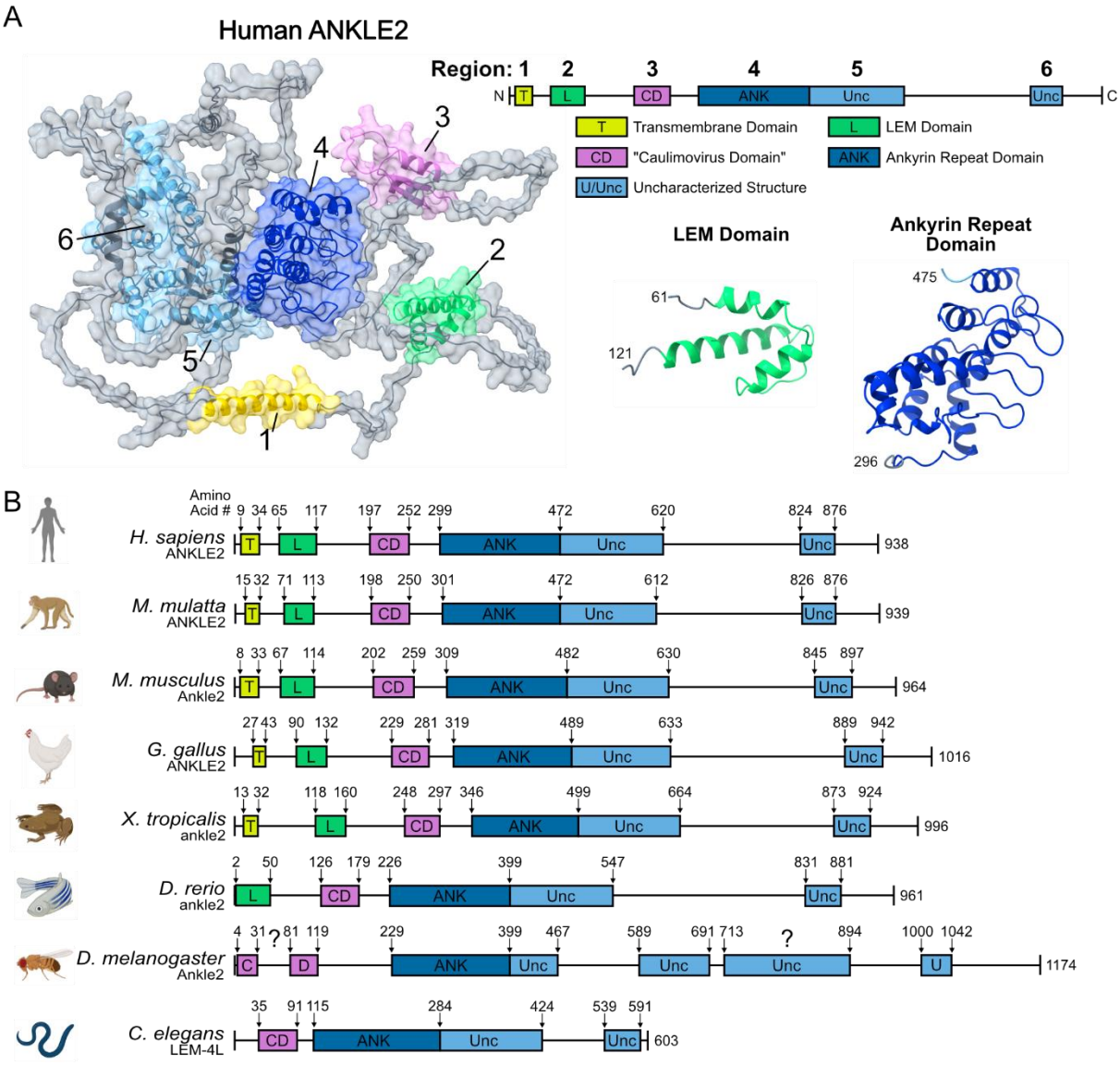
A
Human ANKLE2
Region: 1 2 3 4 5 6
N T L CD ANK Unc Unc C
T Transmembrane Domain
L LEM Domain
CD "Caulimovirus Domain"
ANK Ankyrin Repeat Domain
U/Unc Uncharacterized Structure
LEM Domain
61
121
Ankyrin Repeat Domain
475
296
B
Amino Acid #
H. sapiens ANKLE2 938
M. mulatta ANKLE2 939
M. musculus Ankle2 964
G. gallus ANKLE2 1016
X. tropicalis ankle2 996
D. rerio ankle2 961
D. melanogaster Ankle2 1174
C. elegans LEM-4L 603
C
Total ANKLE2
D
Ankyrin Repeat Domain
E
LEM Domain
H. sapiens
M. mulatta
M. musculus
G. gallus
X. tropicalis
D. rerio
D. melanogaster
C. elegans
Amino Acid Identity (%)

Figure 3-1: Conservation of ANKLE2 structural domains. A) AlphaFold structural prediction of human ANKLE2 (UniProt Q86XL3) with annotated and uncharacterized structural regions highlighted by color and number. **B)** ANKLE2 and orthologous sequences (sequences come from NCBI). Structured domains not previously annotated (such as LEM or ankyrin repeat domain) were identified using AlphaFold (103,104). Regions were considered structured if AlphaFold pLDDT was greater than 70 for each given residue. Transmembrane domains were annotated using DeepTMHMM (105). The Caulimovirus domain in *D. melanogaster* Ankle2 appears to maintain a similar structure but is broken into two segments with a β sheet-disordered region-α helix-β sheet-α helix organization. The region in *D. melanogaster* Ankle2 between 713-894 amino acids represents an uncharacterized structured region between region 5 and 6 with no clear orthologous region among other evaluated orthologs. **C-E)** Amino acid conservation among ANKLE2 orthologs and for specific protein domains (as shown in B) determined using Clustal Omega multiple sequence alignment (106). (C) Amino acid conservation in the total ANKLE2 protein sequence, (D) the ankyrin repeat domain, and (E) the LEM domain, showing that these vital domains have higher degrees of conservation.

Molecular and Cellular Functions of ANKLE2

Studies over the last decade have given insight into the cellular functions of ANKLE2, however, much is still unclear. In this section we will review the known functions of ANKLE2 in aspects of cell division, T cell development, and asymmetric division of neural progenitor cells.

Cell Division

A major feature of cell division is the assembly and disassembly of the nuclear envelope. During eukaryotic interphase, the nuclear envelope exists as a double lipid bilayer membrane. During mitosis, the nuclear envelope must disassemble to allow for chromosome condensation in

prophase and for chromatid segregation into the two daughter cells (30). Thereafter, the nuclear envelope must quickly and efficiently reassemble to enclose the DNA again. The initial disassembly of the nuclear envelope is triggered by phosphorylation of many nuclear envelope proteins (31,32). This includes the DNA-binding protein BAF, which is phosphorylated by the widely expressed serine/threonine kinase VRK1. Despite its small size, BAF has many binding partners and roles in the cell, including gene regulation, DNA damage responses, and defense against DNA viruses (8). BAF's phosphorylation reduces its DNA binding affinity (33) and alters its localization (33,34). During interphase, unphosphorylated BAF localizes diffusely throughout the nucleoplasm, where it interacts with chromatin (35). Early in mitosis, BAF is phosphorylated and becomes evenly distributed throughout the cytoplasm. After metaphase, BAF is dephosphorylated and localizes to the DNA "core region" around centromeres. Interestingly, BAF is the first protein to associate with this region, where it forms an immobile complex with other proteins to enable nuclear envelope reassembly to be initiated (36). The depletion of BAF, or of its kinase VRK1, dramatically alters nuclear envelope architecture, chromatin dynamics during mitosis, and nuclear envelope reassembly in the roundworm *Caenorhabditis elegans* (37) or human cell lines (38). Thus, the coordination of BAF phosphorylation and localization are of crucial importance for nuclear envelope dynamics and for cell division in eukaryotic cells.

The first foundational study of ANKLE2 discovered its role in coordinating BAF-1/BAF phosphorylation and dephosphorylation in *C. elegans* and HeLa cells (39). The *C. elegans* ortholog of *ANKLE2*, named *lem-4 like* (*lem-4L*) due to the lack of a clear LEM domain, also plays a role in nuclear envelope formation and BAF regulation. Temperature-sensitive mutations in *lem-4L* are lethal in early *C. elegans* development and give rise to cells with defective nuclear morphology. Interestingly, a random mutagenesis suppressor screen (Appendix A-3) yielded a *lem-4L C. elegans* mutant line that could grow at previously lethal temperatures due to a newly introduced P69L mutation in the *VRK1* ortholog (*vrk-1*). RNAi silencing of *vrk-1* is tolerated in *lem-4L* mutants, despite being lethal in *lem-4L* wild-type embryos. Depletion *of vrk-1* in *lem-4L* mutants

restores nuclear morphology. This suggests that mutation or reduction of *vrk-1* suppresses the aberrant effects of *lem-4L* mutation. An analysis of BAF-1 phosphorylation states revealed that the silencing of *lem-4L,* but not other LEM genes (*lem-3, lem-2, or emr-1*), increases BAF-1 phosphorylation. Whereas, the silencing or mutation of *vrk-1* dramatically decreases BAF-1 phosphorylation, consistent with its ability to rescue *lem-4L* mutant lethality. Interestingly, the silencing and/or mutation of both *lem-4L* and *vrk-1* leads to balanced BAF-1 phosphorylation. These opposing effects on BAF-1 phosphorylation indicate that LEM-4L plays a role in reversing BAF-1 phosphorylation by VRK-1. Glutathione-S-transferase (GST) pulldown experiments (Appendix A-3) revealed that LEM-4L and VRK-1 physically interact, as do their human orthologs (ANKLE2 and VRK1), although it is unclear if this physical interaction is limited to a particular phase of the cell cycle. *In vitro* kinase assays revealed that both LEM-4L and human ANKLE2 can inhibit the VRK-1-mediated phosphorylation of BAF-1 in a concentration-dependent manner, via a mechanism that was initially unclear (39).

ANKLE2 also interacts with phosphatases. Proteomics studies have previously reported that human ANKLE2 interacts with several subunits of the serine/threonine protein phosphatase 2A (PP2A) complex (40,41). This complex has a broad substrate range and controls cell cycle entry and exit (40,42,43). Asencio et al. demonstrated in their 2012 study that ANKLE2 and PP2A (specifically subunits PP2A-C, PP2A-R1, and PP2A-B55α) physically interact, and that PP2A can directly dephosphorylate BAF *in vitro*. Interestingly, a truncated portion of ANKLE2 (amino acids 162-349) can interact with all these PP2A subunits, but a smaller truncated form (amino acids 255-349) that excludes the Caulimovirus domain (amino acids 197-252) cannot. This suggests that the Caulimovirus domain supports the interaction with PP2A. RNAi depletion of these PP2A subunits in HeLa cells decreases the anaphase recruitment of BAF to chromatin, indicating that PP2A regulates BAF's phosphorylation state to control mitosis. These trends were mirrored in *C. elegans* upon the silencing of the *C. elegans* orthologs *(let-92* and *tag-93* which are the orthologs of human PP2A-C and PP2C-B, respectively) (39).

Further studies in human cells expanded our knowledge of the range of cellular functions of ANKLE2. A study by Snyers et al. used ANKLE2-deficient HeLa cells to determine which regions of ANKLE2 mediate BAF-chromatin association during cell division (44). *ANKLE2* knockout HeLa cells expressing GFP-tagged BAF were analyzed using fluorescence microscopy. In these ANKLE2-deficient cells, the association of BAF with chromatin was dramatically reduced and BAF was diffusely localized in the cytoplasm. To determine which regions of ANKLE2 mediated this process, the authors generated various ANKLE2 truncation mutations and introduced them into the *ANKLE2* knockout cells. Surprisingly, mutants lacking the TM or LEM domain restored BAF's association with chromatin. However, three mutants lacking the Caulimovirus domain or C-terminal uncharacterized region of ANKLE2 (ANKLE2 241-938, 311-938, or 1-822) failed to restore this association (44). This further highlights the importance of the Caulimovirus domain and suggests that these conserved regions, for which the molecular functions are not fully understood, play vital roles in ANKLE2's regulation of BAF (Figure 3-1).

Another study has highlighted a potential mechanism to regulate ANKLE2's control of nuclear envelope reassembly. In 2016, Kaufmann et al. reported that ANKLE2 and the deacetylase, Sirtuin 2 (SIRT2), physically interact *in vitro*. SIRT2 has many substrate proteins that collectively regulate microtubule dynamics and cell cycle progression (45). Both the depletion and overexpression of SIRT2 lead to abnormal nuclear morphologies in U2OS cells, mimicking cells with depleted ANKLE2 (46). However, overexpression of ANKLE2 did not impact nuclear morphology. Kaufmann et al. (2016) then showed that SIRT2 directly deacetylates ANKLE2 and regulates the acetylation and phosphorylation of ANKLE2 during the cell cycle. Importantly, they showed that acetylation of K302 in the N-terminal portion of the ankyrin repeat domain of ANKLE2 is important for nuclear envelope reassembly in U2OS cells (46).

Together, these experiments established the model of ANKLE2-mediated control of nuclear envelope disassembly and reassembly. During interphase, unphosphorylated BAF is present in the nucleoplasm, where it may bind to chromatin and the nuclear envelope via lamins and LEM proteins, including ANKLE2. During interphase, some fraction of phosphorylated BAF may exist in the cytoplasm (35,47). On mitotic entry VRK1 phosphorylates the remaining nuclear BAF, reducing its affinity for DNA and its nuclear retention. Later, ANKLE2 inhibits the VRK1-mediated phosphorylation of BAF and PP2A dephosphorylates BAF, presumably via its physical interactions with ANKLE2. This restores the binding of DNA to BAF, allowing BAF to concentrate at the “core region” after anaphase and to initiate nuclear envelope reassembly (Figure 3-2).

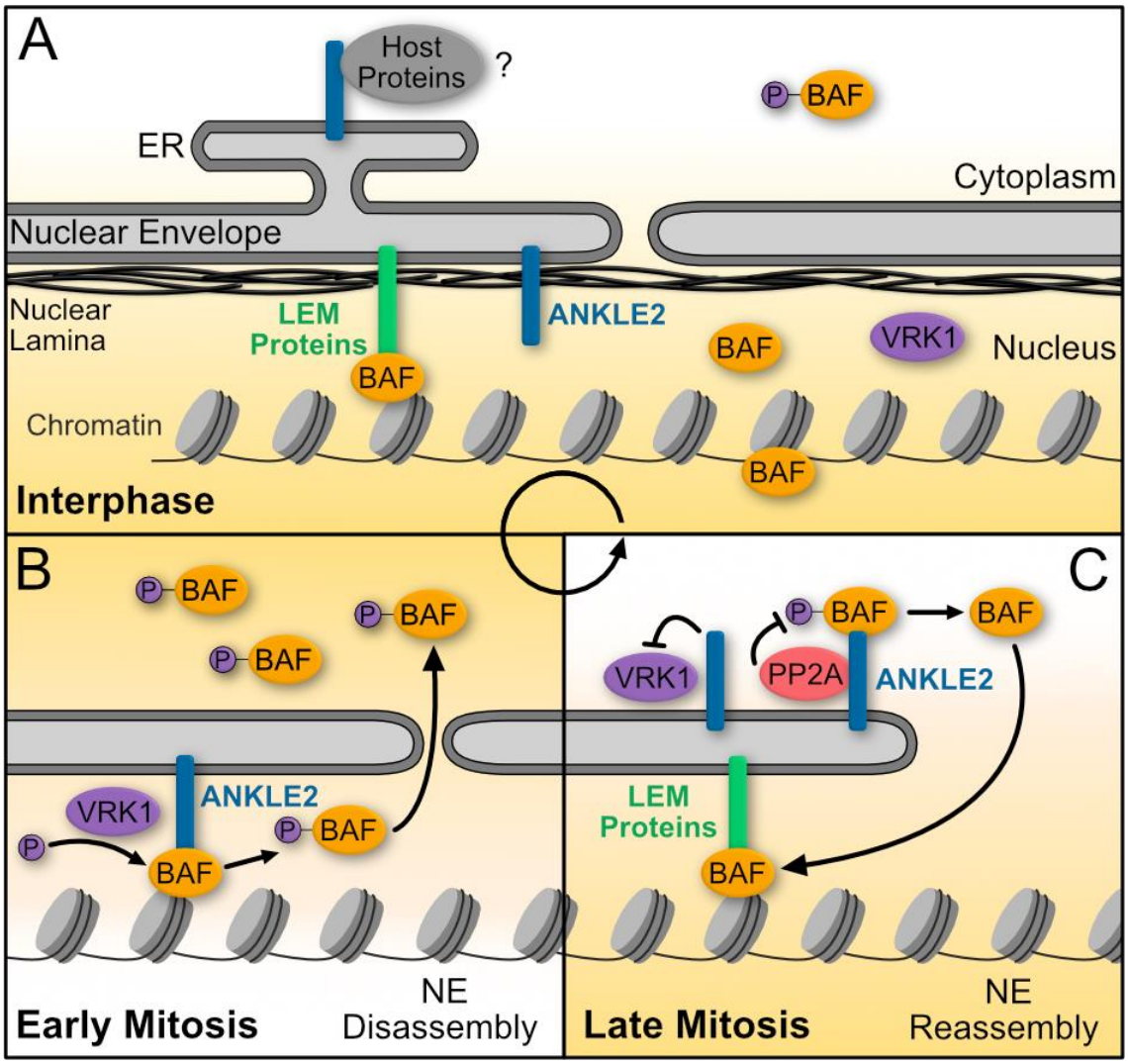

Figure 3-2: Model of ANKLE2's role in nuclear envelope disassembly and reassembly via its regulation of BAF phosphorylation. A) AlphaFold structural prediction of human ANKLE2 (UniProt Q86XL3) with annotated and uncharacterized structural regions highlighted by color and number. B) ANKLE2 and orthologous sequences (sequences come from NCBI). Structured domains not previously annotated (such as LEM or ankyrin repeat domain) were identified using AlphaFold (105,106). Regions were considered structured if AlphaFold pLDDT was greater than 70 for each given residue. Transmembrane domains were annotated using DeepTMHMM (107). The Caulimovirus domain in *D. melanogaster* Ankle2 appears to maintain a similar structure but is broken into two segments with a β sheet-disordered region-α helix-β sheet-α helix organization. The region in *D. melanogaster* Ankle2 between 713-894 amino acids represents an uncharacterized structured region between region 5 and 6 with no clear orthologous region among other evaluated orthologs. C-E) Amino acid conservation among ANKLE2 orthologs and for specific protein domains (as shown in B) determined using Clustal Omega multiple sequence alignment (108). (C) Amino acid conservation in the total ANKLE2 protein sequence, (D) the ankyrin repeat domain, and (E) the LEM domain, showing that these vital domains have higher degrees of conservation.

ANKLE2 is expressed throughout the body in human adults (48), and likely plays a fundamental role in mitosis. In humans *ANKLE2* is seemingly expressed throughout development, from 10 weeks post conception. Its expression has also been observed in all seven evaluated tissues (brain, cerebellum, heart, kidney, liver, ovary, and testis), supporting that *ANKLE2* is ubiquitously expressed in humans throughout life (49). It is also expressed throughout development in other organisms, including in mice *(Mus musculus)* (50), zebrafish *(Danio rerio)* (51), and fruit flies (*D. melanogaster)* (52). In the remainder of this section, we review what we know about the

temporospatial patterns of *ANKLE2* expression and what this tells us about its specific roles in development.

Immune Cell Development

ANKLE2 has been recently implicated in immune cell development, and specifically in T cell maturation. This occurs via ANKLE2's transcriptional regulation by the zinc finger protein 335 (ZFP335), which regulates *ANKLE2* expression by binding to its promoter. ZFP335 is a C2H2 zinc-finger, transcription factor protein that is essential for vertebrate embryonic development and functions in T cell maturation (53,54). In mice that harbor a Zfp335 R1092W mutation, Zfp335's binding to *Ankle2's* promoter is abolished, reducing the expression of *Ankle2*. This loss of Ankle2 is accompanied by T cell maturation defects throughout multiple stages of T cell development, and results in a decreased number of T cells. *In vitro* overexpression of mouse *Ankle2* in a Zfp335 mutant background partially rescues T cell maturation. This finding indicates that Ankle2 is a downstream target of Zfp335 required for T cell maturation (54). Another recent study found that the continuous expression of Zfp335 and Ankle2 is necessary for DN4 thymocyte (Appendix A-3) survival in mice and for the proper late stage T cell development in the thymus. The authors of this study hypothesized that decreased levels of Ankle2 might lead to increased levels of hyperphosphorylated Baf, and thus disrupt nuclear envelope assembly. The resulting nuclear envelope morphology defects would in turn lead to increased levels of cytoplasmic DNA, thereby activating cGAS/STING-mediated apoptosis (Appendix A-3). Thus, the loss of Zfp335 resulted in impaired T cell development due to the disruption of the Zfp335/Ankle2/Baf axis, ultimately triggering DN4 cell death through cGAS/STING signaling (55). These findings are supported by previous studies showing that depleted levels of ANKLE2 (and of its orthologs) disrupt nuclear envelope morphology (26,39,56). In human cells, BAF has direct roles in cGAS/STING signaling as a modulator of basal cell-intrinsic immunity in response to viral infection. It does so by

regulating cGAS-dependent interferon-stimulated gene homeostasis, as well as affecting the levels of cytoplasmic DNA (57). However, whether ANKLE2 directly participates in this signaling is unknown.

Asymmetric Cell Division in Neural Progenitor Cells

ANKLE2 also plays a specialized role in regulating asymmetric cell division in neural progenitor cells (NPCs). To maintain stemness, NPCs segregate their stem-like proteins asymmetrically during cell division. The mutation of *Ankle2* in *D. melanogaster* results in aberrant NPC division, with reduced cell proliferation and increased cell death (58). The depletion or mutation of *D. melanogaster Ankle2* also leads to the disruption of the ER and nuclear envelope, which in turn causes the release of the VRK1 ortholog, Ballchen, into the cytosol. Interestingly, this is accompanied by defects in NPC polarity and spindle alignment, which are both required for asymmetric cell division. There are also defects in the phosphorylation of atypical protein kinase C (aPKC) in *D. melanogaster Ankle2* mutants. aPKC is part of the Par complex together with Par-3 and Par-6. This complex localizes apically during mitosis in NPCs, and the activity of this complex ensures asymmetric cell division proceeds properly. Phosphorylation of aPKC is thought to be associated with its activation (59) (Appendix A-3). The Par complex is negatively regulated by physical interaction between aPKC and Lethal (2) giant larvae (L(2)gl), but when aPKC is active it phosphorylates L(2)gl to prevent it from binding aPKC (60,61). Defects in NPC asymmetric division in *Ankle2* mutant *D. melanogaster* can be rescued by partial loss of *ballchen*, or a temperature sensitive mutation in *l(2)gl*, suggesting both Ball and L(2)gl are overactive in *Ankle2* mutants and providing a genetic link between Ankle2 and the Par complex (26) (Figure 3-3).

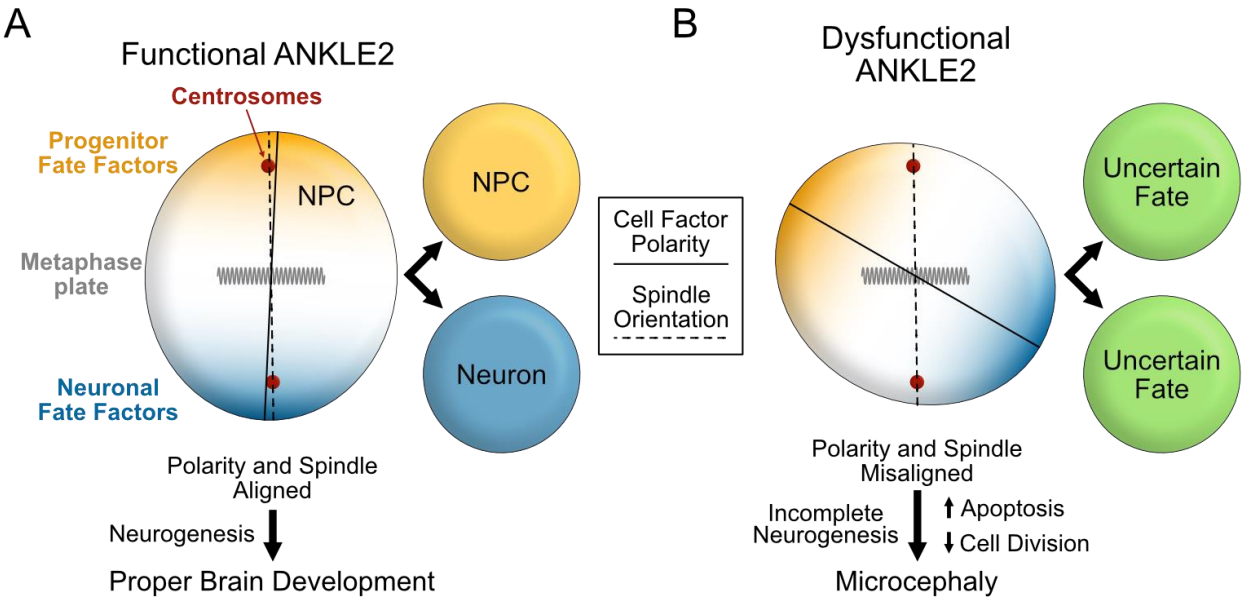

Figure 3-3: Model of the ANKLE2-mediated dysregulation of asymmetric division in neural progenitor cells, leading to microcephaly. A) During brain development, neural progenitor cells (NPCs) divide asymmetrically to give rise to two daughter cells: one acquires a neuronal fate, and the other a fate that retains it as a progenitor. These differing daughter cell fates are brought about by the polarization of fate-determining factors in NPCs across the metaphase plate. Thus, this process depends on the alignment of cell polarity with the mitotic spindle and is required for proper neurogenesis and brain development. B) In ANKLE2-deficient cells the polarity of cell fate factors becomes misaligned relative to the mitotic spindle. The resulting dysregulation of NPC polarity leads to a reduction in neuronal cell numbers generated during neurogenesis. This effect is compounded by increased apoptosis and by decreased cell division, resulting in microcephaly.

In summary, ANKLE2 has multiple roles in cell biology through its functions in regulating nuclear envelope dynamics, T cell maturation, and asymmetric cell division. Next, we will expand our review to the physiological human diseases caused by disruption of ANKLE2 function.

Roles of ANKLE2 in human disease

The control of cell division during development is a complex and carefully coordinated process that can be perturbed in many ways, with often disastrous consequences for a cell and/or organism. Given ANKLE2's role in regulating cell division, its altered or inhibited function can lead to severe cellular defects that ultimately result in dysregulated neurodevelopment or cancer.

Microcephaly

Microcephaly describes a neurological condition in which brain and head size are greatly reduced. In clinical terms, someone with a head circumference 2-3 standard deviations (SD) below the mean for their age and sex is classified as having microcephaly, with a reduction of >3 SD being classified as severe microcephaly (62). While head circumference is the main criteria for diagnosing microcephaly, it is often characterized by a disproportionally small brain and head size relative to the rest of the face and body.

Microcephaly can be caused by a wide range of factors, including toxins (63), pathogen infection during pregnancy (64–67), metabolic conditions such as maternal phenylketonuria (68), traumatic brain injuries (69), and genetic mutations in a wide array of genes (70–72). Microcephaly can be further broken down into two main types, primary and secondary microcephaly. Primary microcephaly (MCPH) describes microcephaly that is present at birth, usually due to neurodevelopmental defects. Secondary microcephaly occurs when a normally sized brain at birth does not grow appropriately with age. There is no cure for microcephaly nor are treatments available to restore brain size or growth. The condition is commonly accompanied by seizures, severe developmental delays, and impaired motor, vision, or auditory functions (62).

Genetic MCPH was first identified through autozygosity mapping in two consanguineous families, which revealed a genetic locus (*MCPH1*) for autosomal recessive MCPH (73). There are 30 known genes whose mutations cause primary microcephaly, and more MCPH genes are identified almost every year, suggesting that yet more genes contribute to this condition (74). Of the 30

genes identified so far, more than 20 are linked to the molecular regulation of mitosis (74–76). ANKLE2 was first discovered to cause MCPH in a *D. melanogaster* forward mosaic genetic screen (Appendix A-3) that identified a neurodevelopmental phenotype in an *Ankle2* mutant (58). Flies harboring a L326H mutation in *Ankle2* had reduced brain size without an overall growth defect at the third instar larval stage of development (26,58). In *Ankle2* CRISPR-null mutant flies, brain size was even further decreased and associated with smaller overall animal size and failure to survive beyond the third instar stage (26). A corresponding search of human whole-exome sequencing data identified a patient who recessively inherited MCPH through a compound heterozygous *ANKLE2* mutation. This compound mutation consisted of one allele with an L573V missense mutation, and another allele with a nonsense mutation, Q782X. L573 lies in the structured region following the ankyrin repeat domain and Q782X results in a truncated ANKLE2 lacking the last structured region (Figures 3-1 and 3-4). This individual presented with severe microcephaly at birth, and at 5.5 years old had a frontal-occipital circumference of –9 SD. A sibling with the same mutations also had severe microcephaly, but unfortunately died shortly after birth. To establish whether human ANKLE2 was directly responsible for the neurodevelopmental defects diagnosed in this family, a rescue experiment was performed via human ANKLE2 expression in *Ankle2* mutant flies. The expression of wild-type human ANKLE2 restored brain development to near normal levels, highlighting that ANKLE2's role in brain development is functionally conserved between humans and *Drosophila* (26,58).

Due to its association with MCPH, *ANKLE2* is sometimes called *MCPH16*. MCPH16 is also the clinical name for microcephaly arising from mutations in *ANKLE2.* Additional studies have expanded the range of *ANKLE2* mutations and allele combinations associated with this disease (Figure 3-4 and Appendix A-4) (26,77,78). Other studies have also implicated *VRK1* (72) and *ZFP335* (53) mutations in MCPH, further supporting a role for the ANKLE2 pathway in neurodevelopment. In addition, in depth imaging and clinical evaluation of ANKLE2-associated microcephaly in humans revealed 12 additional MCPH16 cases and new pathogenic *ANKLE2*

variants located in various domains of *ANKLE2* (Figure 3-4 and Appendix A-4). In ten of these cases, MCPH16 patients had missense mutations and in two cases, the patients had nonsense mutations that resulted in premature protein termination. These pathogenic mutations were associated with a broad range of structural brain abnormalities and developmental delays, with speech and language delays being the most common abnormality (78).

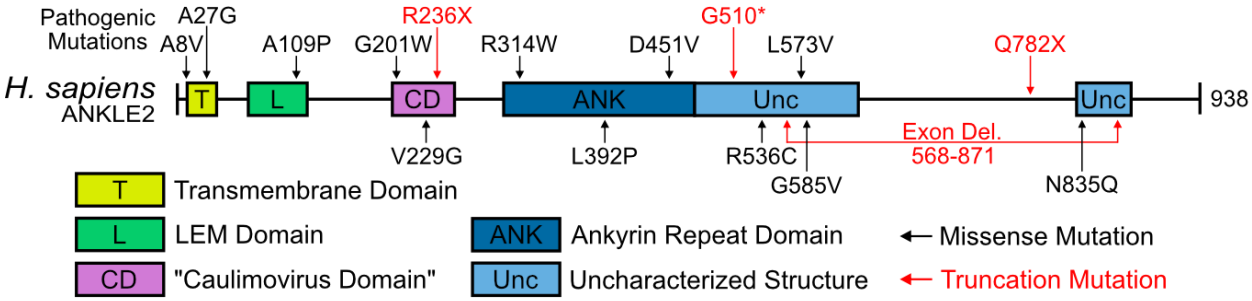

Figure 3-4: Pathogenic mutations in human ANKLE2 associated with primary congenital microcephaly. ANKLE2 protein structure, showing sites of known pathogenic mutations, as originally described in (26,58,72,77,78). Point mutations leading to missense mutations are shown in black, while mutations leading to protein truncations are shown in red. G510* describes a hypothesized splicing mutation that leads to premature protein termination (c. 1421-1 G>C), which was identified in a compound heterozygous individual along with A109P (26). Allele combinations are described in Appendix A-4.

In addition to clinical studies, animal models have elucidated how ANKLE2 regulates brain development and how *ANKLE2* mutations lead to the formation of MCPH16. While pathogenic mutations in *ANKLE2* were first uncovered in the invertebrate model *D. melanogaster* (26,58), the role of ANKLE2 in vertebrate brain development has only recently been explored using a zebrafish model (56). Surprisingly, in zebrafish (*D. rerio*), *ankle2* null mutation resulted in normal body and brain size at 6- or 14-days post fertilization (dpf). However, at 14 dpf, radial glial progenitor cell numbers and locomotor activity were significantly reduced. Reduced brain size in *ankle2* null adult

fish manifested later, at 3-4 months post fertilization (mpf), with the cerebellum and telencephalon (Appendix A-3) being primarily impacted. These brain regions are consistent with those impacted in humans with pathogenic *ANKLE2* mutations, despite the delay in phenotype onset in zebrafish. While brain size is clearly affected in these animals, it is unclear if these impacts were specific or accompanied by general reductions in animal size. Nonetheless, the small brain phenotype could be rescued using morpholino-based *vrk1* knockdown, recapitulating the previously established relationship between these two genes (26,39). Finally, in this zebrafish model, the depletion of *ankle2* also led to infertility due to defective spermatogenesis that was partially rescued by mutation of *vrk1* (56). The finding that *vrk1* is involved in fertility is supported by observations from *D. melanogaster* in which *vrk1* mutations also lead to fertility defects (79–81). Currently, the impacts of ANKLE2 on fertility and on spermatogenesis have yet to be explored in humans, although alternative *ANKLE2* transcripts have been identified in human spermatid cells (24).

Congenital Zika Syndrome

In 2015-2016, Zika virus (ZIKV) emerged as a global public health threat due to an epidemic across South and Central America. ZIKV is often clinically mild in healthy adults, except for rare cases of Guillan-Barré Syndrome (82) (Appendix A-3). In pregnant women ZIKV can be vertically transmitted and *in utero* infections can cause congenital Zika syndrome (CZS). CZS is characterized by a range of significant birth defects, including congenital contractures, ocular abnormalities (83), hip displacement (84), and in the most severe cases MCPH (66,85,86). The occurrence of microcephaly after congenital ZIKV exposure is roughly 5% and varies dramatically based on gestational timing (87), as well as many other environmental- and viral-associated factors (88,89). CZS-associated microcephaly has a mortality rate of approximately 10%, but this also varies with severity of disease and other factors (90). Similar to other etiologies of microcephaly, CZS-associated microcephaly can present with multiple neurological defects,

including ventriculomegaly, hypoplasia, simplified gyral patterns, and calcifications (91). The molecular mechanisms by which ZIKV causes microcephaly are still not fully understood and are likely to be multifactorial (92).

To investigate the molecular mechanisms of CZS, we assessed protein interactions between ZIKV and host proteins using a global proteomics approach. In these experiments, individual ZIKV proteins were expressed in HEK293T cells and subjected to affinity purification and mass spectrometry (Appendix A-3) to identify protein-protein interactions between each viral protein and the host proteome. This pipeline identified hundreds of high-confidence ZIKV-host protein-protein interactions, including an interaction between ZIKV non-structural protein 4A (NS4A) and host ANKLE2 (93). Transgenic expression of ZIKV NS4A under different ubiquitous or tissue-specific promoters in *D. melanogaster* larvae induced a small brain phenotype. As in *Ankle2* mutant flies, this virally induced small brain phenotype could be rescued by human ANKLE2 expression, by partial loss of *VRK1* ortholog *ballchen,* or a temperature sensitive mutation in the polarity regulator *l(2)gl.* The expression of pathogenic loss-of-function ANKLE2 mutant Q782X failed to rescue this small brain phenotype, further underlining ZIKV NS4A inhibition of ANKLE2 (26,58,93). Interestingly, while *Ankle2* heterozygous animals had normal brain development, expression of ZIKV NS4A in these heterozygous animals led to more severe brain development phenotypes than observed for ZIKV NS4A expression in wild-type animals. This suggests that typically non-pathogenic variation in *ANKLE2* may sensitize individuals to ZIKV-induced microcephaly, tipping the scales from haplosufficiency to haploinsufficiency. This could also provide a host genetic basis for the spectrum of clinical outcomes observed in CZS (93).

In addition to inhibiting gross brain development, ZIKV NS4A also inhibits cellular functions of *Ankle2.* In the same *Drosophila* model described above, ZIKV NS4A expression induced similar disruption of NPC polarity and spindle alignment in wild-type flies as those seen in *Ankle2* mutants (26) (Figure 3-5). Together, these findings suggest that ZIKV NS4A interacts with host ANKLE2 to inhibit its functions in cell division, subsequently dysregulating NPC development, leading to

microcephaly. Identifying the physical determinants of this protein-protein interaction is vital in understanding the mechanism behind ZIKV NS4A inhibition of ANKLE2. While these determinants are not fully established, they are of continuing interest to our group (25).

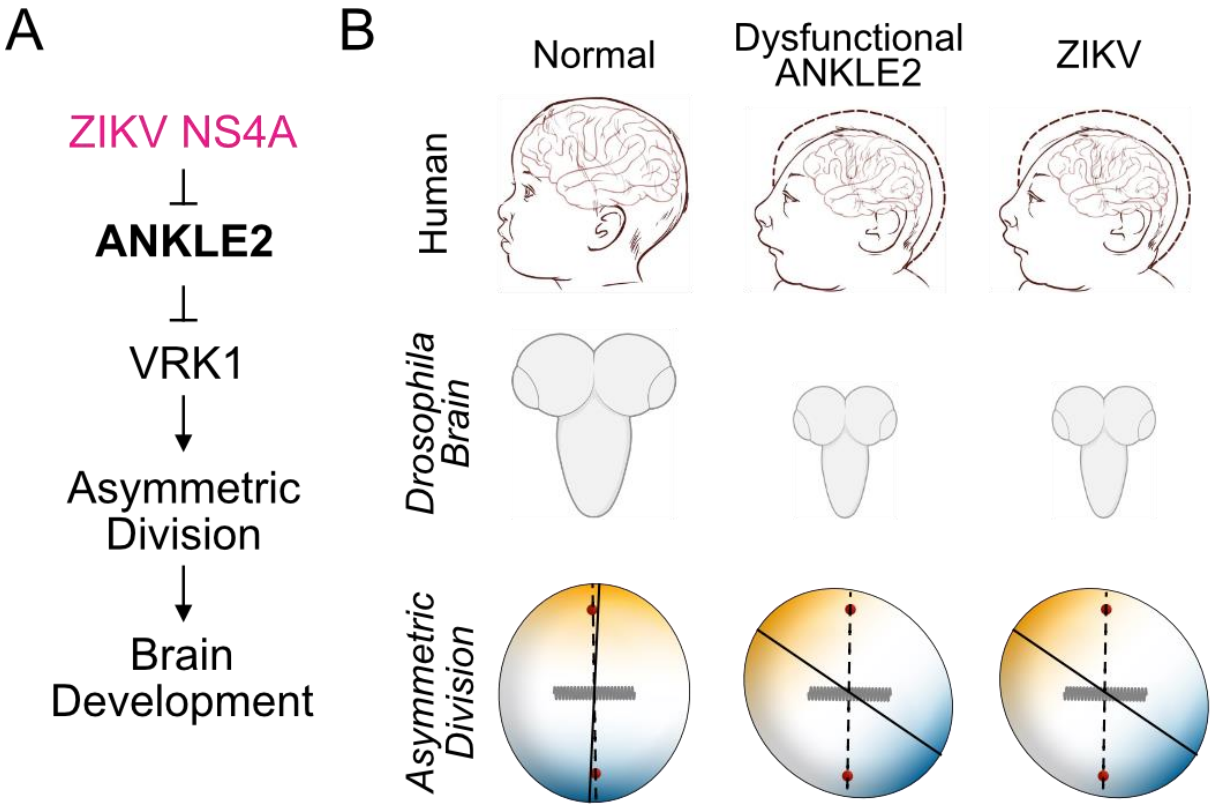

Figure 3-5: Zika virus NS4A inhibits ANKLE2 and causes similar pathogenic outcomes. (A) During mitosis, ANKLE2 interacts with BAF, VRK1, and PP2A to regulate nuclear envelope dynamics. During asymmetric cell division the ANKLE2-VRK1 pathway is crucial for establishing proper cell polarity. Zika virus (ZIKV) NS4A interacts with ANKLE2 and inhibits its function to cause microcephaly. (B) Cartoon examples of normal human brain development compared to microcephaly arising from dysfunction ANKLE2 or from congenital Zika syndrome (top). Small brain phenotypes (middle) and defects in asymmetric neuroblast division (bottom) are also mirrored in larval *Drosophila* brains.

Cancer

ANKLE2's function as a mitotic regulator also has implications in ovarian and breast cancer. Cancer arises due to defects in cell cycle control mechanisms leading to abnormal mitosis and unchecked cell proliferation. In high grade serous ovarian carcinoma (HGS-OvC), *ANKLE2* is part of a network of 12 genes that interact with *VIRMA*, an RNA methylation/adenylation gene that contributes to tumor aggressiveness through N6-methylation of adenosine (m6A), which targets RNA for their ultimate destination (94). RNAi silencing of *ANKLE2* in various human ovarian cancer cell lines (SKOV3, OVCAR, and APOCC) decreases cell viability and cell migration, and increases chemosensitivity to paclitaxel, a common chemotherapy used in ovarian cancer (95). Similarly, in estrogen receptor-positive (ER+) human breast cancer cells lines (T47D, BT474, and MCF7), ANKLE2 overexpression contributes to tamoxifen resistance and accelerated tumor growth (96). In ER+ human breast cancer, ANKLE2 acts as a scaffold by stabilizing and facilitating the phosphorylation of estrogen receptor alpha (ERα) through Aurora-A kinase, thus activating ERα signaling and increasing DNA binding and transactivation. Phosphorylated ERα directly targets cyclin D to cause tamoxifen resistance (97). Gao et al., 2018 also showed that ANKLE2 facilitates phosphorylation of the tumor suppressor retinoblastoma protein (Rb), activating the cyclin D-CDK4-Rb signaling axis to promote tamoxifen resistance by sending the cell from G1 to S phase (96). For other cancers, such as prostate adenocarcinoma, LEM-domain containing proteins, including ANKLE1, EMD, and LEMD2, can serve as prognostic markers. However, in this type of prostate cancer, there were no significant changes in ANKLE2 expression (98).

Conclusions

ANKLE2 is a multifunctional protein with established and emerging roles throughout the cell. In its most studied function in cell division, ANKLE2 acts as a scaffold to regulate BAF phosphorylation and control nuclear envelope dynamics. These roles in cell division are directly

linked to development in multicellular organisms. While clearly important for brain development and neurogenesis, the ubiquitous expression of ANKLE2 implies it has broader functionality. We speculate that ANKLE2 has at least two functionalities, depending on its subcellular localization and cell type. At the INM it interacts with and regulates BAF, while at the ER its interactions or roles are not understood. This hypothesis arises from the observation that ANKLE2 has distinct and conserved localization to the ER, while most LEM-domain containing proteins are primarily nuclear or retained to the INM. This observation, along with the ubiquitous expression of ANKLE2, suggests the potential for a broader post-mitotic function in the ER. Our group has explored this unknown ER function and recently showed in a preprint that it may be coopted for ZIKV replication (25). It is enticing to speculate that the scaffolding function of ANKLE2 could be hijacked by viral proteins, including ZIKV NS4A, to mediate aspects of virus replication in the ER that are otherwise inefficient.

Though not as well established, a post-mitotic function of ANKLE2 may also regulate the development of tauopathies. Tauopathies, including Alzheimer's Disease, are a group of neurodegenerative disorders characterized by the aggregation of tau protein as intracellular neurofibrillary tangles in neurons (99). It is speculated that these aggregations are driven by changes in tau phosphorylation (100,101), and ANKLE2 may in fact prevent tau aggregation. Knockdown of *ANKLE2* in HEK293T tau biosensor cells led to the aggregation of insoluble and phosphorylated tau, as well as nuclear proteins like BAF in the cytoplasm (102). Another study involving *ANKLE2* knockdown in similar cells identified ANKLE2 as a key regulator in the development of both exosomal and vesicle-free aggregates of tau outside of the cell (103). Together, these studies raise the potential for a post-mitotic role of ANKLE2 in regulating tau phosphorylation. While the mechanism by which ANKLE2 interacts with and regulates tau is still unclear, these data suggest a potentially important role for ANKLE2 in the development of neurodegenerative diseases. Notably, we recently showed that ZIKV NS4A not only inhibits fly brain development in an ANKLE2-dependent manner, but it also causes retinal

neurodegeneration in adult flies (104). It is interesting to speculate that this degenerative phenotype is also ANKLE2-dependent and disrupts a post-mitotic role of ANKLE2.

Future research is necessary and warranted to explore these possibilities and the roles of ANKLE2 in human diseases. As a scaffolding protein, evaluating protein-protein interactions is an obvious avenue to identify potential processes in which ANKLE2 is involved. A current significant challenge is the lack of an experimentally determined structure, complicated by many disordered regions. A well-defined structure would allow for a clearer understanding of how ANKLE2 interacts with other host proteins, such as BAF, PP2A, VRK1, tau, or others. This may also illuminate how naturally occurring mutations or ZIKV NS4A may inhibit these interactions to cause disease. Understanding how this set of ANKLE2-interacting proteins varies between different stages of development (NPCs vs. post-mitotic neurons) or cell states (interphase vs. mitotic, healthy vs. diseased, etc.) will provide new insights into the dynamic nature of ANKLE2, and how changes in these interactions can cause disease.

References

1. Lee KK, Wilson KL. All in the family: evidence for four new LEM-domain proteins Lem2 (NET-25), Lem3, Lem4 and Lem5 in the human genome. Symp Soc Exp Biol. 2004;(56):329–39.
2. Cai M, Huang Y, Ghirlando R, Wilson KL, Craigie R, Clore GM. Solution structure of the constant region of nuclear envelope protein LAP2 reveals two LEM-domain structures: one binds BAF and the other binds DNA. The EMBO Journal. 2001 Aug 15;20(16):4399–407.
3. Lin F, Blake DL, Callebaut I, Skerjanc IS, Holmer L, McBurney MW, et al. MAN1, an inner nuclear membrane protein that shares the LEM domain with lamina-associated polypeptide 2 and emerin. J Biol Chem. 2000 Feb 18;275(7):4840–7.

4. Laguri C, Gilquin B, Wolff N, Romi-Lebrun R, Courchay K, Callebaut I, et al. Structural characterization of the LEM motif common to three human inner nuclear membrane proteins. Structure. 2001 Jun;9(6):503–11.
5. Shumaker DK, Lee KK, Tanhehco YC, Craigie R, Wilson KL. LAP2 binds to BAF.DNA complexes: requirement for the LEM domain and modulation by variable regions. EMBO J. 2001 Apr 2;20(7):1754–64.
6. Mansharamani M, Wilson KL. Direct Binding of Nuclear Membrane Protein MAN1 to Emerin in Vitro and Two Modes of Binding to Barrier-to-Autointegration Factor*. Journal of Biological Chemistry. 2005 Apr 8;280(14):13863–70.
7. Cai M, Huang Y, Suh JY, Louis JM, Ghirlando R, Craigie R, et al. Solution NMR structure of the barrier-to-autointegration factor-Emerin complex. J Biol Chem. 2007 May 11;282(19):14525–35.
8. Sears RM, Roux KJ. Diverse cellular functions of barrier-to-autointegration factor and its roles in disease. Journal of Cell Science. 2020 Aug 17;133(16):jcs246546.
9. Umland TC, Wei SQ, Craigie R, Davies DR. Structural Basis of DNA Bridging by Barrier-to-Autointegration Factor. Biochemistry. 2000 Aug 1;39(31):9130–8.
10. Bradley CM, Ronning DR, Ghirlando R, Craigie R, Dyda F. Structural basis for DNA bridging by barrier-to-autointegration factor. Nat Struct Mol Biol. 2005 Oct;12(10):935–6.
11. Samson C, Petitalot A, Celli F, Herrada I, Ropars V, Le Du MH, et al. Structural analysis of the ternary complex between lamin A/C, BAF and emerin identifies an interface disrupted in autosomal recessive progeroid diseases. Nucleic Acids Res. 2018 Nov 2;46(19):10460–73.
12. Kohl A, Binz HK, Forrer P, Stumpp MT, Plückthun A, Grütter MG. Designed to be stable: Crystal structure of a consensus ankyrin repeat protein. Proceedings of the National Academy of Sciences. 2003 Feb 18;100(4):1700–5.

13. Mosavi LK, Cammett TJ, Desrosiers DC, Peng Z yu. The ankyrin repeat as molecular architecture for protein recognition. Protein Sci. 2004 Jun;13(6):1435–48.
14. Kumar A, Balbach J. Folding and Stability of Ankyrin Repeats Control Biological Protein Function. Biomolecules. 2021 Jun;11(6):840.
15. Sharma N, Bham K, Senapati S. Human ankyrins and their contribution to disease biology: An update. J Biosci. 2020 Nov 24;45(1):146.
16. Brachner A, Braun J, Ghodgaonkar M, Castor D, Zlopasa L, Ehrlich V, et al. The endonuclease Ankle1 requires its LEM and GIY-YIG motifs for DNA cleavage in vivo. J Cell Sci. 2012 Feb 15;125(4):1048–57.
17. Song J, Freeman ADJ, Knebel A, Gartner A, Lilley DMJ. Human ANKLE1 Is a Nuclease Specific for Branched DNA. J Mol Biol. 2020 Oct 2;432(21):5825–34.
18. Przanowski P, Przanowska RK, Guertin MJ. ANKLE1 cleaves mitochondrial DNA and contributes to cancer risk by promoting apoptosis resistance and metabolic dysregulation. Commun Biol. 2023 Mar 1;6(1):231.
19. Gupta GD, Coyaud É, Gonçalves J, Mojarad BA, Liu Y, Wu Q, et al. A dynamic protein interaction landscape of the human centrosome-cilium interface. Cell. 2015 Dec 3;163(6):1484–99.
20. Hein MY, Hubner NC, Poser I, Cox J, Nagaraj N, Toyoda Y, et al. A Human Interactome in Three Quantitative Dimensions Organized by Stoichiometries and Abundances. Cell. 2015 Oct 22;163(3):712–23.
21. Go CD, Knight JDR, Rajasekharan A, Rathod B, Hesketh GG, Abe KT, et al. A proximity-dependent biotinylation map of a human cell. Nature. 2021 Jul;595(7865):120–4.
22. Huttlin EL, Bruckner RJ, Navarrete-Perea J, Cannon JR, Baltier K, Gebreab F, et al. Dual proteome-scale networks reveal cell-specific remodeling of the human interactome. Cell. 2021 May 27;184(11):3022-3040.e28.

23. Brachner A, Foisner R. Evolvement of LEM proteins as chromatin tethers at the nuclear periphery. Biochemical Society Transactions. 2011 Nov 21;39(6):1735–41.

24. Elkhatib RA, Paci M, Boissier R, Longepied G, Auguste Y, Achard V, et al. LEM-domain proteins are lost during human spermiogenesis but BAF and BAF-L persist. Reproduction. 2017 Oct;154(4):387–401.

25. Fishburn AT, Kenaston MW, Lopez NJ, Hoang V, Shiu TN, Arcé STH, et al. Zika virus NS4A hijacks host ANKLE2 to promote viral replication [Internet]. bioRxiv; 2022 [cited 2023 Oct 12]. p. 2022.03.15.484510. Available from: https://www.biorxiv.org/content/10.1101/2022.03.15.484510v2

26. Link N, Chung H, Jolly A, Withers M, Tepe B, Arenkiel BR, et al. Mutations in ANKLE2, a ZIKA Virus Target, Disrupt an Asymmetric Cell Division Pathway in *Drosophila* Neuroblasts to Cause Microcephaly. Dev Cell. 2019 Dec 16;51(6):713-729.e6.

27. Wintermantel WM, Anderson EJ, Schoelz JE. Identification of domains within gene VI of cauliflower mosaic virus that influence systemic infection of Nicotiana bigelovii in a light-dependent manner. Virology. 1993 Oct;196(2):789–98.

28. van der Lee R, Buljan M, Lang B, Weatheritt RJ, Daughdrill GW, Dunker AK, et al. Classification of Intrinsically Disordered Regions and Proteins. Chem Rev. 2014 Jul 9;114(13):6589–631.

29. Wright PE, Dyson HJ. Intrinsically disordered proteins in cellular signalling and regulation. Nat Rev Mol Cell Biol. 2015 Jan;16(1):18–29.

30. Hetzer MW. The Nuclear Envelope. Cold Spring Harb Perspect Biol. 2010 Mar 1;2(3):a000539.

31. Heald R, McKeon F. Mutations of phosphorylation sites in lamin A that prevent nuclear lamina disassembly in mitosis. Cell. 1990 May 18;61(4):579–89.

32. Macaulay C, Meier E, Forbes DJ. Differential mitotic phosphorylation of proteins of the nuclear pore complex. J Biol Chem. 1995 Jan 6;270(1):254–62.

33. Marcelot A, Petitalot A, Ropars V, Le Du MH, Samson C, Dubois S, et al. Di-phosphorylated BAF shows altered structural dynamics and binding to DNA, but interacts with its nuclear envelope partners. Nucleic Acids Res. 2021 Apr 19;49(7):3841–55.

34. Nichols RJ, Wiebe MS, Traktman P. The Vaccinia-related Kinases Phosphorylate the N′ Terminus of BAF, Regulating Its Interaction with DNA and Its Retention in the Nucleus. MBoC. 2006 May;17(5):2451–64.

35. Haraguchi T, Koujin T, Osakada H, Kojidani T, Mori C, Masuda H, et al. Nuclear localization of barrier-to-autointegration factor is correlated with progression of S phase in human cells. J Cell Sci. 2007 Jun 15;120(Pt 12):1967–77.

36. Haraguchi T, Kojidani T, Koujin T, Shimi T, Osakada H, Mori C, et al. Live cell imaging and electron microscopy reveal dynamic processes of BAF-directed nuclear envelope assembly. Journal of Cell Science. 2008 Aug 1;121(15):2540–54.

37. Gorjánácz M, Klerkx EP, Galy V, Santarella R, López-Iglesias C, Askjaer P, et al. Caenorhabditis elegans BAF-1 and its kinase VRK-1 participate directly in post-mitotic nuclear envelope assembly. The EMBO Journal. 2007 Jan 10;26(1):132–43.

38. Molitor TP, Traktman P. Depletion of the protein kinase VRK1 disrupts nuclear envelope morphology and leads to BAF retention on mitotic chromosomes. Mol Biol Cell. 2014 Mar;25(6):891–903.

39. Asencio C, Davidson IF, Santarella-Mellwig R, Ly-Hartig TBN, Mall M, Wallenfang MR, et al. Coordination of Kinase and Phosphatase Activities by Lem4 Enables Nuclear Envelope Reassembly during Mitosis. Cell. 2012 Jul 6;150(1):122–35.

40. Bollen M, Gerlich DW, Lesage B. Mitotic phosphatases: from entry guards to exit guides. Trends in Cell Biology. 2009 Oct 1;19(10):531–41.

41. Glatter T, Wepf A, Aebersold R, Gstaiger M. An integrated workflow for charting the human interaction proteome: insights into the PP2A system. Molecular Systems Biology. 2009 Jan;5(1):237.

42. Hunt T. On the regulation of protein phosphatase 2A and its role in controlling entry into and exit from mitosis. Adv Biol Regul. 2013 May;53(2):173–8.

43. Wlodarchak N, Xing Y. PP2A as a master regulator of the cell cycle. Crit Rev Biochem Mol Biol. 2016;51(3):162–84.

44. Snyers L, Erhart R, Laffer S, Pusch O, Weipoltshammer K, Schöfer C. LEM4/ANKLE-2 deficiency impairs post-mitotic re-localization of BAF, LAP2α and LaminA to the nucleus, causes nuclear envelope instability in telophase and leads to hyperploidy in HeLa cells. Eur J Cell Biol. 2018 Jan;97(1):63–74.

45. Inoue T, Hiratsuka M, Osaki M, Oshimura M. The molecular biology of mammalian SIRT proteins: SIRT2 in cell cycle regulation. Cell Cycle. 2007 May 2;6(9):1011–8.

46. Kaufmann T, Kukolj E, Brachner A, Beltzung E, Bruno M, Kostrhon S, et al. SIRT2 regulates nuclear envelope reassembly through ANKLE2 deacetylation. J Cell Sci. 2016 15;129(24):4607–21.

47. Berk JM, Wilson KL. Simple Separation of Functionally Distinct Populations of Lamin-Binding Proteins. Methods Enzymol. 2016;569:101–14.

48. Fagerberg L, Hallström BM, Oksvold P, Kampf C, Djureinovic D, Odeberg J, et al. Analysis of the human tissue-specific expression by genome-wide integration of transcriptomics and antibody-based proteomics. Mol Cell Proteomics. 2014 Feb;13(2):397–406.

49. Cardoso-Moreira M, Halbert J, Valloton D, Velten B, Chen C, Shao Y, et al. Gene expression across mammalian organ development. Nature. 2019 Jul;571(7766):505–9.

50. Yue F, Cheng Y, Breschi A, Vierstra J, Wu W, Ryba T, et al. A comparative encyclopedia of DNA elements in the mouse genome. Nature. 2014 Nov 20;515(7527):355–64.

51. White RJ, Collins JE, Sealy IM, Wali N, Dooley CM, Digby Z, et al. A high-resolution mRNA expression time course of embryonic development in zebrafish. Elife. 2017 Nov 1;6:e30860.

52. Brown JB, Boley N, Eisman R, May GE, Stoiber MH, Duff MO, et al. Diversity and dynamics of the *Drosophila* transcriptome. Nature. 2014 Aug;512(7515):393–9.

53. Yang YJ, Baltus AE, Mathew RS, Murphy EA, Evrony GD, Gonzalez DM, et al. Microcephaly Gene Links Trithorax and REST/NRSF to Control Neural Stem Cell Proliferation and Differentiation. Cell. 2012 Nov 21;151(5):1097–112.

54. Han BY, Wu S, Foo CS, Horton RM, Jenne CN, Watson SR, et al. Zinc finger protein Zfp335 is required for the formation of the naïve T cell compartment. Nussenzweig M, editor. eLife. 2014 Oct 24;3:e03549.

55. Ratiu JJ, Barclay WE, Lin E, Wang Q, Wellford S, Mehta N, et al. Loss of Zfp335 triggers cGAS/STING-dependent apoptosis of post-β selection thymocytes. Nat Commun. 2022 Oct 6;13(1):5901.

56. Apridita Sebastian W, Shiraishi H, Shimizu N, Umeda R, Lai S, Ikeuchi M, et al. Ankle2 deficiency-associated microcephaly and spermatogenesis defects in zebrafish are alleviated by heterozygous deletion of vrk1. Biochemical and Biophysical Research Communications. 2022 Oct 8;624:95–101.

57. Ma H, Qian W, Bambouskova M, Collins PL, Porter SI, Byrum AK, et al. Barrier-to-Autointegration Factor 1 Protects against a Basal cGAS-STING Response. mBio. 2020 Mar 10;11(2):e00136-20.

58. Yamamoto S, Jaiswal M, Charng WL, Gambin T, Karaca E, Mirzaa G, et al. A *Drosophila* genetic resource of mutants to study mechanisms underlying human genetic diseases. Cell. 2014 Sep 25;159(1):200–14.

59. Kim S, Gailite I, Moussian B, Luschnig S, Goette M, Fricke K, et al. Kinase-activity-independent functions of atypical protein kinase C in *Drosophila*. J Cell Sci. 2009 Oct 15;122(Pt 20):3759–71.

60. Betschinger J, Mechtler K, Knoblich JA. The Par complex directs asymmetric cell division by phosphorylating the cytoskeletal protein Lgl. Nature. 2003 Mar 20;422(6929):326–30.

61. Rolls MM, Albertson R, Shih HP, Lee CY, Doe CQ. *Drosophila* aPKC regulates cell polarity and cell proliferation in neuroblasts and epithelia. Journal of Cell Biology. 2003 Dec 1;163(5):1089–98.

62. Jayaraman D, Bae BI, Walsh CA. The Genetics of Primary Microcephaly. Annu Rev Genomics Hum Genet. 2018 31;19:177–200.

63. Sawada Feldman H, Lyons Jones K, Lindsay S, Slymen D, Klonoff-Cohen H, Kao K, et al. Prenatal Alcohol Exposure Patterns and Alcohol-Related Birth Defects and Growth Deficiencies: A Prospective Study. Alcoholism: Clinical and Experimental Research. 2012;36(4):670–6.

64. Giles JP, Cooper LZ, Krugman S. The rubella syndrome. The Journal of Pediatrics. 1965 Feb 1;66(2):434–7.

65. McLeod R, Boyer K, Karrison T, Kasza K, Swisher C, Roizen N, et al. Outcome of Treatment for Congenital Toxoplasmosis, 1981–2004: The National Collaborative Chicago-Based, Congenital Toxoplasmosis Study. Clinical Infectious Diseases. 2006 May 15;42(10):1383–94.

66. Mlakar J, Korva M, Tul N, Popović M, Poljšak-Prijatelj M, Mraz J, et al. Zika Virus Associated with Microcephaly. N Engl J Med. 2016 Mar 10;374(10):951–8.

67. Messinger CJ, Lipsitch M, Bateman BT, He M, Huybrechts KF, MacDonald S, et al. Association Between Congenital Cytomegalovirus and the Prevalence at Birth of Microcephaly in the United States. JAMA Pediatr. 2020 Sep 14;e203009.

68. Waisbren SE, Rohr F, Anastasoaie V, Brown M, Harris D, Ozonoff A, et al. Maternal Phenylketonuria: Long-term Outcomes in Offspring and Post-pregnancy Maternal Characteristics. JIMD Rep. 2015 Feb 25;21:23–33.

69. Lo TYM, McPhillips M, Minns RA, Gibson RJ. Cerebral atrophy following shaken impact syndrome and other non-accidental head injury (NAHI). Pediatr Rehabil. 2003;6(1):47–55.

70. Alcantara D, O'Driscoll M. Congenital microcephaly. American Journal of Medical Genetics Part C: Seminars in Medical Genetics. 2014;166(2):124–39.

71. Naveed M, Kazmi SK, Amin M, Asif Z, Islam U, Shahid K, et al. Comprehensive review on the molecular genetics of autosomal recessive primary microcephaly (MCPH). Genet Res (Camb). 2018 Aug 8;100:e7.

72. Shaheen R, Maddirevula S, Ewida N, Alsahli S, Abdel-Salam GMH, Zaki MS, et al. Genomic and phenotypic delineation of congenital microcephaly. Genet Med. 2019;21(3):545–52.

73. Jackson AP, McHale DP, Campbell DA, Jafri H, Rashid Y, Mannan J, et al. Primary autosomal recessive microcephaly (MCPH1) maps to chromosome 8p22-pter. Am J Hum Genet. 1998 Aug;63(2):541–6.

74. Carvalhal S, Bader I, Rooimans MA, Oostra AB, Balk JA, Feichtinger RG, et al. Biallelic BUB1 mutations cause microcephaly, developmental delay, and variable effects on cohesion and chromosome segregation. Science Advances. 2022 Jan 19;8(3):eabk0114.

75. Amberger JS, Bocchini CA, Scott AF, Hamosh A. OMIM.org: leveraging knowledge across phenotype-gene relationships. Nucleic Acids Res. 2019 Jan 8;47(D1):D1038–43.

76. Degrassi F, Damizia M, Lavia P. The Mitotic Apparatus and Kinetochores in Microcephaly and Neurodevelopmental Diseases. Cells. 2020 Jan;9(1):49.

77. Masih S, Moirangthem A, Shambhavi A, Rai A, Mandal K, Saxena D, et al. Deciphering the molecular landscape of microcephaly in 87 Indian families by exome sequencing. European Journal of Medical Genetics. 2022 Jun 1;65(6):104520.

78. Thomas AX, Link N, Robak LA, Demmler-Harrison G, Pao EC, Squire AE, et al. ANKLE2 - related microcephaly: A variable microcephaly syndrome resembling Zika infection. Ann Clin Transl Neurol. 2022 Jul 24;9(8):1276–88.

79. Cullen CF, Brittle AL, Ito T, Ohkura H. The conserved kinase NHK-1 is essential for mitotic progression and unifying acentrosomal meiotic spindles in *Drosophila melanogaster*. J Cell Biol. 2005 Nov 21;171(4):593–602.

80. Ivanovska I, Khandan T, Ito T, Orr-Weaver TL. A histone code in meiosis: the histone kinase, NHK-1, is required for proper chromosomal architecture in *Drosophila* oocytes. Genes Dev. 2005 Nov 1;19(21):2571–82.

81. Lancaster OM, Cullen CF, Ohkura H. NHK-1 phosphorylates BAF to allow karyosome formation in the *Drosophila* oocyte nucleus. J Cell Biol. 2007 Dec 3;179(5):817–24.

82. Cao-Lormeau VM, Blake A, Mons S, Lastère S, Roche C, Vanhomwegen J, et al. Guillain-Barré Syndrome outbreak associated with Zika virus infection in French Polynesia: a case-control study. Lancet. 2016 Apr 9;387(10027):1531–9.

83. Campo M del, Feitosa IML, Ribeiro EM, Horovitz DDG, Pessoa ALS, França GVA, et al. The phenotypic spectrum of congenital Zika syndrome. American Journal of Medical Genetics Part A. 2017;173(4):841–57.

84. da Fonseca JO, de Oliveira Vianna RA, Carvalho FR, Velarde LGC, de Oliveira SA, Cardoso CAA, et al. The Hip of Children with Congenital Zika Syndrome: A Prospective Observational Study. J Pediatr. 2023 May;256:27–32.

85. de Araújo TVB, Rodrigues LC, de Alencar Ximenes RA, de Barros Miranda-Filho D, Montarroyos UR, de Melo APL, et al. Association between Zika virus infection and microcephaly in Brazil, January to May, 2016: preliminary report of a case-control study. Lancet Infect Dis. 2016 Dec;16(12):1356–63.

86. Moore CA, Staples JE, Dobyns WB, Pessoa A, Ventura CV, Fonseca EB da, et al. Characterizing the Pattern of Anomalies in Congenital Zika Syndrome for Pediatric Clinicians. JAMA Pediatr. 2017 01;171(3):288–95.

87. Roth NM. Zika-Associated Birth Defects Reported in Pregnancies with Laboratory Evidence of Confirmed or Possible Zika Virus Infection — U.S. Zika Pregnancy and Infant

Registry, December 1, 2015–March 31, 2018. MMWR Morb Mortal Wkly Rep [Internet]. 2022 ;71. Available from: https://www.cdc.gov/mmwr/volumes/71/wr/mm7103a1.htm

88. Adachi K, Romero T, Nielsen-Saines K, Pone S, Aibe M, Barroso de Aguiar E, et al. Early Clinical Infancy Outcomes for Microcephaly and/or Small for Gestational Age Zika-Exposed Infants. Clin Infect Dis. 2020 Jun 15;70(12):2663–72.

89. Nunes PS, Guimarães RA, Martelli CMT, de Souza WV, Turchi MD. Zika virus infection and microcephaly: spatial analysis and socio-environmental determinants in a region of high *Aedes aegypti* infestation in the Central-West Region of Brazil. BMC Infectious Diseases. 2021 Oct 27;21(1):1107.

90. N. Costa MC, Cardim LL, Teixeira MG, Barreto ML, de Carvalho-Sauer R de CO, R. Barreto F, et al. Case Fatality Rate Related to Microcephaly Congenital Zika Syndrome and Associated Factors: A Nationwide Retrospective Study in Brazil. Viruses. 2020 Oct 29;12(11):1228.

91. de Fatima Vasco Aragao M, van der Linden V, Brainer-Lima AM, Coeli RR, Rocha MA, Sobral da Silva P, et al. Clinical features and neuroimaging (CT and MRI) findings in presumed Zika virus related congenital infection and microcephaly: retrospective case series study. BMJ. 2016 Apr 13;353:i1901.

92. Fishburn AT, Pham OH, Kenaston MW, Beesabathuni NS, Shah PS. Let's Get Physical: Flavivirus-Host Protein–Protein Interactions in Replication and Pathogenesis. Frontiers in Microbiology [Internet]. 2022 [cited 2022 Mar 3];13. Available from: https://www.frontiersin.org/article/10.3389/fmicb.2022.847588

93. Shah PS, Link N, Jang GM, Sharp PP, Zhu T, Swaney DL, et al. Comparative Flavivirus-Host Protein Interaction Mapping Reveals Mechanisms of Dengue and Zika Virus Pathogenesis. Cell. 2018 13;175(7):1931-1945.e18.

94. Miranda-Gonçalves V, Lobo J, Guimarães-Teixeira C, Barros-Silva D, Guimarães R, Cantante M, et al. The component of the m6A writer complex VIRMA is implicated in

aggressive tumor phenotype, DNA damage response and cisplatin resistance in germ cell tumors. J Exp Clin Cancer Res. 2021 Aug 25;40:268.

95. Al-Farsi H, Al-Azwani I, Malek JA, Chouchane L, Rafii A, Halabi NM. Discovery of new therapeutic targets in ovarian cancer through identifying significantly non-mutated genes. Journal of Translational Medicine. 2022 May 26;20(1):244.

96. Gao A, Sun T, Ma G, Cao J, Hu Q, Chen L, et al. LEM4 confers tamoxifen resistance to breast cancer cells by activating cyclin D-CDK4/6-Rb and ERα pathway. Nat Commun. 2018 Oct 9;9(1):4180.

97. Stendahl M, Kronblad Å, Rydén L, Emdin S, Bengtsson NO, Landberg G. Cyclin D1 overexpression is a negative predictive factor for tamoxifen response in postmenopausal breast cancer patients. Br J Cancer. 2004 May 17;90(10):1942–8.

98. He T, Zhang Y, Li X, Liu C, Zhu G, Yin X, et al. Collective analysis of the expression and prognosis for LEM-domain proteins in prostate cancer. World J Surg Oncol. 2022 Jun 2;20:174.

99. Wood JG, Mirra SS, Pollock NJ, Binder LI. Neurofibrillary tangles of Alzheimer disease share antigenic determinants with the axonal microtubule-associated protein tau (tau). Proceedings of the National Academy of Sciences. 1986 Jun;83(11):4040–3.

100. Xia Y, Prokop S, Gorion KMM, Kim JD, Sorrentino ZA, Bell BM, et al. Tau Ser208 phosphorylation promotes aggregation and reveals neuropathologic diversity in Alzheimer's disease and other tauopathies. Acta Neuropathologica Communications. 2020 Jun 22;8(1):88.

101. Meng JX, Zhang Y, Saman D, Haider AM, De S, Sang JC, et al. Hyperphosphorylated tau self-assembles into amorphous aggregates eliciting TLR4-dependent responses. Nat Commun. 2022 May 16;13(1):2692.

102. Prissette M, Fury W, Koss M, Racioppi C, Fedorova D, Dragileva E, et al. Disruption of nuclear envelope integrity as a possible initiating event in tauopathies. Cell Rep. 2022 Aug 23;40(8):111249.

103. Polanco JC, Akimov Y, Fernandes A, Briner A, Hand GR, van Roijen M, et al. CRISPRi screening reveals regulators of tau pathology shared between exosomal and vesicle-free tau. Life Sci Alliance. 2022 Oct 31;6(1):e202201689.

104. Link N, Harnish JM, Hull B, Gibson S, Dietze M, Mgbike UE, et al. A Zika virus protein expression screen in *Drosophila* to investigate targeted host pathways during development. Dis Model Mech. 2024 Jan 12;dmm.050297.

105. Jumper J, Evans R, Pritzel A, Green T, Figurnov M, Ronneberger O, et al. Highly accurate protein structure prediction with AlphaFold. Nature. 2021 Aug;596(7873):583–9.

106. Varadi M, Anyango S, Deshpande M, Nair S, Natassia C, Yordanova G, et al. AlphaFold Protein Structure Database: massively expanding the structural coverage of protein-sequence space with high-accuracy models. Nucleic Acids Research. 2022 Jan 7;50(D1):D439–44.

107. Hallgren J, Tsirigos KD, Pedersen MD, Armenteros JJA, Marcatili P, Nielsen H, et al. DeepTMHMM predicts alpha and beta transmembrane proteins using deep neural networks [Internet]. bioRxiv; 2022 [cited 2023 Jul 26]. p. 2022.04.08.487609. Available from: https://www.biorxiv.org/content/10.1101/2022.04.08.487609v1

108. Sievers F, Wilm A, Dineen D, Gibson TJ, Karplus K, Li W, et al. Fast, scalable generation of high-quality protein multiple sequence alignments using Clustal Omega. Mol Syst Biol. 2011 Oct 1;7:539.

Chapter 4: Microcephaly protein ANKLE2 promotes Zika virus replication

Orthoflaviviruses are positive-sense single-stranded RNA viruses that hijack host proteins to promote their own replication. Zika virus (ZIKV) is infamous among orthoflaviviruses for its association with severe congenital birth defects, notably microcephaly. We previously mapped ZIKV-host protein interactions and identified the interaction between ZIKV non-structural protein 4A (NS4A) and host microcephaly protein ankyrin repeat and LEM domain-containing 2 (ANKLE2). We showed that NS4A induced microcephaly in an ANKLE2-dependent manner. Here, we explore the role of ANKLE2 in ZIKV replication to understand the biological significance of the interaction from a viral perspective. We observe that ANKLE2 localization is drastically shifted to sites of NS4A accumulation during infection. We show that transient knockdown or stable knockout of ANKLE2 reduces ZIKV replication in multiple human cell lines. Using transmission electron microscopy, we observe disrupted virus replication organelles in ANKLE2 knockout cells. Knockdown of the ANKLE2 ortholog in mosquito Aag2 cells also leads to decreased virus replication, suggesting ANKLE2 is a beneficial replication factor across hosts. Finally, we show that NS4A from four other orthoflaviviruses physically interacts with ANKLE2 and that ANKLE2 is beneficial to the replication of dengue virus. Taken together with our previous results, our findings indicate that ZIKV disrupts the physiological function of ANKLE2 to cause disease in the process of hijacking it for replication.

Introduction

Orthoflaviviruses are positive-sense single-stranded RNA viruses that cause severe disease. Many orthoflaviviruses, such as Zika virus (ZIKV), dengue virus (DENV), West Nile virus (WNV), and yellow fever virus (YFV) are transmitted by mosquitoes and represent significant public health

threats worldwide. The RNA genome of orthoflaviviruses is roughly ~11kb. Upon entry, this genome is directly translated into a single viral polyprotein and cleaved by host and viral proteases into 10 individual viral proteins. Three structural proteins (capsid, prM, and envelope [E]) makeup the physical virion, while seven non-structural (NS) proteins (NS1, NS2A, NS2B, NS3, NS4A, NS4B, and NS5) facilitate aspects of virus replication within the host cell (1). Orthoflavivirus replication occurs on the cytoplasmic side of the host endoplasmic reticulum (ER) membrane, which is remodeled by other viral proteins to form virus replication organelles (2,3). These organelles include replication compartments or vesicles (Ve), which bud into the ER membrane to concentrate substrates and conceal newly generated dsRNA from host detection (4). In addition to Ve, orthoflaviviruses also generate amorphous structures called convoluted membranes (CM). CM are believed to mediate aspects of protein translation, maturation, and degradation (5–7). NS4A is integral to the formation of orthoflavivirus replication organelles in the ER by inducing membrane curvature (8,9) and through its interactions with host proteins (10–13).

ZIKV emerged as a global threat in 2015 during an epidemic that spread across South and Central America (14). ZIKV infection in adults typically leads to mild symptoms and very rarely Guillain-Barré Syndrome (15). The primary concern surrounding ZIKV arises from the occurrence of Congenital Zika Syndrome (CZS) in individuals infected *in utero* (16). CZS is a spectrum of disease and can be clinically characterized by multiple hallmark features, including congenital contractures, ocular anomalies, cortical calcifications, and in the most severe cases, microcephaly (17,18). Microcephaly is a condition in which the head and brain size are significantly reduced at birth (more than two standard deviations below the mean), and it is associated with a wide range of complications, including developmental delays, intellectual disability, and predisposition to seizures (19). In recent years, significant research has been dedicated to understanding mechanisms of ZIKV-induced neuropathogenesis. The mechanisms can be non-specific and broadly acting, such as the cytopathic effect of virus replicating in developing tissues, the systemic

immune response, and the disruption of important biological barriers (*e.g.,* placenta, blood-brain-barrier) (20,21). Mechanisms can also be highly specific, such as modulation of neuronal or neural progenitor cell growth through molecular interactions between viral and host components (22–24).

Previously, we used affinity-purification and mass-spectrometry to identify ZIKV-host protein-protein interactions that may contribute to the development of microcephaly in CZS (25). By searching for host proteins with known roles in neurodevelopment or associations with microcephaly, we identified the interaction between ZIKV NS4A and host ankyrin repeat and LEM domain-containing 2 (ANKLE2). ANKLE2 is primarily considered a scaffolding protein, facilitating protein-protein interactions between kinases, phosphatases, and their substrates. ANKLE2 localizes to the ER and inner nuclear membrane where it mediates interactions with proteins, including barrier to autointegration factor (BANF1), vaccinia related kinase 1 (VRK1), and protein phosphatase complex 2A (PP2A), to control nuclear membrane disassembly during cell division (26,27). Pathogenic mutations in *ANKLE2* cause congenital microcephaly in humans (28–30). Loss-of-function mutations in fly *Ankle2* cause small brain phenotypes and cellular defects in neuroblasts of third instar larvae. These phenotypes are rescued by the expression of human ANKLE2, suggesting that human ANKLE2 and fly Ankle2 are functionally conserved in brain development (28,30). Using this *Drosophila* model, we previously showed that transgenic expression of ZIKV NS4A induces similar microcephaly phenotypes which are also rescued by the expression of human ANKLE2. Overall, this suggests NS4A induces microcephaly *in vivo* in an ANKLE2-dependent manner (25,28).

Whether NS4A inhibition of ANKLE2 function during development is simply an unfortunate coincidence, or if there is a functional role for this virus-host protein interaction in ZIKV replication is unknown. In this study we explore the possibility that ANKLE2 plays a role in ZIKV replication. We find ANKLE2 concentrates at sites of NS4A accumulation during infection. Depletion of

ANKLE2 reduces ZIKV replication in multiple cell lines that represent biologically relevant sites of ZIKV infection. Transmission electron microscopy (TEM) of ANKLE2 knockout cells reveals deficiencies in the formation of virus replication organelles, providing insight into a potential mechanism. Further, we show that silencing of the ANKLE2 ortholog in mosquito cells also reduces ZIKV replication, suggesting a conserved role in replication across hosts. The NS4A-ANKLE2 interaction is conserved across mosquito-borne orthoflaviviruses and ANKLE2's role in virus replication is conserved to varying degrees. Altogether, we report the novel function of ANKLE2 in promoting ZIKV infection, providing evidence that NS4A disruption of neurodevelopment through ANKLE2 may arise from an underlying virus replication mechanism.

Results

ANKLE2 colocalizes with NS4A during ZIKV infection

Our previous studies established the interaction between ANKLE2 and NS4A (25), but only in the context of exogenously expressing a single viral protein. Therefore, we evaluated ANKLE2 subcellular localization during ZIKV infection. We generated HEK293T cells that express FLAG affinity tagged fusions of ANKLE2 (ANKLE2-FLAG). As controls, we also generated cells that express GFP-FLAG as a general non-specific control and ANKLE1-FLAG to distinguish between intrinsic localization in this family of proteins, and localization unique to ANKLE2. We infected these cells with three ZIKV strains (PLCal, MR766, and PRVABC59) and evaluated the colocalization of FLAG and NS4A. Strikingly, we found that ANKLE2 distribution became concentrated after infection, with near perfect overlap with NS4A (Figure 4-1A). Conversely, we found that the localization of GFP and ANKLE1 did not change following ZIKV infection (Figure 4-1B-C). We measured colocalization between FLAG and NS4A signal using Pearson's correlation and consistently found very high levels of colocalization between ANKLE2 and NS4A, which was significantly higher than GFP or ANKLE1 with NS4A (Figure 4-1D).

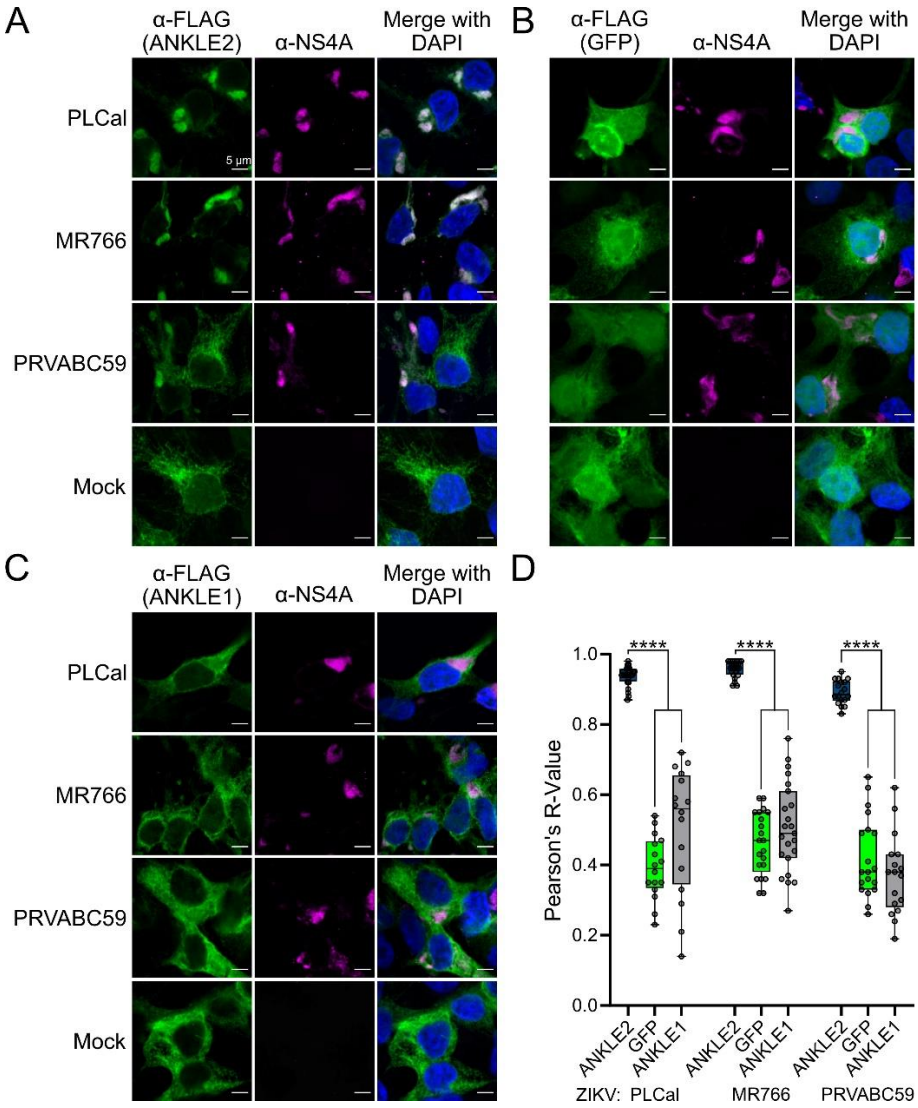

Figure 4-1: ANKLE2 colocalizes with ZIKV NS4A during infection. (A-C) HEK293T cells expressing either ANKLE2-, GFP-, or ANKLE1-3xFLAG were infected with designated ZIKV strain for 48 hours. Cells were then fixed and imaged using confocal microscopy. (D) Pearson's correlation was determined to quantify degree of colocalization between FLAG and NS4A, n = 16-24 cells per condition. **** $p > 0.0001$, one-way ANOVA with Šidák multiple comparisons test. Grey circles represent the values of individual cells. All scale bars = 5 μm.

Given the known role of NS4A in forming orthoflavivirus Ve, we next explored if ANKLE2 colocalizes with dsRNA generated in these Ve. In HEK 293T cells infected with ZIKV MR766, we observed a punctate dsRNA signal compared to ANKLE2 and NS4A (Figure 4-2A and B). Despite this, correlation of ANKLE2 and NS4A with dsRNA was still significantly higher than correlation of ectopically expressed GFP with dsRNA (Figure 4-2C and D), suggesting that this modest correlation is still biologically meaningful. Given the physical interaction and high colocalization between NS4A and ANKLE2, as well as the similarities between the colocalization of these proteins with dsRNA, we speculated that ANKLE2 may be participating in ZIKV replication.

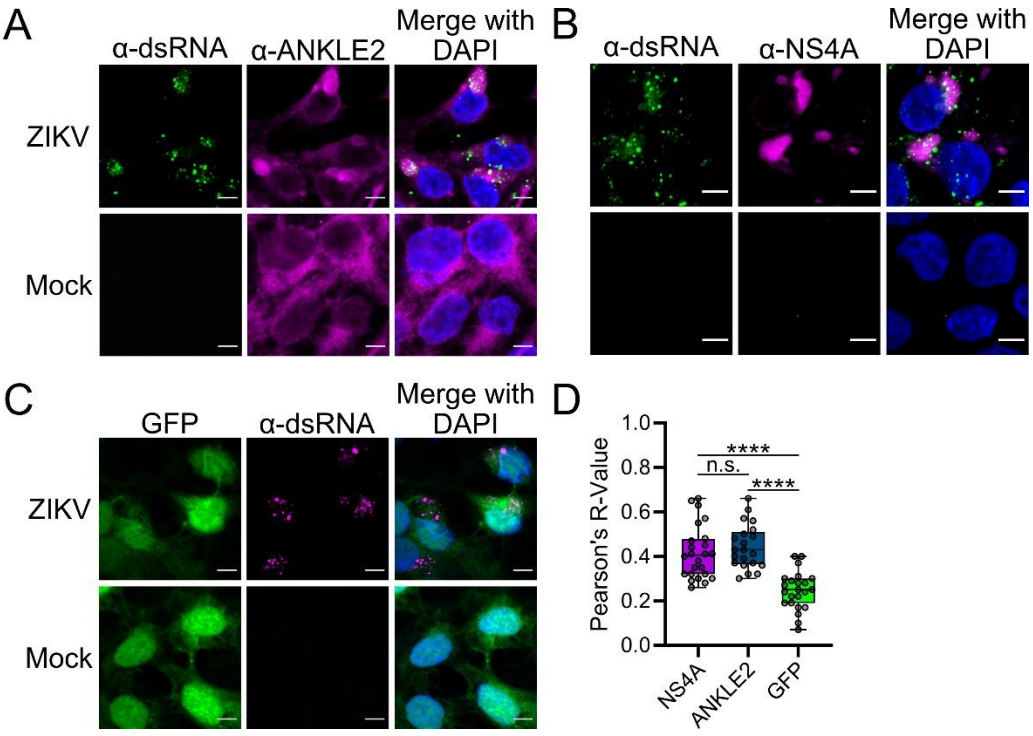

Figure 4-2: ANKLE2 partially colocalizes with ZIKV dsRNA during infection. (A-C) Confocal microscopy of HEK293T cells infected with ZIKV MR766 at MOI 5 for 48 hours. (D) Pearson's correlation was determined to quantify the degree of colocalization between denoted target signal and dsRNA, n = 21-24 cells per condition. One-way ANOVA with Tukey's multiple comparisons test, n.s., not significant, **** $p < 0.0001$. Grey circles represent the values of individual cells. All scale bars = 5 μm.

ANKLE2 depletion reduces ZIKV replication in Huh7 cells

We next tested the role of ANKLE2 in ZIKV replication using a gene perturbation approach. We chose Huh7 cells, derived from a human hepatocarcinoma, since they are readily infected by ZIKV *in vitro* (31,32), and the liver is an established site of ZIKV replication *in vivo* (33–35). We also observed similar localization patterns of ANKLE2 and dsRNA in these cells (Figure 4-4A). Initially, we used a transient CRISPRi knockdown system by reverse-transfecting gRNAs into dCas9-expressing Huh7 cells. We observed modest, but consistent, decreases in ZIKV replication following ANKLE2 knockdown across two ZIKV strains and multiple multiplicities of infection (MOIs) (Figure 4-3). We hypothesized that these modest phenotypes arise from incomplete depletion of ANKLE2 in this system (Figure 4-3C and 1H).

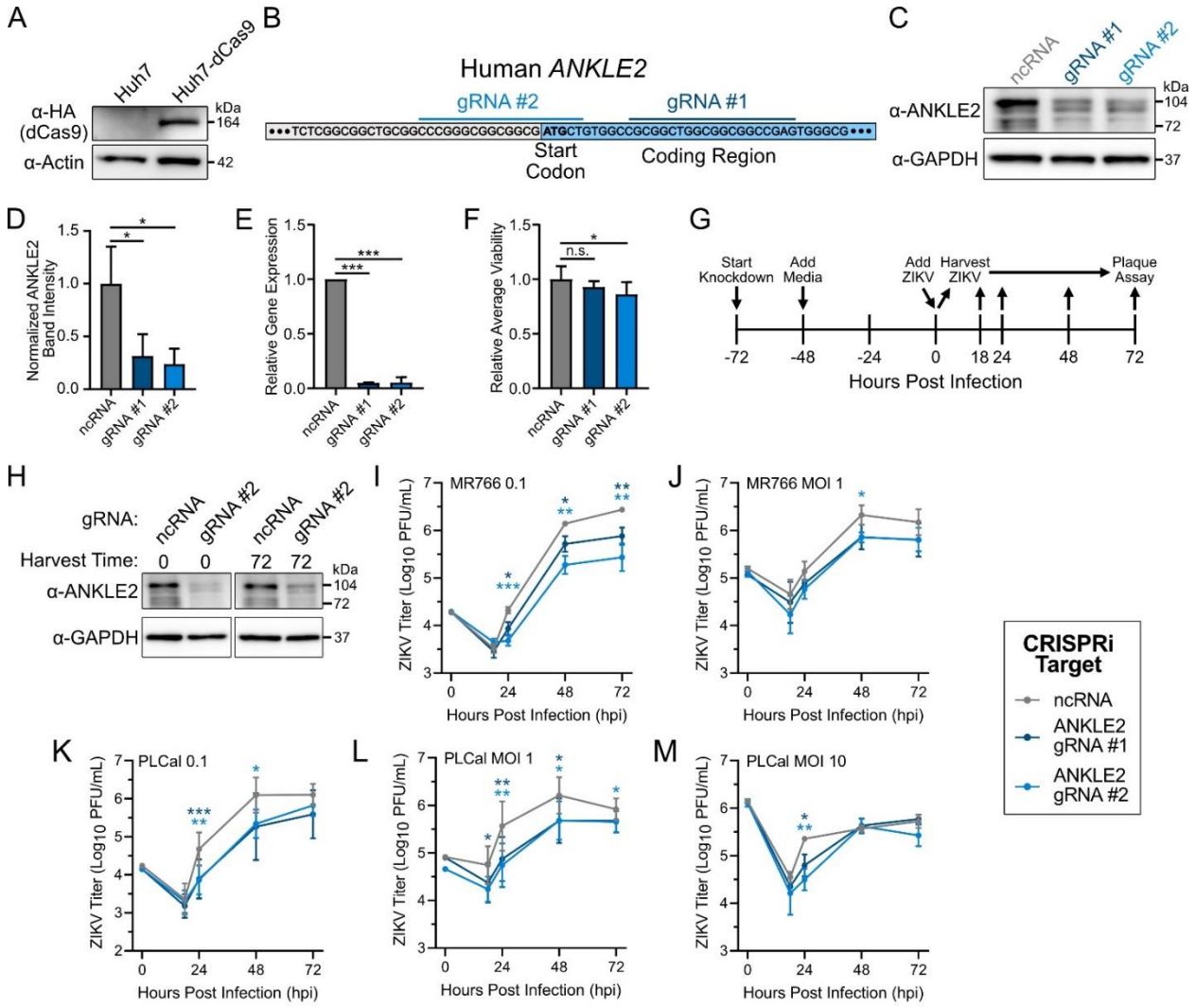

Figure 4-3: CRISPRi knockdown of ANKLE2 in Huh7-dCas9 cells reduces ZIKV replication. (A) Western blot to evaluate the expression of dCas9-HA in Huh7 cells that were used for CRISPRi experiments. (B) Schematic of ANKLE2 and the targeting guide RNAs (gRNA) that were used to knockdown ANKLE2 expression. (C) Western blot to evaluate ANKLE2 expression after CRISPRi knockdown with three different gRNAs. The primary isoform is shown at 104kDa, and the knockdown of various other isoforms can be observed at 76 and 73kdA (Appendix A-1). A known background band associated with this antibody at ~96kDa is visible and unchanged. (D) Densitometry analysis to quantify ANKLE2 band intensity. ANKLE2 band intensity was normalized to its respective loading control and then normalized to ncRNA. Error bars represent the standard

deviation between three biological replicates. (E) ANKLE2 gene expression after knockdown was quantified by qRT-PCR. Error bars represent the standard deviation between three biological replicates. (F) Cell viability was evaluated using ZombieGreen dye. Data represents the average cell viability across ten images for each condition. (G) Schematic for 72-hour CRISPRi knockdown, followed by 72-hour ZIKV infection. Supernatant was harvested from infected cells at 0, 18, 24, 48, and 72 hours post infection and assessed by plaque assay. (H) Western blot validation that ANKLE2 knockdown persists for additional 72 hours after removal of transfection reagents. (I-M) After a 72-hour knockdown, transfected cells were infected with either ZIKV MR766 (I-J) or PLCal (K-M) at designated MOI. Virus titers were determined using plaque assay. All error bars represent the standard deviation. (I, J, M) Three technical replicates. Student's unpaired two-tailed t-test. (K, L) Five biological replicates. Student's paired two-tailed t-test. All statistical tests compared to ncRNA condition, n.s., not significant, * $p < 0.05$, ** $p < 0.01$, *** $p < 0.001$.

We next sought to achieve more complete depletion of ANKLE2 in Huh7 cells using CRISPR mutagenesis. We generated two stable knockout clones by targeting the first exon of *ANKLE2* (hereon referred to as H1 and H2). As a control we also generated a bulk cell line using a non-specific negative control gRNA (referred to as H-ncg). We observed substantial depletion of ANKLE2 in our two clonal populations, with some residual ANKLE2 remaining the H1 clone (Figure 4-4B). We evaluated virus replication in these cells by infecting them with ZIKV PLCal at MOI 0.1 and western blotting for viral proteins at 0, 48, and 72 hours post infection (hpi). We observed substantial depletion of ANKLE2 in our two clonal populations, with some residual ANKLE2 remaining the H1 clone. We observed reduced levels of ZIKV E protein in H1 cells and no E protein detected in H2 cells (Figure 4-4B). We repeated this experiment at MOI 0.1 and 1 and evaluated the abundance of other ZIKV proteins (NS4A and capsid), which were also strongly

reduced in our clonal populations (Figure 4-4C). Next, we measured titers of ZIKV PLCal in these cells and found significant and consistent reduction in ZIKV titers at three MOIs (0.1, 1, or 10), with a maximum decrease of ~2.5 logs in the H2 clone when infected at MOI 0.1 (Figure 4-4D-F). Interestingly, we observed a consistent difference between clones H1 and H2, with H2 having the more dramatic phenotype. This is supported by a small amount of ANKLE2 remaining in the H1 clone (Figure 4-4B). The more modest phenotype in our H1 clone resembles the ~1 log decreases in virus titer that we observed in CRISPRi experiments where ANKLE2 expression was only partially suppressed (Figure 4-3). Further, sequencing our clones revealed H2 had a single *ANKLE2* mutation, while H1 was not entirely a monoclonal population and contained four similarly abundant mutations (Appendix B-2). To validate our results, we infected H-ncg and H2 with other Asian lineage ZIKV strains, PRVABC59, FSS13025, or H/PF/2013, and observed similar ~1-2 log decreases in virus replication at 48 and 72 hpi (Figure 4-4G-I).

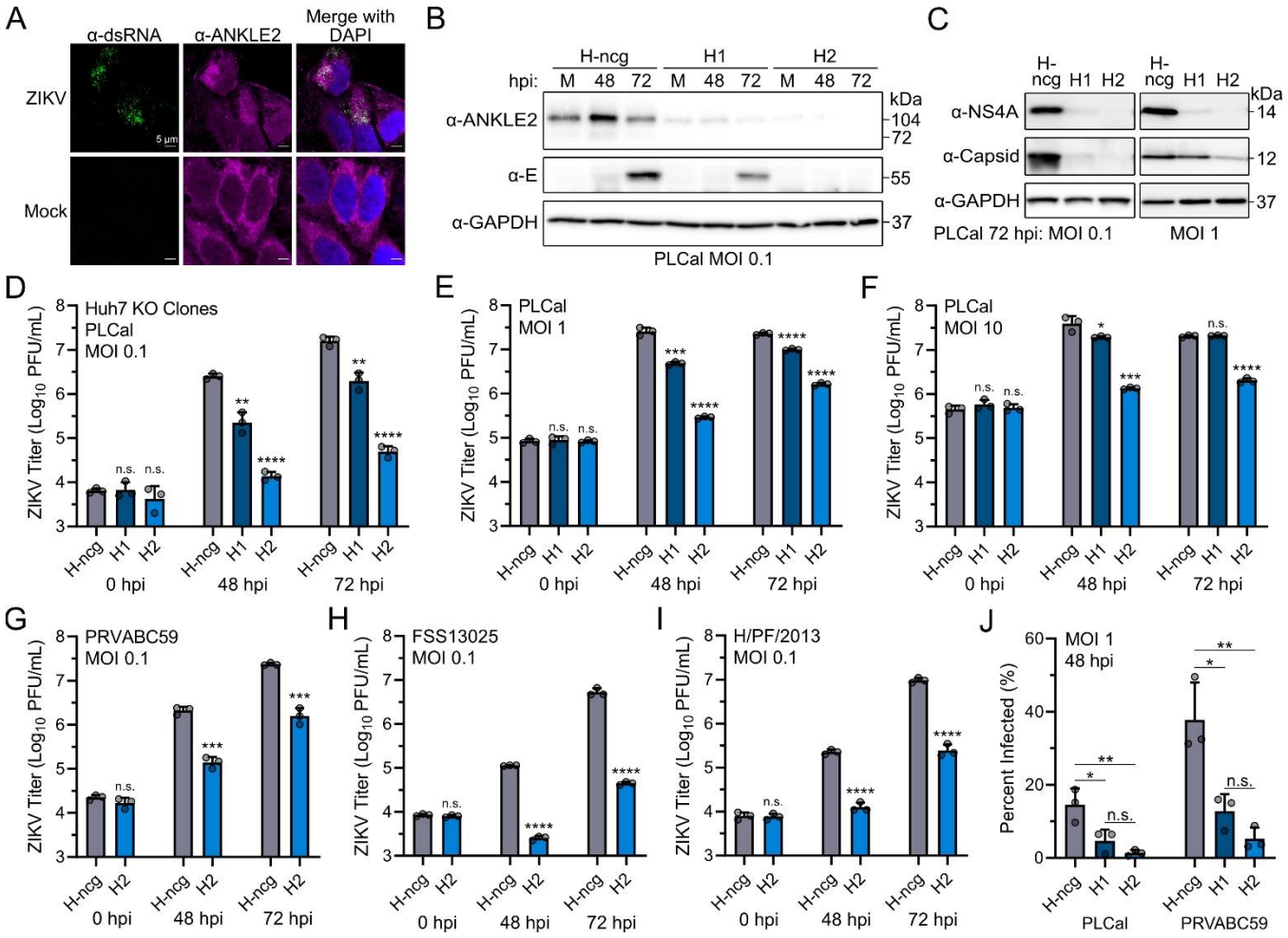

Figure 4-4: Knockout of ANKLE2 reduces ZIKV replication in Huh7 cells. (A) Confocal microscopy of ANKLE2 and dsRNA in ZIKV infected Huh7 cells (MOI 5, 48 hours). (B) Clonal ANKLE2 knockout Huh7 cells (H1 and H2) were generated with CRISPR and infected with ZIKV PLCal at MOI 0.1. Expression of ANKLE2 and viral proteins were assessed by western blot and compared to mock infected cells "M". (C) Cells were infected with ZIKV PLCal at MOI 0.1 or 1 for 72 hours and ZIKV protein levels were evaluated by western blot. (D-F) Knockout cells were infected with ZIKV PLCal at noted MOI. Supernatant was collected at noted times and virus titer was determined by plaque assay. All statistical comparisons are made to negative control guide RNA (H-ncg) cells. (G-I) Replication kinetics of additional ZIKV strains in control and H2 clonal cells. (J) Cells were infected with ZIKV PLCal or PRVABC59 at MOI 1 for 48 hours prior to analysis by immunofluorescence microscopy. Images identities were blinded prior to counting infected

cells. Three biological replicates, at least 10 images per replicate, n = ~2800 - 5600 total cells per condition. Student's two-tailed T-test., n.s., not significant, * $p < 0.05$, ** $p < 0.01$, *** $p < 0.001$, **** $p < 0.0001$.

To further characterize and validate our Huh7 clones we performed confocal and high-throughput fluorescence microscopy, either in mock-, PLCal-, or PRVABC59-infected cells at MOI 1 for 48 hours. We observed a significant reduction in ANKLE2 fluorescence intensity and hypothesize that the residual signal is likely background (Supplemental Figure 4-5A-B). ANKLE2 knockout HeLa cells show dramatic increases in nuclear area (27), however we did not observe any biologically relevant increase in our Huh7 knockout cells (Supplemental Figure 4-5C). We determined the percentage of cells infected based on the presence of E signal, as measured by 4G2 staining. This recapitulated the results of our previous titration experiments, with decreases in H1 and H2 for both PLCal and PRVABC59 strains (Figure 4-4I, Figure 4-5D). Due to the established role of ANKLE2 in nuclear envelope disassembly and neuroprogenitor division (26,28), we hypothesized we might observe aberrations in cell division. However, we observed no difference in the number of mitotic cells in either clone, in the absence or presence of virus infection (Figure 4-5E).

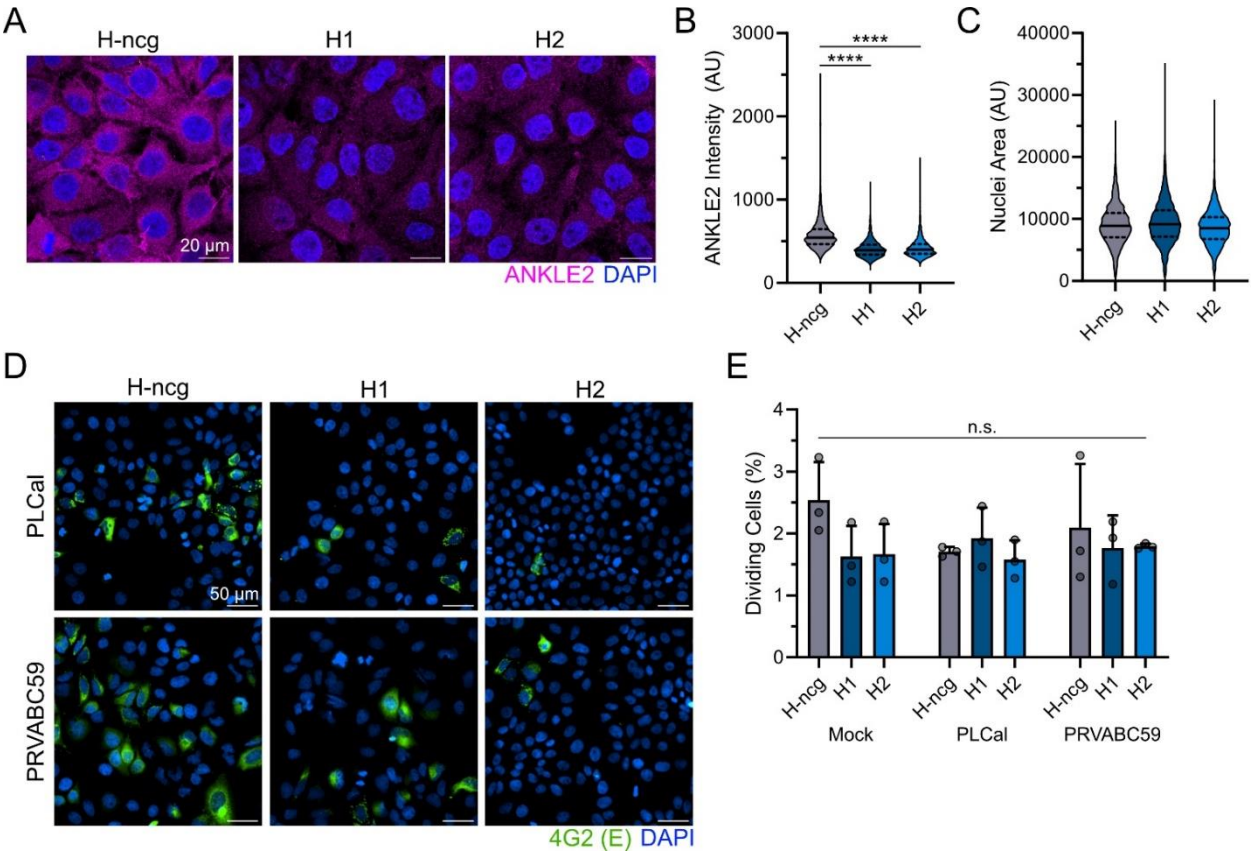

Figure 4-5: Morphological characterization of ANKLE2 knockout cells. (A) Confocal microscopy of Huh7 ANKLE2 knockout cells. Evaluating ANKLE2 (magenta) and DAPI (blue). (B) ANKLE2 fluorescence intensity was measured across three biological replicates, n = ~1500 - 2100 cells per condition. (C) Nuclei area was determined using cellpose masking. Three biological replicates, n = ~2600 - 3300 cells per condition. (D) Representative images of cells infected with ZIKV (PLCal or PRVABC59) at MOI 1 for 48 hours used to determine percent of cells infected (Figure 2I). (E) Images were assessed for cells visibly in any stage of mitosis. Grey circles represent the average value of each technical replicate (at least ten images per replicate). One-way ANOVA with Dunnett's multiple comparisons when appropriate. All statistical tests compared to ncgRNA condition, n.s., not significant, **** $p < 0.0001$.

To eliminate the possibility of off-target effects we sought to complement ANKLE2 expression to our knockout cells. We transduced our H-ncg or H2 cells with lentivirus to stably induce expression of ANKLE2-mCherry-3xFLAG (A2) or mCherry (Ch) alone as a control. Confocal microscopy showed expression of our fusion protein and that expression in rescued cells was higher than endogenous levels (Figure 4-6A). The fusion protein also retained correct ER localization (Figure 4-6B). ZIKV infection of these cells revealed nearly complete absence of ZIKV E protein in H2+Ch cells, with a moderate increase in H2+A2 cells, however this was still much less than either H-ncg population, suggesting only a partial rescue of the replication phenotype (Figure 4-6C). This was consistent with virus titers which showed a ~0.5 log increase in our rescue population compared to the knockout (H2+A2 vs H2+Ch) (Figure 4-6D). Evaluation of > 7,000 cells using immunofluorescence microscopy revealed a rescue rate of only ~8%, suggesting that our partial rescue is due to incomplete ANKLE2 restoration (Figure 4-6E). It is unclear if this is due to transcriptional silencing, incomplete selection, or instability of the fusion protein. We measured the infection rate by immunofluorescence of this same cell population and observed a partial rescue of this infection rate, similar to our virus titer measurements (Figure 4-6F). In fact, a Fisher's exact test revealed that the small number of successfully rescued H2 cells were more likely to be infected than those without rescue (p-value = 0.00015). Altogether, these results suggest that our rescue phenotypes would be stronger if ANKLE2 expression were more homogeneously restored and that ANKLE2 supports ZIKV infection in Huh7 cells.

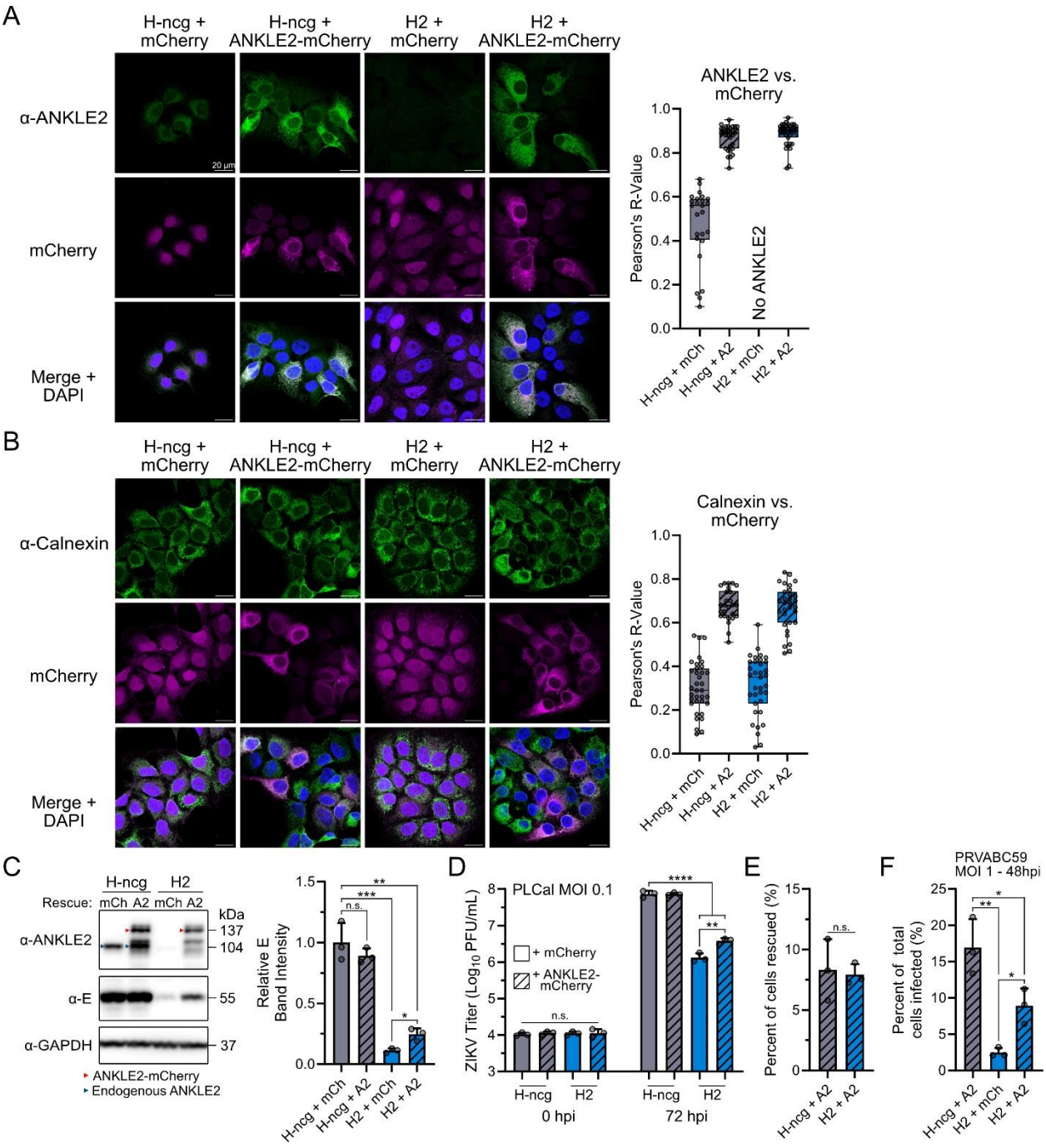

Figure 4-6: Restoration of ANKLE2 to Huh7 knockout cells partially rescues virus replication phenotype. Huh7-ncg control or H2 knockout cells were transduced with lentivirus to express mCherry (mCh) or ANKLE2-mCherry-3xFLAG (A2). (A-B) Cells were immunostained for ANKLE2 (A) or ER marker Calnexin (B) and evaluated by confocal microscopy. Pearson's Correlation was used to measure colocalization. Grey dots represent individual cells, n = 25-35

cells. All scale bars = 20 μm. (C-D) Cells were infected with ZIKV PLCal at MOI 0.1 for 72 hours. ANKLE2 and ZIKV E protein levels were assessed by western blot and measured by densitometry. Virus titers were measured using plaque assay. Grey dots represent technical replicates. (E-F) Cells were plated on coverslips and infected with ZIKV PRVABC59 at MOI 1 for 48 hours. Cells were immunostained for FLAG and ZIKV E protein using the 4G2 antibody. Fluorescent images were acquired (at least ten per replicate) and identities were blinded prior to counting the number of rescue and infected (4G2 positive) cells. Grey dots represent rescue or infection rate from all cells within each of three technical replicates (n = 2100-3400 cells per replicate).

ANKLE2 is not associated with ZIKV entry or internalization

To begin exploring potential mechanisms by which ANKLE2 appears to promote ZIKV replication we sought to initially eliminate entry or internalization as possibilities. We hypothesized that these steps would not be mediated by ANKLE2 based on its established localization to the ER. To test this, we chilled H-ncg or H2 cells on ice to inhibit endocytosis, prior to adding ZIKV PRVABC59 at MOI 2 for 90 minutes. Incubating the inoculum on ice allows for ZIKV binding of host receptors, but not for entry into the cell. After incubation, the cells were thoroughly washed to remove any unbound virions, such that only receptor-bound viruses remained (Figure 4-7A). To assess binding efficiency, RNA was collected immediately after these washes, while the cells remained on ice. If ANKLE2 was an entry receptor for ZIKV then its absence would result in a significant decrease in bound virus and less viral RNA, however we did not observe this, confirming that ANKLE2 is not a receptor for ZIKV (Figure 4-7B). To assess internalization this process was repeated and after virus binding/washing the cells were reintroduced to 37°C to initiate endocytosis. RNA was then collected at 3, 6, 12, 24, or 48 hpi. 3 and 6 hpi represent ZIKV internalization, while 12, 24, and 48 hpi represent the progression of ZIKV replication and spread.

Here, we observed no significant differences at 3 or 6 hpi, supporting our hypothesis that ANKLE2 is not associated with ZIKV internalization. However, we did observe a significant decrease in H2 ZIKV RNA starting at 12 hpi, with progressively larger decreases at 24 and 48 hpi (Figure 4-7B). This additionally manifested in decreased virus titer at 24 and 48 hpi as measured by plaque assay (Figure 4-7C). Similar virus titers at 12 hpi suggest that the initial round of virus production may not be impaired, but genome replication and virus production in H2 is much less efficient as infection progresses.

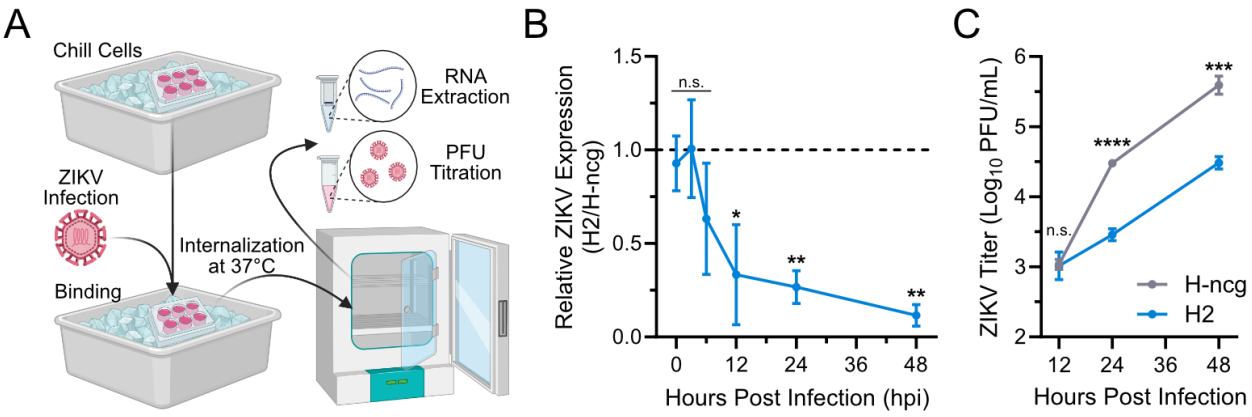

Figure 4-7: ANKLE2 is not necessary for ZIKV entry or internalization. (A) Visual representation of entry/internalization assay. Huh7 cells were chilled on ice to inhibit endocytosis. ZIKV was added and allowed to bind host cell receptors. Cells were then washed thrice to remove unbound viruses, prior to warming cells to allow for virus entry. After 0, 3, 6, 12, 24, or 48 hours of incubation, RNA was harvested to measure relative amounts of ZIKV bound or internalized. At 12, 24, and 48 hours, virus-supernatant was also collected for quantification by plaque assay. (B) Quantification of relative ZIKV RNA by qRT-PCR. H2 (blue line) normalized to H-ncg, represented by dashed line. (C) ZIKV titers at 12, 24, or 48 hours post infection as measured by plaque assay. Data represent average ± standard deviation of four (0, 3, 6 hpi) or three (12, 24, 48 hpi) biological replicates. Student's two-tailed T-test, n.s., not significant, * $p < 0.05$, ** $p < 0.01$, *** $p < 0.001$, **** $p < 0.0001$.

Electron microscopy analysis of ZIKV-induced ER remodeling in ANKLE2 knockout cells

Given that ANKLE2 colocalized with NS4A, we hypothesized that ANKLE2 mediates aspects of ER remodeling and generation of virus replication organelles. To explore this, we examined the structure of the ER and virus replication organelles in control H-ncg cells and ANKLE2 knockout H2 cells by transmission electron microscopy (TEM). The ER in mock infected cells appeared normal in both H-ncg and H2 cells, suggesting that ANKLE2 is not inherently involved in higher-level ER integrity, organization, or structure (Figure 4-8A and B). In ZIKV infected H-ncg cells, we observed stereotypical virus replication organelles in 12 out of 34 cells analyzed, including clusters of CM and Ve which matched the expected size and organization (Figure 4-8C) (2). In ZIKV-infected H2 cells we only observed replication organelles in two out of 38 cells, and the structure of CM was poorly defined (Figure 4-8D). Overall, we observed significantly fewer CM clusters per cell in H2 cells (Figure 4-8E). These data support the idea that ANKLE2 promotes the formation of virus replication organelles to facilitate virus replication.

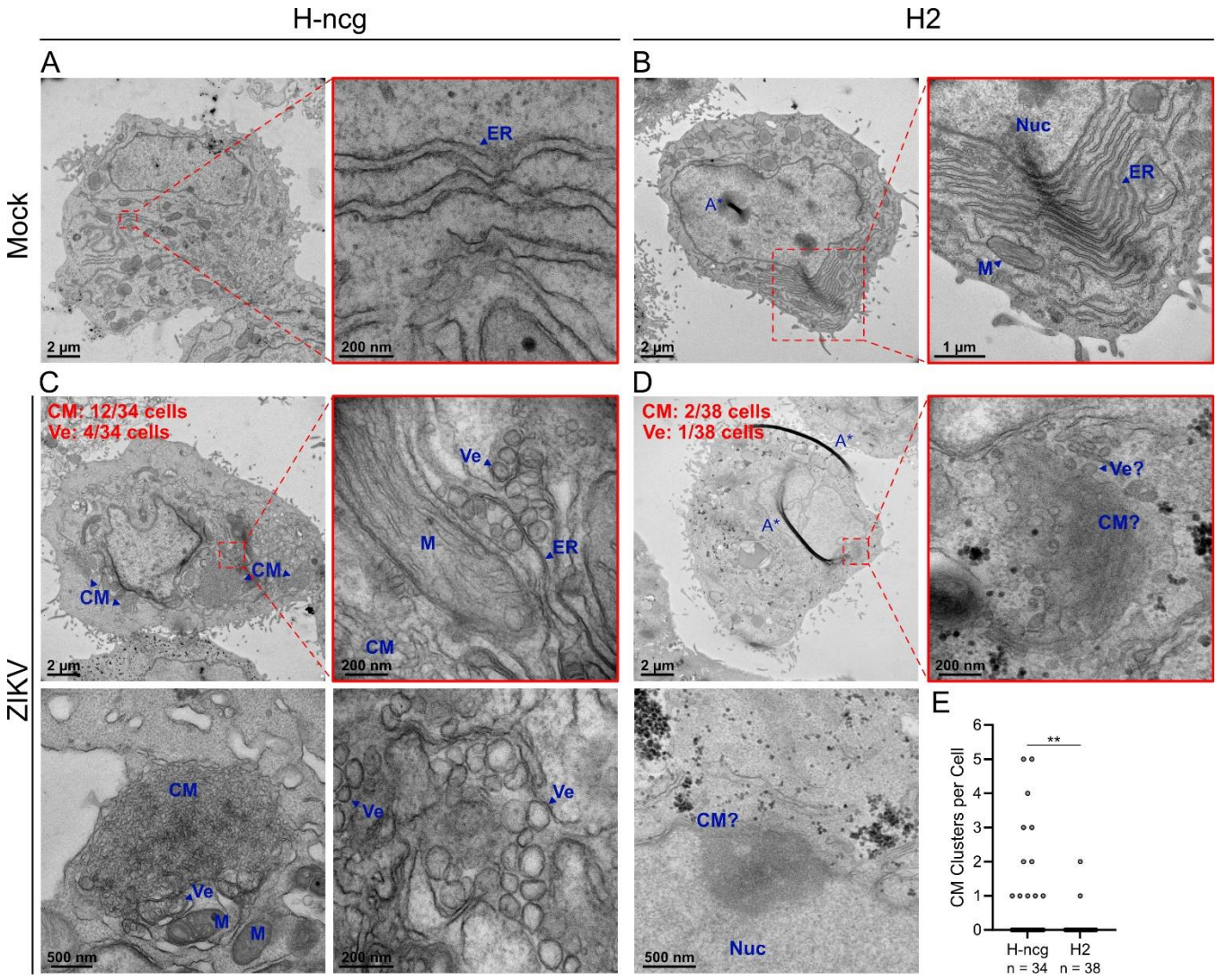

Figure 4-8: Evaluation of ZIKV replication organelles in ANKLE2 knockout Huh7 cells. (A-D) TEM images of ~100-nm thin sections and resin-embedded Huh7 cells. Cells were mock infected (A-B) or infected with ZIKV PRVABC59 at MOI 1 for 48 hours (C-D). Red boxes indicate enlarged images. (C) Stereotypical flavivirus replication organelles were consistently observed in infected H-ncg cells, including virus induced replication vesicles (Ve) and convoluted membranes (CM). Replication organelles were often adjacent or in close association with mitochondria (M). (D) In ZIKV-infected ANKLE2 knockout H2 cells, fewer ZIKV replication organelles were observed and were poorly defined compared to structures observed in control cells. Additional enlarged images of CM and Ve included in C and D from separate cells. The number of cells with observed

CM and Ve are noted in the top left corners. (E) ZIKV-infected H-ncg and H2 cells were indiscriminately imaged and evaluated for presence and amount of CM, which often appeared in discrete clusters throughout the cell. Mann Whitney test, ** $p < 0.01$. Other abbreviations: ER = endoplasmic reticulum, Nuc = nucleus, A* = TEM artifact.

ANKLE2 depletion reduces ZIKV replication in SK-N-SH and JEG-3 cells

We next investigated cell lines representative of tissues targeted by ZIKV during human infection. ZIKV replicates in the developing brain, and we therefore examined the role of ANKLE2 in the neuroblastoma SK-N-SH cell line. We generated a bulk knockout population (SK-g1), with an accompanying control line (SK-ncg). Western blotting revealed a modest ~50% decrease in ANKLE2 protein levels in SK-g1 cells (Figure 4-9A). Unfortunately, SK-N-SH cells were difficult to grow at low cell densities in our hands, so we were unable to generate clonal knockout populations in this cell line. ZIKV infection in SK-g1 cells revealed substantial reduction of ZIKV capsid protein compared to SK-ncg control cells (Figure 4-9A). Virus titers were also significantly reduced across the 72-hour infection for SK-g1 cells (Figure 4-9B).

The placenta is also actively infected during human ZIKV infection and this process is very likely responsible for vertical transmission (36,37). We therefore generated additional knockout clones in placental choriocarcinoma JEG-3 cells (referred to as J1 and J2) with an accompanying control line (J-ncg). ANKLE2 depletion was confirmed by western blotting (Figure 4-9C). We infected these cells with ZIKV and observed reduced levels of ZIKV E and NS4A proteins in J1 and J2 cells by western blotting (Figure 4-9C). We also observed a strong ~1-2 log reduction in virus titers in J1 and J2 cells compared to J-ncg (Figure 4-9D). As a complementary approach we infected all our control and knockout lines and evaluated the fold change of viral genomic material using RT-qPCR. Here, we observed very strong decreases in all our ANKLE2-depleted cell lines (Figure 4-9E). As we did with our Huh7 knockouts, we sought to rescue replication phenotypes

by restoring ANKLE2 expression in JEG-3 cells. We transduced our J-ncg or J2 cells with lentivirus to stably induce expression of ANKLE2-mCherry-3xFLAG (A2) (Figure 4-9F-G) or mCherry (Ch) (not shown). Virus titers showed that J2+A2 had similar virus titers to J-ncg cells, and significantly more than J2+Ch (Figure 4-9H). We did not observe any further increase in E protein or virus titers from J-ncg+Ch to J-ncg+A2 cells, suggesting that overexpression of ANKLE2 does not further increase ZIKV replication. Taken together, we conclude that ANKLE2 supports ZIKV replication in multiple human cell lines and types.

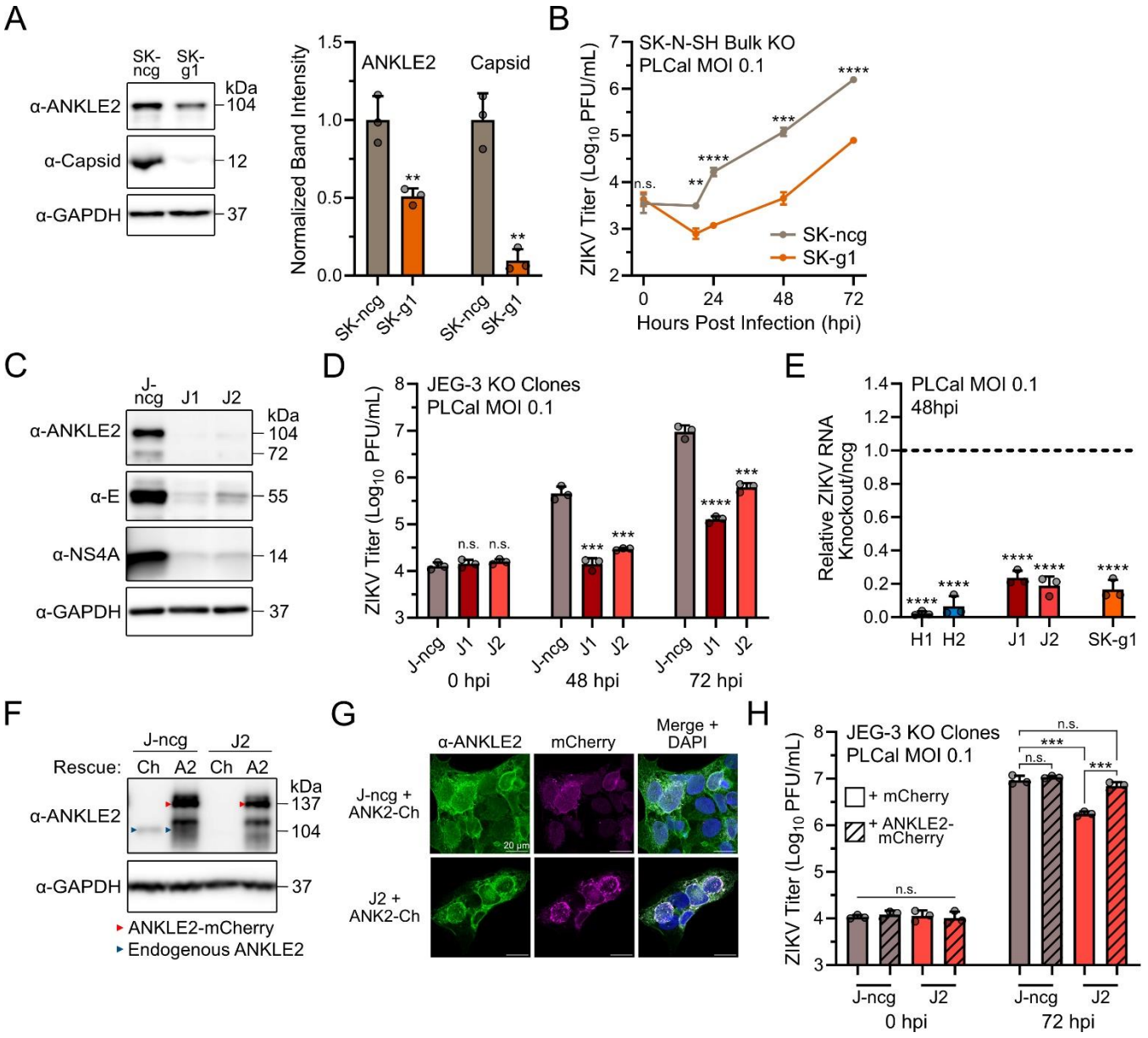

Figure 4-9: Knockout of ANKLE2 reduces ZIKV replication in SK-N-SH and JEG-3 cells. (A-B) A bulk population of ANKLE2 knockout SK-N-SH cells were generated by CRISPR. Cells were infected with ZIKV PLCal at MOI 0.1. ANKLE2 and ZIKV E protein from infected cells were assessed by western blot and virus titer was measured by plaque assay. (C-D) Clonal ANKLE2 knockout JEG-3 cells (J1 and J2) were generated with CRISPR and infected with ZIKV PLCal at MOI 0.1. Expression of ANKLE2 and viral proteins were assessed by western blot. Virus titers from infected-cell supernatant were measured by plaque assay. (E) ANKLE2 knockout Huh7, JEG-3, and SK-N-SH lines were infected with ZIKV PLCal at MOI 0.1 for 48 hours. RNA was harvested and ZIKV replication relative to corresponding ncg line was measured by qRT-PCR. Student's unpaired t-test compared to corresponding normalized ncg control (dashed line). (F-G) JEG-3 cells were transduced with lentivirus to induce expression of mCherry (Ch) or ANKLE2-mCherry-3xFLAG (A2). Confirmation of expression and expected localization was confirmed by western blot and confocal microscopy. (H) Rescued JEG-3 cells were infected with ZIKV PLCal at MOI 0.1 for 72 hours. Virus titers were measured by plaque assay. All bar values shown are means + standard deviation of three infection technical replicates. Grey circles represent the value of each individual replicate. Student's unpaired t-test, n.s., not significant, * $p < 0.05$, ** $p < 0.01$, *** $p < 0.001$, **** $p < 0.0001$.

Mosquito ANKLE2 also promotes ZIKV replication

While ZIKV can be transmitted between humans sexually, vertically, and via blood or organ donation, it is primarily an arbovirus transmitted by *Aedes aegypti* mosquitoes. Successful transmission requires active replication in the mosquito vector. The predicted ANKLE2 ortholog in *A. aegypti* (LOC5576059, UniProtID A0A6I8U7J4) has not been previously characterized, but appears to contain an ankyrin repeat domain very similar to that of human ANKLE2. Given that ZIKV benefits from ANKLE2 in human cells, we hypothesized that ZIKV similarly uses mosquito

ANKLE2 in some capacity as a conserved replication host factor. To test this hypothesis, we performed dsRNA knockdown of ANKLE2 *in vitro* using *Aedes aegypti* Aag2 cells with a GFP targeting dsRNA as a control (Figure 4-10A). Here, we achieved modest decreases in ANKLE2 mRNA expression after 48 hours (Figure 4-10B). We then infected these cells with three strains of ZIKV at three MOIs each and assessed virus titers by plaque assay. We observed consistent decreases in ZIKV titer at 48 hpi across MOIs and ZIKV strains (Figure 4-10C-E, Appendix B-1). These experiments support our hypothesis that the ANKLE2 ortholog is beneficial for ZIKV replication in mosquito cells and may serve as a conserved ZIKV replication factor.

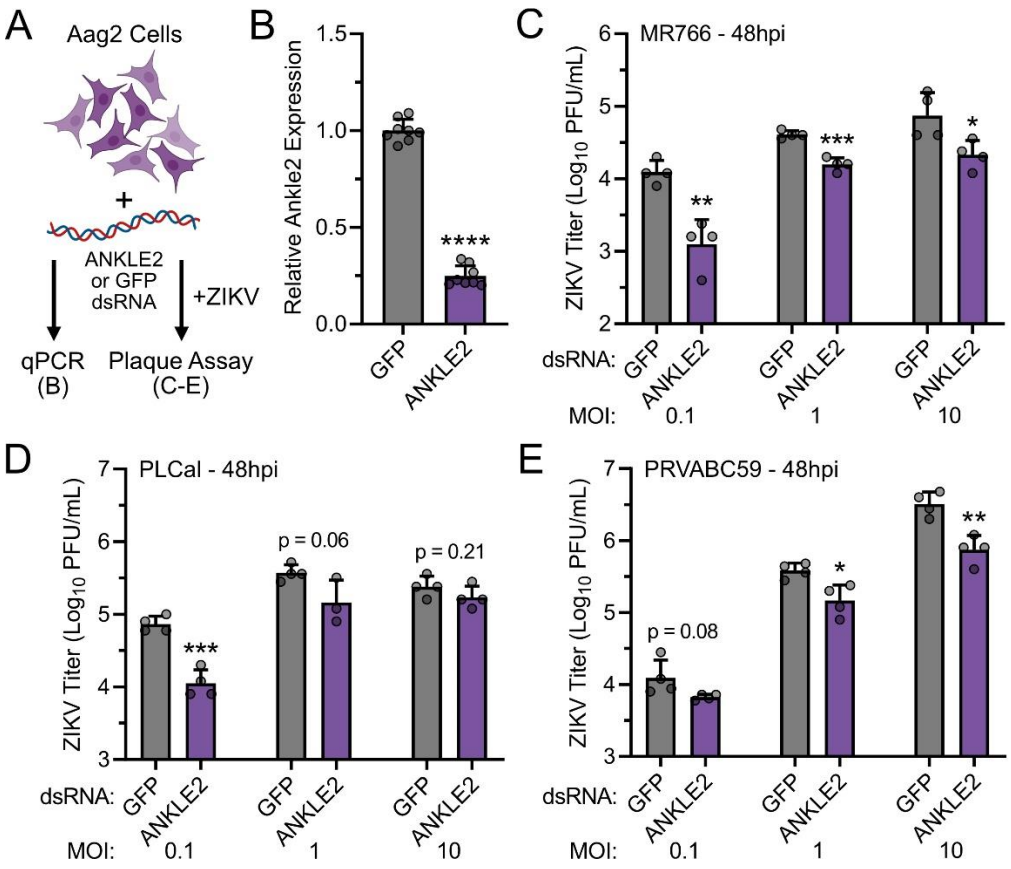

Figure 4-10: Silencing of ANKLE2 ortholog in mosquito Aag2 cells reduces ZIKV replication. (A) Experimental design for evaluating impact of Ankle2 mosquito ortholog in ZIKV replication. Aag2 cells were transfected with either GFP- or Ankle2-targeting dsRNA for 48 hours prior to qRT-PCR or ZIKV infection. (B) After dsRNA transfection, expression of ANKLE2 was

measured by qRT-PCR in eight transfection replicates across two experiments. (C-E) After dsRNA transfection, cells were infected with noted ZIKV strain at either MOI 0.1, 1, or 10. Viral supernatant was harvested and virus titers were measured by plaque assay. Four knockdown/infection technical replicates were performed for each condition. Grey circles represent the value of each individual replicate. Student's unpaired T-test. All statistical tests compared to corresponding GFP condition, * $p < 0.05$, ** $p < 0.01$, *** $p < 0.001$, **** $p < 0.0001$.

Conservation of orthoflavivirus NS4A and its interaction with ANKLE2

Given that ANKLE2 promotes ZIKV replication, we next sought to explore the conservation of this interaction. Comparing NS4A amino acid similarity showed moderately high conservation amongst mosquito-borne orthoflaviviruses (Figure 4-11A). Our previous work established the physical interaction between ZIKV NS4A and ANKLE2 (25), so we next tested the extent to which this interaction was conserved for other mosquito-borne orthoflaviviruses. We generated NS4A C-terminal strep-tagged fusions for four additional mosquito-borne orthoflaviviruses (DENV, WNV, YFV, and JEV) and evaluated their physical interaction with ANKLE2-3xFLAG using FLAG affinity purification and western blotting. We observed that these NS4As expressed higher than ZIKV NS4A, and all were immunoprecipitated by ANKLE2-3xFLAG (Figure 4-11B). This suggests that the NS4A-ANKLE2 physical interaction is conserved across mosquito-borne orthoflaviviruses. To evaluate a potential role for ANKLE2 in orthoflavivirus replication beyond ZIKV, we infected our Huh7 and SK-N-SH ANKLE2 knockout cells with WNV (NY2000) and DENV (serotype 2 16681). For WNV we observed statistically significant but biologically irrelevant decreases in virus replication (Figure 4-11C-D). However, DENV infection resulted in an early replication deficit in H2 cells (Figure 4-11E) and a sustained replication defect in SK-g1 cells (Figure 4-11F). Together, these data suggest that multiple orthoflaviviruses interact with ANKLE2, though its impact on orthoflavivirus replication *in vitro* is variable.

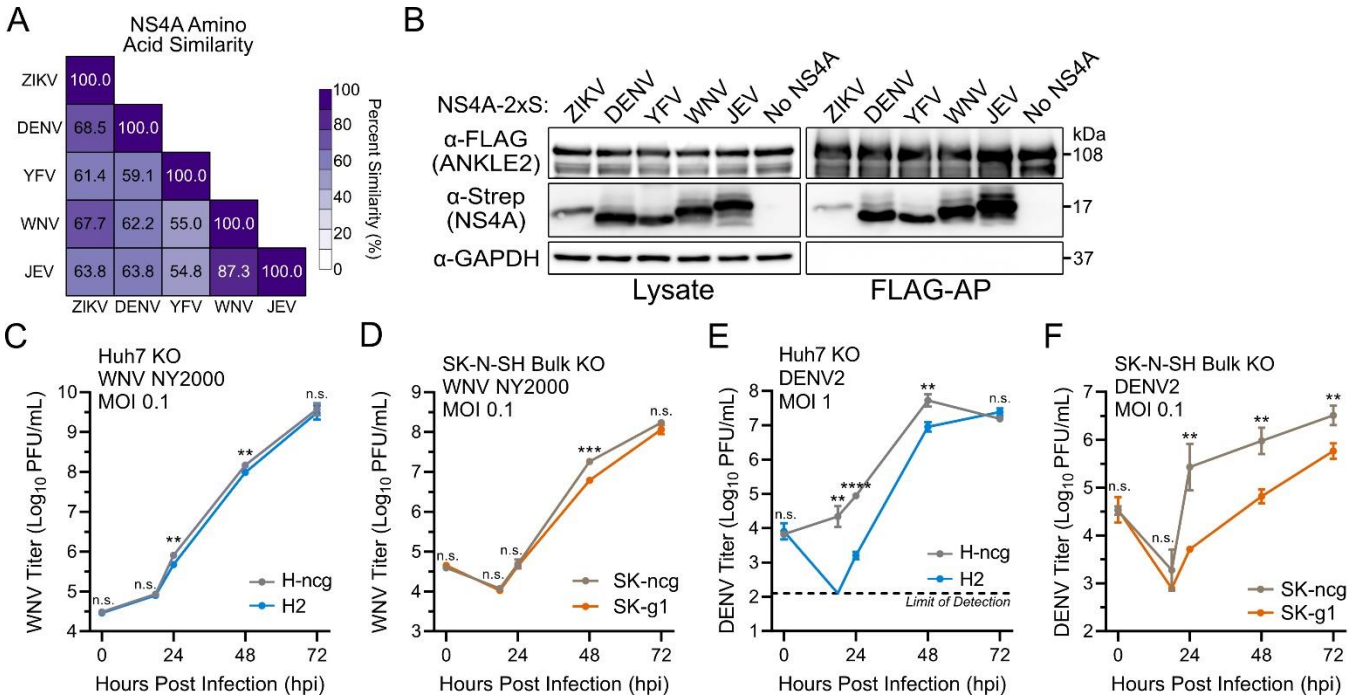

Figure 4-11: The NS4A-ANKLE2 interaction is conserved across mosquito-borne orthoflaviviruses but the role of ANKLE2 in virus replication varies. (A) NS4A total amino acid biochemical similarity using EMBOSS Needle (38). (B) HEK293T cells were co-transfected with ANKLE2-3xFLAG and NS4A-2xStrep from corresponding flavivirus. FLAG affinity purification (AP) and western blot were performed to determine physical interaction between proteins. NS4A-2xStrep bands vary in size corresponding to each virus. (C-D) Huh7 or SK-N-SH ANKLE2 knockout cells were infected with WNV NY2000. Virus titers at 0, 18, 24, 48, and 72 hours post infection were measured using plaque assay. (E-F) Huh7 or SK-N-SH ANKLE2 knockout cells were infected with DENV2 16681 at MOI 1 or 0.1. Virus titers at 0, 18, 24, 48, and 72 hours post infection were measured using plaque assay. All values shown are means + standard deviation of three technical replicates. Error bars represent standard deviation, assume bars not shown are within the bounds of the dot. All statistical tests compared to corresponding ncgRNA condition, n.s., not significant, * $p < 0.05$, ** $p < 0.01$, *** $p < 0.001$, **** $p < 0.0001$. ncg = negative control CRISPR gRNA control.

Conclusions and Discussion

In this study we explore the relationship between ZIKV and host ANKLE2, with a focus on virus replication. ANKLE2 actively colocalizes with ZIKV NS4A during infection and depletion of ANKLE2 in human cells leads to consistent reduction in ZIKV replication. TEM revealed that knockout of ANKLE2 results in fewer and more poorly formed virus replication organelles. Interestingly, dsRNA knockdown of the ANKLE2 ortholog in mosquito cells also produces similar, albeit modest, decreases in ZIKV replication, suggesting that ANKLE2 may be a conserved host factor. Further, we showed that the physical interaction between NS4A and ANKLE2 is conserved across four additional mosquito-borne orthoflaviviruses, and that ANKLE2 promotes DENV replication.

The conserved role of ANKLE2 in replication across hosts and orthoflaviviruses revises our model in which ZIKV NS4A inhibits ANKLE2 to cause microcephaly (25,28). Though ANKLE2 has a very specific and non-redundant role during fetal brain development, it may have additional roles in cell physiology when expressed in other tissues. Our data suggests that ANKLE2 may be hijacked by orthoflaviviruses in general to facilitate replication in many different tissues. We speculate that other orthoflavivirus NS4As can inhibit ANKLE2 function through a conserved protein interaction to cause neurodevelopmental defects, however non-teratogenic orthoflaviviruses lack the ability to access the fetal brain during the time in which ANKLE2 inhibition can cause neuropathogenesis. This is supported by our previous data that shows transgenic expression of DENV NS4A also leads to reduced brain size in larval fruit flies (25).

The supportive role of ANKLE2 in ZIKV replication raises exciting possibilities about ANKLE2 function during orthoflavivirus replication. Beyond BANF1, PP2A, and VRK1 (26,27), ANKLE2 also interacts with many other host proteins. For example, ANKLE2 also influences the cell cycle by interacting with Aurora-A and estrogen receptor alpha (ERα) to mediate ERα phosphorylation (39). Plentiful other ANKLE2-host protein interactions have been found in proteomic screens (40–

43). It is particularly appealing to speculate that ZIKV leverages the protein interaction/scaffolding function of ANKLE2 to facilitate protein interactions within orthoflavivirus replication organelles. Orthoflavivirus non-structural proteins interact with ER associated degradation (ERAD) factors, which regulate CM morphogenesis, virus propagation, and virus-induced cell death (7,44,45). DENV utilizes the host protein HMGCR in the process of replication complex formation, which is significant as HMGCR is also regulated by PP2A (46). Many other host factors are co-opted by orthoflaviviruses to remodel the ER and assist in the formation of replication compartments or complexes (10,12,47–51), and ANKLE2 may play a scaffolding role in this remodeling process. Future mechanistic studies exploring ANKLE2 protein interactions during orthoflavivirus infection will be valuable in uncovering the molecular mechanisms by which ANKLE2 accelerates orthoflavivirus replication.

To our knowledge, the NS4A-ANKLE2 interaction is a rare example of a ZIKV-host protein interaction that dysregulates the host function to cause neuropathogenesis (25,28) in the process of promoting ZIKV replication. Several other protein interactions impact aspects of neurodevelopment but appear distinct from virus replication. ZIKV NS3 cleaves host BMP2, inducing osteogenesis and intracranial calcification commonly seen in CZS (22). Expression of NS2A *in vivo* impacts neurodevelopment by disrupting adherens junctions in radial glial cells (24). Expression of NS4A and NS4B impairs the growth of neural stem cells *in vitro* and perturbs autophagy (52). While the host factors from these studies are involved in pathogenesis, they were not linked to virus replication directly. A notable exception is the interaction between ZIKV capsid and Dicer. Capsid interacts with Dicer and inhibits its antiviral activity to promote ZIKV replication while simultaneously inducing neurodevelopmental defects (53). These types of virus-host interactions, which result in compounding losses for the host, represent an exciting system to simultaneously study virus replication and neuropathogenesis.

Materials and Methods

Cells. HEK293T (gift of Dr. Sam Díaz-Muñoz), Huh7 (gift of Dr. Raul Andino), JEG-3 (ATCC), SK-N-SH (ATCC), and Vero (ATCC) cell lines were maintained in Dulbecco's modified Eagle's medium (DMEM, Gibco ThermoFisher) supplemented with 10% fetal bovine serum (FBS, Gibco ThermoFisher) at 37ºC, 5% CO_2. Cells we washed with Dulbecco's phosphate buffered saline (D-PBS, Life Technologies) and dissociated with 0.05% Trypsin-EDTA (Life Technologies). Cells were tested for *Mycoplasma spp.* monthly by PCR. Mosquito Aag2 (*Aedes aegypti*) cells were cultured at 27°C in Schneider's *Drosophila* Medium (Gibco; +Glutamate) supplemented with 7% FBS and antibiotics (100 units mL penicillin, 100 µg/mL streptomycin, 5 µg/mL gentamicin).

Plasmids. Lentiviral plasmid (pHR-UCOE-EF1α-KRAB-dCas9-P2A-Bls) encoding a catalytically dead Cas9 (dCas9) with a C-terminal hemagglutinin (HA) tag was a gift from Dr. Sean Collins. For stable, inducible expression in HEK293T cells, ANKLE2 and GFP sequences were amplified by PCR and cloned into pLVX-TetOne-Puro, cut with EcoRI, using Gibson assembly. Codon-optimized ANKLE1 sequence was acquired from Twist BioSciences and similarly inserted into pLVX-TetOne-Puro, cut with EcoRI, with C-terminal APEX2 and 3xFLAG affinity tags. Orthoflavivirus (DENV, YFV, WNV, JEV) NS4A sequences were acquired from Twist Bioscience and inserted into pcDNA4_TO, cut with BamHI and XhoI, with C-terminal 2xStrep tags using Gibson assembly. ANKLE2-mCherry-3xFLAG-P2A-BLS rescue fusions were cloned into pHR-UCOE-EF1α-KRAB-dCas9-P2A-Bls cut with MluI and NotI remove dCas9. Gene fragments were acquired from Twist BioSciences and inserted with Gibson Assembly. All plasmids were prepared in Stbl3 or DH5α using MiniPrep (Sigma-Aldrich) or MidiPrep (Macherey-Nagel) kits and verified using sequencing services provided by GeneWiz. All sequence accession numbers are available in Appendix B-5. Primer sequences used for the generation of all our constructs are available in Appendix B-6.

Lentiviral packaging, transduction, and cell selection. Lentiviral packaging and transduction were performed as previously described (54) using the calcium phosphate protocol (Yu and Schaffer, 2006). In short, 3.5 µg of cloning product plasmid were transfected into HEK293T with lentiviral packaging plasmids including 1.8 µg pMDLg/p-RRE, 1.25 µg pCMV-VSV-g and 1.5 µg pRSV-Rev. After 48 hours lentivirus particles were collected, and cell debris was removed by centrifugation (Eppendorf centrifuge 5810 R, Rotor S-4-104, 94 g, 5 minutes) and filtration through a 0.45 µm filter. The resulting lentiviral stocks were used to transduce HEK293T cells. Transduced cells were bulk selected for puromycin or blasticidin resistance (1 or 10 µg/mL, respectively, ThermoFisher). A control lentiviral plasmid encoding GFP without a selection marker was used in tandem as a control to ensure efficient packaging, transduction, and selection.

Viruses and stock preparation. All virus (ZIKV, DENV, WNV) stocks were propagated in Vero cells and monitored for CPE. Supernatant was then harvested, and cell debris was removed by centrifugation (Eppendorf centrifuge 5810 R, Rotor S-4-104, 211 g, 5 minutes, 4°C) Cleared supernatant was then distributed into 1 mL aliquots and frozen at -80°C. Each aliquot was only used once to prevent repetitive freeze-thaw. Aliquots were titered by plaque assay (method below). Strains used were ZIKV PLCal/2013 (gift of Dr. Richard Wozniak), ZIKV PRVABC59 (gift of Dr. Lark Coffey), ZIKV FSS13025 (gift of Dr. Helen Lazear), ZIKV H/PF/2013 (gift of Dr. Helen Lazear), ZIKV MR766 (BEI Resources, NIAID, NIH, as part of the WRCEVA program: Zika Virus, MR 766, NR-50065), DENV2 16681 (25), and WNV NY2000 (gift of Dr. Helen Lazear).

Western blot. For whole cell lysates, cells were lysed in RIPA buffer (150 mM NaCl, 50 mM Tris Base, 1% Triton X-100, 0.5% sodium deoxycholate) supplemented with protease inhibitors for 5 minutes at room temperature. Cell lysate was incubated on ice for 30 minutes prior to centrifugation (Eppendorf centrifuge 5424 R, Rotor FA-45-24-11, 13,500 g, 4ºC, 20 min). When

possible, the total protein concentration of each sample was normalized by BCA assay. Protein samples (lysates or IP eluates) were resuspended in NuPAGE LDS sample buffer supplemented with TCEP and boiled at 95ºC for 10 minutes. Samples were run on 7.5-12% polyacrylamide gels for ~1 hour at 150V and transferred to PVDF membranes (VWR) for 1 hour at 330 mA on ice. Membranes were then blocked in 5% milk solution for 1 hour prior to overnight incubation in primary antibodies (Appendix B-4) at 4ºC. Membranes were washed three times in Tris-buffered saline with Tween-20 (TBS-T) (150 mM NaCl, 20 mM Tris Base, 0.1% Tween-20, Fisher) and incubated with HRP-conjugated secondary antibodies in 5% milk for 1 hour at room temperature. Membranes were again washed three times in TBS-T and 1x in TBS (without Tween-20) prior to Pierce™ ECL activation (Fisher). Membranes were imaged using Amersham Imager 600 (GE). Western blot images were analyzed using Fiji. Densitometry was calculated by measuring the band intensity ratio of the experimental band to the loading control band.

ANKLE2 CRISPRi knockdown and ZIKV Infection. Custom synthetic guide RNAs (gRNA) were acquired from Sigma and resuspended to 3 μM in TE buffer (10 mM Tris Base, 1 mM EDTA, pH 8.0). For Huh7-dCas9 knockdown in 12-well dishes 30 μL of each gRNA was combined with 7 μL TransIT-CRISPR transfection reagent (Sigma) in 363 μL OPTI-MEM (Life Technologies) and complexed at room-temperature for 20 minutes prior to being added to each well (90nM final gRNA concentration). A total of $1.2x10^5$ Huh7-dCas9 cells were then added and grown overnight at 37ºC. Additional DMEM was then added 24 hpt. Viability experiments were done 72 hpt with ZombieGreen dye (BioLegend, gift of Dr. Scott Dawson) diluted 1:100 in D-PBS and incubated on live cells for 5 minutes. Ten images were taken for each condition and total and dead cells were then counted to determine viability. ZIKV replication after *ANKLE2* knockdown was done by removing media from each well 72 hpt. 2 mL of fresh DMEM and appropriate volume of ZIKV

stock was then added to each well. Supernatant aliquots were harvested at 0, 18, 24, 48, and 72 hpi and frozen at –80ºC.

Aag2 cell dsRNA knockdown. Gene-specific dsRNA was generated using PCR primers designed to amplify *Ae. aegypti ANKLE2* and containing the T7 promoter sequence. Aag2 cell cDNA generated using the High-Capacity cDNA reverse transcription kit (Applied Biosystems) was used as a template to amplify a 355 bp fragment of the *ANKLE2* transcript for dsRNA synthesis. After PCR amplification, dsRNA was generated via *in vitro* transcription using the MEGAScript™ RNAi kit (Thermo Fisher). As a non-specific control dsRNA, GFP dsRNA was generated from a GFP containing plasmid. For Aag2 knockdown in 24-well plates, 500ng of dsRNA was combined with 1.5 µL of Lipofectamine RNAiMAX (Thermo Fisher), diluted to a total volume of 100 µL in Opti-MEM (Thermo Fisher), and complexed at room-temperature for 20 minutes prior to being added to each well. A total of $2x10^5$ cells in 1 mL of culture media was then added to each well. Cells were incubated for 48 h before RNA extraction or virus infection. Aag2 cells were infected with ZIKV by removing the culture media and adding the appropriate volume of ZIKV diluted in a total of 200 µL of DMEM (no additives). After 1 h, the virus-containing media was removed and replaced with 1 mL of complete culture media. Supernatant aliquots were harvested at 0, 24, 48, and 72 hpi and frozen at –80ºC.

Plaque assay. Vero cells were grown as a monolayer in 6-well dishes overnight. Virus aliquots were thawed on ice then subjected to 10-fold serial dilution. Media was removed from Vero cells and the monolayer was washed with 1mL D-PBS. For ZIKV and WNV 500 µL of each virus dilution was then added and incubated for 1 hour at 37ºC with periodic rocking. Virus was then removed and cells were overlayed with 3 mL of DMEM with 0.8% methylcellulose (Sigma), 1% FBS, 1% penicillin/streptomycin (Thomas Scientific) and incubated at 37ºC for 4 days. For DENV, cells

were infected with 800 µL for 2 hours at 37ºC and incubated in DMEM/methylcellulose mixture for 8 days. Cells were then fixed with 4% formaldehyde (Fisher) for 30 minutes at room temperature. Formaldehyde and media were then removed, and cells were stained with 0.23% crystal violet solution (Fisher) for 30 minutes. Solution was then removed, and plaques were counted.

Quantitative RT-PCR. RNA was harvested using *Quick*-RNA Miniprep kit per manufacturer's instructions (Zymo). Purified RNA (500 ng) was then used to make cDNA using iScript™ cDNA synthesis kit (Bio-Rad). After cDNA synthesis each sample was resuspended to a total volume of 100 µL using RNase-Free water. A total of 2 µL of cDNA was then used for each qPCR reaction (with 2-3 replicate wells for each gene measurement) using LightCycler 480 SYBR Master Mix (Fisher). Samples were run in a Roche LightCycler® 480 II Instrument using relative quantification and temperatures of 95°C (5 sec), 55°C (10 sec), and 72°C (30 sec) for melting, annealing, and elongation, respectively. Quantification of SYBR signal was measured at the end of each elongation step for 40-45 cycles. Changes in gene expression were calculated using the Livak method ($2^{\Delta\Delta Ct}$) comparing to GAPDH expression as an internal control (55). Primer sequences are listed in Appendix B-6.

Immunofluorescence microscopy. HEK293T, Huh7, or JEG-3 cells cultured on #1.5 coverslips were fixed with 4% paraformaldehyde (Fisher) for 15 minutes at room temperature. Cells were permeabilized with 0.1% Triton X-100 (Integra) for 10 minutes and blocked with 5% goat serum (Sigma) in PBS-Tween (0.1% Tween-20, Fisher). Coverslips were incubated with primary antibodies overnight at 4°C. Coverslips were then washed in PBS-Tween and incubated in secondary antibody at room temperature for 1 hour. Nuclei were visualized with Hoechst (Invitrogen). Confocal images were acquired using an Olympus FV1000 Spectral Scan point-scanning confocal fitted to an Olympus IX-81 inverted microscope using a PlanApo 60x/NA1.40

oil immersion lens (Figures 4-1, 4-2, and 4-4) or Zeiss Airyscan LSM980 with Axiocam using a 63x/NA1.40 oil immersion lens (Figures 4-5A, 4-6, 4-9). Laser lines at 405, 488, and 543nm were employed sequentially for each image using optics and detector stock settings in the “Dye List” portion of the FluoView microscope-controlling software. Other microscopy images (Figures 4-5D) were captured using a Nikon Ti2 inverted microscope, CFI PLAN APO LAMBDA 40X CF160 Plan Apochromat Lambda 40X objective lens, N.A. 0.95, W.D. 0.17–0.25 mm, F.O.V. 25 mm, DIC, Correction collar 0.11–0.23 mm, Spring Loaded, and using Andor Zyla VSC-08688 camera. All antibodies and dilutions are listed in Appendix B-4. Microscopy images were analyzed using ImageJ (Fiji) software (56). Signal colocalization was quantified using Pearson’s correlation coefficient (R-value) determined with the “Colocalization 2” analysis tool within Fiji after masking signal in entire individual cells across at least five images.

ZIKV Entry/Internalization Assay.

Cells were seeded into 6-well plates one day prior to infection. On the day of the infection cells were pre-cooled on ice for 10 minutes. Media was removed and the cells were washed with chilled D-PBS. Equal amounts of chilled binding buffer (DMEM pH ~7.4 containing 0.2% BSA, 2mM MgCl2, and 1mM CaCl2) was added to each well. ZIKV PRVABC59 was added at MOI of 2 and incubated on ice for 90 minutes. After incubation, the binding buffer was removed, and cells were washed three times with ice cold PBS. Fresh media (DMEM pH~7.4 containing 10% FBS) was added to the wells and rapidly warmed up to 37°C. At indicated times cells were washed once with D-PBS and lysed in Zymo RNA lysis buffer for RNA purification. 500 ng of total RNA was converted to cDNA and used for qRT-PCR with either GAPDH or ZIKV primers (see previous). Media supernatant was harvested at later timepoints for PFU quantification using plaque assay.

Transmission Electron Microscopy. Cells were mock-infected or infected with ZIKV PRVABC59 for 48 hours prior to collection. Cells were washed with D-PBS and then placed in fixative (2.5% glutaraldehyde, 2% paraformaldehyde, 0.1M sodium phosphate buffer) for at least 3 hours. Cells were washed with 0.1M sodium phosphate buffer prior to secondary fixation in 1% osmium tetroxide, 1.5% potassium ferrocyanide for 1 hour. Cells were washed with cold water 3 times and then serially dehydrated in ethanol (30%, 50%, 70%, 95%, 3x 100%, 10 minutes each). Cells were then washed with propylene oxide twice for 10 minutes each. Half resin (dodecenyl succinic anhydride, Araldite 6005, Epon 812, Dibutyl Phthalate, Benzyldimethylamine) and half propylene oxide were allowed to infiltrate overnight at room temperature. The mixture was then removed and replaced with 100% resin and left to infiltrate for 4 hours. Resin was then replaced with fresh resin and allowed to polymerize at 70°C overnight. Resin blocks were sectioned on Leica EM UC6 ultramicrotome at approximately 100 nm. Sections were collected onto copper grids and dried at 60°C for 20 minutes. Grids were stained with 4% aqueous uranyl acetate and 0.1% lead citrate in 0.1N NaOH. Sections were imaged using FEI Talos L120C at 80kV with a 4k x 4k Ceta camera.

ANKLE2 and NS4A co-transfection and FLAG affinity-purification. For transfection $5x10^6$ HEK293T cells were plated in 10 cm dishes and grown overnight. Transfection was performed by combining 3.5 µg of each corresponding plasmid DNA with 700 µL of serum-free DMEM. Next, 21 µL of PolyJet transfection reagent (SignaGen) was combined with 700 µL serum-free DMEM and added to each plasmid DNA tube. Samples were mixed and incubated at room temperature for 15 minutes prior to addition to cells. Cells were then grown for an additional 24 hours. Transfection efficiency was confirmed using a GFP encoding plasmid. Media was then removed from each plate. To dissociate cells, 5 mL of D-PBS supplemented with 10 mM EDTA was added and allowed to incubate for several minutes. Cells were resuspended in 5 mL of D-

PBS and transferred to 15 mL conical tubes prior to centrifugation 94 g, 4ºC for 5 minutes (Eppendorf centrifuge 5810 R, Rotor S-4-104). Cell pellets were washed with 5 mL D-PBS and centrifugation was repeated. Supernatant was removed and pellets were then resuspended in 1 mL IP buffer (50 mM Tris Base, 150 mM NaCl, 0.5 M EDTA, pH 7.4) with Pierce™ protease inhibitor tablets (Thermo Scientific) supplemented with 0.5% NP-40 Substitute (Igepal™ CA-630, Affymetrix). Cells were lysed for 30 minutes at 4ºC, and lysate was then centrifugated at 845 g, 4ºC, for 20 minutes (Eppendorf centrifuge 5424 R, Rotor FA-45-24-11). A portion of each lysate (60-100 µL) was collected, normalized by BCA assay (Thermo Scientific), and saved for western blot analysis. Remaining lysate was added to 40 µL of magnetic FLAG beads (Sigma) and incubated overnight at 4ºC with gentle rotation. Beads were then washed four times with 1 mL IP buffer with 0.05% NP-40 and once with 1 mL IP buffer without NP-40. Beads were then incubated in 40 µL of 100 ng/mL 3x FLAG peptide (APExBIO) at 211 g for 1 hour at room temperature (Eppendorf ThermoMixerC). Eluate was then removed. Eluate and lysate were resuspended in NuPAGE LDS sample buffer and bond-breaker TCEP (Thermo Scientific) according to manufacturer's recommendation. Samples were boiled for 10 minutes at 95ºC prior to evaluation by western blot (below).

Statistical analysis.

Statistical analysis and plotting were performed using GraphPad Prism 6 software (GraphPad Prism 6.0; GraphPad Software Inc., La Jolla, CA, USA). Error bars represent standard deviations. Data were considered statistically significant when a $p < 0.05$ was determined by Student's T-test or one-way ANOVA with noted multiple-comparison test.

References

1. Fishburn AT, Pham OH, Kenaston MW, Beesabathuni NS, Shah PS. Let's Get Physical: Flavivirus-Host Protein-Protein Interactions in Replication and Pathogenesis. Front Microbiol. 2022;13:847588.
2. Cortese M, Goellner S, Acosta EG, Neufeldt CJ, Oleksiuk O, Lampe M, et al. Ultrastructural Characterization of Zika Virus Replication Factories. Cell Rep. 2017 Feb 28;18(9):2113–23.
3. Welsch S, Miller S, Romero-Brey I, Merz A, Bleck CKE, Walther P, et al. Composition and three-dimensional architecture of the dengue virus replication and assembly sites. Cell Host Microbe. 2009 Apr 23;5(4):365–75.
4. Paul D, Bartenschlager R. Flaviviridae Replication Organelles: Oh, What a Tangled Web We Weave. Annu Rev Virol. 2015 Nov;2(1):289–310.
5. Arakawa M, Morita E. Flavivirus Replication Organelle Biogenesis in the Endoplasmic Reticulum: Comparison with Other Single-Stranded Positive-Sense RNA Viruses. Int J Mol Sci. 2019 May 11;20(9):2336.
6. Neufeldt CJ, Cortese M, Acosta EG, Bartenschlager R. Rewiring cellular networks by members of the Flaviviridae family. Nature Reviews Microbiology. 2018;16(3):125.
7. Tabata K, Arakawa M, Ishida K, Kobayashi M, Nara A, Sugimoto T, et al. Endoplasmic Reticulum-Associated Degradation Controls Virus Protein Homeostasis, Which Is Required for Flavivirus Propagation. Journal of Virology. 2021 Jul 12;95(15):10.1128/jvi.02234-20.
8. Miller S, Kastner S, Krijnse-Locker J, Bühler S, Bartenschlager R. The non-structural protein 4A of dengue virus is an integral membrane protein inducing membrane alterations in a 2K-regulated manner. J Biol Chem. 2007 Mar 23;282(12):8873–82.

9. Roosendaal J, Westaway EG, Khromykh A, Mackenzie JM. Regulated cleavages at the West Nile virus NS4A-2K-NS4B junctions play a major role in rearranging cytoplasmic membranes and Golgi trafficking of the NS4A protein. J Virol. 2006 May;80(9):4623–32.
10. Aktepe TE, Liebscher S, Prier JE, Simmons CP, Mackenzie JM. The Host Protein Reticulon 3.1A Is Utilized by Flaviviruses to Facilitate Membrane Remodelling. Cell Reports. 2017 Nov 7;21(6):1639–54.
11. He Z, Zhu X, Wen W, Yuan J, Hu Y, Chen J, et al. Dengue Virus Subverts Host Innate Immunity by Targeting Adaptor Protein MAVS. J Virol. 2016 Aug 15;90(16):7219–30.
12. Teo CSH, Chu JJH. Cellular vimentin regulates construction of dengue virus replication complexes through interaction with NS4A protein. J Virol. 2014 Feb;88(4):1897–913.
13. Zhang J, Lan Y, Li MY, Lamers MM, Fusade-Boyer M, Klemm E, et al. Flaviviruses Exploit the Lipid Droplet Protein AUP1 to Trigger Lipophagy and Drive Virus Production. Cell Host Microbe. 2018 Jun 13;23(6):819-831.e5.
14. Kindhauser MK, Allen T, Frank V, Santhana RS, Dye C. Zika: the origin and spread of a mosquito-borne virus. Bull World Health Organ. 2016 Sep 1;94(9):675-686C.
15. Cao-Lormeau VM, Blake A, Mons S, Lastère S, Roche C, Vanhomwegen J, et al. Guillain-Barré Syndrome outbreak associated with Zika virus infection in French Polynesia: a case-control study. Lancet. 2016 Apr 9;387(10027):1531–9.
16. de Araújo TVB, Rodrigues LC, de Alencar Ximenes RA, de Barros Miranda-Filho D, Montarroyos UR, de Melo APL, et al. Association between Zika virus infection and microcephaly in Brazil, January to May, 2016: preliminary report of a case-control study. Lancet Infect Dis. 2016 Dec;16(12):1356–63.
17. Campo M del, Feitosa IML, Ribeiro EM, Horovitz DDG, Pessoa ALS, França GVA, et al. The phenotypic spectrum of congenital Zika syndrome. American Journal of Medical Genetics Part A. 2017;173(4):841–57.

18. Moore CA, Staples JE, Dobyns WB, Pessoa A, Ventura CV, Fonseca EB da, et al. Characterizing the Pattern of Anomalies in Congenital Zika Syndrome for Pediatric Clinicians. JAMA Pediatr. 2017 01;171(3):288–95.

19. Boonsawat P, Joset P, Steindl K, Oneda B, Gogoll L, Azzarello-Burri S, et al. Elucidation of the phenotypic spectrum and genetic landscape in primary and secondary microcephaly. Genetics in Medicine. 2019 Sep 1;21(9):2043–58.

20. Filgueiras IS, Torrentes de Carvalho A, Cunha DP, Mathias da Fonseca DL, El Khawanky N, Freire PP, et al. The clinical spectrum and immunopathological mechanisms underlying ZIKV-induced neurological manifestations. PLoS Negl Trop Dis. 2021 Aug;15(8):e0009575.

21. Giraldo MI, Gonzalez-Orozco M, Rajsbaum R. Pathogenesis of Zika Virus Infection. Annu Rev Pathol. 2023 Jan 24;18:181–203.

22. Chen W, Foo SS, Hong E, Wu C, Lee WS, Lee SA, et al. Zika virus NS3 protease induces bone morphogenetic protein-dependent brain calcification in human fetuses. Nat Microbiol. 2021 Apr;6(4):455–66.

23. Chavali PL, Stojic L, Meredith LW, Joseph N, Nahorski MS, Sanford TJ, et al. Neurodevelopmental protein Musashi-1 interacts with the Zika genome and promotes viral replication. Science. 2017 Jul 7;357(6346):83–8.

24. Yoon KJ, Song G, Qian X, Pan J, Xu D, Rho HS, et al. Zika-Virus-Encoded NS2A Disrupts Mammalian Cortical Neurogenesis by Degrading Adherens Junction Proteins. Cell Stem Cell. 2017 Sep 7;21(3):349-358.e6.

25. Shah PS, Link N, Jang GM, Sharp PP, Zhu T, Swaney DL, et al. Comparative Flavivirus-Host Protein Interaction Mapping Reveals Mechanisms of Dengue and Zika Virus Pathogenesis. Cell. 2018 13;175(7):1931-1945.e18.

26. Asencio C, Davidson IF, Santarella-Mellwig R, Ly-Hartig TBN, Mall M, Wallenfang MR, et al. Coordination of kinase and phosphatase activities by Lem4 enables nuclear envelope reassembly during mitosis. Cell. 2012 Jul 6;150(1):122–35.

27. Snyers L, Erhart R, Laffer S, Pusch O, Weipoltshammer K, Schöfer C. LEM4/ANKLE-2 deficiency impairs post-mitotic re-localization of BAF, LAP2α and LaminA to the nucleus, causes nuclear envelope instability in telophase and leads to hyperploidy in HeLa cells. Eur J Cell Biol. 2018 Jan;97(1):63–74.

28. Link N, Chung H, Jolly A, Withers M, Tepe B, Arenkiel BR, et al. Mutations in ANKLE2, a ZIKA Virus Target, Disrupt an Asymmetric Cell Division Pathway in *Drosophila* Neuroblasts to Cause Microcephaly. Dev Cell. 2019 Dec 16;51(6):713-729.e6.

29. Thomas AX, Link N, Robak LA, Demmler-Harrison G, Pao EC, Squire AE, et al. ANKLE2 - related microcephaly: A variable microcephaly syndrome resembling Zika infection. Ann Clin Transl Neurol. 2022 Jul 24;9(8):1276–88.

30. Yamamoto S, Jaiswal M, Charng WL, Gambin T, Karaca E, Mirzaa G, et al. A *Drosophila* genetic resource of mutants to study mechanisms underlying human genetic diseases. Cell. 2014 Sep 25;159(1):200–14.

31. Chan JFW, Yip CCY, Tsang JOL, Tee KM, Cai JP, Chik KKH, et al. Differential cell line susceptibility to the emerging Zika virus: implications for disease pathogenesis, non-vector-borne human transmission and animal reservoirs. Emerg Microbes Infect. 2016 Aug 24;5:e93.

32. Vicenti I, Boccuto A, Giannini A, Dragoni F, Saladini F, Zazzi M. Comparative analysis of different cell systems for Zika virus (ZIKV) propagation and evaluation of anti-ZIKV compounds in vitro. Virus Research. 2018 Jan 15;244:64–70.

33. Adams Waldorf KM, Stencel-Baerenwald JE, Kapur RP, Studholme C, Boldenow E, Vornhagen J, et al. Fetal brain lesions after subcutaneous inoculation of Zika virus in a pregnant nonhuman primate. Nature Medicine. 2016 Nov;22(11):1256–9.

34. Lazear HM, Govero J, Smith AM, Platt DJ, Fernandez E, Miner JJ, et al. A Mouse Model of Zika Virus Pathogenesis. Cell Host & Microbe. 2016 May 11;19(5):720–30.

35. Wu Y, Cui X, Wu N, Song R, Yang W, Zhang W, et al. A unique case of human Zika virus infection in association with severe liver injury and coagulation disorders. Sci Rep. 2017 Sep 12;7(1):11393.

36. Langerak T, Broekhuizen M, Unger PPA, Tan L, Koopmans M, Gorp E van, et al. Transplacental Zika virus transmission in ex vivo perfused human placentas. PLOS Neglected Tropical Diseases. 2022 Apr 20;16(4):e0010359.

37. Villazana-Kretzer DL, Wuertz KM, Newhouse D, Damicis JR, Dornisch EM, Voss KM, et al. ZIKV can infect human term placentas in the absence of maternal factors. Commun Biol. 2022 Mar 18;5(1):1–15.

38. Sievers F, Wilm A, Dineen D, Gibson TJ, Karplus K, Li W, et al. Fast, scalable generation of high-quality protein multiple sequence alignments using Clustal Omega. Mol Syst Biol. 2011 Oct 1;7:539.

39. Gao A, Sun T, Ma G, Cao J, Hu Q, Chen L, et al. LEM4 confers tamoxifen resistance to breast cancer cells by activating cyclin D-CDK4/6-Rb and ERα pathway. Nat Commun. 2018 Oct 9;9(1):4180.

40. Go CD, Knight JDR, Rajasekharan A, Rathod B, Hesketh GG, Abe KT, et al. A proximity-dependent biotinylation map of a human cell. Nature. 2021 Jul;595(7865):120–4.

41. Gupta GD, Coyaud É, Gonçalves J, Mojarad BA, Liu Y, Wu Q, et al. A Dynamic Protein Interaction Landscape of the Human Centrosome-Cilium Interface. Cell. 2015 Dec 3;163(6):1484–99.

42. Hein MY, Hubner NC, Poser I, Cox J, Nagaraj N, Toyoda Y, et al. A Human Interactome in Three Quantitative Dimensions Organized by Stoichiometries and Abundances. Cell. 2015 Oct 22;163(3):712–23.

43. Huttlin EL, Bruckner RJ, Navarrete-Perea J, Cannon JR, Baltier K, Gebreab F, et al. Dual proteome-scale networks reveal cell-specific remodeling of the human interactome. Cell. 2021 May 27;184(11):3022-3040.e28.

44. Anton A, Mazeaud C, Freppel W, Gilbert C, Tremblay N, Sow AA, et al. Valosin-containing protein ATPase activity regulates the morphogenesis of Zika virus replication organelles and virus-induced cell death. Cell Microbiol. 2021 Apr;23(4):e13302.

45. Mazeaud C, Anton A, Pahmeier F, Sow AA, Cerikan B, Freppel W, et al. The Biogenesis of Dengue Virus Replication Organelles Requires the ATPase Activity of Valosin-Containing Protein. Viruses. 2021 Oct 18;13(10):2092.

46. Soto-Acosta R, Bautista-Carbajal P, Cervantes-Salazar M, Angel-Ambrocio AH, Del Angel RM. DENV up-regulates the HMG-CoA reductase activity through the impairment of AMPK phosphorylation: A potential antiviral target. PLoS Pathog. 2017 Apr;13(4):e1006257.

47. Tabata K, Arimoto M, Arakawa M, Nara A, Saito K, Omori H, et al. Unique Requirement for ESCRT Factors in Flavivirus Particle Formation on the Endoplasmic Reticulum. Cell Reports. 2016 Aug 30;16(9):2339–47.

48. Monel B, Rajah MM, Hafirassou ML, Sid Ahmed S, Burlaud-Gaillard J, Zhu PP, et al. Atlastin Endoplasmic Reticulum-Shaping Proteins Facilitate Zika Virus Replication. J Virol. 2019 Dec 1;93(23):e01047-19.

49. Tran PTH, Asghar N, Johansson M, Melik W. Roles of the Endogenous Lunapark Protein during Flavivirus Replication. Viruses. 2021 Jul;13(7):1198.

50. Hoffmann HH, Schneider WM, Rozen-Gagnon K, Miles LA, Schuster F, Razooky B, et al. TMEM41B Is a Pan-flavivirus Host Factor. Cell. 2021 Jan 7;184(1):133-148.e20.

51. Shue B, Chiramel AI, Cerikan B, To TH, Frölich S, Pederson SM, et al. Genome-Wide CRISPR Screen Identifies RACK1 as a Critical Host Factor for Flavivirus Replication. J Virol. 2021 Nov 23;95(24):e0059621.

52. Liang Q, Luo Z, Zeng J, Chen W, Foo SS, Lee SA, et al. Zika Virus NS4A and NS4B Proteins Deregulate Akt-mTOR Signaling in Human Fetal Neural Stem Cells to Inhibit Neurogenesis and Induce Autophagy. Cell Stem Cell. 2016 Nov 3;19(5):663–71.

53. Zeng J, Dong S, Luo Z, Xie X, Fu B, Li P, et al. The Zika Virus Capsid Disrupts Corticogenesis by Suppressing Dicer Activity and miRNA Biogenesis. Cell Stem Cell. 2020 Oct 1;27(4):618-632.e9.

54. Petit MJ, Kenaston MW, Pham OH, Nagainis AA, Fishburn AT, Shah PS. Nuclear dengue virus NS5 antagonizes expression of PAF1-dependent immune response genes. PLoS Pathog. 2021 Nov 19;17(11):e1010100.

55. Livak KJ, Schmittgen TD. Analysis of relative gene expression data using real-time quantitative PCR and the 2(-Delta Delta C(T)) Method. Methods. 2001 Dec;25(4):402–8.

56. Schindelin J, Arganda-Carreras I, Frise E, Kaynig V, Longair M, Pietzsch T, et al. Fiji: an open-source platform for biological-image analysis. Nat Methods. 2012 Jul;9(7):676–82.

Chapter 5: Determining the molecular determinants of the NS4A-ANKLE2 protein interaction

Introduction

Our work presented in Chapter 4 suggests that ANKLE2 promotes ZIKV replication by facilitating aspects of ER remodeling. Given our previous work that showed ZIKV NS4A interacts with and inhibits the function of ANKLE2, we hypothesize that NS4A specifically hijacks ANKLE2 to promote ZIKV replication. However, showing that the beneficial role of ANKLE2 in ZIKV replication is dependent on interaction with NS4A is not trivial. Further, understanding the interaction can allow for expanded study of how the NS4A-ANKLE2 interaction impacts neurodevelopment *in vivo*. To show that the physical interaction is directly what mediates the role of ANKLE2 in ZIKV replication and that NS4A inhibits ANKLE2 to cause microcephaly, the physical determinants of this interaction must be determined. Following this, the interaction can be broken at the amino acid level and the impacts on these processes can be evaluated. In this Chapter, we explore the physical determinants of the NS4A-ANKLE2 interaction from both sides and establish general regions required for the physical interaction.

As we have previously introduced, ANKLE2 is a 938 amino acid long resident of the ER and inner nuclear membrane, where it is anchored to the membrane by the single N-terminal transmembrane domain from amino acids 9-34 (Figure 3-1). The remaining majority of ANKLE2 is outstretched from the membrane towards the cytoplasmic side of the ER or the nuclear side of the inner nuclear membrane. On the other hand, orthoflavivirus NS4A has a more complex membrane orientation, despite its small size of 150-151 amino acids (depending on the virus). The topology of the polyprotein is such that the N-terminal portion of NS4A, following NS3, lies on the cytoplasmic portion of the ER membrane, where it is cleaved from NS3 by the viral protease (1). An N-terminal portion of approximately 50 amino acids remains outstretched on this side of

the membrane. Following this portion are a series of transmembrane domains which we will refer to as TM1 – 4. TM1 spans the membrane to the lumenal side, where it is quickly followed by TM2 which interestingly remains integrated horizontally in the membrane without spanning it. This integrated portion is followed by TM3 which spans the membrane back to the cytoplasmic side. Following this is TM4 or the "2K-peptide", which spans the membrane again to the ER lumen (2). NS4B follows 2K and begins on the lumenal side of the membrane (Figure 2-1). Studies on Kunjin virus (KUNV) NS4A-2K-NS4B have shown that NS4A is cleaved from 2K-NS4B first by NS3, followed by 2K separation from NS4B by host signal peptidase (3). It is assumed that the processing of other orthoflavivirus NS4A follows these temporal steps, but that has never been explicitly shown. The cleavage of NS4A from 2K is a seemingly important step, but the ability for NS4A to induce membrane rearrangements appears to vary by specific virus. DENV NS4A was shown to only induce membrane rearrangements after removal of 2K, while for KUNV, both NS4A with and without 2K were able to accomplish this (3), although it is worth noting that the data in this study suggests that NS4A-2K would not exist separated from NS4B. In this Chapter, we will refer to NS4A with 2K as "NS4A-2K" and NS4A without 2K as "NS4A ΔTM4".

Results

ANKLE2 interacts with NS4A through its TM and LEM domains

To further understand the biophysical interaction between NS4A and ANKLE2, we sought to determine which domains of ANKLE2 were necessary for the interaction. The structure of ANKLE2 has not yet been experimentally resolved. Thus, we employed the structural prediction provided by AlphaFold2 (4,5). This revealed high-confidence structured regions corresponding to the known TM, LEM, and ankyrin repeat (ANK) domains. Surprisingly, this also revealed three previously uncharacterized high-confidence structures (Figure 3-1). Using this predicted structure as a template, we then generated seven C-terminal truncation mutants with progressively fewer

of these domains or structures, each with FLAG affinity tags (3xF) (Figure 5-1). To characterize the biochemical behavior of these truncations we performed subcellular fractionation to enrich cytosolic, membrane, and nuclear/nuclear lamina compartments. Western blotting analysis of these fractions showed the presence of each primarily in the membrane-bound (including ER, Golgi, etc.) and nuclear/nuclear-lamina fractions (Figure 5-1B). We attempted to quantify this using the relative densitometry of FLAG vs. each compartment's marker (GAPDH, SERCA2, Lamin A/C) (Figure 5-1C). This result is expected given the established localization of ANKLE2 to the ER and inner nuclear membrane (6–8), and the role of the TM, which was not deleted, in facilitating ER localization (9). To evaluate interaction of these ANKLE2 truncations with NS4A we co-transfected each with C-terminally Strep-tagged NS4A-2K plasmid we generated previously (10) and then performed FLAG affinity purification (FLAG-AP). Intriguingly, FLAG co-AP revealed that each truncation maintained its interaction with NS4A-2K, although Δ54-938 only very weakly interacted (Figure 5-1D). Intriguingly, we observed consistent FLAG bands above and below the band at the expected mass. We interpret the lower bands as N-terminal degradation products, as the C-terminal FLAG tag must be maintained for western blot detection. We speculate that the higher mass bands may be dimers or aggregations of variously sized ANKLE2 products. Together, these results showed the C-terminal deletions of ANKLE2 do not substantially impact its localization or interaction with ZIKV NS4A, except for Δ54-938 which may have reduced interaction.

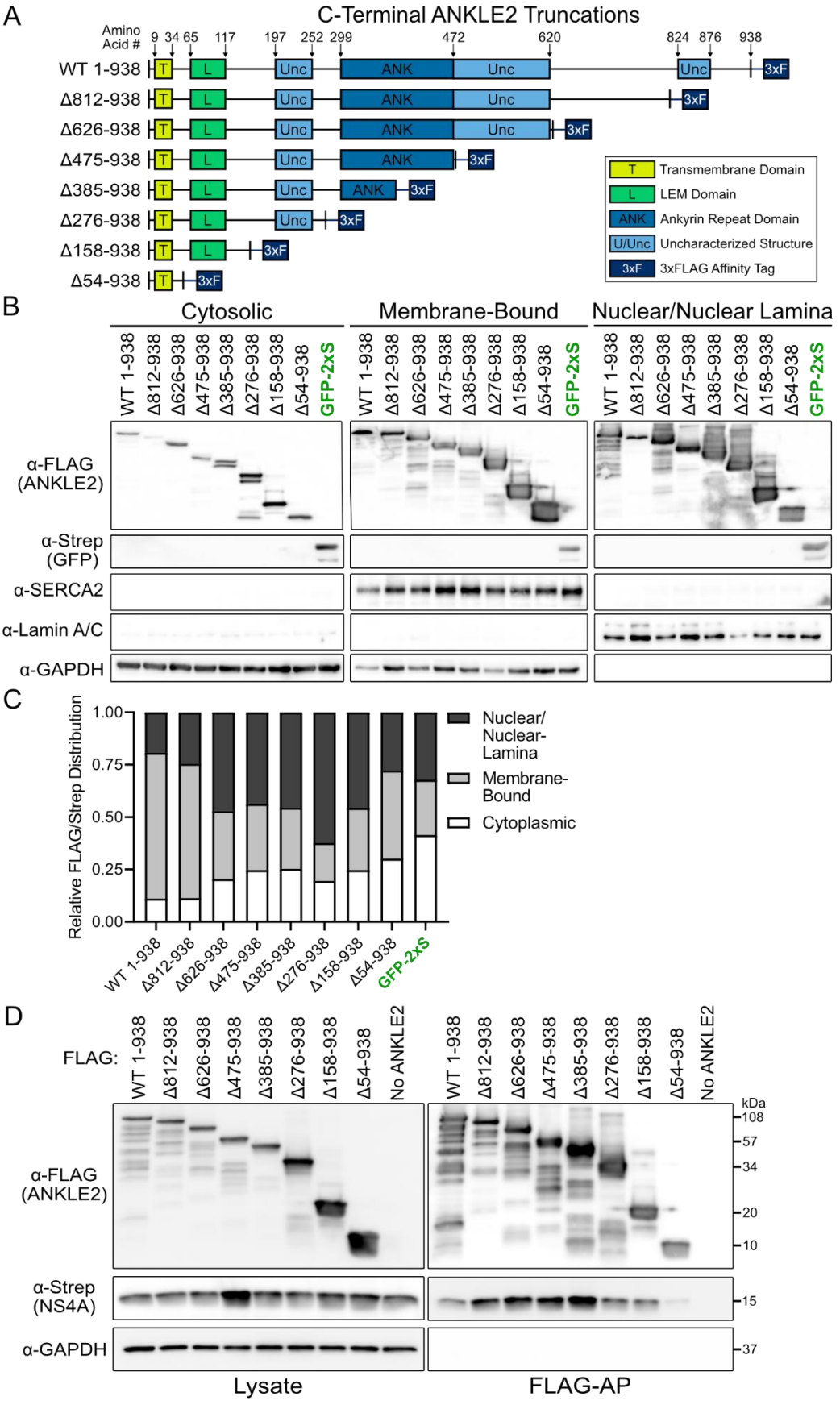
A
C-Terminal ANKLE2 Truncations
Amino Acid #
9 34 65 117 197 252 299 472 620 824 876 938
WT 1-938
Δ812-938
Δ626-938
Δ475-938
Δ385-938
Δ276-938
Δ158-938
Δ54-938
T
L
Unc
ANK
3xF
Transmembrane Domain
LEM Domain
Ankyrin Repeat Domain
Uncharacterized Structure
3xFLAG Affinity Tag
B
Cytosolic
Membrane-Bound
Nuclear/Nuclear Lamina
GFP-2xS
α-FLAG (ANKLE2)
α-Strep (GFP)
α-SERCA2
α-Lamin A/C
α-GAPDH
C
Relative FLAG/Strep Distribution
1.00
0.75
0.50
0.25
0.00
Nuclear/ Nuclear-Lamina
Membrane-Bound
Cytoplasmic
D
FLAG:
No ANKLE2
α-FLAG (ANKLE2)
α-Strep (NS4A)
α-GAPDH
kDa
108
57
34
20
10
15
37
Lysate
FLAG-AP

Figure 5-1: C-terminal truncations of ANKLE2 reveal retained localization patterns and physical interaction with ZIKV NS4A. (A) Schematic of C-terminal ANKLE2 truncations, using AlphaFold structural prediction as guide for characterized and uncharacterized domains (Fig S4). (B) ANKLE2 truncations were transfected into HEK293T cells and lysate was fractionated. Fractions were then assessed by western blot using indicated cellular markers. (C) Densitometry analysis to determine relative abundance of each truncation in different cellular spaces. (D) HEK293T cells were co-transfected with ZIKV NS4A-2xStrep and each ANKLE2 truncation. ANKLE2 interaction with NS4A was determined by FLAG affinity-purification (FLAG-AP) and western blot.

Given that C-terminal deletions did not significantly impact ANKLE2 or its interaction with NS4A, we generated additional mutants with either N-terminal deletions of the TM domain only (Δ2-53), the TM and LEM domains (Δ2-157), the LEM domain only (Δ54-158), or the LEM through ANK domains (Δ54-474) (Figure 5-2A). We performed similar subcellular fractionation analysis which showed that Δ2-53 and Δ2-157 were enriched in the cytosolic fraction and depleted in the nuclear/nuclear lamina fraction but maintained some membrane (ER) localization (Figure 5-2B-C). Confocal microscopy of Δ2-53 and Δ2-157 showed disperse signal in the cytosol with decreased overlap with the ER marker Calreticulin, whereas WT ANKLE2 and internal deletions Δ54-158 and Δ54-474 had high colocalization with the ER as measured by Pearson's correlation (Figure 5-2D-E). Thus, both ER and nuclear/nuclear lamina localization were disrupted in the Δ2-53 and Δ2-157 mutant. Co-transfection with NS4A-2K and FLAG-AP of these ANKLE2 mutants revealed that deletion of both the TM and LEM domains (Δ2-157) strongly ablated interaction with NS4A-2K, whereas deletion of either the TM or LEM domain alone retained the interaction with NS4A-2K (Figure 5-2F). This was somewhat surprising since deletion of the TM substantially altered subcellular localization that could preclude the interaction with NS4A in cells. To corroborate this biochemical finding, we visualized the subcellular localization of these ANKLE2

truncations along with NS4A during infection. Here, we clearly observed similar clusters of NS4A that colocalized with wild-type ANKLE2, but not the Δ2-157 mutant. Instead, we observed our Δ2-157 ANKLE2 mutant appeared to be distinctly separated from sites of NS4A accumulation (Figure 5-2G). Altogether, these results suggest that while the TM domain controls ER and nuclear lamina localization of ANKLE2, both the TM and LEM regions together contribute to the interaction with NS4A, with presence of at least one being sufficient for the biochemical interaction.

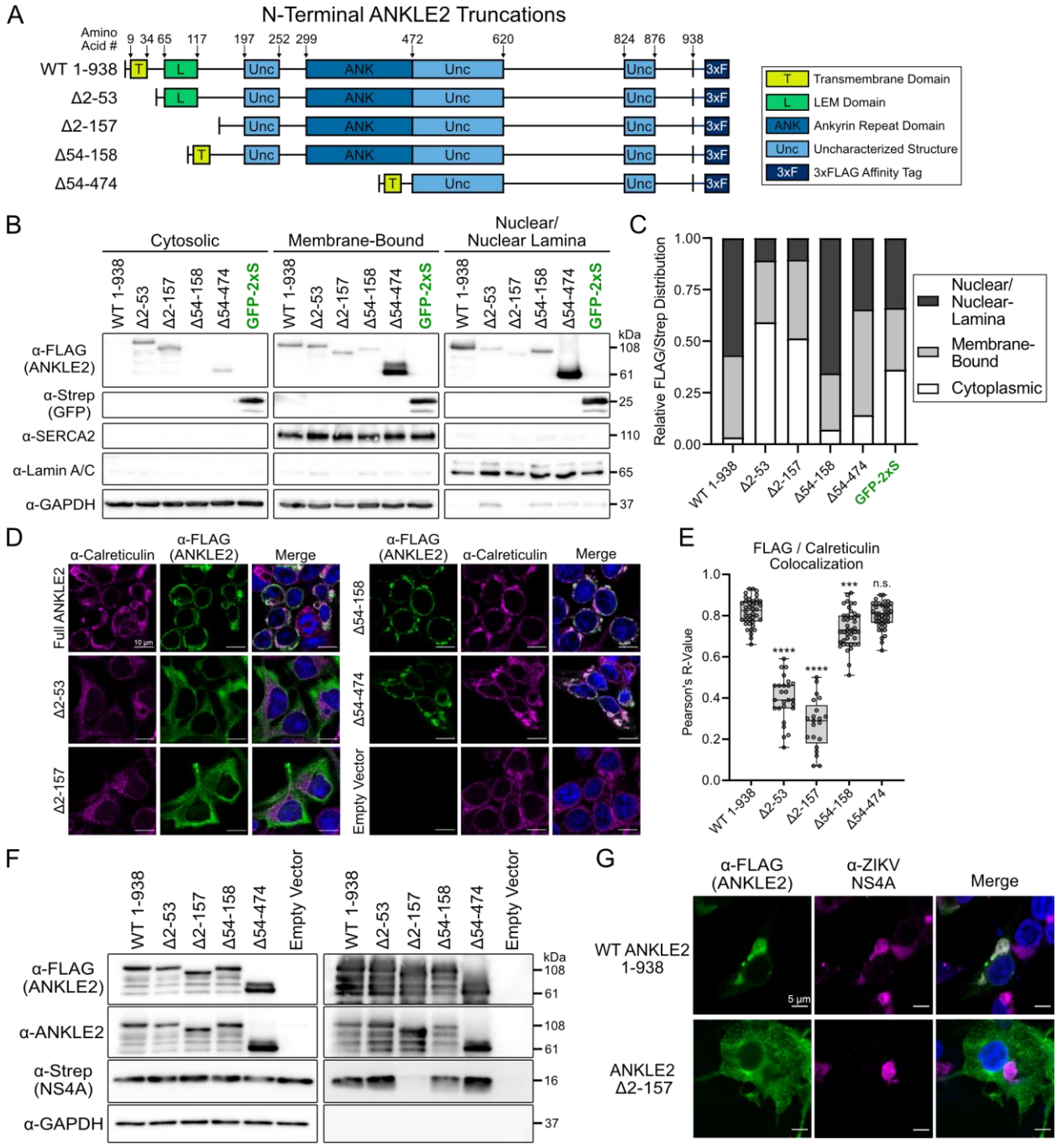

Figure 5-2: ANKLE2 N-terminal truncation mutations reveal physical determinants for localization and interaction with ZIKV NS4A. (A) Schematic of human ANKLE2 N-terminal truncations with known domains and predicted structural regions mapped. (B) HEK293T cells transfected with ANKLE2 truncations. After transfection, lysate was fractionated and assessed by western blot. (C) Densitometry analysis of (B) using each fractions marker to normalize

expression levels within each fraction (Cytoplasmic = GAPDH, Membrane-Bound = SERCA2, Nuclear/Nuclear Lamina = Lamin A/C. (D) HEK293T cells were transfected as done in (B) and localization of each mutant was compared to the ER marker calreticulin using confocal microscopy. Scale bars = 10 μm. € Pearson's correlation was quantified from n = 21-41 cells across 5-11 images for each condition. Grey circles represent individual cells. One-way ANOVA with Dunnett's multiple comparison test compared to WT ANKLE2, n.s., not significant, *** $p > 0.001$, **** $p > 0.0001$. (F) HEK293T were co-transfected with ZIKV NS4A-2xStrep and designated ANKLE2 truncation. 24 hours post transfection, cell lysate was collected and FLAG affinity-purification was performed to assess physical interaction with NS4A. The presence of N-terminal degradation bands was confirmed using ANKLE2 antibody. Endogenous ANKLE2 is present in Lysate but too faint to visualize. (G) HEK293T cells were infected with ZIKV MR766 (MOI 5). 24 hours post infection cells were transfected with each ANKLE2 truncation as done previously. 24 hours post transfection (48hpi) cells were fixed and examined using confocal microscopy. Scale bars = 5 μm.

NS4A-ANKLE2 interaction is dependent on NS4A TM2 and TM3

To further explore the determinants of the NS4A-ANKLE2 interaction, we sought to generate NS4A truncation mutants. Using a previous evaluation of dengue virus (DENV) NS4A as a template (2), we initially generated plasmids encoding one of three C-terminal truncations, each removing an additional TM domain (Figure 5-3A and B). As done previously with our ANKLE2 truncations, we characterized the localization of these NS4A truncations using subcellular fractionation and confocal microscopy. Contrary to the relatively disperse localization of ANKLE2, fractionation experiments on NS4A truncations revealed very distinct localization to the membrane fraction, with very little signal detected in the cytoplasmic or nuclear portions (Figure 5-3C-D). Confocal microscopy further confirmed ER retention of all truncations as all had similar

colocalization with the ER-marker Calnexin (Figure 5-3E-F). We considered N-terminal truncation mutants of NS4A as well but were concerned about proper membrane insertion and topology, so these mutants were not evaluated.

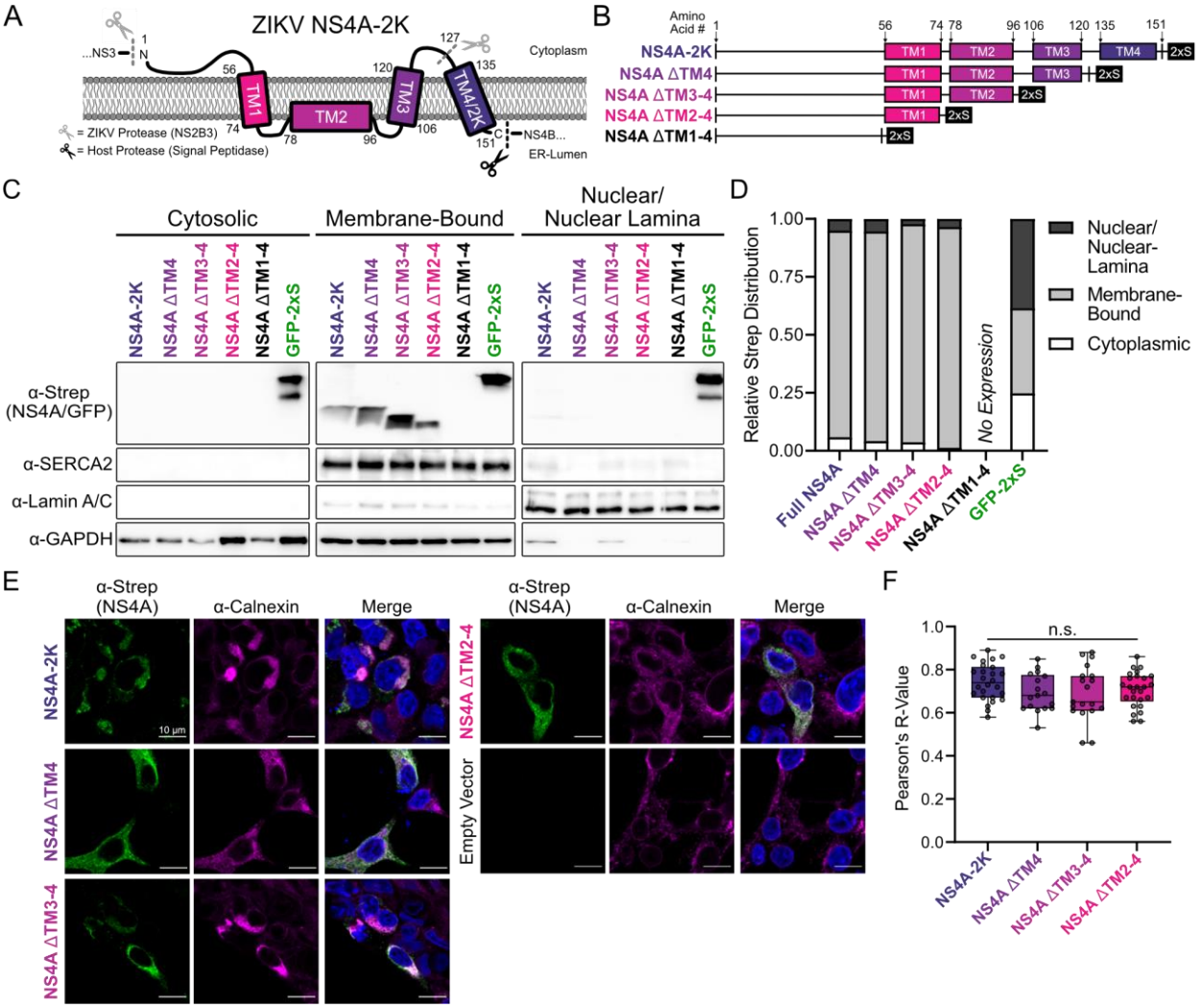

Figure 5-3: C-terminal truncations of ZIKV NS4A do not alter ER localization. (A) Schematic of ZIKV NS4A in the ER membrane based on previous studies (Miller 2007) and using TMHMM2.0 which was later upgraded to DeepTMHMM (Hallgren). (B) Schematic of cloned C-terminal NS4A truncations with 2xStrep tags for purification and identification. (C) Western blot analysis of subcellular fractions of cells transfected with the indicated NS4A construct. SERCA2 and Lamin A/C antibodies were used to validate enrichment of membrane-bound and nuclear fractions,

respectively, while GAPDH was used as a cytoplasmic marker. We were unable to detect NS4A ΔTM1-4 in these experiments. (D) Densitometry analysis was performed on western blot images by measuring the intensity of Strep bands relative to each fraction's marker. These values were then plotted as a fractional distribution for relative intensity across all fractions. (E) Confocal microscopy of HEK293T cell transfected with noted NS4A-2xS truncations. Scale bars = 10 μm. (F) Pearson's correlation was determined to quantify the degree of colocalization between NS4A-2xStrep and Calnexin. Signal in five images for each condition. N = 17-26 cells per condition. Grey circles represent the value of each individual replicate. One-way ANOVA, n.s., not significant.

Next, we expressed these NS4A truncations in HEK293T cells and performed affinity-purification against the Strep affinity tag (Strep-AP) to determine interaction with endogenous ANKLE2 (Figure 5-4A). The first of these truncations, NS4A ΔTM4 representing processed NS4A, appeared to have better expression and interaction with ANKLE2 than our full-length NS4A-2K. This also represents a biologically relevant form of NS4A during ZIKV infection, since the 2K-peptide is first cleaved at the C-terminus of NS4A to separate NS4A from 2K-NS4B (3). The other truncations, NS4A ΔTM3-4 and ΔTM2-4, had significantly reduced to no visible interaction with ANKLE2, suggesting that at least TM3 is crucial for stabilizing the interaction with ANKLE2 (Figure 5-4A). To corroborate this result, we co-transfected our ANKLE2-3xFLAG and NS4A-2xStrep truncation constructs and performed FLAG-AP (Figure 5-4B). Here, to display the importance of NS4A TM domains, we additionally generated a fourth NS4A truncation that does not express any TM domains (NS4A ΔTM1-4). In this experiment we observed that NS4A ΔTM3-4 had detectable but dramatically reduced interaction with ANKLE2. However, NS4A ΔTM2-4 had no detectable interaction. Additionally, ΔTM1-4 had very low expression and we could not draw conclusions regarding its ability to interact with ANKLE2. Our Strep-AP results indicate that both TM2 and TM3 contribute to the interaction with ANKLE2. Finally, we evaluated the effect of the

2K-peptide on the interaction between NS4A and ANKLE2 Δ2-158, which had strongly reduced interaction with NS4A-2K previously (Figure 5-2F). We observed faint and reduced interaction between ANKLE2 Δ2-157 and NS4A-2K, but no detectable interaction between ANKLE2 Δ2-157 and NS4A ΔTM4, suggesting that the 2K-peptide may stabilize the interaction outside of the TM and LEM domains, but that the processed form of NS4A requires these ANKLE2 domains for interaction.

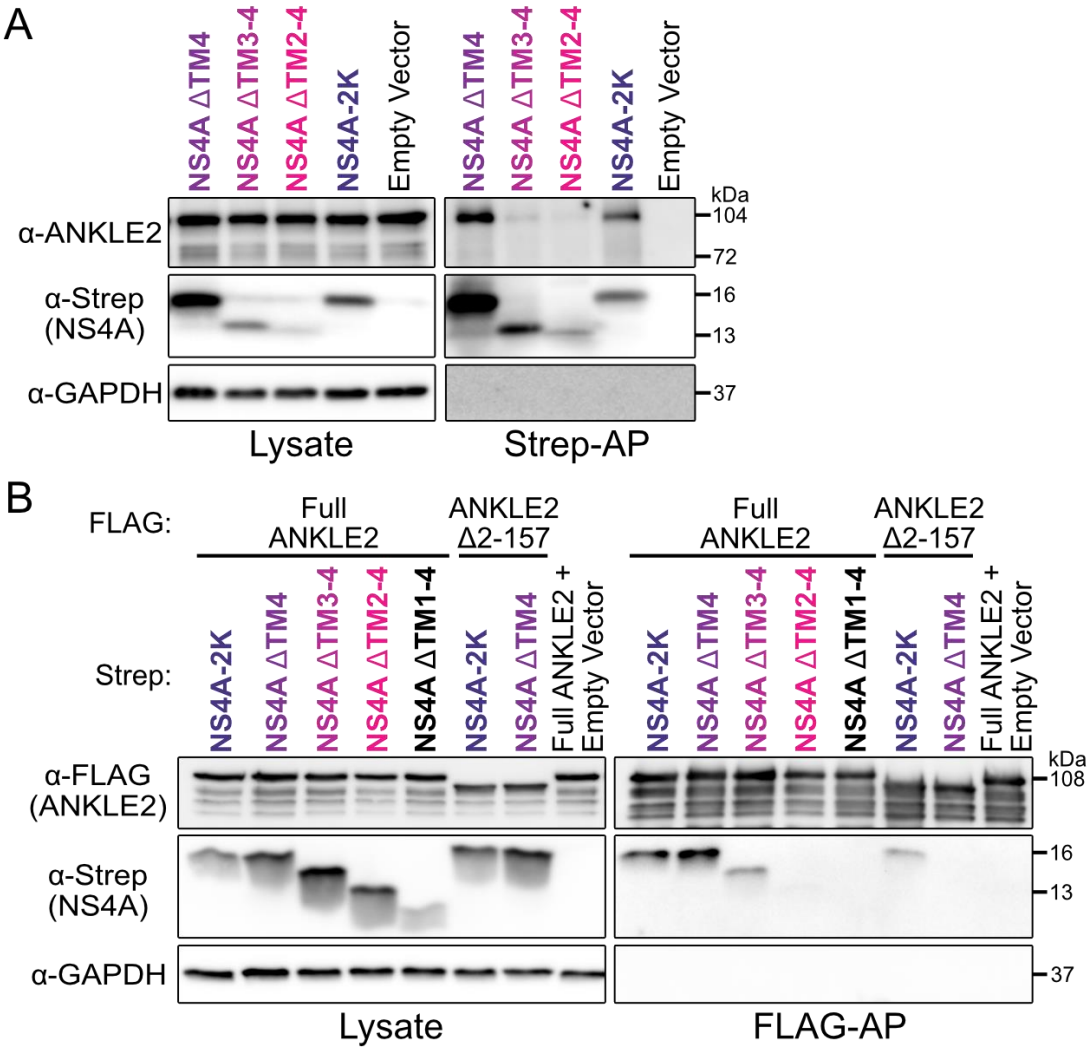

Figure 5-4: C-terminal truncation of ZIKV NS4A reveal physical determinants for interaction with ANKLE2. (A) NS4A-2xS truncations were transfected in HEK293T cells and interaction with endogenous ANKLE2 was determined using Strep affinity-purification (Strep-AP) and western

blot. (B) NS4A-2xS truncations and WT ANKLE2-3xF or ANKLE2-3xF Δ2-157 were co-transfected in HEK293T cells. Interaction between the two proteins was achieved with FLAG affinity-purification (FLAG-AP) and western blot.

Given the apparent conservation of the physical interaction we hypothesized that conserved amino acids within NS4A may be contributing. To further investigate this, we used Jensen-Shannon divergence to measure NS4A conservation at each amino acid position for a variety of other medically relevant orthoflaviviruses (all DENV serotypes, St. Louis encephalitis virus [SLEV], Powassan virus [POWV] and Langat virus [LGTV]) (Figure 5-5A) (11). The location of the TM domains for ZIKV are included as a general reference, although the exact positioning varies for each virus. The regions outside of the TM domains generally had higher conservation, highlighted by the stretch prior to TM1, between TM1 and 2, and after TM3 (Jensen-Shannon divergence score > 0.7). Sequence logo analysis of this region revealed several amino acids in the interaction domain that were highly conserved, including G84, W96, A106, L115, L119, and the entire stretch from 121-127. (Figure 5-5B). Amino acids 121-127 likely have very high conservation due to acting as a signal for cleavage by NS3 to separate NS4A from 2K, although this does not exclude the possibility these residues also play a role in mediating interaction with ANKLE2.

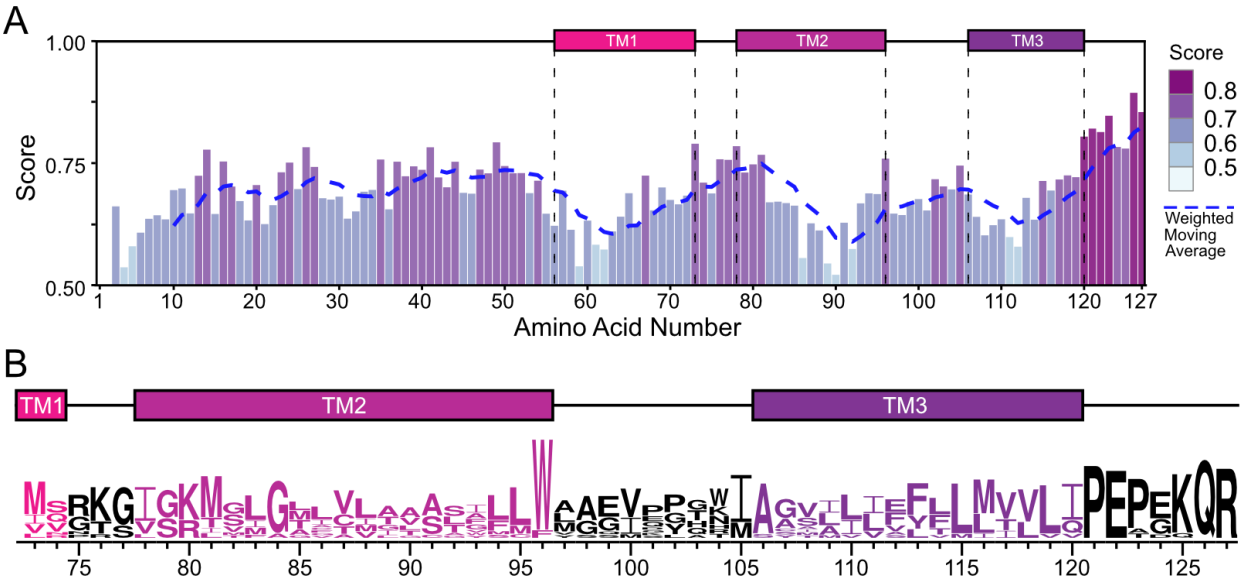

Figure 5-5: Amino acid conservation of orthoflavivirus NS4A by residue. (A) Conservation of NS4A across 12 orthoflaviviruses measured by Jensen-Shannon divergence at each amino acid position (11). (B) Logo analysis of the ANKLE2 interaction domain of NS4A (TM2 and TM3, amino acids 73-127), compiled from 12 orthoflaviviruses, with consensus TM domains from ZIKV NS4A overlayed (12,13). Only a portion of TM1 is shown as a reference.

Conclusions and Discussion

Our work provides molecular-level insight into the biophysical nature of the NS4A-ANKLE2 interaction. AP studies revealed that both the TM and LEM domains of ANKLE2 together mediate the interaction. Loss of the TM alone is sufficient to disrupt the colocalization of ANKLE2 to sites of NS4A during infection, though physical interaction appears to remain possible. The TM anchors ANKLE2 to the ER and nuclear envelope, and its loss reduces this localization in favor of cytoplasmic localization (9). This deletion separates ANKLE2 from NS4A, which would otherwise interact with the LEM domain. This does not imply an inherent necessity of the TM domain for the interaction with NS4A. The presence of this domain varies between organisms with no clear

phylogenetic separation. Mammalian (human, primate, mouse, etc.) ANKLE2 and the *C. elegans* homolog LEM-4L all contain an N-terminal TM. *Drosophila* Ankle2 lacks a clear TM but does have structured elements at the N-terminus, although these appear to be more similar to the "Caulimovirus domain" rather than a TM domain (Figure 3-1). Despite this, *Drosophila* Ankle2 still localizes to the ER and is inhibited by NS4A (8), suggesting its ER localization is mediated by other factors or regions. Moreover, the interaction with NS4A could still be detected biochemically by AP for the TM-deleted ANKLE2. This is likely due to mixing of cytoplasmic and ER compartments during lysis, which enables the interaction through the LEM domain even in the absence of correct ER localization. Thus, ER localization and the TM and LEM domains are the major contributors to the interaction. Dissecting this interaction with amino acid resolution in the future has the potential to identify ANKLE2 mutants that do not interact with NS4A (or vice versa). This would enable direct testing of the importance of this protein interaction for ZIKV replication. Ultimately it could reveal protective ANKLE2 variants which are functional in brain development, but do not interact with NS4A and thus do not support replication.

Finally, we identified the NS4A determinants of the interactions and demonstrated that the NS4A-ANKLE2 protein interaction is highly conserved amongst mosquito-borne flaviviruses. The conserved nature of the interactions suggests that while inhibition of ANKLE2 to cause microcephaly may be unique to ZIKV, co- opting ANKLE2 to promote replication maybe a general feature of flaviviruses. By analyzing the sequence of this interaction domain (TM2 and TM3) for diverse flaviviruses, we were able to identify highly conserved amino acids in this region that may mediate the interaction with ANKLE2. Mutagenesis of this region will be critical to generating a ZIKV mutant that does not interact with ANKLE2. Such a mutant could be evaluated for replication, and if viable, neuropathogenesis.

Materials and Methods

Plasmids. ANKLE2 truncations were designed based on AlphaFold2 structural prediction (Jumper, Varadi) using NM_015114.3 accession sequence (searched August 8th, 2021). Codon optimized DNA fragments with C-terminal 3xFLAG affinity-tags were acquired from Twist Bioscience and inserted into pcDNA4_TO, cut with KpnI and ApaI, using Gibson assembly. A full length pcDNA4_TO ZIKV NS4A-2xStrep plasmid was previously generated (10) and used as a template for generation of NS4A truncation sequences using PCR amplification. Products were inserted into pcDNA4_TO cut with BamHI and EcoRI upstream of 2xStrep using Gibson assembly.

Cells. HEK293T (gift of Dr. Sam Díaz-Muñoz) and HeLa (gift of Dr. Luc Snyers) cell lines were maintained as previously described in Chapter 4.

Subcellular fractionation. Proteins were isolated from the cytosol, membrane-bound organelles, and the nucleus using a previously established protocol for cultured cells (10). In brief, cells were sequentially lysed in buffer (3 M NaCl, 1 M HEPES, 1 M glycerol, 1X protease inhibitor) containing increasingly stronger detergents. Following cell trypsinization, buffer with digitonin (25 µg/mL) disrupted the plasma membrane over the course of gentle rotation at 4ºC. Buffer with Igepal (1% v:v, NP-40 substitute) permeabilized membrane-bound organelles during incubation on ice. The nuclear membrane was disrupted by buffer containing sodium deoxycholate (0.5% w:v) and sodium dodecyl sulfate (0.1 % w:v), with subsequent sonification to disrupt genomic DNA. All separations were performed by centrifugation (Eppendorf centrifuge 5424 R, Rotor FA-45-24-11, 4ºC). Cell fractions were evaluated by western blot.

Western blot. Performed as previously described in Chapter 4.

ANKLE2 and NS4A co-transfection and FLAG affinity-purification. For transfection $5x10^6$ HEK293T cells were plated in 10 cm dishes and grown overnight. Transfection was performed by combining 3.5 µg of each corresponding plasmid DNA with 700 µL of serum-free DMEM. Next, 21 µL of PolyJet transfection reagent (SignaGen) was combined with 700 µL serum-free DMEM and added to each plasmid DNA tube. Samples were mixed and incubated at room temperature for 15 minutes prior to addition to cells. Cells were then grown for an additional 24 hours. Transfection efficiency was confirmed using a GFP encoding plasmid. Media was then removed from each plate. To dissociate cells, 5 mL of D-PBS supplemented with 10 mM EDTA was added and allowed to incubate for several minutes. Cells were resuspended in 5 mL of D-PBS and transferred to 15 mL conical tubes prior to centrifugation 94 g, 4ºC for 5 minutes (Eppendorf centrifuge 5810 R, Rotor S-4-104). Cell pellets were washed with 5 mL D-PBS and centrifugation was repeated. Supernatant was removed and pellets were then resuspended in 1 mL IP buffer (50 mM Tris Base, 150 mM NaCl, 0.5 M EDTA, pH 7.4) with Pierce™ protease inhibitor tablets (Thermo Scientific) supplemented with 0.5% NP-40 Substitute (Igepal™ CA-630, Affymetrix). Cells were lysed for 30 minutes at 4ºC, and lysate was then centrifugated at 845 g, 4ºC, for 20 minutes (Eppendorf centrifuge 5424 R, Rotor FA-45-24-11). A portion of each lysate (60-100 µL) was collected, normalized by BCA assay (Thermo Scientific), and saved for western blot analysis. Remaining lysate was added to 40 µL of magnetic FLAG beads (Sigma) or non-magnetic Streptactin beads (Fisher #NC1506023) and incubated overnight at 4ºC with gentle rotation. Beads were then washed four times with 1 mL IP buffer with 0.05% NP-40 and once with 1 mL IP buffer without NP-40. Beads were then incubated in 40 µL of 100 ng/mL 3x FLAG peptide (for FLAG-AP) (APExBIO) or 40 µL of 2.5mM desthiobiotin (for Strep-AP) at 211 g for 1 hour at room temperature (Eppendorf ThermoMixerC). Eluate was then removed. Eluate and lysate were

resuspended in NuPAGE LDS sample buffer and bond-breaker TCEP (Thermo Scientific) according to manufacturer's recommendation. Samples were boiled for 10 minutes at 95ºC prior to evaluation by western blot (below).

Immunofluorescence microscopy. Performed as previously described in Chapter 4. Images in Figure 5-2G were captured using the Olympus FV1000 and Figures 5-2D and 5-3 were captured using Zeiss Airyscan LSM980.

Viruses and stock preparation. Performed as previously described in Chapter 4.

References

1. Cahour A, Falgout B, Lai CJ. Cleavage of the dengue virus polyprotein at the NS3/NS4A and NS4B/NS5 junctions is mediated by viral protease NS2B-NS3, whereas NS4A/NS4B may be processed by a cellular protease. J Virol. 1992 Mar;66(3):1535–42.
2. Miller S, Kastner S, Krijnse-Locker J, Bühler S, Bartenschlager R. The non-structural protein 4A of dengue virus is an integral membrane protein inducing membrane alterations in a 2K-regulated manner. J Biol Chem. 2007 Mar 23;282(12):8873–82.
3. Roosendaal J, Westaway EG, Khromykh A, Mackenzie JM. Regulated cleavages at the West Nile virus NS4A-2K-NS4B junctions play a major role in rearranging cytoplasmic membranes and Golgi trafficking of the NS4A protein. J Virol. 2006 May;80(9):4623–32.
4. Jumper J, Evans R, Pritzel A, Green T, Figurnov M, Ronneberger O, et al. Highly accurate protein structure prediction with AlphaFold. Nature. 2021 Aug;596(7873):583–9.
5. Varadi M, Anyango S, Deshpande M, Nair S, Natassia C, Yordanova G, et al. AlphaFold Protein Structure Database: massively expanding the structural coverage of protein-

sequence space with high-accuracy models. Nucleic Acids Research. 2022 Jan 7;50(D1):D439–44.

6. Asencio C, Davidson IF, Santarella-Mellwig R, Ly-Hartig TBN, Mall M, Wallenfang MR, et al. Coordination of kinase and phosphatase activities by Lem4 enables nuclear envelope reassembly during mitosis. Cell. 2012 Jul 6;150(1):122–35.
7. Snyers L, Erhart R, Laffer S, Pusch O, Weipoltshammer K, Schöfer C. LEM4/ANKLE-2 deficiency impairs post-mitotic re-localization of BAF, LAP2α and LaminA to the nucleus, causes nuclear envelope instability in telophase and leads to hyperploidy in HeLa cells. Eur J Cell Biol. 2018 Jan;97(1):63–74.
8. Link N, Chung H, Jolly A, Withers M, Tepe B, Arenkiel BR, et al. Mutations in ANKLE2, a ZIKA Virus Target, Disrupt an Asymmetric Cell Division Pathway in *Drosophila* Neuroblasts to Cause Microcephaly. Dev Cell. 2019 Dec 16;51(6):713-729.e6.
9. Elkhatib RA, Paci M, Boissier R, Longepied G, Auguste Y, Achard V, et al. LEM-domain proteins are lost during human spermiogenesis but BAF and BAF-L persist. Reproduction. 2017 Oct;154(4):387–401.
10. Shah PS, Link N, Jang GM, Sharp PP, Zhu T, Swaney DL, et al. Comparative Flavivirus-Host Protein Interaction Mapping Reveals Mechanisms of Dengue and Zika Virus Pathogenesis. Cell. 2018 13;175(7):1931-1945.e18.
11. Capra JA, Singh M. Predicting functionally important residues from sequence conservation. Bioinformatics. 2007 Aug 1;23(15):1875–82.
12. Schneider TD, Stephens RM. Sequence logos: a new way to display consensus sequences. Nucleic Acids Res. 1990 Oct 25;18(20):6097–100.
13. Crooks GE, Hon G, Chandonia JM, Brenner SE. WebLogo: a sequence logo generator. Genome Res. 2004 Jun;14(6):1188–90.
14. Baghirova S, Hughes BG, Hendzel MJ, Schulz R. Sequential fractionation and isolation of subcellular proteins from tissue or cultured cells. MethodsX. 2015;2:440–5.

Chapter 6: Investigation of ANKLE2-host interactions and perturbation by ZIKV using proteomics

Introduction

As we discussed in Chapter 3, ANKLE2 is a scaffolding protein with multiple roles in the cell. ANKLE2 itself has no enzymatic or catalytic activity that we can directly measure or detect. Thus, the best way to determine ANKLE2's function is to evaluate the proteins it interacts with. The data presented in Chapter 4 suggests that ANKLE2 colocalizes with sites of ZIKV replication and promotes replication in some aspect of ER remodeling. Together, we hypothesize that ANKLE2 will have new protein-protein interactions during ZIKV infection to facilitate this process, while other interactions are maintained or are less frequent. To test this hypothesis, we will utilize affinity-purification and mass-spectrometry (AP-MS) to purify ANKLE2 and interacting proteins from cells with and without ZIKV infection. From this we specifically hypothesize we will identify a base set of consistent ANKLE2-interactors and subsets of variable interactions that are gained or lost during ZIKV infection. The ultimate goal of these experiments is to pinpoint pathways through which ANKLE2 promotes ZIKV replication and potential pathways that are disrupted during ZIKV infection that could contribute to abnormal neurodevelopment.

For our proteomics experiments we utilized liquid-chromatography tandem mass spectrometry (LC-MS/MS) with data-independent acquisition (DIA). Mass spectrometry is a technically complex and sensitive technique. At its simplest level, proteins are proteolytically digested into smaller peptides by trypsin which non-specifically cleaves at lysine and arginine residues. These peptides

are separated by hydrophobicity on a reverse phase liquid chromatography column so that like peptides are grouped together and enter the mass-spectrometer together. Peptides flow from the column into the machine at a steady rate over time. In the mass-spectrometer these peptides are ionized, accelerated through an electric field, and shot at a detector. The time for the ions to reach

the detector is referred to as the time of flight (ToF), which can be used to determine the mass/charge (m/z) ratio of the specific ion. This information is quantified in the form of mass spectra with the m/z on the x-axis and the arbitrarily quantified intensity of the detected ions on the y-axis. This is referred to as the MS1 spectra, which provides information on the mass and abundance of the peptides detected in a certain time window but does not inform on their individual sequences. To determine this, each individual group of peptide ions is randomly fragmented, resulting in a pool of various fragments. This fragmented population is then shot at the detector again, providing information on the mass of each individual fragmentation product, called the MS2 spectra. This information is more difficult to decipher but sophisticated software can parse the m/z fragmentation data to determine the sequence of the peptide it originated from (Figure 6-1). This is repeated for the thousands of peptides that are measured. With the sequence of each peptide, they can then be mapped back to the human proteome and if they are specific to a particular protein then the amount of that protein in each sample can be quantified. Executing this experimental pipeline with careful biological and statistical controls can reveal protein-protein interactions between our bait protein (ANKLE2 in this case) and the prey proteins which are affinity-purified by it (1).

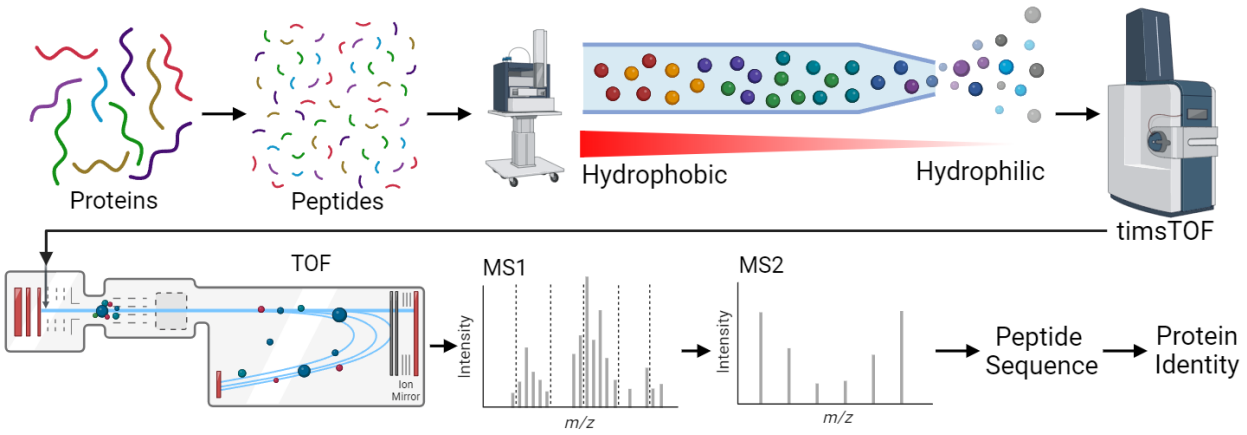

Figure 6-1: Simplified mass spectrometry process. Proteins are purified by affinity-purification and digested by trypsin. Digested peptides are separated by hydrophobicity using liquid

chromatography. This column feeds into the mass spectrometer where peptides are ionized and accelerated towards the detector by an electric field. The flight path is extended by reflecting ions off a reflectron/ion mirror, improving the detection resolution. The mass to charge (m/z) ratio is computed based on the time for the ion to reach the detector and the detected charge. In DIA, windows (dashed lines) of MS1 spectra and fragmented together. The m/z of these fragments are then detected and used to ultimately determine the originating peptide's sequence and precursor protein.

To explore ANKLE2 protein-protein interactions using AP-MS we use HEK293T cells. These cells are ideal for proteomics experiments due to their fast-growing nature, wide array of expressed proteins, and because they are relatively easy to genetically engineer. While not representative of biologically relevant ZIKV infection, we do not anticipate the molecular biology that governs fundamentals of physical protein-protein interactions to change significantly between cell types. However, we will miss interactions for proteins that are not expressed in HEK293T, but are expressed in other cells, and we run the risk of identifying interactions that occur in HEK293T but are not relevant for ZIKV replication in humans because they are with proteins expressed in HEK293T but not in susceptible or relevant tissues.

The work in this Chapter aims to explore ANKLE2 interactions using traditional AP-MS methodology and to explore how to assess the degree to which these interactions are impacted by ZIKV infection.

Results

Generation and validation of cell lines for proteomics

To perform AP-MS on ANKLE2 we chose to stably express human ANKLE2 (NM_015114.3) with a 3x-FLAG affinity tag (3xF), similar to what we used to explore the NS4A-ANKLE2 interaction previously in Chapter 5. We cloned ANKLE2-3xF into the pLenti plasmid backbone which allows for lentivirus packaging. As a control we generated a similar plasmid that encoded for GFP-3xF. HEK293T were then transduced with our generated lentivirus and selected for Zeocin antibiotic resistance. Expression of both ANKLE2-3xF and GFP-3xF was confirmed by western blot. Here, we observed that GFP-3xF expression was much higher than that of ANKLE2-3xF (not shown). We also validated our ANKLE2-3xF cell line using confocal microscopy (Appendix C-1). We observed high colocalization between ANKLE2-3xF and the ER marker SERCA2, and less with the mitochondrial marker TOMM20 or the Golgi marker GRASP65.

For our proteomics experimental setup, we prepared four biological replicates for each cell line. In each replicate half of the plates were infected with ZIKV MR766 at MOI 5 for 48 hours, since this strain was the only ZIKV strain available that can replicate efficiently in these cells (Chapter 4). We confirmed that ZIKV infection in these cells produced the same colocalization between ANKLE2 and NS4A or E (Appendix C-1) as we previously observed (Figure 4-1). Prior to harvest, the cells were illuminated under UV for 60 minutes to inactivate the virus. We confirmed this UV irradiation did not alter GFP fluorescence or short-term cell viability (Appendix C-2). Cells were then collected and lysed in a relatively mild lysis buffer to maintain membrane proteins and complexes as much as possible. Insoluble protein was removed by centrifugation and the remaining lysate was frozen at -80°C until all the replicates were prepared. Next, all the cell lysates were applied to FLAG binding beads overnight at 4°C, followed by a series of washes to remove non-interacting proteins. The beads for each replicate were then split 2:1, with one part continuing to elution with FLAG peptide. This portion was used to confirm expression of target

protein by western blot and pulldown of other proteins by silver stain (Figure 6-2). This strategy of performing all the purifications at once removes one additional point of variability in our experiment. Silver stains revealed that ANKLE2 pulled down many other proteins, while GFP had significantly fewer other proteins visible. We also found that the amount of ZIKV replication during the experiment was significantly different between the ANKLE2-3xF and GFP-3xF expressing cells (Appendix C-3A). Next, the proteins on the remaining two portions of beads were digested by trypsin into peptides for mass-spectrometry analysis. The remaining processing was performed by the UC Davis Proteomics Core.

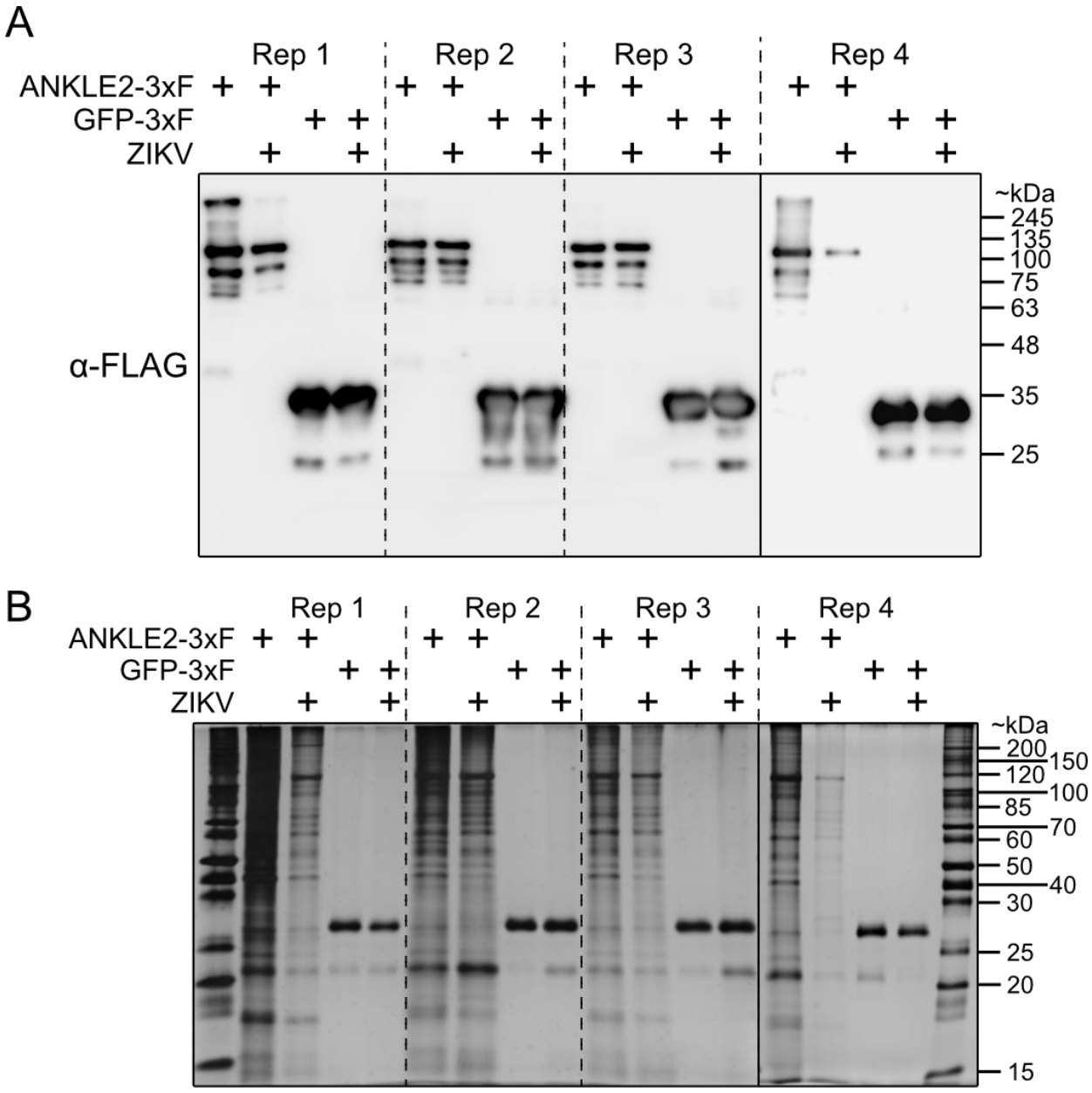

Figure 6-2: Validation of pulldown efficiency in proteomic analysis samples. (A) Western blot analysis of elution product after FLAG affinity purification from ANKLE2-3xF and GFP-3xF HEK293T cells. Cells were either mock infected or infected with ZIKV MR766 at MOI 5 for 48 hours. Both proteins appear at their expected sizes and with N-terminal degradation products. (B) Silver stain of eluted protein confirms the presence of proteins pulled down by ANKLE2.

Assessment and determination of ANKLE2 candidate interactors

Raw LC-MS/MS data was analyzed by the Proteomics Core facility team using the Spectronaut software. Peptides were mapped to the entire human proteome and included a list of individual ZIKV proteins and common contaminants. Unfortunately, one of the samples (replicate #3 of GFP-Mock) was unable to be quantified, although we still had three other replicates so statistical tests could still be performed. Across our remaining 15 samples we detected 119,342 different peptides that were mapped to 8,862 protein groups (Appendix C-3B). Principle component analysis (PCA) of this data revealed two distinct groups, separating the GFP samples from ANKLE2 samples (Appendix C-3C). However, the differences between mock and ZIKV infected appeared to be less substantial.

To initially filter the data, we removed clear contaminant proteins from either non-human species (bacteria, carry-over from bovine serum, etc.) or common human contaminants (keratin, tubulin, etc.). We also removed proteins which were part of non-specific protein groups. These protein groups arise from peptides which are present in multiple, usually very similar proteins, so the precise identity of which protein was present in the sample is ambiguous. In total, this removed 157 identifications, leaving 8,705 proteins in our analysis. To determine which ANKLE interactions may be true interactions we first needed to account for background using our GFP samples. To do this we first compared protein quantities from mock or ZIKV-infected ANKLE2 vs. GFP samples (ZIKV vs. ZIKV or mock vs. mock). To perform this analysis, we used significance analysis of interactome (SAINT), which determines the probability that a specific bait-prey pair interaction is true based on the data in the negative controls (2). This is referred to as a semi-supervised mixture model since the negative distribution is determined from experimental data from negative control purifications, in our case GFP-3xF. The early versions of this model were designed for spectral count data obtained in data-dependent acquisition (DDA) proteomics, but a recent version SAINTexpress was improved to use intensity-based data generated in DIA experiments like ours

(3). SAINTexpress returns several values of interest: a Bayesian false-discovery rate (BFDR), a $\log_2$ fold change in protein quantity between the experimental condition and negative control, and a SAINT score, which ranges from 0 to 1. Our first filter was a BFDR of ≤ to 0.1. Next, we used a ≥ 1.5 $\log_2$ fold change in protein quantity between ANKLE2 and GFP protein IDs to further filter our data. If all the replicates for a sample were 0 then we made the average protein quantity 1 for the sake of this comparison so that this could be computed. We opted to use these cutoffs over the traditional SAINT score cutoff of ≥ 0.95 since these scores were highly sensitive to missing values given our number of replicates. Importantly, our BFDR and $\log_2$ fold change cutoffs were benchmarked by the presence of ANKLE2 in the identified proteins for both mock ($\log_2$ fold change = 2.73, BFDR = 0.06, but SAINT = 0.75) and ZIKV-infected samples ($\log_2$ fold change = 2.47, BFDR = 0.09, but SAINT = 0.5). As a final scoring metric, we used MSstats which we used to compare the samples at both the peptide and protein level. Here, we used an adjusted p-value ≤ 0.005 as our cutoff (4). After these three filters we ended with 711 proteins candidates in the mock condition (Appendix C-4) and 717 in the ZIKV condition (Appendix C-5). Each of these populations represented ~8.2% of the total protein population. Overall, we identified 909 protein candidates, with most overlapping between the mock and ZIKV sets (Figure 6-3). We referred to these 909 proteins as our candidate proteins. It is unlikely and unrealistic to expect that all these proteins are true ANKLE2 interactors, but this systematic analysis provides a strong starting point for further analysis.

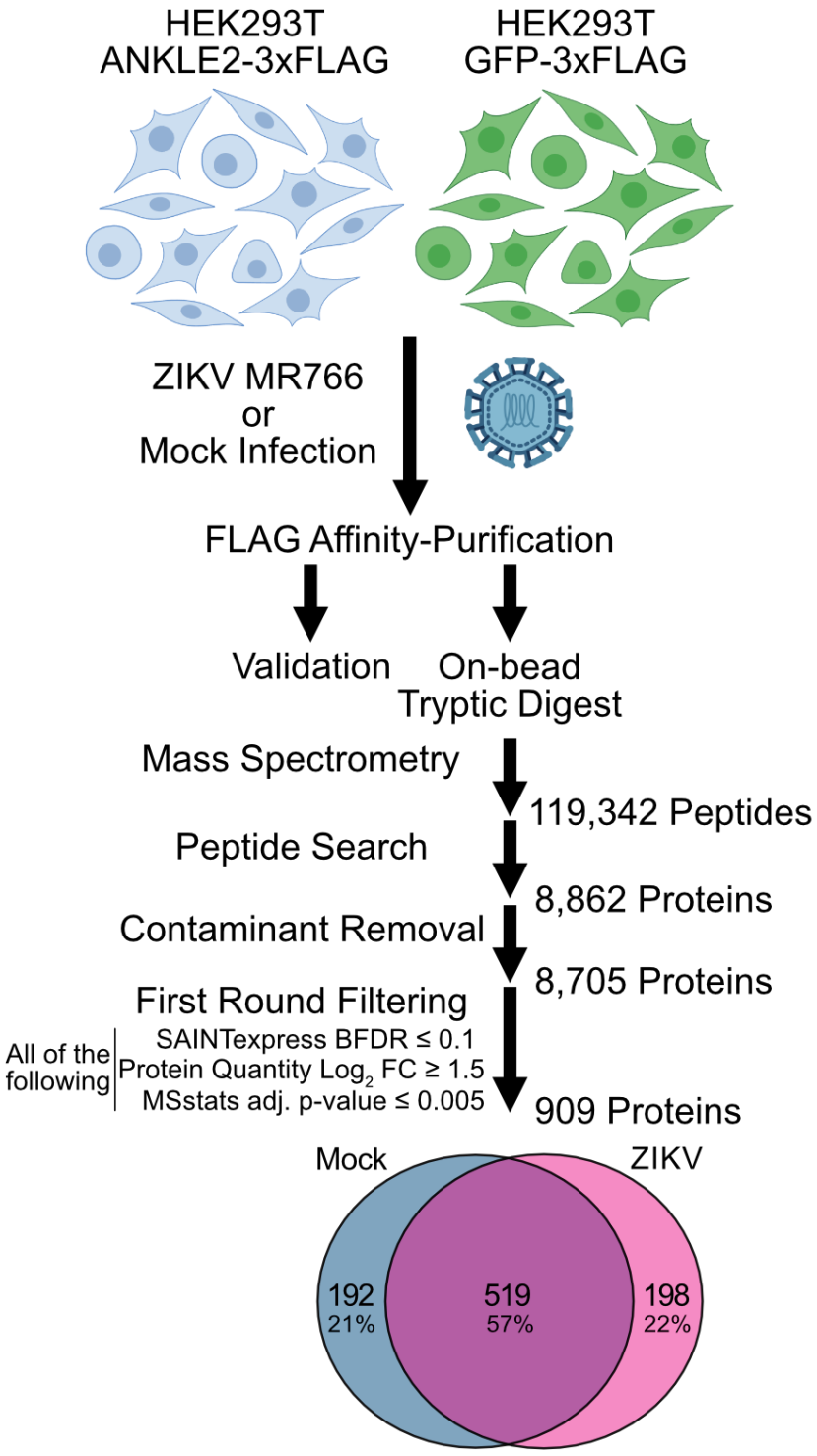

Figure 6-3: Experimental workflow leading from cells to candidate protein interactions. HEK293T cells constitutively expressing ANKLE2 or GFP with 3xFLAG affinity tags were either mock infected or infected with ZIKV MR766 at MOI 5 for 48 hours. Four biological replicates were

performed for each condition. Protein lysates were applied to FLAG affinity beads. After washing, the beads were split for either validation or for on-bead tryptic digest. Digested peptides were given to the UC Davis Proteomics Core for further processing and analysis by liquid chromatography tandem mass-spectrometry. Mass-spectrometry data was analyzed using Spectronaut and then filtered using SAINTexpress (2) and MSstats (4).

Enrichment analysis of candidate proteins

Next, we faced the challenge of determining which of our 909 candidate proteins were biologically feasible for ANKLE2 to interact with, relevant for ZIKV replication or neurodevelopment, or interesting to study. Further, the main questions remained regarding how these protein interactions change during ZIKV infection, and how this may relate to ANKLE2's role in facilitating virus replication or its dysfunction related to abnormal neurodevelopment. To explore this we performed functional gene enrichment analysis using g:GOSt within g:profiler (5). This analysis examines the given genes or proteins in a set and compares to how many proteins in the set are present in pre-defined, manually curated, and experimentally validated enrichment categories. A cumulative hypergeometric test and multiple testing correction (g:SCS) (6) are performed to provide an adjusted p-value for each enrichment category. This analysis integrates multiple databases, including gene ontology (GO) (7), KEGG (8), reactome (9), and CORUM (10), to provide additional confidence that identified categories are not unique to a particular database. The GO database is broken down into three subcategories for biological process (BP), molecular function (MF), and cellular compartment (CC). Additionally, the Human Phenotype Ontology (11) provides insight into how disfunction of the given proteins may be related back to human diseases.

We input each entire candidate proteins from the Mock (711 proteins) or ZIKV (717 proteins) sets or just the overlapping shared proteins (519 protein). Next, we evaluated enriched categories for those with consistently significant scores and realistic biological properties. Since ANKLE2 is

integral to the ER and nuclear envelope, we expected enrichment for membrane pathways. Indeed, categories involved in membrane biology including “organelle membrane,” “ER membrane,” “membrane organization,” and “endomembrane system organization,” are significantly enriched in all protein sets, suggesting this is a foundational aspect of ANKLE2 behavior (Figure 6-4, some not shown). Interestingly, aspects of mitochondrial respiration are also consistently amongst the top enriched categories, including “mitochondrion organization,” “inner mitochondrial membrane protein complex,” “respiratory electron transport chain,” and “ATP synthesis coupled electron transport” (Figure 6-4, some not shown). The potential role of ANKLE2 in mitochondrial respiration has never been explored and changes in metabolic potential have never been described in ANKLE2-deficient cells. Whether ANKLE2 is truly involved in these biological functions requires additional experimentation. Some enrichment categories were especially interesting given the potential role in ZIKV replication or clear changes in score between the mock and ZIKV datasets and will be described individually (bolded in Figure 6-4 and shown in Figure 6-5).

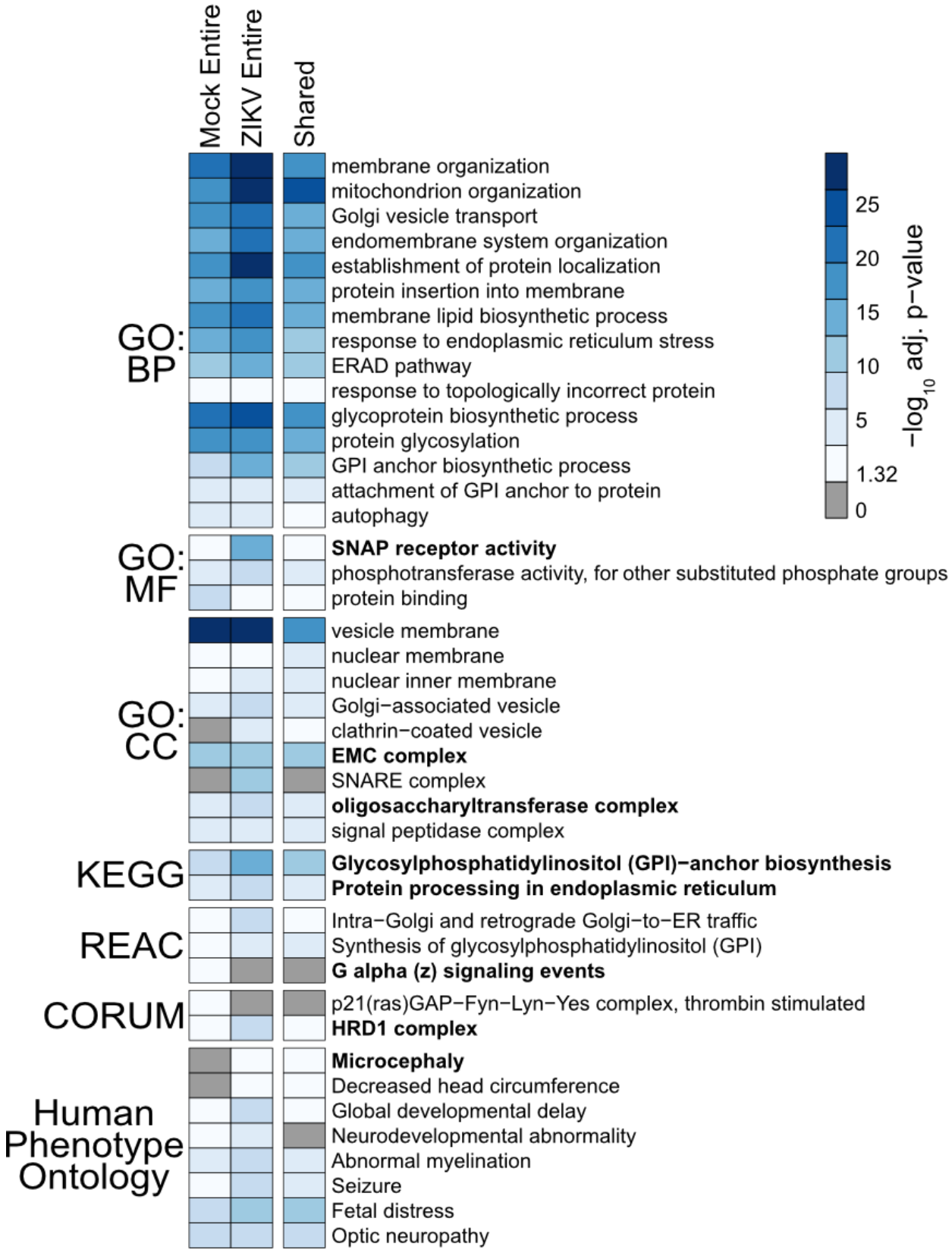
Mock Entire
ZIKV Entire
Shared
GO: BP
membrane organization
mitochondrion organization
Golgi vesicle transport
endomembrane system organization
establishment of protein localization
protein insertion into membrane
membrane lipid biosynthetic process
response to endoplasmic reticulum stress
ERAD pathway
response to topologically incorrect protein
glycoprotein biosynthetic process
protein glycosylation
GPI anchor biosynthetic process
attachment of GPI anchor to protein
autophagy
25
20
15
10
5
1.32
0
−log10 adj. p−value
GO: MF
SNAP receptor activity
phosphotransferase activity, for other substituted phosphate groups
protein binding
GO: CC
vesicle membrane
nuclear membrane
nuclear inner membrane
Golgi−associated vesicle
clathrin−coated vesicle
EMC complex
SNARE complex
oligosaccharyltransferase complex
signal peptidase complex
KEGG
Glycosylphosphatidylinositol (GPI)−anchor biosynthesis
Protein processing in endoplasmic reticulum
REAC
Intra−Golgi and retrograde Golgi−to−ER traffic
Synthesis of glycosylphosphatidylinositol (GPI)
G alpha (z) signaling events
CORUM
p21(ras)GAP−Fyn−Lyn−Yes complex, thrombin stimulated
HRD1 complex
Human Phenotype Ontology
Microcephaly
Decreased head circumference
Global developmental delay
Neurodevelopmental abnormality
Abnormal myelination
Seizure
Fetal distress
Optic neuropathy

Figure 6-4: Protein enrichment analysis of ANKLE2 candidate interactions using gProfiler. Functional gene enrichment analysis of candidate protein from the entire ANKLE2-mock (711 proteins), ANKLE2-ZIKV (717), or overlapping (519) sets. Enrichment categories were selected based on biological relevance and relative significance level (adjusted p-values less than $\times 10^{-30}$ were avoided for the sake of visualization). Categories were considered significantly enriched if the adjusted p-value was less than 0.05 ($-\log_{10}(0.05) = 1.32$). Categories not enriched in a given set are colored grey. Abbreviations: GO = gene ontology, BP = biological process, MF = molecular function, CC = cellular compartment, KEGG = Kyoto Encyclopedia of Genes and Genomes, REAC = reactome, CORUM = comprehensive resource of mammalian protein complexes, ERAD = ER-associated degradation, GPI = glycosylphosphatidylinositol, EMC = ER membrane complex, SNAP = soluble N-ethylmaleimide-sensitive factor attachment proteins, SNARE = SNAP receptors.

SNAP Receptor Activity

Soluble N-ethylmaleimide-sensitive fusion (NSF) attachment proteins (SNAPs) and related proteins mediate vesicle targeting and fusion (12). The enrichment category contains a wide array of proteins with various roles in this process, including syntaxins (STXs) and vesicle-associated membrane proteins (VAMPs). These SNAP receptor proteins (SNAREs) have established roles in neurotransmitter vesicle docking and release (13). We observe that these categories are more highly enriched in the ZIKV dataset, suggesting this pathway may be a target to enhance ZIKV replication through ANKLE2. While these SNARE proteins are involved in the entry of other enveloped viruses (14), no literature has explored their impact on orthoflavivirus entry or replication. Our previous data suggests that ANKLE2 is not involved in ZIKV entry (Figure 4-7), but it is plausible that other aspects of trafficking to the Golgi may be targets of ANKLE2 function.

ER Protein Processing: EMC, ERAD, and OST Complexes

We identified multiple proteins, pathways, and complexes involved in protein processing and ZIKV replication mechanisms (Figure 6-5). The ER membrane complex (EMC) is a 10-protein complex that spans the ER membrane and plays significant roles in mediating membrane protein topology by facilitating correct insertion of transmembrane domains (15). We identified all 10 of these proteins in our proteomics, with 9/10 being identified as candidates in both datasets (Figure 6-5). Given that orthoflavivirus polyproteins are generated at the ER membrane and contain many transmembrane domains (Figure 2-1), it is no surprise that they heavily rely on the host EMC for their viral protein processing (16,17). Given the presence of the EMC complex in both datasets, ANKLE2 may universally interact with the complex in the ER and may play a beneficial role in orthoflavivirus utilization of this complex.

We identified 8 members of the HRD1 complex which mediates ER-associated degradation (ERAD) through its activity as a ubiquitin ligase complex (18). Orthoflaviviruses have been shown to depend on host ERAD pathways for viral protein homeostasis (19), and several of the complex members (SEL1L, AUP1, and UBE2J1) enhance or are required for flavivirus replication (20–22). We also identified other ERAD related proteins DERL1 and ERLIN1, further supporting that ANKLE2 may participate in ERAD. Another striking complex we identified is the oligosaccharyltransferase (OST) complex. This complex mediates asparagine linked glycosylation on newly produced glycoproteins in the ER which is vital for protein folding and export (23). This complex has repeatedly been shown to be critical for orthoflavivirus RNA genome replication, in a role separate from its catalytic activity (24,25). Both the HRD1 and OST complexes were present in both ANKLE2 datasets, suggesting that again, this may be a universal function of ANKLE2 that is hijacked during orthoflavivirus replication.

GPI

Multiple categories revolving around glycosylphosphatidylinositol (GPI) synthesis and attachment were enriched in all sets (Figure 6-4 and Figure 6-5). The GPI anchor synthesis and attachment pathway occurs on the ER membrane so it is feasible that ANKLE2 could participate in this process, although the catalytic attachment of GPI to the target protein occurs on the ER lumen (26), which contains only a small portion of ANKLE2. Involvement of GPI in orthoflavivirus biology has only been minimally explored, with only one study showing that DENV NS1 having a GPI-anchor attached (27), and the participating GPI proteins were not identified.

G Proteins

One of the most interesting outcomes of our gene enrichment analysis was the presence of proteins related to G protein signaling that only appeared in the mock data set and were lost upon ZIKV infection. G proteins are plasma membrane proteins that bind guanine nucleotides and transmit a wide array of extracellular signals to the intracellular space to facilitate some cellular response. G proteins are activated upon ligand binding to the G protein coupled receptor (GPCR), which induces a conformational change in the G protein, allowing for binding to GTP. GTP-binding induces the dissociation of a G protein into its alpha subunit bound with the GTP (Gα-GTP) and the beta-gamma dimer (Gβγ). Both of these subunits can then independently modulate cell effectors to mediate cell responses (28). In our proteomics data, we identified 12 members involved in these processes, including several G protein subunits and two adenylate cyclases which are activated by Gα-GTP to convert ATP to cyclic AMP. While these processes are interesting due to their foundational roles in cellular behavior, it is unclear how ANKLE2 interacts with these proteins on the plasma membrane.

Src Family Kinases

In addition to these G proteins, we also identified interactions with the Src family tyrosine kinases LYN, FYN, and YES1 only in the mock dataset. These kinases are broadly targeting and have wide roles in regulatory and signal transduction pathways (29–31). Interestingly, these kinases are involved in different aspects of the immune response, including the activation of T cells (32), B cells (33), and NK cells (34). This could provide an interesting connection to the potential inhibition by ZIKV infection. Large scale proteomic analysis also suggests that LYN interacts with the G protein subunits GNAI1, GNAI2, and GNIA3 (35). Small-scale studies have shown interaction between LYN and GNAI3 in human ovarian cells (36) and Fyn or Lyn with undetermined Gα subunits in rat cells (37). Whether these kinases phosphorylate these G protein subunits or have their function influenced by them is unknown, although the activity of G proteins is regularly controlled through post-translational modifications, including tyrosine phosphorylation (38,39). Additionally, these kinases interact with the protein phosphatase complex members PPP2CB, PPP2R1A, and PPP2R5E (Figure 6-5). This array of protein interactions could be the first indication of another substrate-kinase-phosphatase trio regulated by ANKLE2, akin to BAF-VRK1-PP2A we discussed previously (Chapter 3).

Additional Microcephaly Related Factors

In addition to established enrichment categories, we were also interested in candidates associated with either congenital microcephaly or orthoflavivirus replication. Our candidate list does not contain any of the other 29 established primary microcephaly (MCPH) genes (Appendix A-2). Thus, we performed an expanded literature review of all 909 candidate genes for any known involvement in microcephaly. This revealed 48 candidate proteins with published connections to clinical microcephaly (Appendix C-6, rounded rectangles in Figure 6-5). For microcephaly, this is

a slightly challenging investigation since there is less clinical evidence tying these genes to the specific clinical outcome, most of these proteins lack clear interactions with each other, and we did not identify a clear unifying function amongst them (Figure 6-5). Most interesting among these were the genes *GNB1*, a member of our G protein related gene enrichment category (40), the OST complex members *STT3B* (41) and *TUSC3* (42,43), and the protein phosphatase complex members *PPP1R15B* (44,45) and *PPP2R1A* (46,47) (Figure 6-5). The relationship of these proteins with microcephaly through an interaction with ANKLE2 or through its function in neurodevelopment is speculative and requires future exploration.

Additional Orthoflavivirus Replication Factors

We performed a similar literature search of all 909 candidate proteins for any published roles in orthoflavivirus replication. We expanded our search beyond ZIKV because very little molecular level research was performed on ZIKV before 2015. Excitingly, we identified 55 proteins with known roles in orthoflavivirus replication (Appendix C-6, red outline in Figure 6-5), including well established host factors that have been identified in recent years. Perhaps unsurprisingly, most of the replication factors we identified revolve around ER processes, and include some previously mentioned complexes (EMC, OST, HRD1). Additionally, we identified other ER translocation proteins such as SEC62 and all five subunits of the signal peptidase complex (SPC) (SPCS1/2/3 and SEC11A/C) in both mock and ZIKV groups. The SPC is a membrane spanning complex which proteolytically cleaves N-terminal signals as they are translocated into the ER lumen (48). SPCS1 has been shown to facilitate replication of JEV through an interaction with NS2B (49) and is amongst many other protein processing factors identified in a large CRISPR screen (50). We also identified ER remodeling factors we previously discussed in Chapter 2, including ATL2 and ATL3 (51), Lunapark (LNPK) (52), and TMEM41B (53). Given that the mechanisms for how these

proteins facilitate replication is already known, exploring if they are mediated by ANKLE2 is an interesting and promising next step.

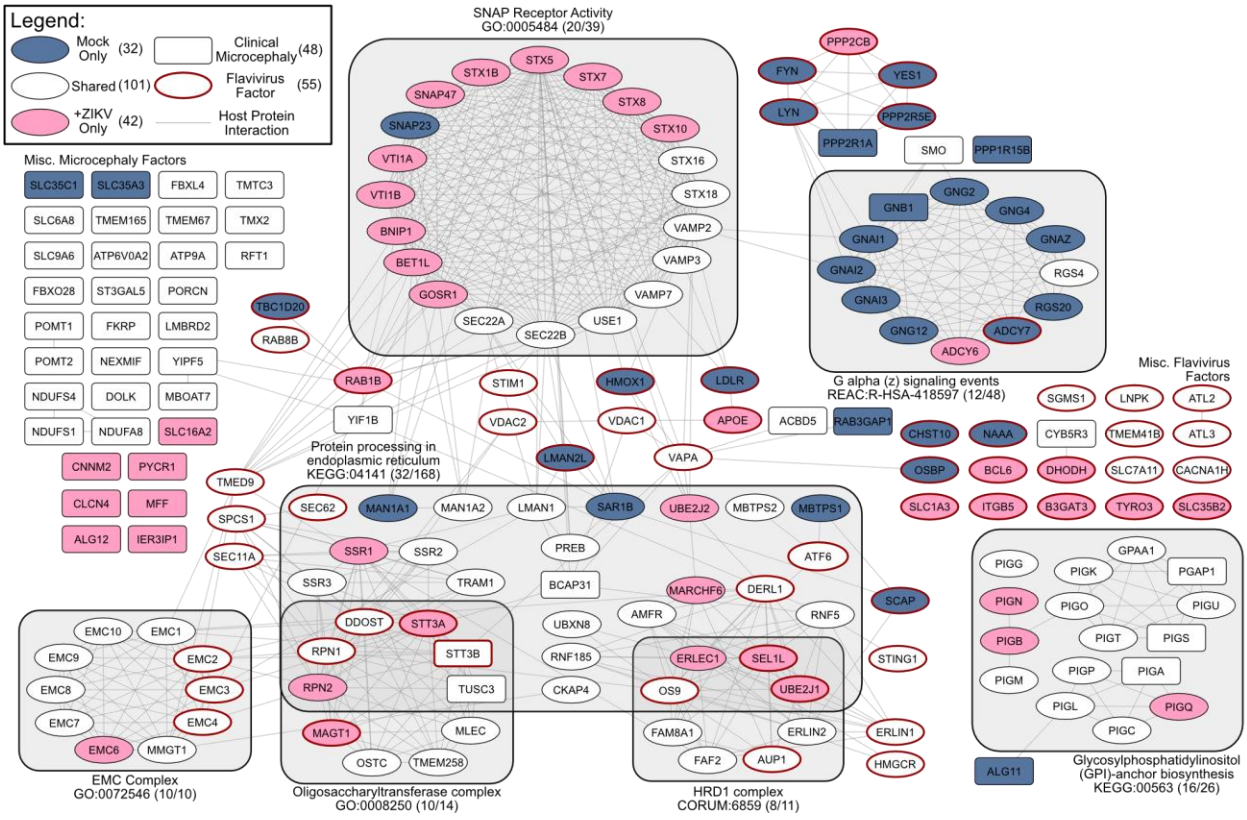

Figure 6-5: Network of proteins from highlighted enrichment categories. Protein interaction networks of selected gene enrichment categories (bolded in Figure 6-4) and candidates with published associations with orthoflavivirus replication (red outline) or clinical microcephaly (rounded rectangle). All selected proteins were entered into STRING to identify supported protein interactions (grey lines) and the networks were formatted in Cytoscape. Individual proteins are colored based on dataset grouping. Proteins belonging to certain enrichment categories are shown in shaded areas with the number of identified proteins out of the total number of proteins in the category.

Direct comparison between mock and infected states

Given that these candidate proteins were determined by comparing ANKLE2 conditions to GFP conditions, we next sought to compare our ANKLE2-ZIKV vs. ANKLE2-mock directly. To do this we used MSstats to directly compare these conditions, but only on our 909 candidate proteins. We considered these candidates mostly free of background since this should have been removed in our initial filtering against the coinciding GFP control. In this direct comparison we used a p-value of less than 0.01 as our only cutoff (Figure 6-6A). For some proteins, they were not identified in any of the four ZIKV-infected replicates and were not imputed so a p-value could not be calculated. We included these in our significantly changing proteins if they appeared in at least three of four mock replicates (FHIP2B, ERC2, MME, and C11orf52) (not shown in Figure 6-6A). Unsurprisingly, ZIKV proteins were the most significantly enriched proteins in the infected state. However, beyond these viral proteins we did not detect many proteins that increased in their interaction with ANKLE2 following ZIKV infection. PPP2CB, MARCHF6, CTDNEP1, and C10orf90 were the only other proteins with a significant p-value and a positive ZIKV vs. mock fold change (Figure 6-6). Interestingly, we did observe more proteins that were significantly enriched in the mock condition over ZIKV infection. This included several of the G protein subunits (GNAI1, GNAI2, GNAI3, GNAZ, and GNG4) and Src family kinases (LYN and FYN) we discussed previously (Figure 6-6B). This provides additional evidence supporting that this pathway is significantly impacted by ZIKV infection. This analysis also revealed contactin-1 (CNTN1) as one of the most significant results. This is exciting since CNTN1 is involved in many aspects of neuronal biology and development (54,55). Other hits, such as limbic system-associated membrane protein (LSAMP) and ubiquitin domain-containing protein 1 (UBTD1) are poorly studied so understanding the significance of finding them amongst our top hits is less clear. Next steps will require the validation of the physical interaction between ANKLE2 and these proteins and evaluation of how much the interaction changes during ZIKV infection.

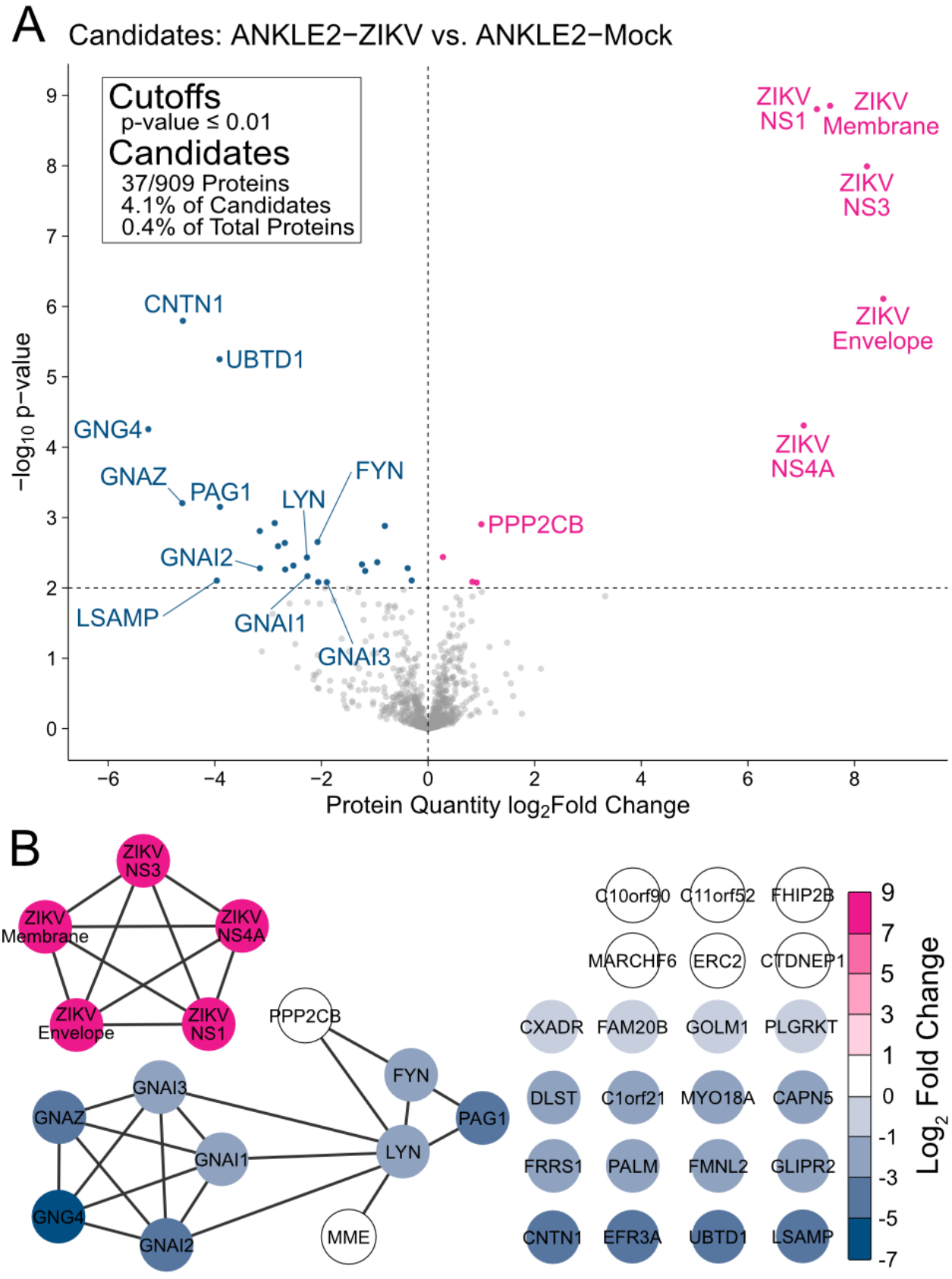
A
Candidates: ANKLE2−ZIKV vs. ANKLE2−Mock
Cutoffs
p-value ≤ 0.01
Candidates
37/909 Proteins
4.1% of Candidates
0.4% of Total Proteins
ZIKV NS1
ZIKV Membrane
ZIKV NS3
ZIKV Envelope
ZIKV NS4A
PPP2CB
CNTN1
UBTD1
GNG4
GNAZ
PAG1
LYN
FYN
GNAI2
LSAMP
GNAI1
GNAI3
−log10 p−value
Protein Quantity log2Fold Change
B
ZIKV NS3
ZIKV Membrane
ZIKV NS4A
ZIKV Envelope
ZIKV NS1
PPP2CB
FYN
GNAI3
GNAZ
PAG1
GNAI1
LYN
GNG4
GNAI2
MME
C10orf90
C11orf52
FHIP2B
MARCHF6
ERC2
CTDNEP1
CXADR
FAM20B
GOLM1
PLGRKT
DLST
C1orf21
MYO18A
CAPN5
FRRS1
PALM
FMNL2
GLIPR2
CNTN1
EFR3A
UBTD1
LSAMP
Log2 Fold Change

Figure 6-6: Statistically significant changes in protein abundance between ANKLE2-ZIKV and ANKLE2-Mock. (A) All 909 candidate proteins were analyzed again using MSstats to compare ANKLE2-ZIKV directly to ANKLE2-Mock. Here, we considered all proteins with a p-value < 0.01 as significantly different from the other condition. Four additional proteins (FHIP2B, ERC2, MME, and C11orf52) were included that had p-values that could not be computed due to no detection in the ZIKV dataset but were found in at least three of four mock replicates. (B) Interaction network of 37 significantly different candidate proteins. Proteins colored by $\log_2$ fold change of ZIKV vs. Mock.

Conclusions and Discussion

Our first exploration of ANKLE2 interactions and the changes induced by ZIKV using affinity-purification and mass-spectrometry revealed over 900 candidate protein interactions. Amongst these proteins are many biologically important pathways that did not appear to have significantly changed upon ZIKV infection. This suggests that ANKLE2's unresolved ER function is multifaceted and that ZIKV interacts with ANKLE2 to utilize these proteins. However, there are significant limitations with this initial study that require recognition prior to complete commitment to these results. First, the utilization of HEK293T is a significant limitation which complicates the analysis in two separate ways. While HEK293T are optimal cells for protein production and expression they are not a reliable representation of any specific tissue or organ, making the ties to any candidate protein with brain development or microcephaly potentially out of place. Second, these cells limit the strains of ZIKV that can be used, with the African lineage MR766 strain being required at high MOI for even partially thorough infection. The utilization of a neuronal cell line in future experiments would alleviate both issues, by placing protein-protein interactions in the context of a biologically relevant cell type and would allow for the use of Asian lineage ZIKV strains

at lower MOIs (Appendix C-7). The difficulty then becomes consistent and complete expression of ANKLE2 in a manner conducive for affinity-purification.

Next, our 909 candidate ANKLE2-protein interactions are likely far too many to be biologically feasible for a single protein. Studies suggest that, on average, yeast proteins have 16 protein interactions (56) and human proteins have 8 interactions, although some proteins certainly have interactions ranging in the hundreds (57). Even after considering that ANKLE2 is a scaffolding protein with potentially numerous roles, it is unrealistic to suggest that every of the 909 proteins that met our initial three-cutoffs is a true interaction. Additionally, the lack of canonical protein interactions (BANF1 or VRK1) even in our broad set of candidates is concerning, although these may be underrepresented due to cell cycle stage dependency. ANKLE2 interactions have been cataloged in large global proteomic screens and current data supports 198 unique physical protein interactions (BioGrid:116758) (57–61). Interestingly, BANF1 or VRK1 are not amongst these interactions either, supporting the hypothesis that identification of these protein-protein interactions by proteomics may not be possible. Of these 198 experimentally supported interactions, 31 are candidates in our data, including PPP2CB and PPP2R1A, which are unsurprisingly the most commonly identified ANKLE2-interactors. Also in this group of overlapping proteins are OST-complex members RPN1 and RPN2, ER processing proteins SEC62, DERL1, LMAN1, and SSR1, and SNAP receptor family protein STX7, supporting the role and involvement of ANKLE2 in these processes. Most of the mitochondrial respiration proteins, G proteins, and GPI-related proteins are missing from this set of supported ANKLE2-interactors, increasing the need to experimentally validate these hits, either to identify novel functions of ANKLE2 or to eliminate them as background.

Several studies have profiled the proteomic landscape of ZIKV proteins. Most were performed by transiently expressing and affinity-purifying individual viral proteins (62–66). These studies often identify hundreds of individual virus-host interactions, which have variable overlap with the

candidate proteins identified in our ZIKV dataset (Appendix C-8). The degree of overlap does not seem to correlate with technique and no unifying protein was identified in all the examined data. A more recent study expanded on this principle by performing fractionation prior to purifying ZIKV-infected ER membranes by pulldown of HA-tagged Calnexin (67). This approach identified proteins expected to be involved in ZIKV replication, although many of the expected orthoflavivirus host factors we discussed previously were not identified. This analysis did reveal novel host factors involved in ZIVK secretion, assembly, RNA processing, and lipid metabolism, although none of these hits overlapped with our candidates. Three proteins identified in their study (IMMT, PHB2, and STOM) were identified in our candidates, although the function of these proteins in orthoflavivirus replication has not been studied (Appendix C-8).

Validating candidate interactions at the individual protein or pathway level is the next major step. While less sensitive, affinity-purification and western blot is a standard tool to confirm physical interactions between proteins identified in mass spectrometry experiments. This is limited by the availability, quality, and cost of specific antibodies against target proteins. Thus, this is often done on a small subset of chosen proteins. Confirming that ANKLE2 interacts with PPP2R1A and PPP2CB is a good initial experiment since these interactions are well established. Next, confirming interactions with individual proteins from the most interesting enrichment categories (G protein signaling, ER processing, GPI attachment, etc.) can provide substantial support for the role of ANKLE2 in these pathways. In coordination with this approach is evaluation of entire pathways potentially associated with ANKLE2. Mitochondrial respiration is a top hit throughout the enrichment analysis and over 50 proteins involved in the electron transport chain were identified as candidates in our data. Assessment of aerobic respiration in wild-type and ANKLE2 knockout cells using a metabolic assay, such as the Seahorse XF assay (68), can provide quick determination regarding whether these are background proteins or truly related to ANKLE2 function.

The pathways identified in this experiment also provide potential insight into how ANKLE2 promotes ZIKV replication. The mechanism by which ANKLE2 influences virus replication has remained elusive to us. This analysis has revealed several interesting ER homeostasis pathways that are certainly important for orthoflavivirus replication, and the main question now becomes if these are mediated in any way by ANKLE2. To test this, we can now explore how the loss of ANKLE2 in our knockout cells (Huh7 or JEG-3) impacts the transcriptional expression and protein function of these pathways or complexes. For example, ATF6 is an ANKLE2 candidate interactor in both mock and ZIKV datasets. ATF6 is a major component of the unfolded protein response (UPR) pathway in the ER. ER stress initiates ATF6 transit from the ER to the Golgi, where it is proteolytically cleaved, yielding a fragment which acts as a transcription factor to upregulate genes involved in maintaining ER folding and homeostasis (69). Activation of this pathway can be evaluated by western blot to determine the degree of this cleavage. Additionally, evaluating the expression of ATF6 or its downstream targets (BiP/GRP78, GRP94, ERDJ3, etc.) by qPCR in WT and ANKLE2 KO cells under mock and ZIKV infected conditions will illuminate if this pathway is mediated by ANKLE2 (70,71). This approach can be expanded to investigate other ER homeostasis pathways including ERAD, lipid metabolism and reticulophagy. In summary, exploration of ANKLE2 interactions using AP-MS has revealed many potential novel ER functions in host processes that could be coopted to promote ZIKV replication.

Materials and Methods

Cells. Cell lines were maintained as previously described in Chapter 4.

Lentiviral packaging, transduction, and cell selection. Lentivirus was prepared as previously described in Chapter 4. Transduced cells were bulk selected for zeocin resistance.

Viruses and stock preparation. ZIKV stocks were prepared as previously described in Chapter 4.

Sample preparation. For proteomic sample preparation $1x10^7$ HEK293T or $5x10^6$ HEK293T cells were plated in 15 cm or 10 cm dishes, respectively and grown overnight. Cells were then mock infected with DMEM or infected with ZIKV MR766 at MOI 5. After 48 hours, a media sample was taken for later determination of virus titer. Lids were then removed, and dishes were left in the hood under UV for 60 minutes to neutralize the remaining virus. Media was then removed from each plate. To dissociate cells, 5 mL of D-PBS supplemented with 10 mM EDTA was added and allowed to incubate for several minutes. Cells were resuspended in D-PBS and transferred to conical tubes prior to centrifugation 94 g, 4ºC for 5 minutes (Eppendorf centrifuge 5810 R, Rotor S-4-104). Cell pellets were washed with D-PBS and centrifugation was repeated. Supernatant was removed and pellets were then resuspended in 1 mL IP buffer (50 mM Tris Base, 150 mM NaCl, 0.5 M EDTA, pH 7.4) with Pierce™ protease inhibitor tablets (Thermo Scientific) supplemented with 0.5% NP-40 Substitute (Igepal™ CA-630, Affymetrix). Cells were lysed for 30 minutes at 4ºC, and lysate was then centrifugated at 845 g, 4ºC, for 20 minutes (Eppendorf centrifuge 5424 R, Rotor FA-45-24-11). The soluble lysate was transferred to a fresh 1.5 mL tube and frozen at -80ºC until all replicates were complete. Once all replicates were ready, the lysate samples were thawed on ice. Lysate was added to 100 µL of ChromoTek DYKDDDDK Fab-Trap™ Agarose (Proteintech) and incubated overnight at 4ºC with gentle rotation. Beads were then washed four times with 1 mL IP buffer with 0.05% NP-40 and once with 1 mL IP buffer without NP-40. Beads were then split (2:1, 66.7 µL:33.3 µL) for on-bead tryptic digest or sample validation. The smaller fraction was incubated in 40 µL of 100 ng/mL 3x FLAG peptide (for FLAG-AP) (APExBIO) at 211 g for 1 hour at room temperature (Eppendorf ThermoMixerC). Eluate was then removed. Eluate and lysate were resuspended in NuPAGE LDS sample buffer and bond-breaker

TCEP (Thermo Scientific) according to manufacturer's recommendation. Samples were boiled for 10 minutes at 95ºC prior to evaluation.

Western blot. Western blot was performed as previously described in Chapter 4.

Silver Stain. Polyacrylamide gels (1.5 mm, 4% stacking / 10% resolving) were manually cast. 4.5 uL PageRuler unstained ladder (Thermo Scientific, #26614) was loaded flanking the samples. 10 uL (ANKLE2) or 2.5 uL (GFP) of sample was loaded into gel. Gel was run at 115 V, 15minutes then 150 V for ~50 minutes. Silver stain was accomplished using the Pierce™ Silver Stain Kit (#24612). In full, the gel was removed from the cast and transferred to a 15 cm dish filled with UltraPure water and washed twice for 5 minutes at ~50-60 rpm. Gel was fixed in 30% Ethanol: 10% Acetic acid solution for 15 minutes twice. Gel was washed twice in 10% ethanol solution for 5 minutes, followed by water twice for 5 minutes. Sensitizer working solution was prepared by adding 50uL sensitized to 25mL UltraPure water and then added to gel for exactly 1 minute. Gel was again washed twice with UltraPure water for 1 minute. Silver stain working solution was prepared by adding 500uL silver stain enhancer to 25mL silver stain and then added to gel for ~45-60 minutes. Silver stain solution was removed, and gel was quickly washed twice with UltraPure water for 20 seconds. Developing solution was prepared by adding 500uL silver stain enhancer to 25mL silver stain developer. Developing solution was added to gel and gently shaken for 1-3 minutes until bands were desired appearance. 5% acetic acid solution was added to stop reaction, shaking vigorously briefly before replacing with new 5% acetic acid. Gel was shaken vigorously for several minutes prior to imaging on Amersham Imager 600 Luminescent Image Analyzer using chemiluminescent setting with diffuser on bottom.

On-bead tryptic digest. The larger fraction of washed FLAG-binding beads was equilibrated in diminishing volumes (200 µL, 100 µL, 50 µL, 25 µL) of 50 mM Triethylammonium bicarbonate (TEAB) buffer (Thermo Scientific) at 4°C for 20 minutes on a tube rotator. At the final wash, 500 ng of Sequencing Grade Modified Trypsin (Promega) was added to each sample. Beads were then incubated under agitation (1300 rpm) overnight (~16 hours) at 37°C. The following morning, digest supernatant was transferred to a new protein LoBind tube (Eppendorf). Another 200 ng of trypsin was added to the beads along with 40 µL of TEAB and incubated for another 2 hours; this digest was combined with the previous extract. Samples were placed on ice and then immediately delivered to the Proteomics Core facility. Raw Spectronaut data revealed missed tryptic cleavage percentages between 44.6%-57% across all 15 replicates.

Mass-spectrometry. Digested peptides were directly loaded onto an Evosep C18 tip and separated using the Evosep One. Peptides were eluted and ionized using a Bruker Captive Spray emitter. A Bruker TimsTof Pro 2 mass spectrometer running in diaPASEF mode was used for acquisition. The acquisition scheme used for diaPASEF consisted of 6x3 50 m/z windows per PASEF scan. DIA data was searched using Spectronaut 17 (Biognosys) against the human UniProt proteome (UP000005640) and ZIKV MR766 protein sequences (DQ859059.1), and the standardized common contaminants database. Direct DIA + workflow was used under default settings. Briefly, trypsin/P Specific was set for the enzyme, allowing two missed cleavages. Fixed Modifications were set for Carbamidomethyl, and variable modification were set to Acetyl (Protein N-term) and Oxidation. For DIA search identification, PSM and Protein Group FDR were set to 0.01%. A minimum of two peptides per protein group were required for quantification. Raw intensities values were normalized to all mapped peptides. Background detections were eliminated by excluding intensity values below the median intensity value for each protein, and

common contaminants were removed. Redundant protein groups were reduced to the intensity values of the most specific group.

Scoring and statistical analysis of candidate interactors. Data was exported from Spectronaut with UniProt ID, gene ID, organism, molecular weight, and protein group quantity value for each sample. Identifications from non-human or ZIKV species and ambiguous protein groups (>1 UniProt ID) were removed from analysis. UniProt IDs were used to map amino acid length using UniProt's ID mapping tool (UniProtKB_AC-ID → UniProtKB-Swiss-Prot). SAINTexpress (choi 2011) was used with default setting (100 replicates, 1 virtual control) via the APOSTL Galaxy Server developed by the Moffitt Cancer Center. ZIKV-infected samples and mock samples were scored separately (ANKLE2-Mock vs. GFP-Mock and ANKLE2-ZIKV vs. GFP-ZIKV). The "bait" files were set up with GFP as the control. The "prey" file was set up with gene ID, amino acid length, and UniProt IDs. The "interaction" files were set up with replicate ID, condition ID, UniProt ID, and determined protein quantity. This output was used to acquire protein quantity $\log_2$ fold change and Bayesian false discovery rate (BFDR). The $\log_2$ fold change was calculated by taking $\log_2$ of the average protein quantity for all replicates of a given condition. If all replicates had 0, then the average was manually set to 1 to calculate acquire a defined value, although arbitrary. A BFDR ≤ 0.1 and $\log_2$ fold change ≥ 1.5 were used as candidate criteria. For the final criteria, MSstats (v4.8.7) was used in R Studio (v4.3.1). A MSstats report was exported directly from Spectronaut and imported into R Studio. The "SpectronauttoMSstatsFormat" function was used with following important parameters: qvalue cutoff = 0.01, useUniquePeptide = TRUE, removeProtein_with1Feature = TRUE. Next, the "dataProcess" function was used with following important parameters: logTrans = 2, normalization = "equalizeMedians", featureSubset = "all", censoredInt = "0", and MBimpute = FALSE. Finally, a comparison matrix was established and the "groupComparison" function was used with default parameters. The adjusted p-value was used

as the final criteria for determining candidate interactors. For instances where MSstats p-value and $\log_2$ fold change could not be computed due to all GFP replicates being 0, the protein was considered a candidate if the BFDR cutoff was met, and the protein was detected (quantity > 0) in 3 out of 4 ANKLE2 replicates.

Enrichment analysis. Gene set enrichment analysis on mock, ZIKV-infected, or shared protein lists was performed using g:GOst functional profiling (version e110_eg57_p18_4b54a898) in g:Profiler. Default parameters were used: statistical domain scope was set to “only annotated genes,” significance threshold was set to “g:SCS threshold,” user threshold was set to 0.05. Ensembl ID with the most GO annotations were used for proteins with multiple annotations. Term IDs and adjusted p-values for all three protein lists were noted for interesting categories.

Data visualization. Volcano plots were generated using R studio (v4.3.1) and the geom_point function within ggplot (v3.4.4). Enrichment analysis heatmap was generated using the pheatmap function (v1.0.12). Protein interaction networks were generated using STRING (v12.0) with active interaction sources set to only include experiments and databases. Cytoscape (v3.10.01) was used for network visualization. Other plots were generated using GraphPad Prism 10.

References

1. Shah PS, Beesabathuni NS, Fishburn AT, Kenaston MW, Minami SA, Pham OH, et al. Systems Biology of Virus-Host Protein Interactions: From Hypothesis Generation to Mechanisms of Replication and Pathogenesis. Annu Rev Virol. 2022 Sep 29;9(1):397–415.

2. Choi H, Larsen B, Lin ZY, Breitkreutz A, Mellacheruvu D, Fermin D, et al. SAINT: Probabilistic Scoring of Affinity Purification - Mass Spectrometry Data. Nat Methods. 2011 Jan;8(1):70–3.
3. Teo G, Liu G, Zhang J, Nesvizhskii AI, Gingras AC, Choi H. SAINTexpress: Improvements and additional features in Significance Analysis of INTeractome software. Journal of Proteomics. 2014 Apr 4;100:37–43.
4. Kohler D, Staniak M, Tsai TH, Huang T, Shulman N, Bernhardt OM, et al. MSstats Version 4.0: Statistical Analyses of Quantitative Mass Spectrometry-Based Proteomic Experiments with Chromatography-Based Quantification at Scale. J Proteome Res. 2023 May 5;22(5):1466–82.
5. Kolberg L, Raudvere U, Kuzmin I, Adler P, Vilo J, Peterson H. g:Profiler—interoperable web service for functional enrichment analysis and gene identifier mapping (2023 update). Nucleic Acids Research. 2023 Jul 5;51(W1):W207–12.
6. Reimand J, Kull M, Peterson H, Hansen J, Vilo J. g:Profiler--a web-based toolset for functional profiling of gene lists from large-scale experiments. Nucleic Acids Res. 2007 Jul;35(Web Server issue):W193-200.
7. Ashburner M, Ball CA, Blake JA, Botstein D, Butler H, Cherry JM, et al. Gene ontology: tool for the unification of biology. The Gene Ontology Consortium. Nat Genet. 2000 May;25(1):25–9.
8. Kanehisa M, Goto S. KEGG: kyoto encyclopedia of genes and genomes. Nucleic Acids Res. 2000 Jan 1;28(1):27–30.
9. Gillespie M, Jassal B, Stephan R, Milacic M, Rothfels K, Senff-Ribeiro A, et al. The reactome pathway knowledgebase 2022. Nucleic Acids Res. 2022 Jan 7;50(D1):D687–92.
10. Tsitsiridis G, Steinkamp R, Giurgiu M, Brauner B, Fobo G, Frishman G, et al. CORUM: the comprehensive resource of mammalian protein complexes-2022. Nucleic Acids Res. 2023 Jan 6;51(D1):D539–45.

11. Köhler S, Gargano M, Matentzoglu N, Carmody LC, Lewis-Smith D, Vasilevsky NA, et al. The Human Phenotype Ontology in 2021. Nucleic Acids Res. 2021 Jan 8;49(D1):D1207–17.

12. Söllner T, Whiteheart SW, Brunner M, Erdjument-Bromage H, Geromanos S, Tempst P, et al. SNAP receptors implicated in vesicle targeting and fusion. Nature. 1993 Mar;362(6418):318–24.

13. Südhof TC, Rothman JE. Membrane Fusion: Grappling with SNARE and SM Proteins. Science. 2009 Jan 23;323(5913):474–7.

14. Wesolowski J, Paumet F. SNARE motif: A common motif used by pathogens to manipulate membrane fusion. Virulence. 2010;1(4):319–24.

15. Chitwood PJ, Hegde RS. The Role of EMC during Membrane Protein Biogenesis. Trends in Cell Biology. 2019 May 1;29(5):371–84.

16. Ngo AM, Shurtleff MJ, Popova KD, Kulsuptrakul J, Weissman JS, Puschnik AS. The ER membrane protein complex is required to ensure correct topology and stable expression of flavivirus polyproteins. Gao G, Kirkegaard K, Sanyal S, editors. eLife. 2019 Sep 13;8:e48469.

17. Lin DL, Inoue T, Chen YJ, Chang A, Tsai B, Tai AW. The ER Membrane Protein Complex Promotes Biogenesis of Dengue and Zika Virus Non-structural Multi-pass Transmembrane Proteins to Support Infection. Cell Rep. 2019 May 7;27(6):1666-1674.e4.

18. Wu X, Siggel M, Ovchinnikov S, Mi W, Svetlov V, Nudler E, et al. Structural basis of ER-associated protein degradation mediated by the Hrd1 ubiquitin ligase complex. Science. 2020 Apr 24;368(6489):eaaz2449.

19. Tabata K, Arakawa M, Ishida K, Kobayashi M, Nara A, Sugimoto T, et al. Endoplasmic Reticulum-Associated Degradation Controls Virus Protein Homeostasis, Which Is Required for Flavivirus Propagation. Journal of Virology. 2021 Jul 12;95(15):10.1128/jvi.02234-20.

20. Zhang J, Lan Y, Li MY, Lamers MM, Fusade-Boyer M, Klemm E, et al. Flaviviruses Exploit the Lipid Droplet Protein AUP1 to Trigger Lipophagy and Drive Virus Production. Cell Host Microbe. 2018 Jun 13;23(6):819-831.e5.

21. Ma H, Dang Y, Wu Y, Jia G, Anaya E, Zhang J, et al. A CRISPR-Based Screen Identifies Genes Essential for West-Nile-Virus-Induced Cell Death. Cell Reports. 2015 Jul 28;12(4):673–83.

22. Lan Y, van Leur SW, Fernando JA, Wong HH, Kampmann M, Siu L, et al. Viral subversion of selective autophagy is critical for biogenesis of virus replication organelles. Nat Commun. 2023 May 10;14(1):2698.

23. Cherepanova N, Shrimal S, Gilmore R. N-linked glycosylation and homeostasis of the endoplasmic reticulum. Current Opinion in Cell Biology. 2016 Aug 1;41:57–65.

24. Marceau CD, Puschnik AS, Majzoub K, Ooi YS, Brewer SM, Fuchs G, et al. Genetic dissection of Flaviviridae host factors through genome-scale CRISPR screens. Nature. 2016 Jul 7;535(7610):159–63.

25. Puschnik AS, Marceau CD, Ooi YS, Majzoub K, Rinis N, Contessa JN, et al. A Small-Molecule Oligosaccharyltransferase Inhibitor with Pan-flaviviral Activity. Cell Rep. 2017 Dec 12;21(11):3032–9.

26. Kinoshita T. Biosynthesis and biology of mammalian GPI-anchored proteins. Open Biology. 2020 Mar 11;10(3):190290.

27. Jacobs MG, Robinson PJ, Bletchly C, Mackenzie JM, Young PR. Dengue virus nonstructural protein 1 is expressed in a glycosyl-phosphatidylinositol-linked form that is capable of signal transduction. The FASEB Journal. 2000;14(11):1603–10.

28. Weis WI, Kobilka BK. The Molecular Basis of G Protein–Coupled Receptor Activation. Annual Review of Biochemistry. 2018;87(1):897–919.

29. Xu Y, Harder KW, Huntington ND, Hibbs ML, Tarlinton DM. Lyn Tyrosine Kinase: Accentuating the Positive and the Negative. Immunity. 2005 Jan 1;22(1):9–18.

30. Guglietti B, Sivasankar S, Mustafa S, Corrigan F, Collins-Praino LE. Fyn Kinase Activity and Its Role in Neurodegenerative Disease Pathology: a Potential Universal Target? Mol Neurobiol. 2021 Nov 1;58(11):5986–6005.

31. Parsons SJ, Parsons JT. Src family kinases, key regulators of signal transduction. Oncogene. 2004 Oct;23(48):7906–9.

32. Fuertes MB, Molinero LL, Toscano MA, Ilarregui JM, Rubinstein N, Fainboim L, et al. Regulated expression of galectin-1 during T-cell activation involves Lck and Fyn kinases and signaling through MEK1/ERK, p38 MAP kinase and p70S6 kinase. Mol Cell Biochem. 2004 Dec;267(1–2):177–85.

33. Rolli V, Gallwitz M, Wossning T, Flemming A, Schamel WWA, Zürn C, et al. Amplification of B Cell Antigen Receptor Signaling by a Syk/ITAM Positive Feedback Loop. Molecular Cell. 2002 Nov 1;10(5):1057–69.

34. Lowin-Kropf B, Kunz B, Schneider P, Held W. A role for the src family kinase Fyn in NK cell activation and the formation of the repertoire of Ly49 receptors. Eur J Immunol. 2002 Mar;32(3):773–82.

35. Buljan M, Ciuffa R, van Drogen A, Vichalkovski A, Mehnert M, Rosenberger G, et al. Kinase Interaction Network Expands Functional and Disease Roles of Human Kinases. Mol Cell. 2020 Aug 6;79(3):504-520.e9.

36. Miotti S, Bagnoli M, Tomassetti A, Colnaghi MI, Canevari S. Interaction of folate receptor with signaling molecules lyn and G(alpha)(i-3) in detergent-resistant complexes from the ovary carcinoma cell line IGROV1. J Cell Sci. 2000 Jan;113 Pt 2:349–57.

37. Miki T, Kaneda M, Iida K, Hasegawa G, Murakami M, Yamamoto N, et al. An anti-sulfatide antibody O4 immunoprecipitates sulfatide rafts including Fyn, Lyn and the G protein α subunit in rat primary immature oligodendrocytes. Glycoconj J. 2013 Dec 1;30(9):819–23.

38. Torres MP, Clement ST, Cappell SD, Dohlman HG. Cell Cycle-dependent Phosphorylation and Ubiquitination of a G Protein α Subunit*. Journal of Biological Chemistry. 2011 Jun 10;286(23):20208–16.

39. Li B, Tunc-Ozdemir M, Urano D, Jia H, Werth EG, Mowrey DD, et al. Tyrosine phosphorylation switching of a G protein. Journal of Biological Chemistry. 2018 Mar 30;293(13):4752–66.

40. Lee J, Park JE, Lee C, Kim AR, Kim BJ, Park WY, et al. Genomic Analysis of Korean Patient With Microcephaly. Front Genet. 2021 Jan 28;11:543528.

41. Shrimal S, Ng BG, Losfeld ME, Gilmore R, Freeze HH. Mutations in STT3A and STT3B cause two congenital disorders of glycosylation. Human Molecular Genetics. 2013 Nov 15;22(22):4638–45.

42. El Chehadeh S, Bonnet C, Callier P, Béri M, Dupré T, Payet M, et al. Homozygous Truncating Intragenic Duplication in TUSC3 Responsible for Rare Autosomal Recessive Nonsyndromic Intellectual Disability with No Clinical or Biochemical Metabolic Markers. JIMD Rep. 2015;20:45–55.

43. Al-Amri A, Saegh AA, Al-Mamari W, El-Asrag ME, Ivorra JL, Cardno AG, et al. Homozygous single base deletion in TUSC3 causes intellectual disability with developmental delay in an Omani family. Am J Med Genet A. 2016 Jul;170(7):1826–31.

44. Abdulkarim B, Nicolino M, Igoillo-Esteve M, Daures M, Romero S, Philippi A, et al. A Missense Mutation in PPP1R15B Causes a Syndrome Including Diabetes, Short Stature, and Microcephaly. Diabetes. 2015 Nov;64(11):3951–62.

45. Kernohan KD, Tétreault M, Liwak-Muir U, Geraghty MT, Qin W, Venkateswaran S, et al. Homozygous mutation in the eukaryotic translation initiation factor 2alpha phosphatase gene, PPP1R15B, is associated with severe microcephaly, short stature and intellectual disability. Hum Mol Genet. 2015 Nov 15;24(22):6293–300.

46. Lenaerts L, Reynhout S, Verbinnen I, Laumonnier F, Toutain A, Bonnet-Brilhault F, et al. The broad phenotypic spectrum of PPP2R1A-related neurodevelopmental disorders correlates with the degree of biochemical dysfunction. Genet Med. 2021 Feb;23(2):352–62.

47. Melas M, Mathew MT, Mori M, Jayaraman V, Wilson SA, Martin C, et al. Somatic variation as an incidental finding in the pediatric next-generation sequencing era. Cold Spring Harb Mol Case Stud. 2021 Dec;7(6):a006135.

48. Liaci AM, Steigenberger B, Telles de Souza PC, Tamara S, Gröllers-Mulderij M, Ogrissek P, et al. Structure of the human signal peptidase complex reveals the determinants for signal peptide cleavage. Mol Cell. 2021 Oct 7;81(19):3934-3948.e11.

49. Ma L, Li F, Zhang JW, Li W, Zhao DM, Wang H, et al. Host Factor SPCS1 Regulates the Replication of Japanese Encephalitis Virus through Interactions with Transmembrane Domains of NS2B. J Virol. 2018 Jun 15;92(12):e00197-18.

50. Zhang R, Miner JJ, Gorman MJ, Rausch K, Ramage H, White JP, et al. A CRISPR screen defines a signal peptide processing pathway required by flaviviruses. Nature. 2016 Jul 7;535(7610):164–8.

51. Neufeldt CJ, Cortese M, Scaturro P, Cerikan B, Wideman JG, Tabata K, et al. ER-shaping atlastin proteins act as central hubs to promote flavivirus replication and virion assembly. Nat Microbiol. 2019 Dec;4(12):2416–29.

52. Tran PTH, Asghar N, Johansson M, Melik W. Roles of the Endogenous Lunapark Protein during Flavivirus Replication. Viruses. 2021 Jul;13(7):1198.

53. Hoffmann HH, Schneider WM, Rozen-Gagnon K, Miles LA, Schuster F, Razooky B, et al. TMEM41B Is a Pan-flavivirus Host Factor. Cell. 2021 Jan 7;184(1):133-148.e20.

54. Bizzoca A, Corsi P, Polizzi A, Pinto MF, Xenaki D, Furley AJW, et al. F3/Contactin acts as a modulator of neurogenesis during cerebral cortex development. Dev Biol. 2012 May 1;365(1):133–51.

55. Çolakoğlu G, Bergstrom-Tyrberg U, Berglund EO, Ranscht B. Contactin-1 regulates myelination and nodal/paranodal domain organization in the central nervous system. Proc Natl Acad Sci U S A. 2014 Jan 21;111(3):E394-403.

56. Michaelis AC, Brunner AD, Zwiebel M, Meier F, Strauss MT, Bludau I, et al. The social and structural architecture of the yeast protein interactome. Nature. 2023 Dec;624(7990):192–200.

57. Huttlin EL, Bruckner RJ, Navarrete-Perea J, Cannon JR, Baltier K, Gebreab F, et al. Dual proteome-scale networks reveal cell-specific remodeling of the human interactome. Cell. 2021 May 27;184(11):3022-3040.e28.

58. Go CD, Knight JDR, Rajasekharan A, Rathod B, Hesketh GG, Abe KT, et al. A proximity-dependent biotinylation map of a human cell. Nature. 2021 Jul;595(7865):120–4.

59. Hein MY, Hubner NC, Poser I, Cox J, Nagaraj N, Toyoda Y, et al. A Human Interactome in Three Quantitative Dimensions Organized by Stoichiometries and Abundances. Cell. 2015 Oct 22;163(3):712–23.

60. Antonicka H, Lin ZY, Janer A, Aaltonen MJ, Weraarpachai W, Gingras AC, et al. A High-Density Human Mitochondrial Proximity Interaction Network. Cell Metab. 2020 Sep 1;32(3):479-497.e9.

61. Bagci H, Sriskandarajah N, Robert A, Boulais J, Elkholi IE, Tran V, et al. Mapping the proximity interaction network of the Rho-family GTPases reveals signalling pathways and regulatory mechanisms. Nat Cell Biol. 2020 Jan;22(1):120–34.

62. Shah PS, Link N, Jang GM, Sharp PP, Zhu T, Swaney DL, et al. Comparative Flavivirus-Host Protein Interaction Mapping Reveals Mechanisms of Dengue and Zika Virus Pathogenesis. Cell. 2018 13;175(7):1931-1945.e18.

63. Coyaud E, Ranadheera C, Cheng D, Gonçalves J, Dyakov BJA, Laurent EMN, et al. Global Interactomics Uncovers Extensive Organellar Targeting by Zika Virus. Mol Cell Proteomics. 2018;17(11):2242–55.

64. Scaturro P, Stukalov A, Haas DA, Cortese M, Draganova K, Płaszczyca A, et al. An orthogonal proteomic survey uncovers novel Zika virus host factors. Nature. 2018 Sep;561(7722):253–7.

65. Golubeva VA, Nepomuceno TC, Gregoriis G de, Mesquita RD, Li X, Dash S, et al. Network of Interactions between ZIKA Virus Non-Structural Proteins and Human Host Proteins. Cells. 2020 Jan 8;9(1):E153.

66. Zeng J, Dong S, Luo Z, Xie X, Fu B, Li P, et al. The Zika Virus Capsid Disrupts Corticogenesis by Suppressing Dicer Activity and miRNA Biogenesis. Cell Stem Cell. 2020 Oct 1;27(4):618-632.e9.

67. Denolly S, Stukalov A, Barayeu U, Rosinski AN, Kritsiligkou P, Joecks S, et al. Zika virus remodelled ER membranes contain proviral factors involved in redox and methylation pathways. Nat Commun. 2023 Dec 5;14(1):8045.

68. Gu X, Ma Y, Liu Y, Wan Q. Measurement of mitochondrial respiration in adherent cells by Seahorse XF96 Cell Mito Stress Test. STAR Protocols. 2021 Mar 19;2(1):100245.

69. Hetz C, Zhang K, Kaufman RJ. Mechanisms, regulation and functions of the unfolded protein response. Nat Rev Mol Cell Biol. 2020 Aug;21(8):421–38.

70. Wu J, Rutkowski DT, Dubois M, Swathirajan J, Saunders T, Wang J, et al. ATF6α Optimizes Long-Term Endoplasmic Reticulum Function to Protect Cells from Chronic Stress. Developmental Cell. 2007 Sep 4;13(3):351–64.

71. Shoulders MD, Ryno LM, Genereux JC, Moresco JJ, Tu PG, Wu C, et al. Stress-Independent Activation of XBP1s and/or ATF6 Reveals Three Functionally Diverse ER Proteostasis Environments. Cell Reports. 2013 Apr 25;3(4):1279–92.

Chapter 7: Ongoing experimental goals and final conclusions.

Introduction

In previous Chapters we have explored the interaction between ZIKV NS4A and host ANKLE2 using a variety of approaches and techniques. This has led to the developed projects with interpretable findings and conclusions presented in the previous three Chapters. However, we have also explored other questions that are still in earlier stages of execution and designed projects that are still in development. In this final Chapter we will briefly introduce these preliminary studies as a platform for highlighting the various future experiments and inquiries regarding, ANKLE2, NS4A, ZIKV, and the birth defects arising from them all.

Ongoing Projects

Comparative proteomics of naturally occurring, pathogenic ANKLE2 variants

As discussed in Chapter 3, pathogenic mutations in *ANKLE2* are now well known for their association with congenital primary microcephaly in humans (Figure 3-4). In the previous Chapter we performed proteomic analysis on wild-type ANKLE2 after ZIKV infection to determine what interactions may be perturbed to cause abnormal neurodevelopment during CZS. We hypothesize that these pathways are the same that are perturbed during natural *ANKLE2*-related congenital microcephaly and that different pathogenic ANKLE2 mutants will have similar disruption of key developmental pathways. To test this, we have cloned six ANKLE2 pathogenic variants (A109P, G201W, V229G, R236X, R536C, and Q782X) with C-terminal 3xFLAG affinity tags into expression vectors so we can determine their interactions using a proteomics approach similar to what we used in Chapter 6 (Figure 7-1). We expect the two nonsense mutants, R236X and Q782X, to have the most differences from WT ANKLE2, due to the dramatic loss in protein content. A109P is an interesting mutation because it is the only known pathogenic mutation in the

LEM domain, and this amino acid substitution may significantly alter the structure or function of this region (Figure 3-4) (1). The G201W and V229G mutations are especially interesting because they are the only known pathogenic homozygous mutations, with G201W being identified in two separate patients (Appendix A-4) (2). Finally, R536C was identified in two separate patients, but each time as one of two alleles in compound heterozygous pairings (Appendix A-4) (3). This missense mutation to cysteine also provides the opportunity for dramatic changes in protein behavior arising from new disulfide bonds formed between cysteine residues (4). This combination of variants supplies a variety of nonsense and missense mutations throughout the ANKLE2 protein, which we hypothesize will yield an interesting array of interactions for which to compare against WT ANKLE2.

To further improve our proteomics experiment in this new exploration we also generated additional controls to account for the spatial differences between different organelles. GFP-3xF is still an ideal general control, due to its widespread localization, but additional controls to account for the compartments ANKLE2 resides in may give additional insight into the background present in these locations. We hope that identification and removal of this background will improve determination of true ANKLE2-interactors. To account for ER background, we generated a construct of GFP-3xF with an N-terminal C1 ER signal sequence from cytochrome P450 2C1, which is sufficient for ER retention (5). Since ANKLE2 also localizes to the inner nuclear membrane we generated a GFP-3xF fusion with a C-terminal nuclear localization signal (NLS) with a linker and transmembrane domain, however expression of this construct requires further optimization (Figure 7-1).

The protein-protein interactions detected between our variants and other host proteins will be detected using the same techniques applied in Chapter 6. After background removal and scoring these interactions can be compared at the pathway level to WT ANKLE2 to identify disrupted biological processes.

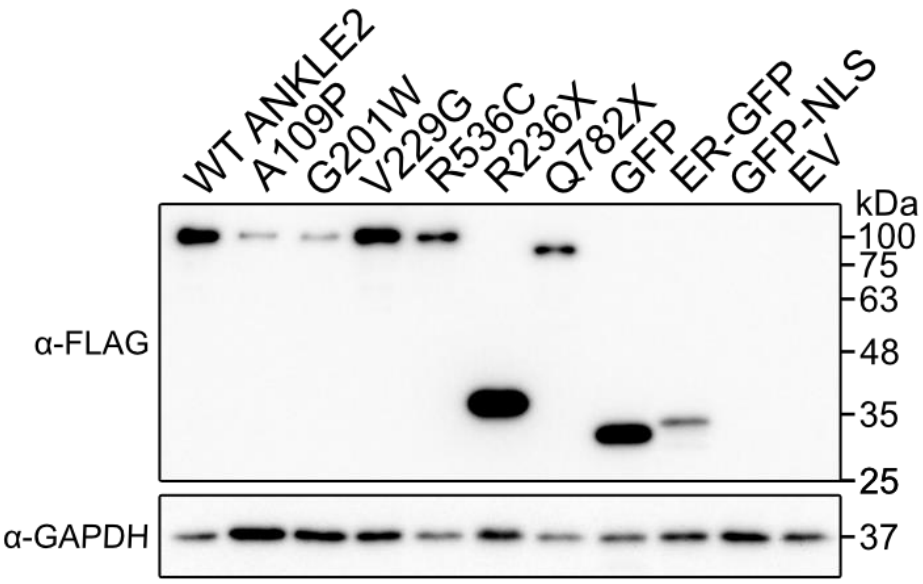

Figure 7-1: Expression of pathogenic ANKLE2 variants for proteomic studies. HEK293T cells were transfected with expression vectors containing pathogenic variants of ANKLE2 or GFP controls. Relative expression and size of each protein was confirmed by western blot.

Potential for the ANKLE2 interaction with NS4A from tick-borne orthoflaviviruses

In Chapter 4 we established that ANKLE2 supports replication for ZIKV and DENV and is capable of physically interacting with NS4A from other mosquito-borne orthoflaviviruses (YFV and JEV) (Figure 4-11). To determine if this physical interaction was conserved beyond mosquito-borne orthoflaviviruses into those transmitted by tick, we cloned NS4A from tick-borne encephalitis virus (TBEV) and Powassan virus (POWV) into the same plasmid backbone we used previously. Using a similar co-transfection and affinity-purification strategy were able to show that ANKLE2 can interact with these NS4A as well (Figure 7-2). Due to serious health risks both of these viruses have high biosecurity ratings and require BSL-3 containment to study. However, Langat virus, within the TBEV complex of viruses, only requires BSL-2 and is not known to cause human disease (6), potentially allowing for future evaluation of a role for ANKLE2 in tick-borne orthoflavivirus replication. These tick-borne viruses are much less studied than their mosquito-

borne counterparts but in general they are believed to generally replicate with similar mechanisms, albeit slower (7). Exploring if ANKLE2 is involved in the replication of tick-borne orthoflaviviruses will be important to determine how far reaching a potential beneficial role in replication may be. Certainly, pan-flavivirus host factors exist, such as TMEM41B (8), while other host factors only promote replication of viruses transmitted by specific host species (9).

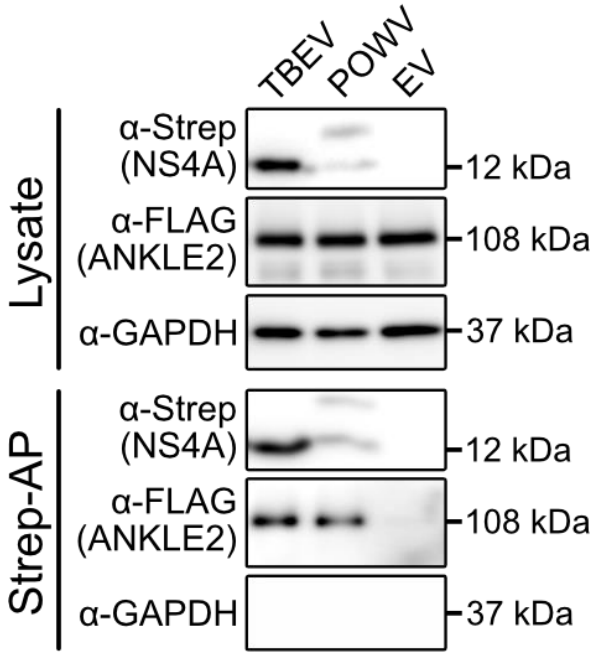

Figure 7-2: Interaction between ANKLE2 and tick-borne orthoflavivirus NS4A. HEK293T cells were co-transfected with ANKLE2-3xFLAG and NS4A-2xStrep from TBEV or POWV. After transfection, cell lysate was collected and purified on Strep-binding beads. Whole cell lysate and affinity-purified eluate were examined for the presence of ANKLE2 and NS4A by western blot.

Animal models to explore role of ANKLE2 in ZIKV pathogenesis

The natural progression of this work is to transition our *in vitro* findings into *in vivo* animal models where the results can be more closely related to human biology and disease. Mice are commonly used for the study of orthoflavivirus replication, pathogenesis, and transmission, as well as the

development of antiviral therapies or vaccines against these viruses (10–12). Mouse ANKLE2 (mANKLE2) has a similar structural organization to that of human ANKLE2 (Figure 3-1, Figure 7-3A), but it was unclear if it could interact with ZIKV NS4A. To test this, we cloned mouse Ankle2 with a 3xFLAG affinity tag into an expression vector and co-transfected it along with ZIKV NS4A-2xStrep, as done previously in Chapter 5. Affinity purification revealed that mANKLE2 could indeed physically interact with ZIKV NS4A (Figure 7-3B). Further, confocal microscopy of transfected HeLa cells revealed similar colocalization between human and mANKLE2 with the ER marker Calnexin, supporting it retains the expected ER localization (Figure 7-3C). Microscopy of ZIKV infected cells also reveals high colocalization between mANKLE2 and NS4A, supporting it may be utilized in replication similar to human ANKLE2 (Figure 7-3D). These results provide important biochemical validation that mANKLE2 can interact with ZIKV NS4A and behaves in a similar manner as human ANKLE2, providing support that mice will serve as a good model for further study of the NS4A-mANKLE2 interaction *in vivo*.

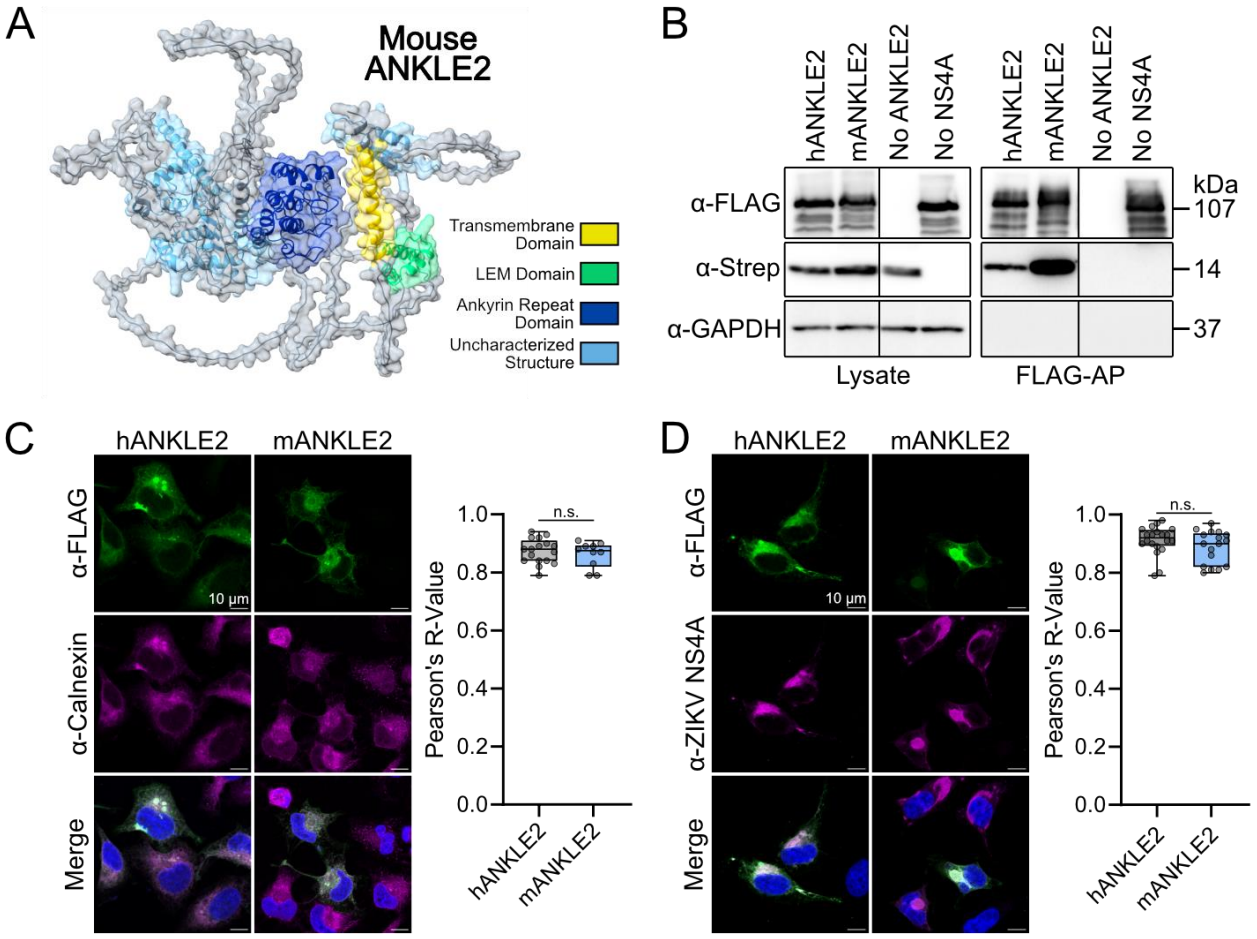

Figure 7-3: Structure of mANKLE2 and physical interaction with ZIKV NS4A. (A) AlphaFold2 structural prediction of mANKLE2 (UniProt ID Q6P1H6) with domains annotated by color (13,14). (B) HEK293T cells were co-transfected with human ANKLE2-3xFLAG (hANKLE2) or mouse ANKLE2-3xFLAG (mANKLE2) with ZIKV NS4A-2xStrep. After transfection, whole cell lysate was affinity-purified on FLAG binding beads. Physical interaction was determined by evaluating the eluate for the presence of ZIKV NS4A. “No NS4A” condition includes hANKLE2. (C) Confocal microscopy of HeLa cells transfected with either hANKLE2 or mANKLE2. After transfection, cells were fixed and immunostained for FLAG and the ER-marker Calnexin. Pearson’s correlation was quantified to determine colocalization. (D) HeLa cells were similarly transfected, and then infected with ZIKV MR766 at MOI 5 for 24 hours, prior to fixation and immunostaining for FLAG and ZIKV

NS4A. Dots represent values from individual cells, n = 10-20 cells per condition, Student's unpaired t-test, n.s. = not significant.

To examine potential impacts of *Ankle2* on ZIKV replication and pathogenesis *in vivo* we sought to perform experiments in *Ankle2* deficient mice. Unfortunately, *Ankle2* null mice (*Ankle2*$^{-/-}$) are non-viable and are resorbed during development. While this is currently anecdotal and unpublished, this observation has been recapitulated in our hands, given that our crosses of *Ankle2*$^{+/-}$ heterozygous mice have never yielded an *Ankle2*$^{-/-}$ offspring. Therefore, we performed experiments in heterozygous mice to test if any depletion, even minor, influenced ZIKV replication. We generated *Ankle2*$^{+/-}$;*Ifnar1*$^{-/-}$ mice and infected them with 1000 PFU of ZIKV PRVABC59 via subcutaneous footpad injection at ~7 weeks old. This route of inoculation most closely resembles a natural mosquito bite into the skin. These infections are done in an immunodeficient Ifnar1$^{-/-}$ background in order for ZIKV to induce pathogenesis (15), which does not readily occur in immunocompetent mice. Infection was allowed to progress for 5 days, in which no significant differences in weight were observed between *Ankle2*$^{+/}$;*Ifnar1*$^{-/-}$ and our *Ankle2*$^{+/+}$;*Ifnar1*$^{-/-}$ control mice (Figure 7-4A). We then performed necropsy and harvested serum, brain, spleen, eyes, and gonads from all infected mice. We observed no significant differences in viral titer in the serum, brain, spleen, or eyes (Figure 7-4B-E). We observed sex differences in ZIKV titer in the gonads, with the male testes having higher ZIKV burden than female ovaries (Figure 7-4F), but we did not observe a meaningful difference between *Ankle2* genotypes. This is supported by established observation of persistent ZIKV infection in the testes (16). We hypothesized the lack of phenotype in these experiments could be due to incomplete depletion of ANKLE2 in heterozygous mice, which was explored by western blot (Figure 7-4G-H). This experiment revealed seemingly variable expression of ANKLE2 between different tissues. The brain appeared to have the highest expression levels, with no difference between genotypes, while the spleen had no detectable

signal in either genotype. The eyes of the heterozygous mouse did have less than the wild-type, however only a lower molecular weight band was expressed, and both observed bands appeared lower than the expected size of 106 kDa. In a wild-type mouse testes we observed low expression of a band at the expected size. These preliminary results suggest either variable expression of mouse ANKLE2 isoforms or inadequate detection by our antibody designed against human ANKLE2.

Overall, this experiment is limited by the scale, both in the number of mice used and in the length of the infection. Additionally, data suggests that ZIKV PRVABC59 is less pathogenic in this model than other Asian lineage strains FSS13025 or H/PF/2013 (17,18). Additional experiments using these strains and a longer course of infection may improve our ability to identify a difference between *Ankle*$^{+/+}$ and *Ankle*$^{+/-}$ mice. One future option may also be the generation of conditional knockouts, which may produce viable *Ankle2*$^{-/-}$ offspring for use in experimentation, although this is time-consuming and technically difficult (19), thus this option remains outside our current project scope.

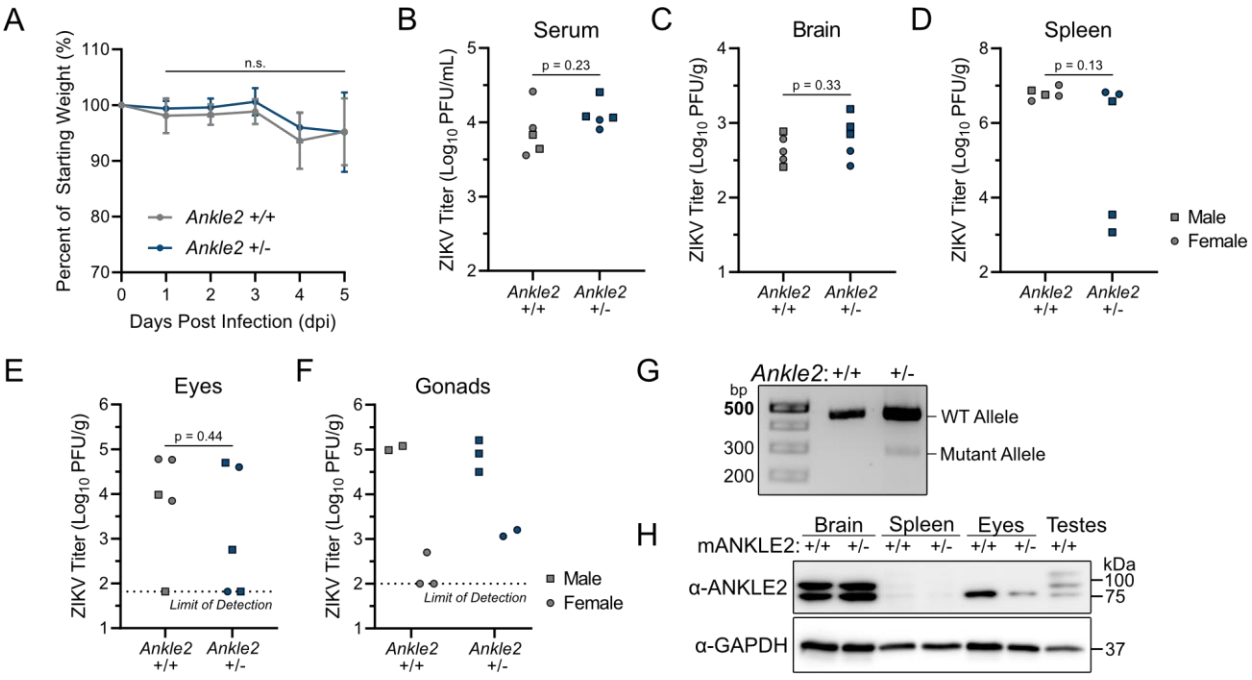

Figure 7-4: Initial evaluation of ZIKV PRVABC59 replication in wild-type and *Ankle2*$^{+/-}$ mice. ~7-week-old C57BL/6 mice (mix of male/female and Ifnar1$^{-/-}$, *Ankle2*$^{+/-}$ or $^{+/+}$) were infected with 1000 PFU of ZIKV PRVABC59 via footpad intradermal injection. (A) Mice were weighed prior to infection (dpi = 0) and every 24 hours for 5 days. (B-F) Serum and tissues were harvested from infected mice and homogenized. Viral titer in homogenate was determined by plaque assay. (G) Representative *Ankle2* genotyping by PCR. (H) Attempted western blot probing for mouse ANKLE2 using human ANKLE2 antibody (SAB3500750) with expected reactivity against the mouse homolog. Two bands appeared at lower size than expected for mouse ANKLE2 (106.2 kDa). Student's two-tailed T-test, unpaired, n.s. = not significant ($p > 0.05$).

Animal models to explore genetic predisposition to adverse congenital ZIKV syndrome outcomes

While the inability to easily perform experiments on *Ankle2*$^{-/-}$ mice certainly limits our ability to explore the role of *Ankle2* in ZIKV pathogenesis and vertebrate brain development, we can still leverage *Ankle2*$^{+/-}$ animals to explore other interesting questions. As discussed earlier, in heterozygous *dAnkle2*^{A} flies, brain development occurs normally (20). However, when NS4A was expressed in these flies, the phenotypes were much more severe and required growth at lower temperatures to allow survival until the third instar larval stage for brain dissection. This phenomenon suggests that *dAnkle2*^{A} heterozygosity sensitized animals to a more severe NS4A outcome. The major question remains if this can be recapitulated in a vertebrate *ANKLE2* heterozygote with more complex brain development. Beyond this lies the larger question of whether this haploinsufficiency is *ANKLE2* specific or does heterozygosity of any number of genes underlie variable disease outcomes. This hypothesis could serve to explain the apparent multitude in disease outcomes from CZS and many other diseases.

To test this hypothesis, we will aim to determine if *Ankle2* heterozygosity results in worse fetal outcomes from vertically transmitted ZIKV. In this proposed experiment we will mate immunodeficient *Ankle2*$^{+/+}$, *Ifnar1*$^{-/-}$ or *Ankle2*$^{+/-}$, *Ifnar*1$^{-/-}$ female mice (dams) with immunocompetent wild-type male mice (sires). Mating with an immunocompetent sire allows for ZIKV to replicate effectively in the pregnant immunodeficient dam, while limiting pathogenesis in the pups themselves, so that only pathology arising from differences in *Ankle2* is observed. ZIKV infection at E7 or E9 has been shown to induce fetal pathology in the pups in the form of embryo resorption or intrauterine growth restriction (IUGR) (17). Embryonic resorption occurs when the embryo experiences significant development abnormalities or dies during development, with the remnants being resorbed by the maternal immune cells (21). In mice, the resorbed embryos are retained within the placenta and can be counted during necropsy along with any remaining, viable embryos. The rate of resorption after ZIKV heavily depends on gestational timing (22) and can be a relatively rare outcome after infection at E9 (17). IUGR arises from ineffective or inefficient development, resulting in overall growth restrictions, and is also observed after ZIKV in varying frequencies. Microcephaly, by the true definition of reduced head and brain size, is not a feasible experimental readout for this model since the fetal heads are so small and measuring brain size itself would be prone to inaccuracies. Instead, the virus burden within the entire fetal head can be determined, along with relative fetal weight and size of the fetus by crown-rump length (17). Histological analysis of viable embryo brains is also a powerful experimental tool to gain insight into the architecture of the developing brain and the specific cell types present. If our hypothesis is correct, then significantly more embryos from *Ankle2*$^{+/-}$ dams will exhibit these abnormal developmental phenotypes than embryos from *Ankle2*$^{+/+}$ dams. If successful, this approach could serve as a powerful model system for exploring the impact of other genes on sensitizing adverse developmental outcomes from ZIKV.

Final Conclusions and Discussion

ZIKV is an orthoflavivirus that recently emerged as a global health threat due to the risk of birth defects, including microcephaly, associated with congenital infection. Exploration into the mechanisms driving ZIKV neuropathogenesis revealed the physical interaction between ZIKV NS4A and host ANKLE2, a protein involved in cell division and mutation which also causes congenital microcephaly. Early experiments showed that NS4A induces a small brain, microcephaly-like phenotype, in larval fruit flies in an ANKLE2 dependent manner, suggesting that ZIKV NS4A induces this phenotype by perturbing ANKLE2. The work presented here initially summarized and reviewed how orthoflaviviruses hijack their hosts to facilitate replication and cause disease (Chapter 2), and the roles of ANKLE2 in cellular functions and how dysregulation of these functions causes human disease (Chapter 3).

One of the major questions we explored was if ANKLE2 played a role in ZIKV replication, and if this function could explain why ZIKV interacts with it in the first place? In Chapter 4 we showed that ANKLE2 colocalizes with sites of ZIKV protein and around sites of dsRNA suggesting ANKLE2 may be involved during replication (Figures 4-1 and 4-2). Next, genetic depletion of ANKLE2 by knockdown or knockout showed reduced ZIKV replication in several different cell types and conditions (Figures 4-3, 4-4, and 4-9). Electron microscopy revealed that ZIKV replication organelles were fewer and appeared less developed in ANKLE2 knockout cells compared to controls, suggesting that ANKLE2 may function in ER remodeling or the formation of these virus-induced structures (Figure 4-8). Depletion of the ANKLE2 ortholog in mosquito cells by dsRNA also showed consistent reduction in ZIKV replication, supporting the hypothesis that ANKLE2 is utilized by ZIKV across hosts (Figure 4-10). Finally, we showed that NS4A from other mosquito borne orthoflaviviruses (DENV, YFV, and WNV) can also physically interact with ANKLE2, and while WNV replication was altered to a relevant degree, DENV replication was

significantly reduced (Figure 4-11). This raises the potential for ANKLE2 to being a beneficial host factor across different orthoflaviviruses.

The degree to which ANKLE2 enhances replication appears to vary on cell type and virus and is an alluring future line of investigation. Further, the specific molecular mechanisms by ANKLE2 supports replication are very interesting. Determining what specific regions of ANKLE2 are required to provide this benefit may provide initial evidence for this function. Specifically, if ANKLE2 knockout cells are rescued with various truncation mutants of ANKLE2 can restore virus replication phenotypes. For example, if ANKLE2 without an ankyrin repeat domain does not rescue the ZIKV phenotype, it may imply that the function provided by this domain is utilized in supporting virus replication. This line of experimentation would certainly require a more optimized rescue system than currently developed (Figure 4-6). These results provide initial support for the hypothesis that ZIKV NS4A interacts with ANKLE2 to facilitate this beneficial function. However, whether the beneficial role of ANKLE2 in orthoflavivirus replication is dependent on interaction with NS4A is still uncertain.

We explored the physical determinants of this interaction in Chapter 5. We found that C-terminal truncations of ANKLE2 did not alter the ability to interact with NS4A (Figure 5-1). Alternatively, an N-terminal deletion of amino acids 2-157 did ablate interaction with NS4A (Figure 5-2). This region makes logical sense as it is set within and proximal to the ER membrane where NS4A resides. The fact that truncations of 1-53 and 54-938 also interact with NS4A further suggests that there are multiple contact sites between ANKLE2 and NS4A, at least one in the transmembrane domain region and at least one in the LEM domain or surrounding region. Using truncations of NS4A we showed that the C-terminal region of NS4A is required for the interaction (Figure 5-4). This alone does not deny the possibility of interacting residues in the N-terminal portions, and investigating this region is complicated due to the apparent difficulty in expressing these regions alone. The cytoplasmic region of NS4A (1-56) has inconsistent expression levels and appears to induce high

toxicity in transfected cells (not shown). Both the low expression and toxicity may be due to misfolding of the truncated protein. These effects were also observed in early trials of other N-terminal NS4A truncations (not shown). Together, our experiments revealed that C-terminal regions of NS4A interact with N-terminal portions of ANKLE2.

Much is still left to do in determining the specific physical determinants of this interaction at the residue level. Initial trials attempted to disrupt the interaction by targeting the conserved amino acids in the C-terminal portion of NS4A between 121-127, due to the high degree of conservation in this region (Figure 5-5), however these substitution of these residues to alanine did not appear to change their ability to interact with ANKLE2 (not shown). The standard alanine scanning approach is likely ineffective in resolving the interacting residues, due to observation that multiple different domains interact and disruption of both is required to ablate interaction. Systemically performing alanine scanning on many different residues in different regions would be experimentally exhaustive and inefficient. However, it is still important to explore this. Therefore, we have begun developing alternative strategies to determine which residues are likely mediating the interaction. Using molecular dynamics simulation (23), we have begun to explore ANKLE2's structure beyond its AlphaFold prediction shown earlier (Figure 3-1). While not shown here, this structure resembles a more realistic and compact orientation of the protein. With this we have used molecular docking to simulate the physical interaction between NS4A and ANKLE2 (24). After allowing the two proteins to interact and stabilize *in silico* we can examine the amino acid residues in contact between the two proteins. Indeed, this approach has revealed compelling candidate residues in both NS4A and ANKLE2 that could facilitate the interaction, however experimentally exploring this *in vitro* is still underway.

Determining the specific interacting residues is powerful in two contexts, one for each protein. If the specific NS4A residues can be broken, then an infectious clone of the virus harboring that mutation can be created. Whether that mutant virus can be rescued and is capable of replicating

in cells is highly dependent on which residues are changed and what mutations are required. Indeed, substitutions to amino acids other than alanine may be able to ablate interaction while being less detrimental to the function of NS4A in virus replication. To identify the spectrum of flexibility in the amino acids of NS4A we have collaborated with Matthew Evan's group to perform deep mutational scanning (DMS) of ZIKV MR766 NS4A. This approach employs the use of a library of infectious clones with the residues of a given protein substituted for every other amino acid so that every possible change is present in the population. Cells are infected with this library of viruses and after allowing several rounds of infection to occur the remaining viruses are sequenced. The ratio of the final abundance of each specific virus (each containing a specific residue mutation) is compared to the starting amount to determine if the virus was successful in replicating or not. This is interpreted as fitness advantage or disadvantage provided by the specific mutation present in that virus (25). In our case we would use the DMS data as a guide when designing mutations in NS4A that ablate the interaction with ANKLE2, while maintaining the overall replicative ability of the virus. If successful, this would be an extremely alluring and powerful tool in investing the contribution of the NS4A-ANKLE2 interaction to CZS. We would hypothesize that ZIKV which encodes an NS4A that does not interact with ANKLE2 to have reduced developmental neuropathogenesis, and this could be experimentally tested using the vertical transmission mouse model described earlier.

The second application of fully understanding the residues which mediate the NS4A-ANKLE2 interaction is related to potentially protective *ANKLE2* alleles. Protective alleles occur when proteins are mutated in such a way that prevents disease, usually through some loss-of-function mutation (26). In this hypothetical case, if the interaction mediating residues of ANKLE2 were known, human genetic data could be scoured for randomly occurring missense mutations in those sites that may maintain proper ANKLE2 cellular function, while losing the interaction with NS4A, and potentially protecting from CZS.

As introduced in Chapter 3, the ER localization of ANKLE2 is a distinguishing feature compared to other LEM-domain proteins. The role of ANKLE2 in ER-based ZIKV replication certainly suggests some function in this cellular compartment. Our proteomics in Chapter 6 revealed hundreds of candidate protein interactions, which will serve as the base for future exploration into what additional functions ANKLE2 has in the cell. Further, how these functions are hijacked by ZIKV to promote virus replication is especially interesting, given the conserved nature of the interaction between NS4A and ANKLE2. While there is certainly much more work to be done on ANKLE2 and its relationships with virus replication and disease, the future is bright and ripe with opportunities for exciting new findings.

Materials and Methods

Plasmids. ANKLE2 variant sequences were made by taking the wild-type sequence (NM_015114.3), performing human codon optimization, and then making the desired amino acid substitution. Fragments with C-terminal 3xFLAG tags were synthesized by Twist Biosciences in two parts and inserted into pcDNA4_TO cut with KpnI and ApaI using Gibson Assembly. NS4A sequence from TBEV (strain Sofjin, JX498940.1) and POWV (strain LB, L06436.1) was human codon optimized. The sequence was synthesized by Twist Biosciences and cloned into pcDNA4_TO cut with BamHI and EcoRI upstream of the 2xStrep tag as done previously. Mouse Ankle2 (NM_001253814.1) was human codon optimized and synthesized with a C-terminal 3xFLAG tag. It was cloned into pcDNA4_TO cut with KpnI and ApaI using Gibson Assembly.

Strep-Affinity Purification. Affinity purification was performed on TBEV and POWV NS4A by co-transfecting ANKLE2-3xF and NS4A-2xS plasmids in equal amounts (3.5 µg each). Cell lysate was harvested and purified on Streptactin beads as previously described in Chapter 5.

Western Blot. Western blot was performed as previously described in Chapter 4.

Confocal Microscopy. HeLa cells were plated on cover slips and transfected with human or mouse ANKLE2 and then mock-infected or infected with ZIKV. Cover slips were prepared and imaged as previously described in Chapter 4.

Mouse Husbandry. C57BL/6 (Jackson Labs) were housed with similar sexes (unless breeding) (1-5 per cage) in ventilated isolation cages and fed standard rodent diet and autoclaved tap water *ad libitum*. Vivarium was set to a 12:12 hour light:dark cycle with an ambient temperature of 22-27°C with 20-30% relative humidity. Breeding pairs were setup with one male with one or two females. After 10-14 days, haram breeding females were separated from each other to allow for separate litters. Between the age of 10-14 days litter pups were uniquely identified by ear clipping and tail tissue was collected for genotyping. Pups were weaned at 20-23 days old. All animal procedures were conducted under the accordance of the University of California Davis Institutional Animal Care and Use Committee (IACUC).

Mouse Genotyping. Tail tissue was collected from mice between the age of 10-14 days and placed in 250 µL lysis buffer (100 mM Tris, 5 mM EDTA, 0.2% SDS, 250 mM NaCl) supplemented with 6.25 µL of Proteinase K (NEB, #P8107S) overnight in a 55°C water bath. Tubes were centrifugated at ~17,000 g for 10 minutes. Supernatant was carefully transferred to a fresh tube and combined with 250 µL 100% isopropanol to precipitate genomic DNA. Tubes were centrifugated again. Supernatant was removed from the DNA pellet and allowed to ambiently dry for ~1 hour. Pellet was resuspended in 50 µL nuclease-free water and DNA was used for nested PCR using 2X MyTaq HS Red Mix (Thomas Scientific, #C755G96).

Mouse Infection and Evaluation of ZIKV Replication. 45- to 49-day-old mice (C57BL/6, Ifnar1$^{-/-}$, and either Ankle2$^{+/+}$ or Ankle2$^{+/-}$, n = 5 each) were transferred from the ABSL1 space to the ABSL2 space in the same cages and allowed to acclimate to the new environment for 2 days. In the ABSL2 space, mice were housed with similar sex (2-3 per cage) in ventilated isolation cages and fed 18% protein irradiated rodent diet and autoclaved tap water *ad libitum*. Vivarium was set to a 12:12 hour light:dark cycle with an ambient temperature of 22-27°C with 20-30% relative humidity. Mice were weighed and anesthetized with isoflurane (NDC 13985-528-60) in a bell jar system (2-5% saturation). They were then inoculated with 10^3 PFU of ZIKV PRVABC59 in 10 µL sterile D-PBS via footpad injection. Mice were returned to original housing after a recovery period. Body weight was measured daily and wellness checks were performed three times daily. Mice were monitored for hunched posture, decreased mobility, pilorection, weight loss >20% of starting, and overall conditioning. After 5 days of ZIKV infection, mice were euthanized by CO_2 exposure. Blood was collected from the heart and necropsy was performed to harvest spleen, brain, gonads (testes or ovaries), and eyes. Tissues were placed in 2 mL round bottom tubes with a 5 mm glass bead (Neta Scientific, WLMD-LG-6750-102) and weighed. DMEM media was then added to each tube and tissues were homogenized using a TissueLyser (Retsch MM400) at 30 Hz for 4 minutes. Tubes were then centrifugated at 12,000 g for 4 minutes and stored at -80°C.

Plaque Assay. Plaque assays were performed as previously described in Chapter 4.

References

1. Link N, Chung H, Jolly A, Withers M, Tepe B, Arenkiel BR, et al. Mutations in ANKLE2, a ZIKA Virus Target, Disrupt an Asymmetric Cell Division Pathway in *Drosophila* Neuroblasts to Cause Microcephaly. Dev Cell. 2019 Dec 16;51(6):713-729.e6.

2. Shaheen R, Maddirevula S, Ewida N, Alsahli S, Abdel-Salam GMH, Zaki MS, et al. Genomic and phenotypic delineation of congenital microcephaly. Genet Med. 2019;21(3):545–52.
3. Thomas AX, Link N, Robak LA, Demmler-Harrison G, Pao EC, Squire AE, et al. ANKLE2 - related microcephaly: A variable microcephaly syndrome resembling Zika infection. Ann Clin Transl Neurol. 2022 Jul 24;9(8):1276–88.
4. Wiedemann C, Kumar A, Lang A, Ohlenschläger O. Cysteines and Disulfide Bonds as Structure-Forming Units: Insights From Different Domains of Life and the Potential for Characterization by NMR. Front Chem. 2020 Apr 23;8:280.
5. Ahn K, Szczesna-Skorupa E, Kemper B. The amino-terminal 29 amino acids of cytochrome P450 2C1 are sufficient for retention in the endoplasmic reticulum. J Biol Chem. 1993 Sep 5;268(25):18726–33.
6. Gritsun TS, Lashkevich VA, Gould EA. Tick-borne encephalitis. Antiviral Res. 2003 Jan;57(1–2):129–46.
7. Beltz LA. Chapter 1 - Introduction to Flaviviruses. In: Beltz LA, editor. Zika and Other Neglected and Emerging Flaviviruses [Internet]. Elsevier; 2021. p. 1–18. Available from: https://www.sciencedirect.com/science/article/pii/B9780323825016000050
8. Hoffmann HH, Schneider WM, Rozen-Gagnon K, Miles LA, Schuster F, Razooky B, et al. TMEM41B Is a Pan-flavivirus Host Factor. Cell. 2021 Jan 7;184(1):133-148.e20.
9. Sun P, Nie K, Zhu Y, Liu Y, Wu P, Liu Z, et al. A mosquito salivary protein promotes flavivirus transmission by activation of autophagy. Nat Commun. 2020 Jan 14;11(1):260.
10. Chen RE, Diamond MS. Dengue mouse models for evaluating pathogenesis and countermeasures. Curr Opin Virol. 2020 Aug;43:50–8.
11. Alves dos Santos E, Fink K. Animal Models for Dengue and Zika Vaccine Development. In: Hilgenfeld R, Vasudevan SG, editors. Dengue and Zika: Control and Antiviral Treatment

Strategies. Singapore: Springer; 2018. p. 215–39. (Advances in Experimental Medicine and Biology).

12. Li QH, Kim K, Shresta S. Mouse models of Zika virus transplacental transmission. Antiviral Res. 2023 Feb;210:105500.

13. Varadi M, Anyango S, Deshpande M, Nair S, Natassia C, Yordanova G, et al. AlphaFold Protein Structure Database: massively expanding the structural coverage of protein-sequence space with high-accuracy models. Nucleic Acids Research. 2022 Jan 7;50(D1):D439–44.

14. Jumper J, Evans R, Pritzel A, Green T, Figurnov M, Ronneberger O, et al. Highly accurate protein structure prediction with AlphaFold. Nature. 2021 Aug;596(7873):583–9.

15. Lazear HM, Govero J, Smith AM, Platt DJ, Fernandez E, Miner JJ, et al. A Mouse Model of Zika Virus Pathogenesis. Cell Host & Microbe. 2016 May 11;19(5):720–30.

16. Julander JG, Siddharthan V. Small-Animal Models of Zika Virus. The Journal of Infectious Diseases. 2017 Dec 16;216(suppl_10):S919–27.

17. Casazza RL, Philip DT, Lazear HM. Interferon Lambda Signals in Maternal Tissues to Exert Protective and Pathogenic Effects in a Gestational Stage-Dependent Manner. mBio. 2022 Apr;13(3):e03857-21.

18. Carbaugh DL, Zhou S, Sanders W, Moorman NJ, Swanstrom R, Lazear HM. Two Genetic Differences between Closely Related Zika Virus Strains Determine Pathogenic Outcome in Mice. J Virol. 2020 Sep 29;94(20):e00618-20.

19. Pritchard CEJ, Kroese LJ, Huijbers IJ. Direct Generation of Conditional Alleles Using CRISPR/Cas9 in Mouse Zygotes. Methods Mol Biol. 2017;1642:21–35.

20. Shah PS, Link N, Jang GM, Sharp PP, Zhu T, Swaney DL, et al. Comparative Flavivirus-Host Protein Interaction Mapping Reveals Mechanisms of Dengue and Zika Virus Pathogenesis. Cell. 2018 13;175(7):1931-1945.e18.

21. Flores LE, Hildebrandt TB, Kühl AA, Drews B. Early detection and staging of spontaneous embryo resorption by ultrasound biomicroscopy in murine pregnancy. Reprod Biol Endocrinol. 2014 May 10;12:38.

22. Nakayama E, Kawai Y, Taniguchi S, Hazlewood JE, Shibasaki K ichi, Takahashi K, et al. Embryonic Stage of Congenital Zika Virus Infection Determines Fetal and Postnatal Outcomes in Mice. Viruses. 2021 Sep;13(9):1807.

23. Collier TA, Piggot TJ, Allison JR. Molecular Dynamics Simulation of Proteins. In: Gerrard JA, Domigan LJ, editors. Protein Nanotechnology: Protocols, Instrumentation, and Applications. New York, NY: Springer US; 2020. p. 311–27. (Methods in Molecular Biology).

24. Santos LHS, Ferreira RS, Caffarena ER. Integrating Molecular Docking and Molecular Dynamics Simulations. Methods Mol Biol. 2019;2053:13–34.

25. Sourisseau M, Lawrence DJP, Schwarz MC, Storrs CH, Veit EC, Bloom JD, et al. Deep Mutational Scanning Comprehensively Maps How Zika Envelope Protein Mutations Affect Viral Growth and Antibody Escape. J Virol. 2019 Dec 1;93(23):e01291-19.

26. Harper AR, Nayee S, Topol EJ. Protective alleles and modifier variants in human health and disease. Nat Rev Genet. 2015 Dec;16(12):689–701.

Appendix A:

Wild-Type ANKLE2 (NM_015114.3)

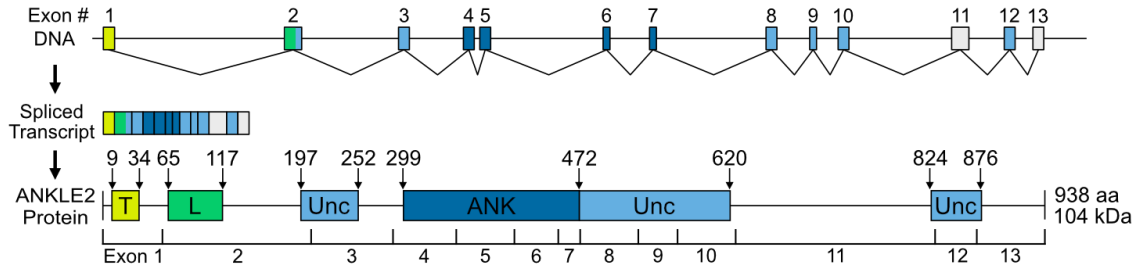

Isoform X1 (XM_005266159.4)

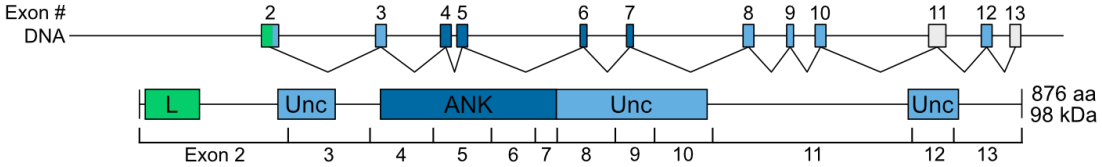

Isoform X2 (XM_006719735.2)

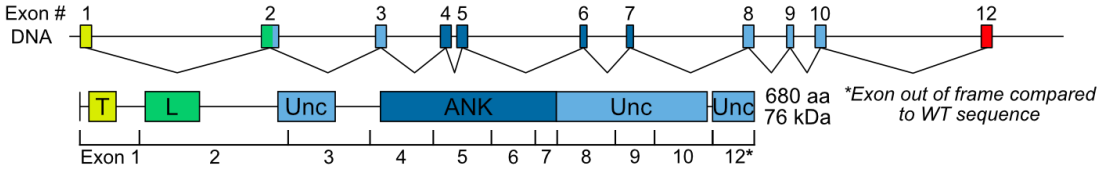

Isoform X3 (XM_011534788.2)

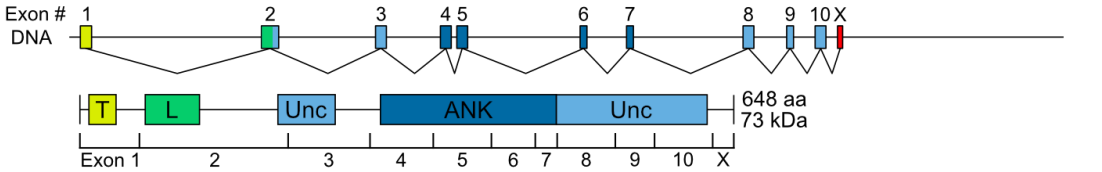

Isoform X4 (XM_047428585.1)

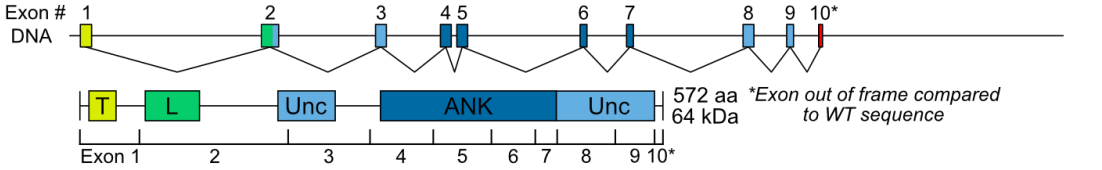

Isoform X5 (XM_024448899.2)

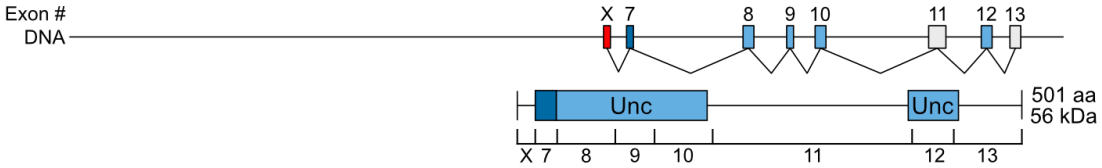

Isoform X6 (XM_047428586.1)

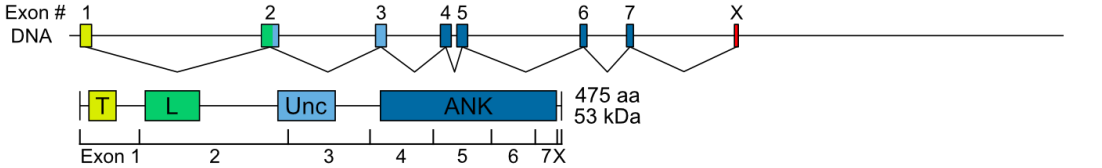

Appendix A-1: Known ANKLE2 isoforms. Sequence of human ANKLE2 isoforms were obtained from NCBI (Gene ID: 23141). Two separate transcript variants were identified for isoform X3 (XM_011534787.4 and XM_011534788.2 both produce XP_011533089.1), but only the latter is shown for simplicity.

Appendix A-2: List of Known Primary Microcephaly (MCPH) Genes

Primary Gene Name	Alternative Gene Name	Cellular Function	First Publication(s) Establishing Association with Microcephaly
MCPH1	N/A	Chromosome condensation and DNA damage responses	Jackson et al., 2002, *American Journal of Human Genetics*
WDR62	MCPH2	Centriole duplication	Roberts et al., 1999, *European Journal of Human Genetics*
CDK5RAP2	MCPH3	Mitotic checkpoint and centrosome regulation	Moynihan et al., 2000, *American Journal of Human Genetics*
KNL1	MCPH4	Kinetochore scaffold	Jamieson et al., 1999, *American Journal of Human Genetics*
ASPM	MCPH5	Microtubule regulation at spindle poles	Pattison et al., 2000, *American Journal of Human Genetics*
CENPJ	MCPH6	Centriole duplication	Leal et al., 2003, *Journal of Medical Genetics*
STIL	MCPH7	Regulation of centriole duplication	Kumar et al., 2009, *American Journal of Human Genetics*
CEP135	MCPH8	Centriole biogenesis	Hussain et al., 2012, *American Journal of Human Genetics*
CEP152	MCPH9	Centrosome scaffold	Guernsey et al., 2010, *American Journal of Human Genetics*
ZNF335	MCPH10	Transcription factor, component of histone methyltransferase complexes	Yang et al., 2012, *Cell*
PHC1	MCPH11	Transcriptional regulation through development	Awad et al., 2013, *Human Molecular Genetics*
CDK6	MCPH12	Cell cycle control and differentiation	Hussain et al., 2013, *Human Molecular Genetics*
CENPE	MCPH13	Kinetochore motor, chromosome congression	Mirzaa et al., 2014, *Human Genetics*
SASS6	MCPH14	Centriole scaffolding	Khan et al., 2014, *Human Molecular Genetics*
MFSD2A	MCPH15	Sodium-dependent lysophosphatidylcholine symporter, involved in blood-brain barrier formation and function	Alakbarzade et al., 2015, *Nature Genetics* Guemez-Gamboa et al., 2015, *Nature Genetics*
ANKLE2	MCPH16	Nuclear envelope dynamics	*Yamamoto et al., 2014, Cell*
CIT	MCPH17	Regulation of cytokinesis	Li et al., 2016, *American Journal of Human Genetics* Harding et al., 2016, *American Journal of Human Genetics*
WDFY3	MCPH18	Selective macroautophagy	Kadir et al., 2016, *PLoS Genetics*
COPB2	MCPH19	Golgi budding and vesicular trafficking	DiStasio et al., 2017, *Human Molecular Genetics*
KIF14	MCPH20	Microtubule motor protein	Moawia et al., 2017, *Annals of Neurology*
NCAPD2	MCPH21	Regulatory subunit of condensin complex	Martin et al., 2016, *Genes and Development*
NCAPD3	MCPH22	Regulatory subunit of condensin-2 complex	Martin et al., 2016, *Genes and Development*

NCAPH	MCPH23	Regulatory subunit of condensin complex	Martin et al., 2016, *Genes and Development*
NUP37	MCPH24	Component of nuclear pore complex	Braun et al., 2018, *Journal of Clinical Investigation*
TRAPPC14	MCPH25	Subunit of vesicle tethering complex	Perez et al., 2019, *Brain*
LMNB1	MCPH26	Component of nuclear lamina	Cristofoli et al., 2020, *American Journal of Human Genetics*
LMNB2	MCPH27	Component of nuclear lamina	Parry et al., 2021, *Genetics in Medicine*
RRP7A	MCPH28	rRNA processing in nucleoli	Farooq et al., 2020, *Nature Communications*
PDCD6IP	MCPH29	Endocytosis, membrane repair, cytokinesis, apoptosis, etc.	Khan et al., 2020, *Clinical Genetics*
BUB1	MCPH30	Mitotic checkpoint control	Carvalhal et al., 2022, *Science Advances*

Appendix A-3: Chapter 3 Glossary

Term	Description
Affinity-purification and mass-spectrometry	In Shah et al., 2018, individual ZIKV proteins with C-terminal Strep affinity tags were expressed in HEK293T cells by transfection. Cell lysate is harvested and applied to Strep-binding beads which purifies the ZIKV protein and any physically interacting proteins. The beads are washed, and bound proteins are eluted, processed, and submitted for mass-spectrometry analysis which identifies and quantifies the proteins in the sample.
cGAS/STING-mediated apoptosis	Cytosolic DNA is sensed by cGAS, resulting in transcriptional expression of cGAS-STING induced interferons which enhance apoptosis progression (Xu et al., 2023).
DN4 thymocyte	In the initial stages of T cell development within the thymus, precursor cells exhibit no expression of CD4 and CD8 and are denoted as double negative (DN) thymocytes. There are four early differentiation stages (DN1-4). DN4 thymocytes are the last stage of development before functional maturation is completed.
Forward mosaic genetic screen	In Yamamoto et al., 2014, adult male *Drosophila* were mutagenized with ethyl methane-sulfonate. This results in stocks harboring random mutations which were then screened for various visual phenotypes. Flies with interesting phenotypes were then sequenced to identify the mutated gene underlying the phenotype.
Glutathione S-transferase (GST) pulldown	A common biochemical technique to determine physical protein-protein interactions. A GST-fusion bait protein is expressed and bound to a glutathione sepharose matrix. Cell lysate is incubated on the matrix and proteins that interact with the bait are retained. These proteins are later eluted and can be detected by a number of other methods.
Guillan-Barré Syndrome (GBS)	A rare autoimmune disorder in which the host immune system damages the myelin sheathes of peripheral nerves. Commonly, it causes weakness in the extremities and can cause paralysis or difficulty breathing in severe cases.
Inner nuclear membrane (INM)	The inner membrane of the double phospholipid nuclear envelope. Enriched for proteins involved in maintaining nuclear structure and chromatin organization.
Intrinsically disordered protein	Proteins or portions of a protein which lack fixed, organized, or stable three-dimensional structure. Disordered regions can serve as flexible linkers between other structured regions or act as linear motifs which can mediate interactions between the protein and other substrates (protein, RNA, DNA, etc.) (Trivedi et al., 2022).
Nuclear envelope	The nucleus is surrounded by a double phospholipid membrane which separates the nucleoplasm from the rest of the cell. This barrier can be bypassed through nuclear pore complexes. The nuclear lamina on the inner side of the envelope is composed of filament lamin proteins and provides structure to the nucleus.

Par complex	A protein complex composed of proteins responsible for asymmetrically partitioning developmental determinants, allowing for variable daughter cell fate outcomes during embryogenesis.
Random mutagenesis suppressor screen	In Asencio et al., 2012, temperature sensitive *lem-4L(ax475)* mutant *C. elegans* were randomly mutagenized ethyl methane-sulfonate. Mutagenized populations were then screened for those that randomly acquired mutations which allowed for growth and reproduction at previously lethal temperatures.
Telencephalon	In vertebrate brain development, the brain first forms with three distinct sections, the forebrain (prosencephalon), midbrain (mesencephalon), and hindbrain (rhombencephalon). Later the forebrain develops into two parts, the telencephalon and diencephalon. The telencephalon is also known as the cerebrum which contains multiple lobes, each with many functions.

Appendix A-4: Pathogenic variants of ANKLE2 associated with congenital microcephaly. The type of mutation along with the DNA sequence (c.) and subsequent protein sequence (p.) changes in each allele. For L573V/Q782X, two individuals were identified from one family (Yamamoto et al., 2014), while for homozygous G201W, two individuals were identified from two separate families (Shaheen et al., 2019).

Type	Allele 1	Allele 2	Reference(s)
Compound Heterozygous (Two individuals)	c.1717 C>G, p. L573V	c.2344 C>T, p. Q782X	Yamamoto et al., 2014; Thomas et al., 2022
Homozygous	c. 1745 G>T, p. G585V	c. 1745 G>T, p. G585V	Shaheen et al., 2019; Thomas et al., 2022
Homozygous (Two individuals)	c. 601 G>T, p. G201W	c. 601 G>T, p. G201W	Link et al., 2019; Shaheen et al., 2019; Thomas et al., 2022
Homozygous	c. 686 T>G, p. V229G	c. 686 T>G, p. V229G	Link et al., 2019; Thomas et al., 2022
Compound Heterozygous	c. 325 G>C, p. A109P	c. 1421-1 G>C, splicing	Link et al., 2019; Thomas et al., 2022
Compound Heterozygous	c. 706 C>T, p. R236X	c. 1606 C>T, p. R536C	Link et al., 2019; Thomas et al., 2022
Compound Heterozygous	c. 23 C>T, p. A8V	c. 80 C>G, p. A27G	Link et al., 2019;
Compound Heterozygous	Exon 11/12 deletion	c. 1606 C>T, p. R536C	Thomas et al., 2022
Compound Heterozygous	c. 940 C>T, p. R314W	c. 2505 T>G, p. N835E	Thomas et al., 2022
Compound Heterozygous	c. 1175 T>C, p. L392P	c. 1352 A>T, p. N451V	Thomas et al., 2022

Appendix B:

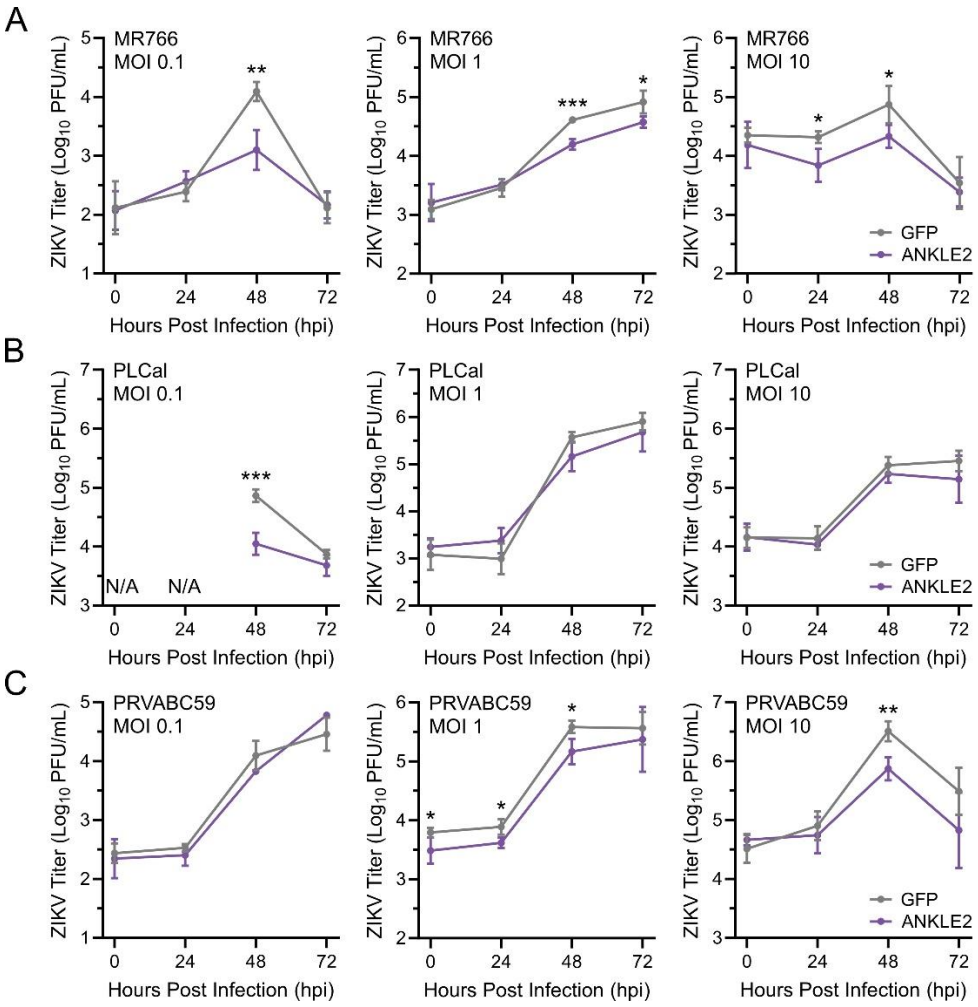

Appendix B-1: Full time-courses of dsRNA ANKLE2 silencing in mosquito Aag2 cells. (A-C) After dsRNA transfection, Aag2 cells were infected with noted ZIKV strain at either MOI 0.1, 1, or 10. Viral supernatant was harvested and virus titers were measured by plaque assay. Student's unpaired T-test, * $p < 0.05$, ** $p < 0.01$, *** $p < 0.001$. Any timepoints without stars are not statistically significant ($p > 0.05$).

Appendix B-2: Summary of Huh7 CRISPR *ANKLE2* Mutagenesis Sequencing

Target Sequence	Reads	Type	Percent
H-ncg			
CCCCAGTTCCTCCGCCAAGCGCGGCCGCCGCC	83652	WT	77.36
CCCCAG-TCCTCCGCCAAGCGCGGCCGCCGCC	3693	Deletion	3.42
CCCCAGT----------GCCGCCGCC	2778	Deletion	2.57
CCCCA--TCCTCCGCCAAGCGCGGCCGCCGCC	2409	Deletion	2.23
CCC----TCCTCCGCCAAGCGCGGCCGCCGCC	2103	Deletion	1.94
Other	13501	N/A	12.48
H1			
CCCCAG-TCCTCCGCCAAGCGCGGCCGCCGCC	37801	Deletion	23.74
CCC----TCCTCCGCCAAGCGCGGCCGCCGCC	37507	Deletion	23.55
CCCCA--TCCTCCGCCAAGCGCGGCCGCCGCC	36867	Deletion	23.15
CCCCAGT----------GCCGCCGCC	30720	Deletion	19.29
CCCCAGTTCCTCCGCCAAGCGCGGCCGCCGCC	1408	WT	0.88
Other	14955	N/A	9.39
H2			
CCCCAG-TCCTCCGCCAAGCGCGGCCGCCGCC	39059	Deletion	54.97
CCCCAGTTCCTCCGCCAAGCGCGGCCGCCGCC	5934	WT	8.35
CCCCAGT----------GCCGCCGCC	5453	Deletion	7.67
CCC----TCCTCCGCCAAGCGCGGCCGCCGCC	4663	Deletion	6.56
CCCCA--TCCTCCGCCAAGCGCGGCCGCCGCC	4618	Deletion	6.50
Other	11325	N/A	15.95

Appendix B-3: Summary of JEG-3 CRISPR *ANKLE2* Mutagenesis Sequencing

Target Sequence	Reads	Type	Percent
J-ncg			
CCCCAGTTCCTCCGCCAAGCGCGGCCGCCGCC	266944	WT	82.78
CCCCAGTTCCTCCGCCAAGCGCGGCCGCCGCC	4197	Insertion	1.30
CCCCAGTTCCTCCGCCAAGCGCGGCCGCCGCC	912	1 Base Change	0.28
CCCCAGTTCCTCCGCCAAGCGCGGCCGCCGCC	777	1 Base Change	0.24
CCCCAGTTCCTCCGCCAAGCGCGGCCGCCGCC	747	1 Base Change	0.23
Other	41651	N/A	15.17
J1			
CCCCA--TCCTCCGCCAAGCGCGGCCGCCGCC	327688	Deletion	84.48
CCCCA--TCCTCCGCCAAGCGCGGCCGCCGCC	3680	Insertion and Deletion	0.95
CCCCAGTTCCTCCGCCAAGCGCGGCCGCCGCC	1957	WT	0.50
CCCCA--TCCTCCGCCAAGCGCGGCCGCCGCC	1489	Deletion	0.38
CCCCA--TCCTCCGCCAAGCGCGGCCGCCGCC	1131	Deletion	0.29
Other	43350	N/A	13.40
J2			
TCTGG----------TCCTCCGC	129939	Deletion	83.11
TCTGGGCCGCAGCGGGACCCCAGTTCCTCCGC	4884	WT	3.12
TCTGG----------TCCTCCGC	1356	Insertion and Deletion	0.87
TCTGG----------TCCTCCGC	648	Deletion	0.41
TCTGG----------TCCTCCGC	409	Deletion	0.26
Other	19114	N/A	12.23

Appendix B-4: Antibodies. WB = Western blot, IF = Immunofluorescence

Antibody	Host Species	Dilution Used	Supplier (Catalog #)	RRID
GAPDH	Mouse	1:1000 (WB)	Fisher (PIMA515738)	AB_2537652
FLAG-M2	Mouse	1:200 (IF), 1:1000 (WB)	MilliporeSigma (F1804)	AB_262044
Strep	Mouse	1:1000 (WB)	Qiagen (34850)	AB_2810987
4G2 (Flavivirus E)	Mouse	1:250 (IF)	ATCC (HB-112)	CVCL_J890
rJ2 (dsRNA)	Mouse	1:40 (IF)	MilliporeSigma (MABE1134)	AB_2819101
Lamin A/C (4C11)	Mouse	1:1000 (WB)	Cell Signaling (4777) Gift from Dr. Jodi Nunnari	AB_10545756
SERCA2	Mouse	1:100 (IF), 1:500 (WB)	Invitrogen (MA3919)	AB_325502
FLAG Tag	Rabbit	1:400 (IF)	Cell Signaling (14793)	AB_2572291
ANKLE2	Rabbit	1:80 (IF)	Atlas Antibodies (HPA074838)	N/A
ANKLE2	Rabbit	1:1000 (WB)	Atlas Antibodies (HPA003602)	AB_1858349
ANKLE2	Rabbit	1:1000 (WB)	Bethyl Labs (A302-966A-M)	AB_2780882
ZIKV Envelope (E)	Rabbit	1:1000 (WB)	GeneTex (GTX637298)	N/A
ZIKV NS4A	Rabbit	1:1000 (IF, WB)	GeneTex (GTX133704)	AB_2887067
ZIKV Capsid	Rabbit	1:1000 (WB)	GeneTex (GTX133317)	AB_2756861
DENV NS5	Rabbit	1:1000 (WB)	GeneTex (GTX103350)	AB_1240701
DENV Capsid	Rabbit	1:1000 (WB)	GeneTex (GTX103343)	AB_1240697
Actin	Rabbit	1:5000 (WB)	Sigma (A2066)	AB_476693
Anti-Mouse IgG-HRP	Rabbit	1:5000 (WB)	SouthernBiotech (6170-05)	AB_2796243
Calnexin	Rabbit	1:250 (IF)	Proteintech (10427-2-AP) Gift from Dr. Jodi Nunnari	AB_2069033
TOMM20	Rabbit	1:250 (IF)	Proteintech (11802-1-AP)	AB_2207530
GRASP65	Rabbit	1:250 (IF)	Gift from Dr. Nevan Krogan	N/A
HA	Rat	1:2000 (WB)	MilliporeSigma (3F10) Gift from Dr. Joanna Chiu	AB_2314622
Anti-Rabbit IgG-HRP	Goat	1:5000 (WB)	SouthernBiotech (4030-05)	AB_2687483
Anti-Mouse AlexaFlour-488	Goat	1:1000 (IF)	Invitrogen (A28175)	AB_2536161
Anti-Mouse AlexaFlour-555	Goat	1:1000 (IF)	Invitrogen (A21422)	AB_2535844
Anti-Rabbit AlexaFlour-488	Goat	1:1000 (IF)	Invitrogen (A11008)	AB_143165
Anti-Rabbit AlexaFlour-555	Goat	1:1000 (IF)	Invitrogen (A27039)	AB_2536100
Anti-Mouse AlexaFlour-680	Goat	1:1000 (IF)	Invitrogen (A21057)	AB_2535723

Appendix B-5: Sequences

Sequence	Accession Number	Relevant Figure(s)
Human ANKLE2	NM_015114.3	4-1, 4-3, 4-6, 4-9, 5-1, 5-2, 5-3, 5-4, 5-5, 6-2, 7-1, 7-3, A-1
Human GAPDH	NM_003860.4	4-3, 4-8
Human ANKLE1	NM_152363.6	4-1
eGFP	UDY80669.1	4-1, 4-10, 5-1, 5-2, 6-2, 7-1, B-1
mCherry	AY678264.1	4-6, 4-9
Mosquito ANKLE2	XM_021856854.1	4-10, B-1
Zika virus (ZIKV) PRVABC59	MK713748.1	4-11, 5-1, 5-2, 5-3, 5-4, 5-5
Dengue virus serotype 1 (DENV1)	QZN14214.1	5-5
Dengue virus serotype 2 (DENV2)	NC_001474.2	4-11, 5-5
Dengue virus serotype 3 (DENV3)	QXM02604.1	5-5
Dengue virus serotype 4 (DENV4)	QTX92397.1	5-5
Yellow Fever virus (YFV) Asibi	KF769016.1	4-11, 5-5
West Nile virus (WNV) NY99	DQ211652.1	4-11, 5-5
Japanese encephalitis virus (JEV)	NC_001437.1	4-11, 5-5
Tick borne encephalitis virus (TBEV) Sofjin	JX498940.1	5-5, 7-2
Powassan virus (POWV) LB	L06436.1	5-5, 7-2
St. Louis encephalitis virus (SLEV)	QVN47903.1	5-5
Langat virus	NP_620108.1	5-5
Mouse Ankle2	NM_001253814.1	7-3, 7-4

Appendix B-6: Oligonucleotides

Oligo Name	Sequence	Application
ANKLE2 CRISPRi gRNA #1	GCGGCTGGCGGCGGCCGAGT	CRISPRi sygRNA
ANKLE2 CRISPRi gRNA #2	GCCGGGCGGCGGCGATGCTG	CRISPRi sygRNA
Negative CRISPRi gRNA	Proprietary sequence from Millipore Sigma	CRISPRi sygRNA
ANKLE2 CRISPR Forward Oligo	CACCGCCGCGCTTGGCGGAGGAACT	CRISPR gRNA
ANKLE2 CRISPR Reverse Oligo	AAACAGTTCCTCCGCCAAGCGCGG	CRISPR gRNA
Negative CRISPR gRNA Forward Oligo	CACCGACCCTCCGAATCGTAACGGA	CRISPR gRNA
Negative CRISPR gRNA Reverse Oligo	AAACTCCGTTACGATTCGGAGGGTC	CRISPR gRNA
ANKLE2 Sequencing Forward w/ Adapter	*ACACTCTTTCCCTACACGACGCTCTTCCGATCT*GTGCTGCTGATCGCTGTG	Sequencing ANKLE2 KOs *(with Illumina Adapter)*
ANKLE2 Sequencing Reverse w/ Adapter	*GACTGGAGTTCAGACGTGTGCTCTTCCGATCT*GTGGTAGAAAGAAGACAGCC	Sequencing ANKLE2 KOs *(with Illumina Adapter)*
GAPDH Forward	ACATCGCTCAGACACCATG	qPCR Control
GAPDH Reverse	TGTAGTTGAGGTCAATGAAGGG	qPCR Control
ANKLE2 Forward	AAAGAGAACCAGGCTTCCATC	qPCR Analysis (Human)
ANKLE2 Reverse	CACGTTGACTACATCTGCATTTC	qPCR Analysis (Human)
ZIKV Forward	CGCCACCAAGATGAACTGATTG	qPCR Analysis
ZIKV Reverse	CATCCATTCTCCCTTTCCATGGAT	qPCR Analysis
ANKLE2 dsRNA Target Forward	*TAATACGACTCACTATAGGG*GCTGGAAATCAAAGCCTACG	Aag2 dsRNA Knockdown *(with T7 Promoter)*
ANKLE2 dsRNA Target Reverse	*TAATACGACTCACTATAGGG*TTTCTCGTCCAGTTGTCGCT	Aag2 dsRNA Knockdown *(with T7 Promoter)*
GFP dsRNA Target Forward	*TAATACGACTCACTATAGGG*ATGGTGAGCAAGGGCGAGGAGCTGTTC	Aag2 dsRNA Knockdown *(with T7 Promoter)*
GFP dsRNA Target Reverse	*TAATACGACTCACTATAGGG*CTGGGTGCTCAGGTAGTGGTTGTCGGGC	Aag2 dsRNA Knockdown *(with T7 Promoter)*
ANKLE2 Forward	CCTCCAGAACTTCCTCGATTTC	qPCR Analysis (*Aedes*)
ANKLE2 Reverse	CGGAGGAGTTCGTCTGATTATTT	qPCR Analysis (*Aedes*)
GFP Forward #1	TAAAGGCCGCCATGGTGAGCAA	Gibson Assembly preparation of GFP-APEX2-3xFLAG
GFP Reverse #1	CGCTCTTGTACAGCTCGTCCAT	Gibson Assembly preparation of GFP-APEX2-3xFLAG
GFP Forward #2	CTTATACCAACTTTCCGTACCACTTCCTACCCTCGTAAAGGCCGCCATGGTGAGCA	Gibson Assembly of GFP-APEX2-3xFLAG
GFP Reverse #2	CAGATCCACCTCCTGAACCACCTCCGCTACCGCCACCGCTCTTGTACAGCTCGTCCATGC	Gibson Assembly of GFP-APEX2-3xFLAG
ANKLE2 Forward #1	TAAAGGCCGCCATGCTGTGGCCGCGG	Gibson Assembly preparation of ANKLE2-APEX2-3xFLAG

ANKLE2 Reverse #1	GCTCAGGGCGGCAAGCTCAGCCAGG	Gibson Assembly preparation of ANKLE2-APEX2-3xFLAG
ANKLE2 Forward #2	ACTTCCTACCCTCGTAAAGGCCGCCATGCTG	Gibson Assembly of ANKLE2-APEX2-3xFLAG
ANKLE2 Reverse #2	CCGCTACCGCCACCGCTCAGGGCGGCAAG	Gibson Assembly of ANKLE2-APEX2-3xFLAG
ANKLE1 Forward #1	GCCGCCATGTGTTCCGAAGCCC	Gibson Assembly preparation of ANKLE1-APEX2-3xFLAG
ANKLE1 Reverse #1	CGCTTCCACGCGCTTGAATATCT	Gibson Assembly preparation of ANKLE1-APEX2-3xFLAG
ANKLE1 Forward #2	ACTTCCTACCCTCGTAAAGGCCGCCATGTGT	Gibson Assembly of ANKLE1-APEX2-3xFLAG
ANKLE1 Reverse #2	TCCGCTACCGCCACCGCTTCCACGCG	Gibson Assembly of ANKLE1-APEX2-3xFLAG
pcDNA Upstream	TGGGAGTTTGTTTTGGAACCA	Sequencing of pcDNA constructs
pcDNA Downstream	CAGATGGCTGGCAACTAGAAG	Sequencing of pcDNA constructs
Mycoplasma Forward #1	TGCACCATCTGTCACTCTGTTAACCTC	For *Mycoplasma sp.* detection
Mycoplasma Reverse #1	GGGAGCAAACAGGATTAGATACCCT	For *Mycoplasma sp.* detection
Mycoplasma Forward #2	GGCGAATGGGTGAGTAACACG	For *Mycoplasma sp.* detection
Mycoplasma Reverse #2	CGGATAACGCTTGCGACCTATG	For *Mycoplasma sp.* detection
NS4A Forward	CTTGGTACCGAGCTCGGATCCGCCACCATGGGAGCCG	Gibson Assembly of ZIKVpr NS4A C-terminal truncations
NS4A 1-54 Reverse	CATCCACCGCCTCCCTCGAGCGTTTCGAGAGTTTCCGGGAG	Gibson Assembly of ZIKVpr NS4A 1-54
NS4A 1-72 Reverse	GTGCTGGATATCTGCAGAATTCAAGGACGAAAAATATACCGAGAGAGACG	Gibson Assembly of ZIKVpr NS4A 1-72
NS4A 1-96 Reverse	GTGCTGGATATCTGCAGAATTCCCACATCAGCCATGCGC	Gibson Assembly of ZIKVpr NS4A 1-96
NS4A 1-127 Reverse	GTGCTGGATATCTGCAGAATTCGCGTTGCTTCTCCGGCT	Gibson Assembly of ZIKVpr NS4A 1-127
Mouse Ankle2 Forward 1	GAGACAAGGTCTCAATCATGTTAATCCACA	For mouse Ankle2 genotyping
Mouse Ankle2 Forward 2	GTGCCAGCTGACATTAGAGACTCTGGAGAA	For mouse Ankle2 genotyping
Mouse Ankle2 Reverse	GCAAGTGTCTTTGAGTCACTTCTGC	For mouse Ankle2 genotyping
Mouse Ifnar1 Forward 1	CGAGGCGAAGTGGTTAAAAG	For mouse Ifnar1 genotyping
Mouse Ifnar1 Forward 2	ACGGATCAACCTCATTCCAC	For mouse Ifnar1 genotyping
Mouse Ifnar1 Reverse	AATTCGCCAATGACAAGACG	For mouse Ifnar1 genotyping

Appendix C:

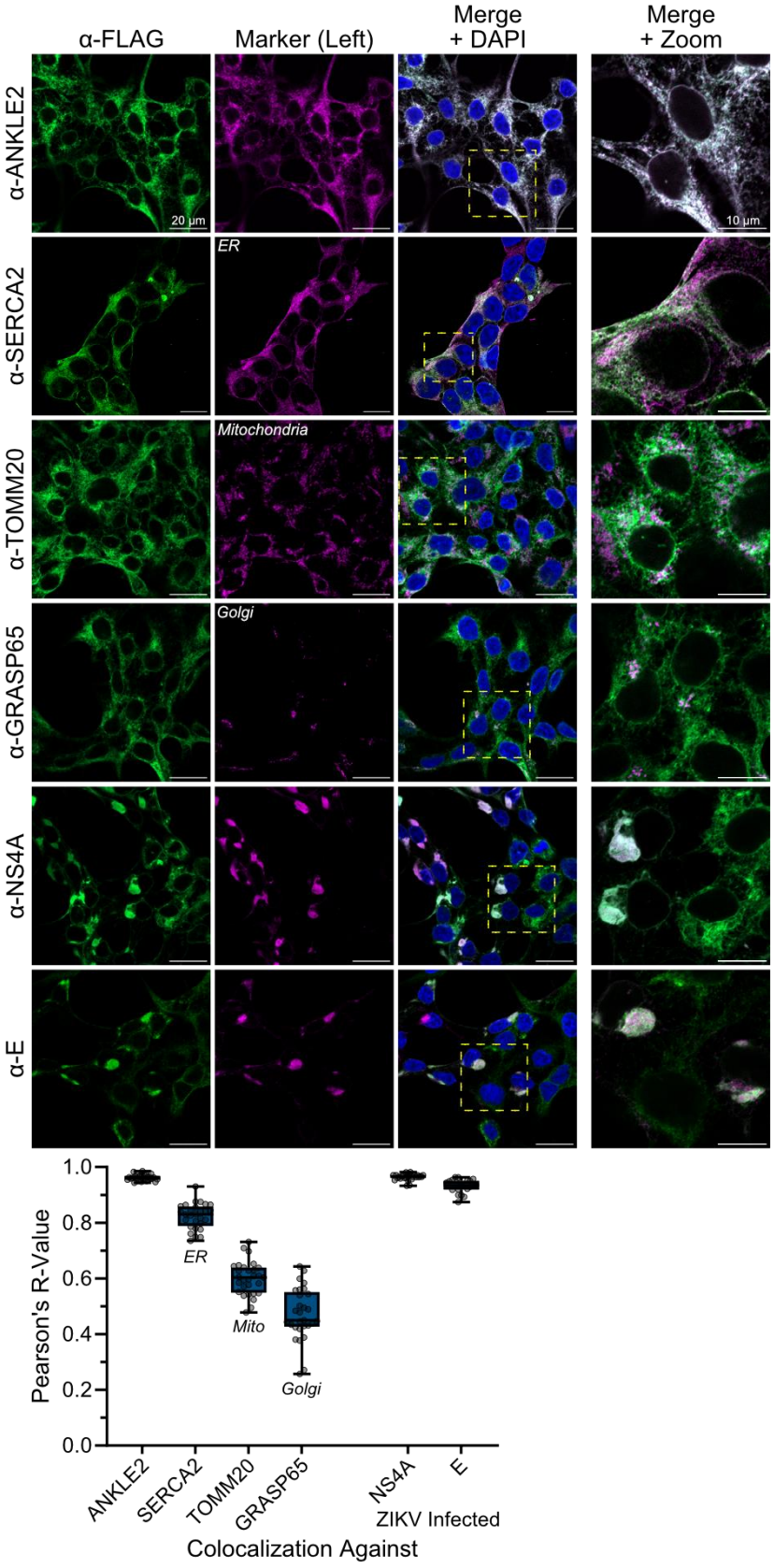
α-FLAG
Marker (Left)
Merge + DAPI
Merge + Zoom
α-ANKLE2
α-SERCA2
α-TOMM20
α-GRASP65
α-NS4A
α-E
20 μm
10 μm
ER
Mitochondria
Golgi
Pearson's R-Value
1.0
0.8
0.6
0.4
0.2
0.0
ER
Mito
Golgi
ANKLE2
SERCA2
TOMM20
GRASP65
NS4A
E
ZIKV Infected
Colocalization Against

Appendix C-1: Colocalization of ANKLE2-3xFLAG with organelle markers and ZIKV proteins. ANKLE2-3xFLAG was stably expressed in HEK293T cells by lentiviral transduction. After antibiotic selection, cells were seeded on cover slips prior to fixation and antibody staining for confocal microscopy visualization. Cells were stained for FLAG (shown in green) to assess localization and expression of ANKLE2-3xFLAG. Cells were counterstained (shown in magenta) for various organelle markers (SERCA2 = ER, TOMM20 = mitochondria, GRASP65 = Golgi). Two wells were infected with ZIKV MR766 at MOI 5 for 48 hours and stained for ZIKV proteins (NS4A and E in magenta). At least five images were captured of each condition and colocalization of between FLAG and the counterstained protein was measured for 22-30 individual cells using ImageJ.

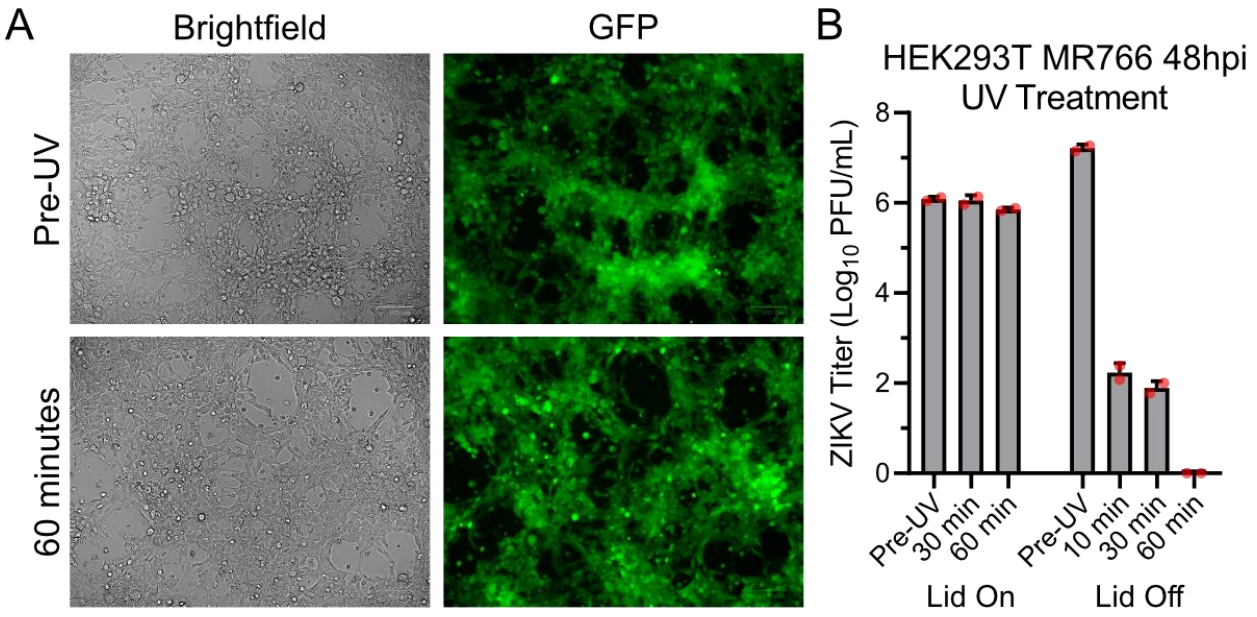

Appendix C-2: Validation of ZIKV neutralization by UV sterilization. (A) HEK293T GFP-3xF cells were infected with ZIKV MR766 at MOI 5 for 48 hours. Brightfield and GFP images were acquired using ZOE Fluorescent Cell Imager (BioRad). (B) ZIKV titer was measured in technical duplicate from the cell media supernatant at shown times after UV sterilization. One plate was left with the polypropylene lid on while the other plate was left in the hood without the lid. ZIKV titer was determined by plaque assay.

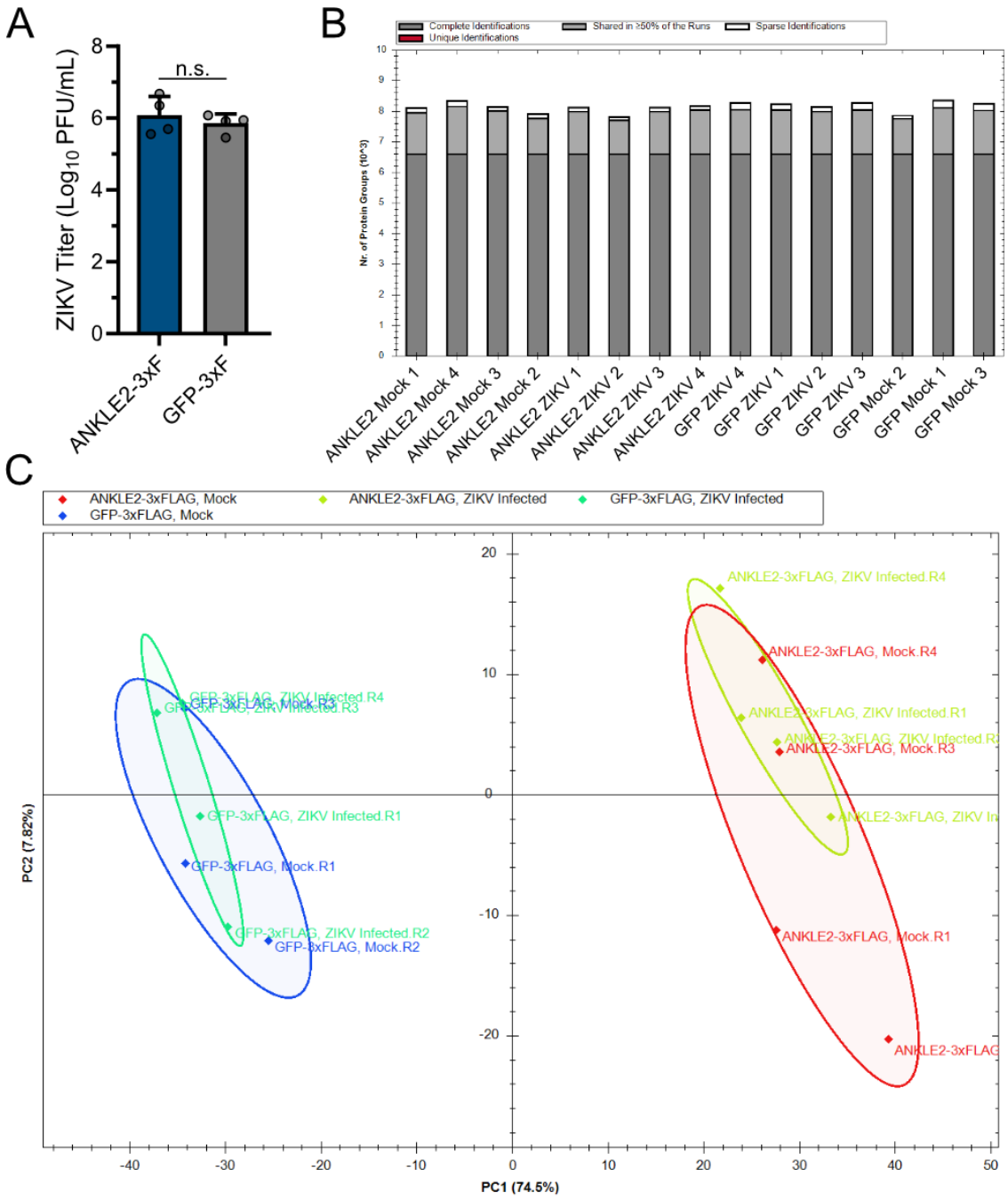

Appendix C-3: Initial validation of ANKLE2 proteomic samples and data. (A) After each infection replicate, a sample of cell media was harvested and frozen at -80ºC. One all replicates were complete, ZIKV titer of each replicate was determined by plaque assay. (B) Analysis plot from Spectronaut™ showing number of identified protein groups per replicate. Colors indicate the number of samples that each protein identification was found. (C) Principal component analysis plot generated by Spectronaut™ showing relative separation of GFP and ANKLE2 datasets.

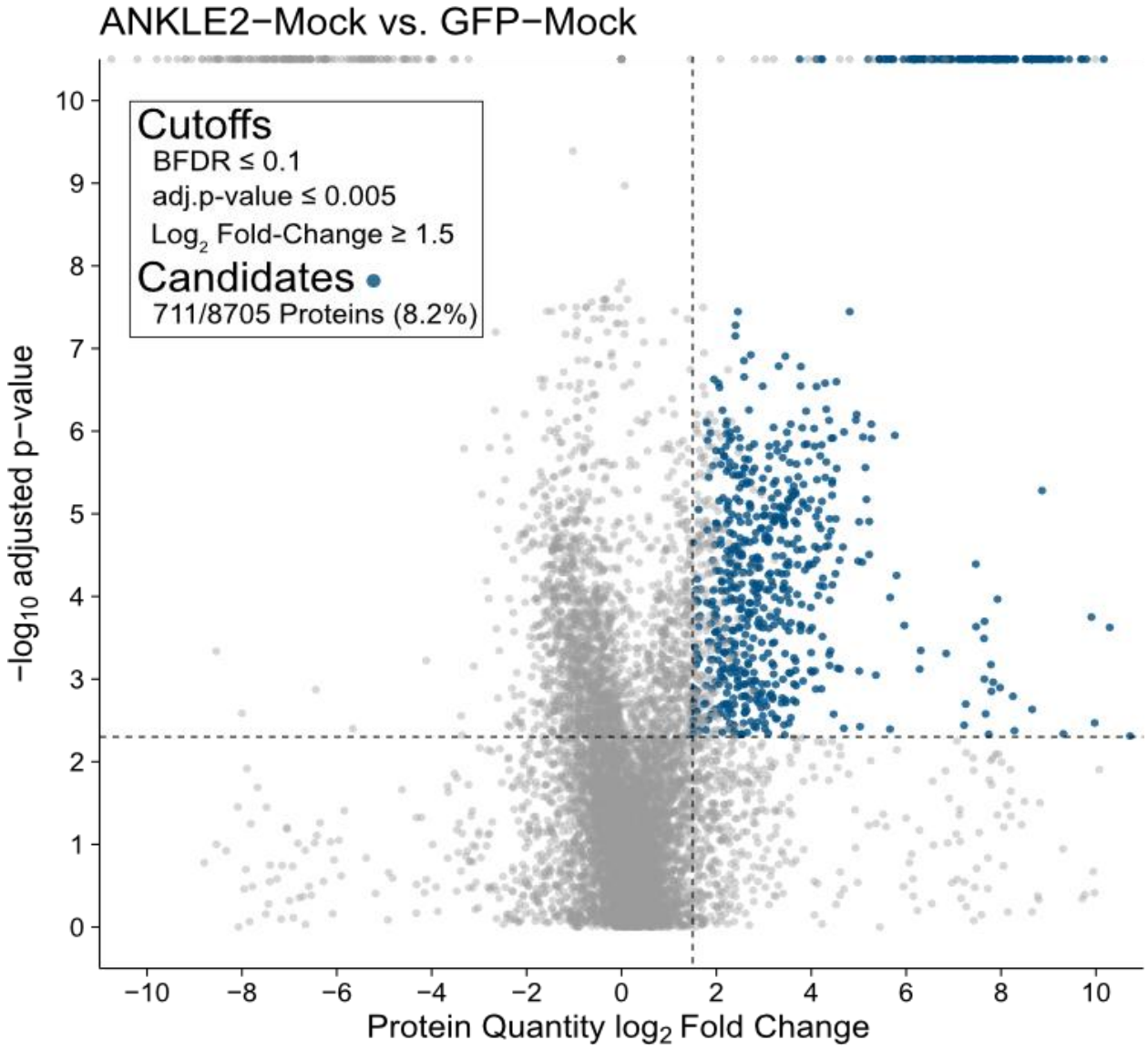

Appendix C-4: Volcano plot of protein identifications from mock infected ANKLE2-3xF vs. GFP-3xF samples. Volcano plot of all proteins identified in ANKLE2 or GFP mock data. On x-axis proteins are distributed by $\log_2$ fold change (ANKLE2/GFP) in protein quantity. On y-axis proteins are distributed by $-\log_{10}$ adjusted p-value calculated by MSstats. Values on top of graph represent identifications with adj. p-value = 0, arising from no identification of the given protein in one set of data. Additionally, candidates were filtered using the Bayesian false-discovery rate (BFDR) using SAINTexpress. Proteins that meet all three criteria are colored blue and represent candidate mock ANKLE2-interactors.

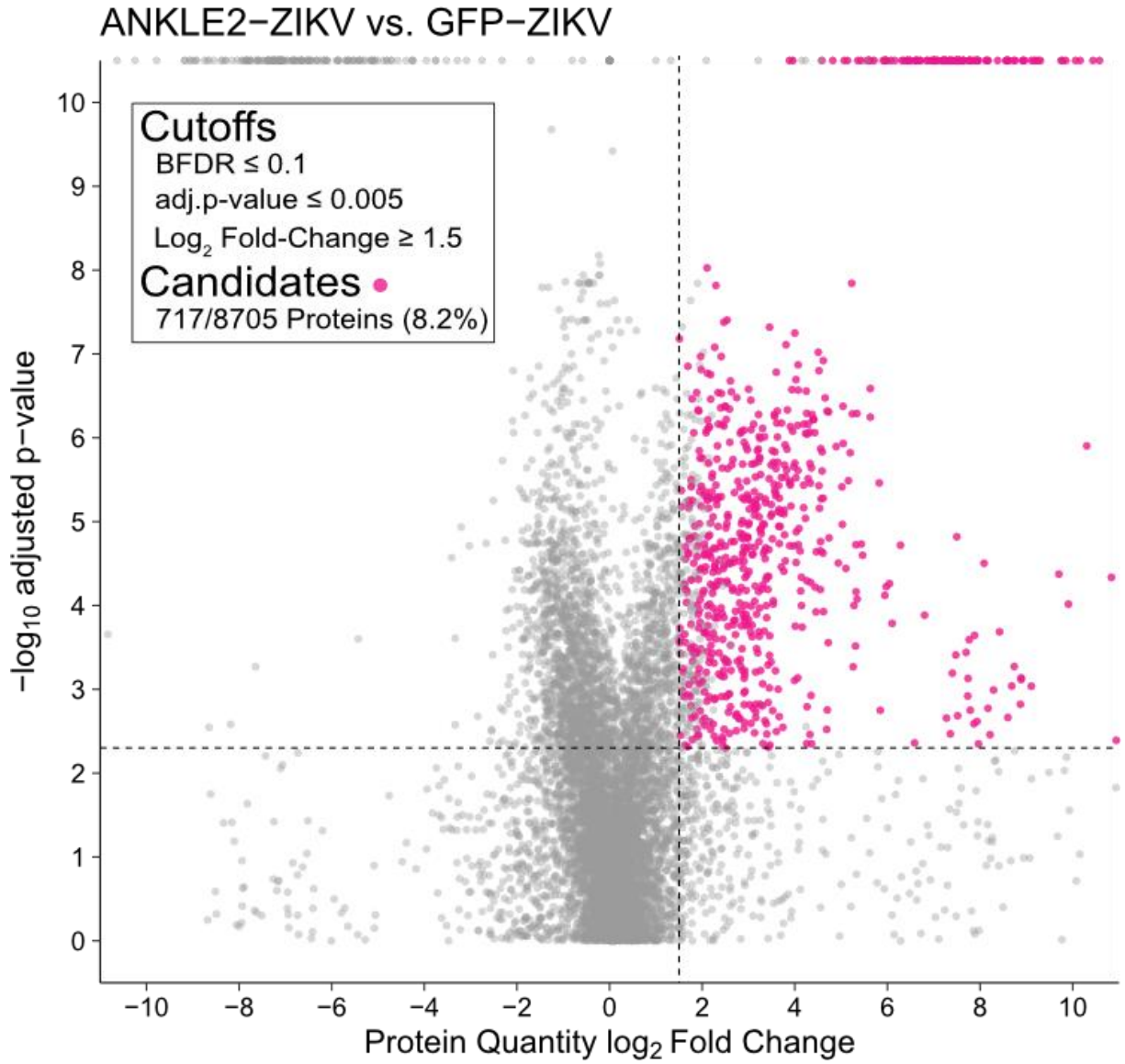

Appendix C-5: Volcano plot of protein identifications from ZIKV infected ANKLE2-3xF vs. GFP-3xF samples. Volcano plot of all proteins identified in ANKLE2 or GFP ZIKV-infected data. On x-axis proteins are distributed by $\log_2$ fold change (ANKLE2/GFP) in protein quantity. On y-axis proteins are distributed by $-\log_{10}$ adjusted p-value calculated by MSstats. Values on top of graph represent identifications with adj. p-value = 0, arising from no identification of the given protein in one set of data. Additionally, candidates were filtered using the Bayesian false-discovery rate (BFDR) using SAINTexpress. Proteins that meet all three criteria are colored pink and represent candidate ZIKV ANKLE2-interactors.

Appendix C-6: Candidate Proteins with ties to orthoflavivirus replication or clinical microcephaly.

Protein	UniProt ID	Search Term	Reference(s)
ACBD5	Q5T8D3	Clinical Microcephaly	Kaiyrzhanov et al., 2013, *Brain*
ADCY7	P51828	Flavivirus Replication	Rossi et al., 2019, *Journal of Internal Medicine*
ALG11	Q2TAA5	Clinical Microcephaly	Regal et al., 2014, *Molecular Genetics and Metabolism Reports* Mulkey et al., 2019, *Pediatric Neurology*
ALG12	Q9BV10	Clinical Microcephaly	Chantert et al., 2002, *Journal of Biological Chemistry*
APOE	P02649	Flavivirus Replication	Tréguier et al., 2022, *Journal of Virology* Faustino et al., 2015, *Science Reports*
ATL2	Q8NHH9	Flavivirus Replication	Neufeldt et al., 2019, *Nature Microbiology*
ATL3	Q6DD88	Flavivirus Replication	
ATP6V0A2	Q9Y487	Clinical Microcephaly	Karacan et al., 2019, *Turkish Journal of Haematology*
ATP9A	O75110	Clinical Microcephaly	Vogt et al., 2022, *Journal of Medical Genetics*
AUP1	Q9Y679	Flavivirus Replication	Zhang et al., 2018, *Cell Host & Microbe*
ATF6	P18850	Flavivirus Replication	Ambrose and Mackenzie, 2013, *Journal of Virology*
B3GAT3	O94766	Flavivirus Replication	Gao et al., 2019, *Virology*
BCAP31	P51572	Clinical Microcephaly	Cacciagli et al., 2013, *American Journal of Health Genetics*
BCL6	P41182	Flavivirus Replication	Guo et al., 2018, *Veterinary Microbiology*
CACNA1H	O95180	Flavivirus Replication	Long et al., 2016, *Genes and Immunity*
CHST10	O43529	Flavivirus Replication	Oliveira et al., 2018, *PLOS Neglected Tropical Diseases*
CLCN4	P51793	Clinical Microcephaly	Veeramah et al., 2013, *Epilepsia* Li et al., 2023, *Frontiers in Neurology*
CNNM2	Q9H8M5	Clinical Microcephaly	Accogli et al., 2019, *European Journal of Medical Genetics*
CYB5R3	P00387	Clinical Microcephaly	Vieira et al., 1995, *Blood* Shirabe et al., 1995, *American Journal of Human Genetics*
DDOST	P39656	Flavivirus Replication	Petrova et al., 2019, *Viruses*
DERL1	Q9BUN8	Flavivirus Replication	Tabata et al., 2021, *Journal of Virology*
DHODH	Q02127	Flavivirus Replication	Tang et al., 2022, *Journal of Medical Virology*
DOLK	Q9UPQ8	Clinical Microcephaly	Komlosi et al., 2021, *Frontiers in Genetics*
EMC2	Q15006	Flavivirus Replication	Ma et al., 2015, *Cell Reports*
EMC3	Q9P0I2	Flavivirus Replication	Marceau et al., 2016, *Nature*
EMC4	Q5J8M3	Flavivirus Replication	Marceau et al., 2016, *Nature* Bagchi et al., 2022, *PLOS Pathogens*
ERLIN1	O75477	Flavivirus Replication	Whitten-Bauer et al., 2019, *Cells*
FBXL4	Q9UKA2	Clinical Microcephaly	El-Hattab et al., 2017, *Human Mutation*
FBXO28	Q9NVF7	Clinical Microcephaly	Schneider et al., 2021, *Epilepsia*
FKRP	Q9H9S5	Clinical Microcephaly	Louhichi et al., 2004, *Neurogenetics*
FYN	P06241	Flavivirus Replication	Wispelaere et al., 2013, *Journal of Virology* Vincetti et al., 2015, *Journal of Medicinal Chemistry*
GNB1	P62873	Clinical Microcephaly	Lee et al., 2020, *Frontiers in Genetics*
HMGCR	P04035	Flavivirus Replication	Soto-Acosta et al., 2017, *PLOS Pathogens*

HMOX1	P09601	Flavivirus Replication	Su et al., 2020, *FASEB* Yan et al., 2023, *Journal of Medical Virology*
IER3IP1	Q9Y5U9	Clinical Microcephaly	Esk et al., 2020, *Science* Söbü et al., 2022, *Journal of Clinical Research in Pediatric Endocrinology*
ITGB5	P18084	Flavivirus Replication	Zhu et al., 2020, *Cell Stem Cell*
LDLR	P01130	Flavivirus Replication	Faustino et al., 2014, *Nanomedicine* Huang et al., 2021, *Emerging Microbes and Infections*
LMAN2L	Q9H0V9	Flavivirus Replication	Xi et al., 2020, *Veterinary Microbiology*
LMBRD2	Q68DH5	Clinical Microcephaly	Malhotra et al., 2021, *Journal of Medical Genetics*
LNPK	Q9C0E8	Flavivirus Replication	Tran et al., 2021, *Viruses*
LYN	P07948	Flavivirus Replication	Li et al., 2020, *Nature Communications*
MAGT1	Q9H0U3	Flavivirus Replication	Lin et al., 2017, *mBio*
MBOAT7	Q96N66	Clinical Microcephaly	Farnè et al., 2020, *American Journal of Medical Genetics Part A*
MFF	Q9GZY8	Clinical Microcephaly	Nasca et al., 2018, *Frontiers in Genetics*
NAAA	Q02083	Flavivirus Replication	Lai et al., 2023, *Antiviral Research*
NDUFA8	P51970	Clinical Microcephaly	Yatsuka et al., 2020, *Clinical Genetics*
NDUFS1	P28331	Clinical Microcephaly	Hoefs et al., 2020, *Molecular Genetics and Metabolism* Roberts et al., 2014, *Gene*
NDUFS4	O43181	Clinical Microcephaly	Budde et al., 2000*, Biochemical and Biophysical Research Communications*
NEXMIF	Q5QGS0	Clinical Microcephaly	Farach and Northrup, 2016, *American Journal of Medical Genetics Part A* Lange et al., 2016, *Journal of Medical Genetics*
OS9	Q13438	Flavivirus Replication	Noack et al., 2014, *Journal of Virology*
OSBP	P22059	Flavivirus Replication	Meutiawati et al., 2018, *Antiviral Research*
PGAP1	Q75T13	Clinical Microcephaly	Granzow et al., 2015, *Molecular and Cellular Probes* Kettwig et al., 2016, *BMC Neurology*
PIGA	P37287	Clinical Microcephaly	Swoboda et al., 2014, *American Journal of Medical Genetics Part A*
PIGS	Q96S52	Clinical Microcephaly	Efthymiou et al., 2021, *Epilepsia*
POMT1	Q9Y6A1	Clinical Microcephaly	Messina et al., 2008, *Neuromuscular Disorders* Mercuri et al., 2009, *Neurology*
POMT2	Q9UKY4	Clinical Microcephaly	
PORCN	Q9H237	Clinical Microcephaly	Castilla-Vallmanya et al., 2021, *International Journal of Molecular Sciences*
PPP1R15B	Q5SWA1	Clinical Microcephaly	Abdulkarim et al., 2015, *Diabetes* Kernohan et al., 2015, *Human Molecular Genetics*
PPP2CB	P62714	Flavivirus Replication	Cao et al., 2019, *International Journal of Molecular Sciences*
PPP2R1A	P30153	Clinical Microcephaly	Melas et al., 2021, *Cold Spring Harbor Molecular Case Studies* Lenaerts et al., 2021, *Genetics in Medicine*
PPP2R5E	Q16537	Flavivirus Replication	Oliveira et al., 2018, *PLOS Neglected Tropical Diseases*
PYCR1	P32322	Clinical Microcephaly	Kouwenberg et al., 2011, *American Journal of Medical Genetics Part A*

RAB1B	Q9H0U4	Flavivirus Replication	Beachboard et al., 2019, *Journal of Biological Chemistry*
RAB3GAP1	Q15042	Clinical Microcephaly	Seemanová et al., 1996, *American Journal of Medical Genetics* Handley et al., 2013, *Human Mutation*
RAB8B	Q92930	Flavivirus Replication	Kobayashi et al., 2016, *Journal of Biological Chemistry*
RFT1	Q96AA3	Clinical Microcephaly	Barba et al., 2016, *Developmental Medicine & Child Neurology*
RPN1	P04843	Flavivirus Replication	Choy et al., 2020, *Cell Reports*
SCAP	Q12770	Flavivirus Replication	Liu et al., 2017, *Journal of Virology*
SEC11A	P67812	Flavivirus Replication	Estoppey et al., 2017, *Cell Reports*
SEC62	Q99442	Flavivirus Replication	Lan et al., 2023, *Nature Communications*
SEL1L	Q9UBV2	Flavivirus Replication	Tabata et al., 2021, *Journal of Virology* Lan et al., 2023, *Nature Communications*
SGMS1	Q86VZ5	Flavivirus Replication	Taniguchi et al., 2016, *Science Reports*
SLC16A2	P36021	Clinical Microcephaly	Tang et al., 2018, *Chinese Journal of Pediatrics*
SLC1A3	P43003	Flavivirus Replication	Mishra et al., 2007, *Neurochemistry International*
SLC35A3	Q9Y2D2	Clinical Microcephaly	Edvardson et al., 2013, *Journal of Medical Genetics* Marini et al., 2017, *American Journal of Medical Genetics Part A*
SLC35B2	Q8TB61	Flavivirus Replication	Gao et al., 2019, *Virology*
SLC35C1	Q96A29	Clinical Microcephaly	Dyment et al., 2020, *American Journal of Medical Genetics Part A*
SLC6A8	P48029	Clinical Microcephaly	Clark et al., 2006, *Human Genetics*
SLC7A11	Q9UPY5	Flavivirus Replication	Carr et al., 2019, *Virus Genetics*
SLC9A6	Q92581	Clinical Microcephaly	Gilfillan et al., 2008, *American Journal of Human Genetics*
SMO	Q99835	Clinical Microcephaly	Le et al., 2020, *American Journal of Human Genetics*
SPCS1	Q9Y6A9	Flavivirus Replication	Zhang et al., 2016, *Nature* Ma et al., 2018, *Journal of Virology*
ST3GAL5	Q9UNP4	Clinical Microcephaly	Cruz et al., 2023, *GeneReviews*
STIM1	Q13586	Flavivirus Replication	Dionicio et al., 2018, *Virus Research*
STING1	Q86WV6	Flavivirus Replication	Wuertz et al., 2019, *PLOS Pathogens*
STT3A	P46977	Flavivirus Replication	Lin et al., 2017, *mBio*
STT3B	Q8TCJ2	Flavivirus Replication	Puschnik et al., 2017, *Cell Reports*
STT3B	Q8TCJ2	Clinical Microcephaly	Shrimal et al., 2013, *Human Molecular Genetics*
TBC1D20	Q96BZ9	Flavivirus Replication	Nevo-Yassaf et al., 2012, *Journal of Virology*
TMED9	Q9BVK6	Flavivirus Replication	Evans et al., 2021, *Journal of Cell Science*
TMEM165	Q9HC07	Clinical Microcephaly	Foulquier et al., 2012, *American Journal of Human Genetics*
TMEM41B	Q5BJD5	Flavivirus Replication	Hoffmann et al., 2021, *Cell* Li et al., 2021, *Journal of Cell Biology* Yousefi et al., 2022, *PLOS Pathogens*
TMEM67	Q5HYA8	Clinical Microcephaly	Tkemaladze et al., 2017, *Georgian Medical News*
TMTC3	Q6ZXV5	Clinical Microcephaly	Liu et al., 2020, *Experimental and Therapeutic Medicine* Hana et al., 2020, *Case Reports in Medicine*

TMX2	Q9Y320	Clinical Microcephaly	Vandervore et al., 2019, *American Journal of Human Genetics*
TUSC3	Q13454	Clinical Microcephaly	Chehadeh et al., 2015, *JIMD Reports* Al-Amri et al., 2016, *American Journal of Medical Genetics Part A*
TYRO3	Q06418	Flavivirus Replication	Perera-Lecoin et al., 2013, *Viruses*
UBE2J1	Q9Y385	Flavivirus Replication	Ma et al., 2015, *Cell Reports*
VAPA	Q9P0L0	Flavivirus Replication	Ramage et al., 2015, *Molecular Cell* Khasa et al., 2020, *Microbial Pathogenesis*
VDAC1	P21796	Flavivirus Replication	Jitobaom et al., 2016, *Science Reports*
VDAC2	P45880	Flavivirus Replication	Pan et al., 2023, *Journal of Virology*
YES1	P07947	Flavivirus Replication	Hirsch et al., 2005, *Journal of Virology*
YIF1B	Q5BJH7	Clinical Microcephaly	Al Muhaizea et al., 2020, *Acta Neuropathologica*
YIPF5	Q969M3	Clinical Microcephaly	Franco et al., 2020, *Journal of Clinical Investigation*

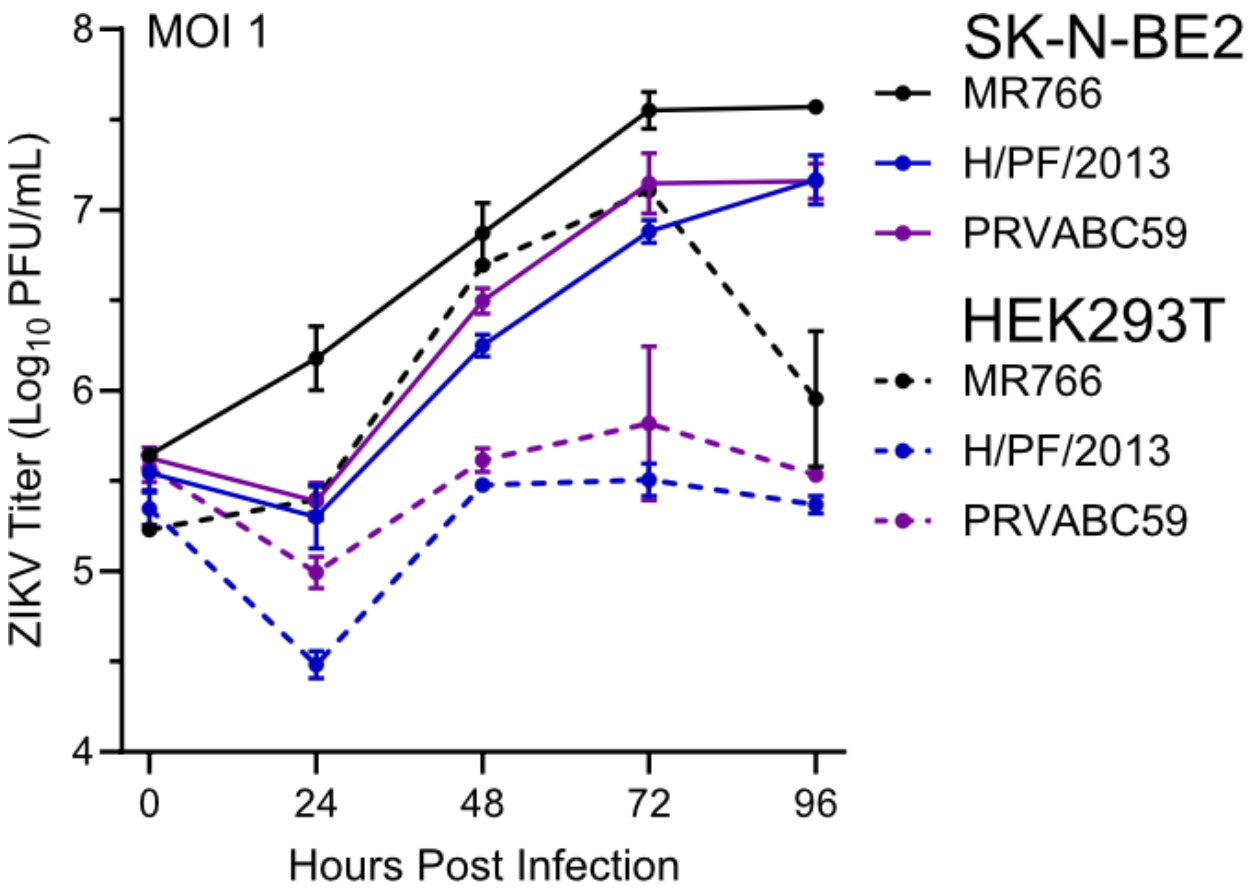

Appendix C-7: Replicative ability of different ZIKV strains in different cell lines. HEK293T or SK-N-BE2 cells were infected with three different ZIKV strains (MR766, Uganda 1947, H/PF/2013, French Polynesia 2013, or PRVABC59, Puerto Rico 2015) at MOI 1. Virus supernatant was harvested every 24 hours and titer was determined by plaque assay.

Appendix C-8: Overlap of ANKLE2-ZIKV proteomic candidates with other ZIKV proteomics studies.

Dataset	# in screen (Unique Proteins)	# of candidate overlap (ZIKV) (717 total)	% of our candidates	% of their data	Technique (Cell Line)
Shah, 2018	366	75	10.46	20.49	Streptactin-AP of ind. ZIKV proteins (HEK293T)
Coyaud, 2018	873	133	18.55	15.23	BioID and FLAG-AP of ind. ZIKV proteins (HEK293T)
Scaturro, 2018	275	45	6.28	16.36	HA-AP of ind. ZIKV proteins (SK-N-BE2)
Golubeva, 2019	150	4	0.56	2.67	Streptavidin-AP of ind. ZIKV NS proteins (HEK293T)
Zeng, 2020	201	10	1.39	4.98	FLAG-AP of ind. ZIKV proteins (Neural Stem Cells)
Denolly, 2023	46	3	0.42	6.52	HA-AP of Calnexin-associated ER membranes after ZIKV infection (A549)